UNIVERSIDADE ESTADUAL DE CAMPINAS
FACULDADE DE ENGENHARIA ELÉTRICA
DEPARTAMENTO DE SEMICONDUTORES INSTRUMENTOS E FOTÔNICA

Corrosão de Tungstênio por Plasma

Autor : Patrick Verdonck
Orientador : Jacobus W. Swart

Abril de 1993

Aan Rudi, Luce en Julia

Agradecimentos

Agradeço primeiramente àqueles sem os quais este trabalho nunca teria sido realizado :

Jacobus W. Swart, meu orientador, pela motivação dada, desde do início do doutorado, pela orientação, sugestões, observações críticas e correções;

Israel Geraldi, pela ajuda na preparação do manuscrito.

Agradeço também :

IMEC v.z.w. e principalmente Gilbert Declerck e Luc Van den hove pela total liberdade que foi dado no uso dos laboratórios e a infraestrutura global de IMEC;

todas as pessoas dos grupos MP e VMT para as discussões e as preparações de amostras, principalmente Pascal De Geyter, Serge Van Haelemeersch, Herman Meynen, Marylinn Stone, Marcel Lux, Johan Vertommen, Peter Vermeulen e Roger Palmans;

Hugo Bender pelas análises Auger e as discussões sobre os resultados;

Cobrain N.V. pelo uso dos equipamentos SWAFER e Matrix 303, e para todas as modificações que foram feitas nestes equipamentos para tornar alguns testes dedicados possíveis;

Guy Brasseur, Cristiane Jehoul, Pierre Bruneel, Johan Vandersmissen, Frank Coosemans e Mark Van Cauwenberghe pelas discussões e pelas preparações de amostras;

LSI-PEE-EPUSP pela total liberdade que foi dada para desenvolver este trabalho;

António Carlos Seabra, Roberto Katsuhiro Yamamoto, Carlos Takeo Akamine, Renato Marcelo Franzin, Ronaldo Domingues Mansano e Nelson Bernardo pela ajuda na preparação do manuscrito;

todas que ajudaram diretamente e indiretamente na realização deste trabalho.

Este trabalho foi feito com o apoio financeiro da RHAE - CNPq.

Resumo.

Neste trabalho apresentamos o desenvolvimento de processos de "back-etch" para a formação de "plugs" e de processos para obter estruturas em tungstênio com paredes verticais. Ao mesmo tempo apresentamos o estudo dos mecanismos da corrosão de tungstênio por plasma.
Neste trabalho usávamos principalmente dois tipos de equipamentos de corrosão por plasma. O primeiro tem a potência aplicada a uma frequência de 25 kHz, ao invés da tradicional 13,56 MHz. O segundo é do tipo reator com confinamento magnético. Em ambos os sistemas é possível obter corrosão química e corrosão induzida por bombardeamento iônico.
Conseguimos obter bons processos de "back-etch" em ambos os equipamentos.
É possível obter estruturas de tungstênio com paredes verticais em ambos os equipamentos. Porém a seletividade de tungstênio para fotorresiste é sempre baixa, tipicamente 1:1. Portanto precisar-se-ia de um tipo de máscara especial para a corrosão de tungstênio quando este é usado como interconexão.
A maioria dos mecanismos, como descritos na literatura foi confirmada neste trabalho. Onde há contradições na literatura, conseguimos determinar qual mecanismo é valido, como no caso de corrosão química, ou em quais circunstâncias qual mecanismo é válido, como no caso da formação e influência do óxido de tungstênio. Podemos também concluir que para a grande maioria dos processos, o mecanismo que limita a taxa de corrosão do tungstênio, é a chegada das espécies reativas na superfície da lâmina. Para os outros processos, há fortes indicações que a interação plasma-tungstênio-resiste causa fenômenos que limitam a taxa de corrosão.
As conclusões deste trabalho não são apenas válidas para os equipamentos estudados aqui, mas também para outros sistemas.

Abstract.

In this work, we present the development of processes to obtain a back etch process for plug formation in via holes and of processes to obtain tungsten structures with vertical walls. At the same time, the mechanisms behind the tungsten etching were studied.
These studies were mainly performed in two different types of equipment. The first one is a system with power applied at 25 kHz, instead of the traditional 13.56 MHz. The second equipment is a magnetically confined reactor. In both systems it is possible to have chemical etching and bombardment enhanced etching.
We were able to develop good back etch processes in both equipment. It is possible to obtain tungsten structures with vertical walls in both equipment, but the selectivity of the tungsten towards the resist is always low, typically 1:1. Therefore, one would need special mask structures or materials for this type of etching of tungsten when it is used as an interconnect material (e.g. as metal 1).
Most of the mechanisms of the tungsten etching as reported in the literature were confirmed in this work. Where there are contradictions, mainly about the possibility of chemical etching of tungsten and the formation and influence on the etching of the tungsten oxide, we were able to draw one conclusion, e.g. that chemical etching is possible, or indicate in which circumstances one mechanism is valid and in which circumstances another mechanism is valid, as in the case of the etch delaying role of tungsten oxide. We could also conclude that the arrival of the active species at the surface of the wafer is the etch rate limiting step most processes. For other processes, we have strong indications that the interaction plasma-tungsten-resist induces some phenomena which limit the etch rate. And for some other processes the removal of the etch product can be indicated as the etch rate limiting step.
These conclusions are not only valid for the systems studied in this work, but also for other types of equipment.

Índice

Lista de símbolos

A : área da lâmina
C : concentração
C_F : concentração do flúor atômico
d: diâmetro da lâmina
D : constante de difusão
E : energia do elétron
E_S : eficiência de excitação
f : fluxo de espécies entrando no reator
f(E): função de distribuição de energia dos elétrons
G : fator de geração de flúor atômico
h : constante de Planck
h_e : distância entre os eletrodos de um reator com eletrodos paralelos
h_i : altura do degrau da medida i
I_X : intensidade da luz emitida pela espécie X
J_F : fluxo de flúor consumido durante a corrosão
J_{WF6} : fluxo da WF_6 dessorvida durante a corrosão
k : constante de Boltzmann
LE : efeito de carregamento
LE_b : efeito de carregamento na borda
LE_c : efeito de carregamento no centro
m : massa molecular
M_i : peso atômico da espécie i
n_i : densidade de espécies i no plasma
ODF : lâmina coberta por uma máscara de óxido PECVD de campo escuro
OLF : lâmina coberta por uma máscara de óxido PECVD de campo claro
p : : pressão
Q : energia de ativação
r : taxa de corrosão
r_{PR} : taxa de corrosão de resiste
r_{SiO2} : taxa de corrosão de óxido
r_W : taxa de corrosão de tungstênio
r_{bDF} : taxa de corrosão de tungstênio na borda de uma lâmina com máscara de campo escuro
r_{bLF} : taxa de corrosão de tungstênio na borda de uma lâmina com máscara de campo claro
r_{cDF} : taxa de corrosão de tungstênio no centro de uma lâmina com máscara de campo escuro
r_{cLF} : taxa de corrosão de tungstênio no centro de uma lâmina com máscara de campo claro
R : constante universal de gases
R^2: fator de correlação
RDF : lâmina coberta com máscara de resiste campo escuro
RLF : lâmina coberta com máscara de resiste campo claro
R_{sp} : resistividade do material
R_{sq} : resistência de folha da camada
S : seletividade
t : tempo

t_l : espessura da camada
t_{PR} : espessura da camada de resiste
t_W : espessura da camada de tungstênio
T : temperatura
T_S :temperatura na superfície da lâmina
U : uniformidade da taxa de corrosão de tungstênio
U_{DF} : uniformidade da taxa de corrosão de tungstênio com máscara campo escuro
U_{LF} : uniformidade da taxa de corrosão de tungstênio com máscara campo claro
U_{PR} : uniformidade da taxa de corrosão de resiste
v(E) : velocidade do elétron, em função da energia do elétron
w : peso da lâmina
x_S : espessura da faixa de depleção de plasma
y : valor médio dos resultados medidos
y_i : resultado experimental, como medido
y_{Ci} : resultado previsto pelo modelo

ν : frequência do fóton
ρ : densidade do material
$\sigma_S(E)$: seção de colisão para excitação
σ_{12} : constante de força de Lennard-Jones
τ : tempo de residência de uma molécula adsorvida
τ_O: período de vibração
Ω_D: função do potencial de Lennard-Jones

Capítulo 1 : Introdução.

Para obter circuitos integrados (CI's) mais e mais potentes, não basta mais simplesmente reduzir as dimensões das estruturas : hoje em dia é indispensável de introduzir novos materiais que aumentarão a performance dos dispositivos. Pode-se dizer que o primeiro material "novo" na tecnologia MOS era o silício policristalino como material que substituiu alumínio como material de porta do transistor. Mais e mais, novos materiais entraram na tecnologia MOS, principalmente metais, tais como Ti e Co como matéria prima para formação de silicetos (e "salicide") e outros metais para formação de barreiras.
Uma das primeiras maneiras de uso de tungstênio em processos MOS era na liga com Ti, formando TiW para uso como barreira. Recentemente, a utilização de tungstênio aumentou bastante [1.1], principalmente como material para interconexão entre dois níveis de metal, os chamados "plugs" [1.2,1.3]. Duas outras aplicações usadas comercialmente hoje são : o uso como material de mascaramento para raios X em máscaras de raios X [1.4] e o uso como primeira camada de metal em estruturas com 3 ou mais camadas de metal [1.5]
Tungstênio é utilizado também como material de porta em MESFETS em GaAs, para a fabricação de transistores auto-alinhados. Também siliceto de tungstênio pode ser usado como material de porta, tanto em tecnologia de Si quanto em tecnologia de GaAs [1.6,1.7]

Tungstênio de corpo tem as seguintes características físicas:
- alta temperatura de ebulição : 3410°C
- peso molecular alto : 183.8 g/mol
- densidade alta : 19.35 kg/dm^3
- resistividade elétrica baixa : 5 µOhmcm

Além disso, tungstênio tem algumas propriedades muito interessantes para a microeletrônica:
- boa estabilidade a alta temperatura
- boa resistência contra eletromigração
- boa resistência contra vários ácidos
- função de trabalho no meio das funções de trabalho de Si tipo p e Si tipo n
- bom mascaramento para raios X
- possibilidade de ser depositado tanto por sputtering quanto por CVD
- possibilidade de ser corroído por plasma tanto com gases fluorados quanto com gases clorados.

Deposição por CVD permite uma cobertura muito conforme de superfícies. Portanto, usando esta técnica é possível encher buracos que têm uma alta razão de aspecto com muito mais confiabilidade do que usando técnicas de sputtering. Como a tecnologia de CVD é muito melhor dominada para tungstênio do que para qualquer outro metal, tungstênio é o

metal preferido para ser utilizado no enchimento de buracos estreitos e profundos, como são tipicamente as "vias" entre dois níveis de metal. Como a corrosão por plasma chamado "back-etching" é também possível, a combinação de deposição de uma camada de tungstênio (sobre uma camada de aderência) sobre um óxido isolante, seguida por uma corrosão por plasma está sendo usado para formar as interconexões entre dois níveis de metal na maioria das aplicações comerciais [1.2,1.3].
O uso de tungstênio como metal de linha de interconexão fica restrito pois a resistividade dele é 3 vezes maior do que do alumínio. Além disso, por causa da baixa seletividade da corrosão de tungstênio para o resiste, a obtenção de paredes verticais em camadas de tungstênio de 1 μm de espessura não é uma tarefa simples [1.8] .
Porém tungstênio tem algumas vantagens sobre alumínio: a primeira é uma estabilidade térmica muito maior: portanto é possível usar ainda processos a alta temperatura quando já há tungstênio nas lâminas. Porém é necessário ter cuidados especiais quanto à presença de oxigênio : pois tungstênio oxida a aproximadamente 250°C na presença de oxigênio. Uma segunda vantagem sobre alumínio é a maior resistência contra eletromigração pois o ponto de fusão é maior e o átomo de tungstênio é muito mais pesado que o átomo de alumínio.
Tungstênio foi usado para metal 1 nos DRAMs de 256k da IBM e será usado de novo nos DRAMs de 64M [1.5].
Cada vez mais usa-se tungstênio como material de mascaramento em litografia de raios X por causa da baixa transmissão dos raios X e por causa da fácil deposição e fácil definição das estruturas quando comparado com ouro [1.4].
Estes aplicações de tungstênio requerem além do domínio de processos de deposição, desenvolvimento de corrosão por plasma.
Na literatura comenta-se que a seletividade tungstênio-resiste é sempre baixa, tipicamente menor que 1:1, para equipamentos RIE tradicionais [1.8]. Isto dificulta bastante a obtenção de linhas com paredes verticais para níveis de interconexão. Portanto pesquisa de processos em equipamentos menos tradicionais é recomendável.
Há grande demanda para processos tipo "back-etch" de tungstênio com alta taxa de corrosão, alta uniformidade, alta seletividade em relação a camadas inferiores e com pouco efeito de área (loading effect).
Para obter processos eficientes e reprodutíveis, precisa-se conhecer os mecanismos básicos de corrosão por plasma de tungstênio.

Objetivos deste trabalho.

Em primeiro lugar, queremos desenvolver processos para obter dois tipos de estruturas : "plugs" de tungstênio e linhas de tungstênio com paredes verticais, que podem servir como linhas de interconexão ou mesmo como portas.

Em segundo lugar, queremos estudar os mecanismos de corrosão por plasma de tungstênio, pois estes mecanismos não são bem conhecidos.

Estrutura da tese.

No capítulo 2 são apresentados os modelos gerais de corrosão por plasma e mecanismos específicos de corrosão por plasma de tungstênio, como relatados na literatura. Dividimos os mecanismos em dois grupos : os que são geralmente aceitos e os mecanismos para os quais existem contradições na literatura. Descrevemos ainda : a tecnologia de fabricar "plugs", a técnica de actinometria e o uso de projeto estatístico de experimentos.
No capítulo 3 resultados experimentais de 3 equipamentos são descritos. Primeiramente os resultados no SWAFER, um equipamento com potência aplicada a 25 kHz e bastante versátil, são apresentados. Testes dedicados para obtenção de linhas com paredes verticais, para obtenção de "plugs", mas também para obter um maior conhecimento de mecanismos são comentados. Um processo de várias etapas para obter "plugs" é apresentado.
No segundo equipamento, um Matrix 303, foram feitos alguns testes para confirmar os resultados obtidos no SWAFER.
O terceiro equipamento é o Tegal 15xx, um sistema com confinamento magnético. Houve ênfase no desenvolvimento de um processo de "plugs", mas discute-se também possibilidades de obter linhas com paredes verticais e os mecanismos de corrosão por plasma de tungstênio.
No capítulo 4 combinam-se os resultados dos capítulos anteriores juntos com os conhecimentos gerais de capítulo 2 para propôr um modelo qualitativo e um modelo quantitativo simples. Através destes modelos é possível esclarecer as contradições encontradas na literatura e explicar a maioria dos testes decritos no capítulo 3.
Finalmente, as conclusões e sugestões para futuros trabalhos são apresentados no capítulo 5.

Referências

[1.1] Swart, "Interconexões e contatos em circuitos integrados", Processos de Microeletrônica, edt. Baranauskas (1990)
[1.2] Saia, Gorowitz, Woodruff, Brown, "Plasma etching methods for the formation of planarized tungsten plugs used in multilevel VLSI metallizations", J. Electrochem. Soc, 135, 936 (1988)
[1.3] Miller, Frazier, Su,"Controlling tungsten etchback on submicron devices", MMT, January 1992,28
[1.4] Kadel, Schomburg, Stern, "X-Ray Masks with Tungsten Absorbersfor use in the LIGA Process", to be published in the Proceedings of the ME92 conference.

[1.5] Arden, "Photolithography Overview for 64 Megabit Production": Presentation at ME 92, abstract A.2.1 published in : Abstracts of the ME 92 Conference, (1992)
[1.6] Kobayashi, Iwata, Yamamoto, Hara, "Highly reliable Tungsten Gate Technology", Proceedings 1987 Materials Research Society, p. 159.
[1.7] Pauleau, "Interconnect Materials for VLSI Circuits", Solid State Technology, vol 30 n°2 p. 61 (1987)
[1.8] S. Tandon, G. Jones, "Reactive Ion Etching of Tungsten in SF6 and CF4", in "Tungsten and other refractory Metals for VLSI Applications IV", Eds. Blewer & Mc. Conica (MRS Proceedings of the 1988 Workshop).

Capítulo 2 : Corrosão de tungstênio por plasma: modelos e técnicas auxiliares.

Introdução:

Os mecanismos gerais da corrosão por plasma são bem conhecidos e descritos na literatura [2.1-2.4]. Como tungstênio é um material relativamente novo na área de fabricação de circuitos integrados (CI's), não existem muitas publicações sobre a sua corrosão. A ref. [2.5] é o artigo mais abrangente, mas não é completo, nem totalmente atual.
Temos os seguintes objetivos para este capítulo :
1) descrever qualitativamente os vários mecanismos envolvidos na corrosão por plasma, aplicados à corrosão de tungstênio;
2) fazer uma revisão bibliográfica resumida de mecanismos e modelos relatados na literatura;
3) descrever em maior detalhe duas técnicas usadas na parte experimental deste trabalho : actinometria e projeto estatístico de experimentos;
4) descrever a aplicação mais usada na indústria : formação de "plugs".

2.1) Revisão dos mecanismos gerais de corrosão por plasma.

O processo de corrosão por plasma pode ser subdividido em vários subprocessos :

1: formação das espécies reativas
2: transporte das espécies reativas até a superfície a ser corroída;
3: adsorção da espécie reativa;
4: quimissorção da espécie reativa;
5: formação do produto volátil;
6: dessorção da molécula volátil e remoção pelo sistema de bombeamento.
Cada subprocesso será descrito sumariamente, com corrosão de tungstênio como aplicação.

2.1.1) Formação das espécies reativas.

Normalmente, não são as moléculas que entram no reator que reagem com o material da superfície, mas os átomos como F, Cl, Br. Mesmo no caso de corrosão de polímeros, são os átomos de O que fazem as ligações com o C e o H, não as moléculas O_2 [2.6].
Uma exceção é a corrosão de alumínio, para a qual a molécula Cl_2 é suficientemente reativa [2.7].
Em geral, o papel principal do plasma é a formação das espécies reativas, que farão a adsorção-quimissorção depois [2.2,2.3,2.5].
Gases tradicionalmente usados na corrosão por plasma são CF_4, SF_6 e NF_3. Se os átomos de flúor não forem liberados, estes gases não removem o material do filme. O papel mais importante do plasma na corrosão de tungstênio é a formação

do flúor atômico, como verificado no capítulo 5. Fazer um modelo quantitativo deste fenômeno é muito difícil, mas começa a ser feito [2.8].

A energia de formação da ligação entre os átomos é um parâmetro muito importante. Na ref. [2.9] acham-se estes valores, mostrados na tabela 2.1 :

Tabela 2.1 : Energias de ligação para algumas moléculas importantes para corrosão por plasma.

CF_3 - F : 128 kcal/mol	C - F : 128 kcal/mol
SF_5 - F : 90 kcal/mol	S - F : 82 kcal/mol
NF_2 - F : 55 kcal/mol	N - F : 63 kcal/mol
	W - F : 131 kcal/mol

Destes valores podemos concluir que é mais fácil gerar F com NF_3 que com SF_6, enquanto que com CF_4 gera-se menos flúor atômico ainda. Portanto a taxa de corrosão é em geral a maior com NF_3, depois com SF_6 e é a menor com CF_4.

É muito difícil determinar valores quantitativos para a concentração de flúor atômico. Através das técnicas de fluorescência induzida por laser (LIF) e actinometria, é possível fazer algumas comparações entre vários processos [2.5,2.10-2.15].
A geração de flúor livre pode ser influenciada pela adição de outros gases. Os sistemas mais conhecidos são : $CF_4 + O_2$ e $CF_4 + H_2$ [2.1-2.4,2.16].
Para o primeiro sistema, as seguintes reações ocorrem (entre outras) :

$$CF_4 + O_2 \rightarrow CO_2 + 4F. \qquad (2.1)$$
$$2\ CF_4 + O_2 \rightarrow 2\ COF_2 + 4F \qquad (2.2)$$

Através destas reações a densidade de flúor livre aumenta. Assim aumenta também a taxa de corrosão para a maioria dos processos.
A presença de carbono, na forma de um eletrodo ou mesmo como elemento do resiste, afeta também a formação do flúor livre. O carbono captura oxigênio através das seguintes reações :

$$C + O_2 \rightarrow CO_2 \qquad (2.3)$$
$$2\ C + O_2 \rightarrow 2\ CO \qquad (2.4)$$

Portanto há menos chances que as reações (2.1) e (2.2) ocorram, assim diminuindo a geração do flúor livre e diminuindo a taxa de corrosão em geral.
Reações similares a (2.1) e (2.2) ocorrem adicionando O_2 a SF_6 e NF_3.
A adição de hidrogênio também influencia diretamente na concentração de flúor livre, através da seguinte reação :

$$2\ F + H_2 \rightarrow 2\ HF \qquad (2.5)$$

Portanto, a adição de hidrogênio diminui a taxa de corrosão. Para modelar o plasma, todas estas reações devem ser consideradas.

2.1.2) Transporte das espécies reativas até a superfície a ser corroída.

Um fator muito importante para a taxa de corrosão é o número de espécies reativas que chegam na superfície do material a ser corroído. Este fluxo é determinado por dois mecanismos :
1: a geração de espécies reativas;
2: o transporte destes espécies para a superfície.

Como visto acima, uma quantização do primeiro mecanismo é extremamente difícil. É possível fazer alguns cálculos para determinar o segundo mecanismo, como mostrado no capítulo 4.

2.1.3) Adsorção e quimissorção.

Uma parte dos átomos de flúor que chegam na superfície não formam o produto volátil WF_6. Uma parte volta para o plasma sem reagir. Porém a maior parte forma uma ligação W-F, através de adsorção e quimissorção. Assim formam-se compostos WF_x com x = 1,2,3 ou 4 [2.17]. Estes compostos WF_x interagem para formar o produto volátil WF_6 como mostrado em 2.1.4.

2.1.4) Formação do produto volátil.

Não é suficiente formar uma ligação W-F : WF não é um produto volátil, porém WF_6 é. Os mecanismos da formação deste produto não são bem conhecidos, mas há vários modelos propostos, como mostrado em 2.2 abaixo. O modelo de dessorção associativo [2.17] assume a formação de compostos de WF_x (x = 1->4) formando WF_6 através das seguintes reações :

$$WF_2 + WF_4 \rightarrow WF_6 + W \qquad (2.6)$$
$$WF_3 + WF_3 \rightarrow WF_6 + W \qquad (2.7)$$

2.1.5) Dessorção.

O produto volátil, no caso de tungstênio WF_6, deve sair da superfície da lâmina e ser removido do reator pelo sistema de bombeamento. Este processo é descrito com mais detalhes na ref. [2.19] e no capítulo 4.

2.2) Revisão bibliográfica resumida de modelos existentes para corrosão de tungstênio por plasma.

Segue uma revisão de artigos sobre corrosão de tungstênio por plasma com gases contendo flúor, que são relevantes para este trabalho.

2.2.1) Observações gerais.

Tabela 2.2 mostra as temperaturas de ebulição de possíveis produtos voláteis na corrosão de W e de Si.

Tabela 2.2 : Ponto de ebulição de produtos voláteis.

SiF_4	-86°C	WBr_5	333°C
$SiCl_4$	57.6°C	WOF_4	188°C
WF_6	17.5°C	$WOCl_4$	228°C
WCl_5	276°C	$WOBr_4$	327°C
WCl_6	347°C		

Estes dados mostram que flúor é o átomo mais indicado para remover W rapidamente. Aumentando a energia, por exemplo por bombardeamento iônico, é possível também corroer W com Cl e Br [2.10,2.20,2.21].
A maioria dos testes publicados aconteceram num reator com potência aplicada a 13,56 MHz, alguns com microondas. Não houve publicações com plasmas de áudio-freqüência (AF).

2.2.2) Influência dos gases usados.

Muitos testes usaram os gases SF_6 e CF_4.
Adições limitadas de O_2 (e N_2) aumentam a concentração do flúor livre, através de reações similares a (2.1) e (2.2). Isto causa um aumento de taxa de corrosão de tungstênio [2.11,2.12,2.15,2.21-2.25]. Porém, adicionando oxigênio em excesso, o fator de diluição se torna mais importante que o fator de aumento de flúor, assim diminuindo a taxa de corrosão.
Taxas de corrosão são mostrados como função de concentração de oxigênio na figura 2.1. Na mesma figura mostra-se a taxa de corrosão de silício policristalino e a concentração relativa de flúor atômico, como medido por actinometria. Combinando estas curvas, espectrometria de massa e análise XPS [2.11,2.23-2.25], o seguinte modelo foi proposto : existem 3 regimes diferentes. O primeiro é quando pouco oxigênio está sendo adicionado. A taxa de corrosão é determinada pela concentração de F, formando WF_6. Na segunda região, no regime intermediário, forma-se também WOF_4, o que ajuda obter ainda uma taxa de corrosão alta apesar do fato de WOF_4 ser menos volátil que WF_6. Adicionando ainda mais oxigênio, há competição entre o F e o O para formar ligações com o W [2.11], ou pode ter diluição demais para ficar com uma taxa alta de corrosão.

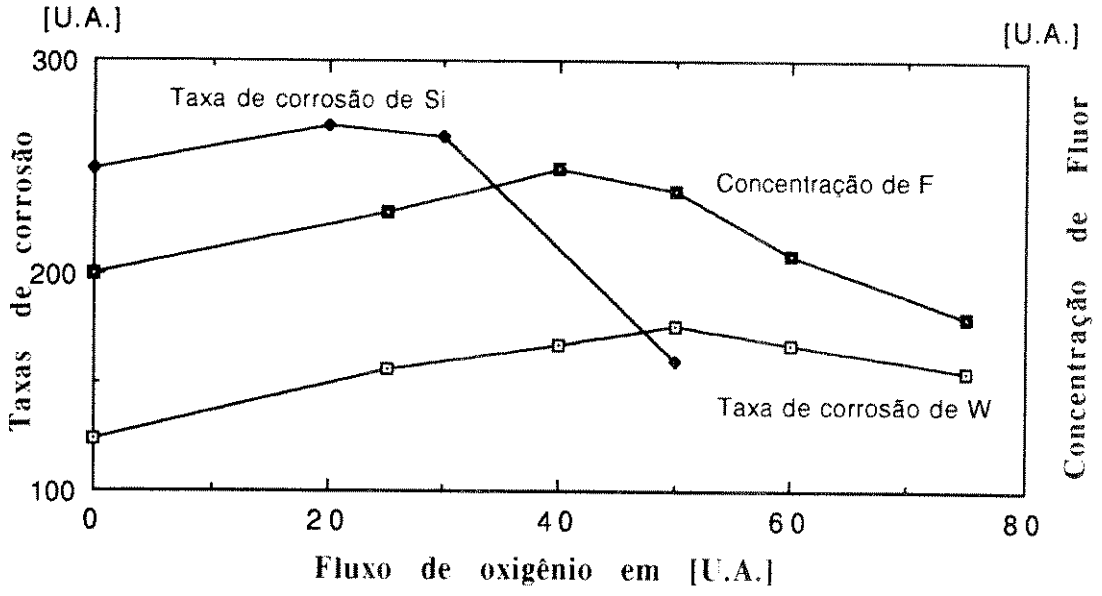

Figura 2.1 : Taxa de corrosão de tungstênio e de silício policristalino e concentração de flúor atômico em função do fluxo de oxigênio.

A diferença com o modelo de corrosão de Si é que fora do produto volátil principal, WF_6, forma-se também um outro produto volátil : WOF_4 quando se adiciona O_2. Esta a razão que o máximo da curva de taxa de corrosão de W está situado num fluxo porcentual maior de O_2 que o máximo da concentração de F. O máximo da curva da taxa de corrosão de Si está situado a um fluxo de oxigênio menor ainda pelas seguintes duas razões :
1) $SiOF_2$ (o equivalente de WOF_4) não é volátil. Portanto não pode contribuir à taxa de corrosão;
2) oxigênio oxida a superfície de Si, impedindo a corrosão de Si pois é muito mais difícil de corroer SiO_2 que Si [2.17].
WO_3 seria uma molécula estável, mas volátil [2.27]. Na literatura acha-se que o óxido de tungstênio impede a corrosão [2.28] mas também que não influencia a corrosão [2.11].
Neste trabalho mostraremos que a influência do óxido de tungstênio depende do modo de corrosão (e da espessura do óxido).
A presença de oxigênio influencia também na anisotropia da corrosão. O oxigênio pode aumentar a anisotropia, quando misturado com SF_6, pelo aumento de bombardeamento iônico [2.25], mas pode também diminuir a anisotropia pela formação de mais flúor livre, aumentando assim a corrosão química (dependente de outros parâmetros de plasma) [2.26].
Adição de um pouco de nitrogênio pode resultar em aumento significativo de taxa de corrosão por 2 razões : geração de mais F e aumento de bombardeamento [2.24,2.26].
Foi relatado que para plasmas de NF_3 + O_2 não se acha WOF_4 [2.29] (para processos em modo RIE). Para estes gases

também propõe-se uma corrosão induzido por danos. Não foi encontrado nenhum artigo sobre corrosão química com NF_3.

2.2.3) A influência de bombardeamento iônico.

Bombardeamento iônico pode ser um fator muito importante na corrosão de W. É possível ter uma corrosão completamente química, mas um bombardeamento iônico, mesmo causado por um campo elétrico de apenas 25 V, já aumenta a taxa de corrosão com um fator 2 [2.23]. O aumento da voltagem DC geralmente resulta em uma taxa de corrosão maior. Este aumento pode ser obtido por um aumento da potência aplicada, pela diminuição de pressão, mas também pela adição de certos gases. Assim esta adição resulta numa maior variação de taxa de corrosão do que pensado se apenas fosse avaliada a função química do gás adicionado.
Bombardeamento iônico forma sítios ativos de W. Ali, o F forma mais facilmente uma ligação química com o W. Assim pode-se aumentar a taxa de corrosão por uma voltagem DC de 100 V por um fator 15 (ou mais) [2.29,2.30].
Os artigos que tratam da anisotropia mostram resultados diferentes [2.23,2.25,2.26,2.35]. Anisotropia depende de vários fatores, tais como : material de resiste, material do eletrodo, adição de oxigênio (ou nitrogênio), além dos fatores tradicionais como : pressão, potência e voltagem DC. Alguns autores assumem que se precisa formar um polímero para proteger a parede de W. Outros mostram que a formação de sítios ativos no W, através de bombardeamento iônico, promove a corrosão vertical em relação à corrosão horizontal.

2.2.4) Corrosão química.

O fato que o ponto de ebulição de WF_6 é 17.5°C indica que corrosão química ocorre menos facilmente para W que para Si. O mecanismo de dessorção associativa foi proposto [2.17]: uma quantidade suficientemente alta de F atômico deve ser gerado para formar compostos WF_x (x = 1->4) através das reações :

$$W + F \rightarrow WF \qquad (2.8)$$
$$WF + F \rightarrow WF_2 \qquad (2.9)$$
$$WF_2 + F \rightarrow WF_3 \qquad (2.10)$$
$$WF_3 + F \rightarrow WF_4 \qquad (2.11)$$

O produto volátil WF_6 forma-se através das seguintes reações:

$$WF_3 + WF_3 \rightarrow WF_6 + W \qquad (2.12)$$
$$WF_4 + WF_2 \rightarrow WF_6 + W \qquad (2.13)$$

Este mecanismo é parecido com a formação de SiF_4 pela dessorção associativa de duas moléculas de SiF_2.

2.2.5) Resumo dos modelos propostos na literatura.

Há concordância para os seguintes itens :
- tungstênio pode ser corroído por flúor livre, mesmo sem bombardeamento;
- bombardeamento iônico aumenta a taxa de corrosão de tungstênio;
- a taxa de corrosão segue a concentração de flúor. Para CF_4 e SF_6 a formação de WOF_4 sustenta a taxa de corrosão, para NF_3 não achou-se WOF_4.

Houve contradições, principalmente nos seguintes dois tópicos:
- adição de oxigênio diminui a taxa de corrosão por causa de formação de um óxido de tungstênio;
- qual o mecanismo responsável para formação de paredes verticais.

A corrosão química de tungstênio não é bem modelada, mas há concordância sobre o modelo de dessorção associativa.

2.3) Actinometria

Uma técnica bastante simples para fazer análise de plasmas é actinometria. Esta técnica é baseada na técnica de espectrometria de emissão. É uma técnica bastante usada pois é muito simples [2.5,2.10-2.15,2.36,2.37]
A intensidade da luz emitida pelos espécies não é apenas proporcional com a densidade das espécies, mas também é função de : densidade e energia dos elétrons e da seção de emissão de luz das espécies. Tendo um gás inerte que tem estas características similares ao gás a ser monitorado é possível fazer uma análise semiquantitativa : para monitorar F, Ar é um gás útil [2.36,2.37]

É necessário excitar o gás pela seguinte reação :

$$e^- + S \rightarrow S^* + e^- \qquad (2.14)$$

onde :
e^- : elétron
S : espécie química
S^* : espécie química excitada

A intensidade da luz é proporcional ao número de espécies excitadas que voltam ao estado básico através de emissão de fótons :

$$S^* \rightarrow S + h\nu \qquad (2.15)$$

Se este relaxamento por emissão de fótons é constante, a intensidade da luz I_S é proporcional à taxa de geração de S^*.

$$I_S \propto k_S [e^-] [S] \qquad (2.16)$$

O constante k_S é proporcional à eficiência de excitação E_S que pode ser expressa como :

$$E_S = \int v(E)\ \sigma_S(E)\ f(E)\ dE \qquad (2.17)$$

onde :
$v(E)$: a velocidade do elétron,
$\sigma_S(E)$: a seção de excitação
$f(E)$: a função de distribuição de energia dos elétrons.

Aplicando estas equações para o gás X a ser monitorado e o gás A de referência :

$$\frac{I_X}{I_A} = \frac{k_X\ [X]}{k_A\ [A]} = \frac{E_{SX}\ [X]}{E_{SA}\ [A]} \qquad (2.18)$$

Escolhendo gás A tal que σ_X e σ_A sejam funções similares da energia dos elétrons, E_{SX} e E_{SA} serão também funções similares da energia dos elétrons. Portanto : k_X/k_A pode ser considerado uma constante.
Para determinar a concentração da espécie X, a concentração do gás A deve ficar constante. Portanto , o fluxo de A deve ser proporcional ao fluxo total.
A concentração [A] é proporcional com a pressão : portanto introduzimos o fator p", um fator proporcional com a pressão total no reator :

$$[X] \propto p''\ I_X\ /\ I_A \qquad (2.19)$$

Para determinar a concentração de flúor atômico, usa-se Ar como gás de referência com sucesso [2.5,2.10-2.15,2.36,2.37]. As linhas usadas são em geral 704 nm para F e 750 nm para Ar.

2.4) Projeto estatístico de experimentos.

Projeto estatístico de experimentos é uma técnica para obter um máximo de informações na maneira mais eficiente de um certo conjunto de testes.[2.38-2.43]
Esta técnica está sendo usado em muitas indústrias, recentemente também na indústria de semicondutores.
Para obter os valores dos parâmetros para o processo ótimo, vários testes devem ser feitos. É importante determinar bem os valores dos parâmetros do conjunto de testes para obter resultados significativos com o mínimo de testes possíveis.
Para este trabalho foi usada a técnica de Metodologia de Superfície de Resposta (Response Surface Method (RSM)).
A RSM consiste de um grupo de técnicas estatísticas que combina a estratégia experimental e análise de dados para gerar uma equação empírica que represente as respostas do processo. Este método pode ser aplicado a qualquer processo desde que as respostas possam ser quantificadas, tenham comportamento de uma função contínua e os fatores possam ser manipulados independentemente. As regiões de mudança brusca

no comportamento devem ser evitadas por causa de sua natureza instável. Em geral, as regiões de interesse são contínuas e podem ser explorados criando-se uma expressão polinomial para representá-las [2.39-2.41].
O projeto de experimento para a superfície de resposta é um fatorial fracionado em três ou mais níveis para cada fator. Em geral, o projeto deve ser escolhido de modo a poder ajustar um modelo quadrático. Um modelo quadrático é da seguinte forma :

$$Y = b_o + \sum_{i=1}^{f} b_i X_i + \sum_{i=1}^{f-1} \sum_{j=2}^{f} b_{ij} X_i X_j + \sum_{i=1}^{f} b_{ii} X_i^2 \quad (j>i) \quad (2.20)$$

onde :
Y : a resposta
X_i : os parâmetros do processo
b_{ix} : os coeficientes do polinômio
f : o número de fatores.

O projeto mais comum para casos de três variáveis é o projeto Box-Behnken, mostrado na figura 2.2.
Este projeto tem repetições dos experimentos no ponto central para a estimativa do erro puro.
Os coeficientes b_{ix} são determinados pelo método dos mínimos quadrados.

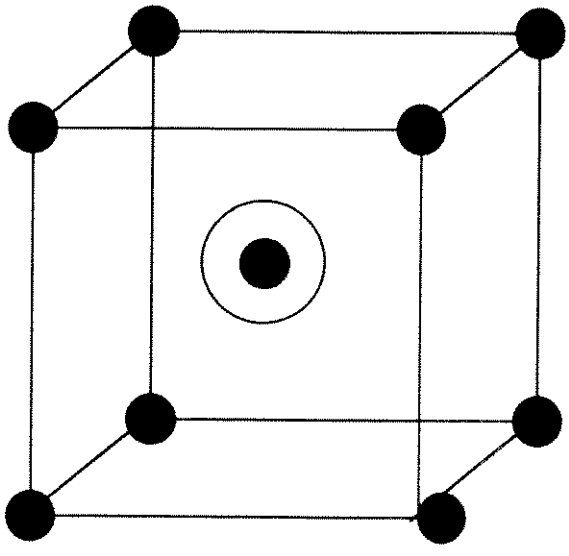

Figura 2.2 : Representação geométrica do projeto Box-Behnken [2.39].

A validade do modelo pode ser verificado através da avaliação do fator de correlação R^2 e da análise de variâncias.

O fator de correlação é determinado da seguinte maneira :

$$R^2 = \Sigma (y_{ci} - y)^2 / \Sigma (y_i - y)^2 \qquad (2.21)$$

Onde :
y : o valor médio
y_{ci} : o resultado calculado pelo modelo
y_i : o resultado experimental
portanto $0 < R^2 < 1$.
Como explicado na ref [2.40] quanto mais perto R^2 se aproxime de 1, melhor o modelo.
O teste para verificar o ajuste do modelo criado, utiliza a análise de variância. Neste teste, utiliza-se o resíduo : a diferença entre o resultado experimental e o calculado pelo modelo proposto. O resíduo consiste de dois termos de erros: o erro experimental e o erro devido à falta de ajuste do modelo proposto.
O erro experimental pode ser estimado por repetições dos experimentos numa dada condição experimental. A variação entre elas nos dá a estimativa do desvio padrão dos experimentos.
O erro de ajuste do modelo criado, pode ser estimado fazendo mais experimentos que o mínimo necessário para poder estimar todos os coeficientes b_i do modelo proposto e calcular o desvio entre o modelo e os dados experimentais.
O erro de ajuste indica se a funcionalidade do modelo ajustado é suficiente para representar a realidade.
Na análise de variâncias comparem-se estes dois tipos de erros : se o erro do ajuste for grande a análise indica que o modelo não é válido.

2.5) Corrosão de "plugs" de tungstênio.

A aplicação mais usada de corrosão de tungstênio por plasma é a "back-etch" para formar "plugs" nas vias. A deposição de tungstênio é bem descrito na literatura, mas a corrosão não. Alguns artigos descrevem o processo e o problema de efeito de área [2.44-2.46].
A figura 2.3 mostra o objetivo desta corrosão. Uma camada de W é depositada por cima da camada de óxido, para formar uma camada planar. Deve-se tirar a parte sobre o óxido para que fiquem apenas os "plugs".
Para obter um bom processo de "plugs", é preciso ter uma camada de óxido bem planar, uma camada uniforme de W por cima de uma camada de aderência, em geral TiW ou TiN.

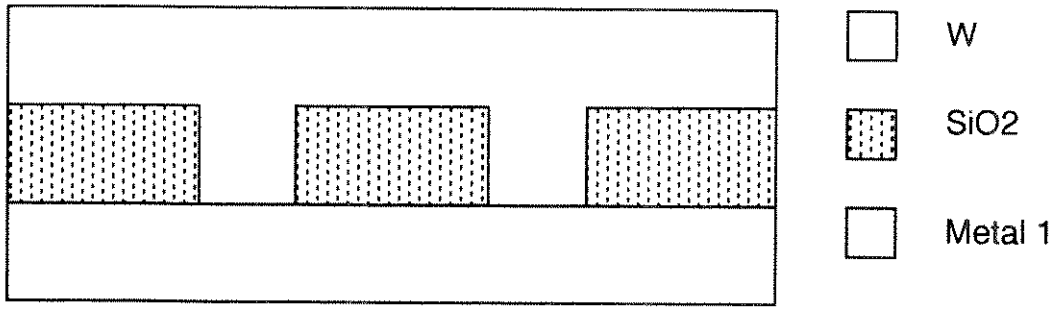

Fig. 2.3.a: Formação de "plugs" : depois de deposição por CVD

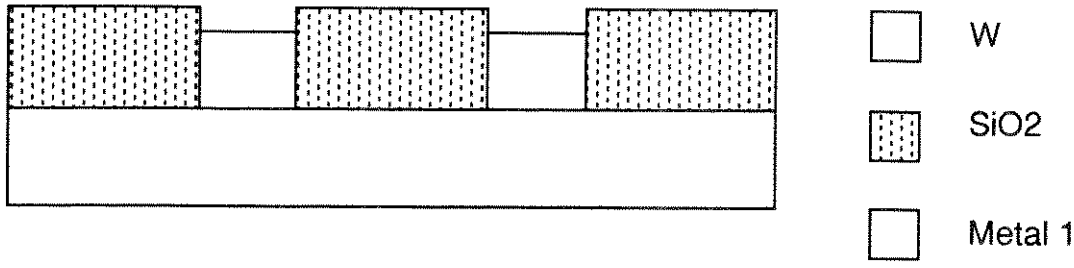

Fig. 2.3.b: Formação de "plugs" : depois de corrosão

Figura 2.3 : O processo "back-etch" para a formação de "plugs".

O processo de corrosão deve ter as seguintes características:
- boa uniformidade;
- boa seletividade em relação ao óxido ou à camada de aderência;
- boa detecção do ponto final;
- nenhum problema de efeito de área.

Esta quarta característica é em geral a mais difícil para se obter. O problema fundamental do efeito de área é que no momento que a corrosão acaba de remover o W sobre o óxido, a área de material que está sendo corroído rapidamente muda drasticamente : de 100 % da área para alguns % da área. Portanto o consumo do flúor livre é muito menor, o que significa que há muito mais flúor disponível para remover o W dos "plugs" de dentro das "vias". É possível remover todo o W dos "plugs" em alguns segundos (para certos processos). Também ocorre que se remove todo o W dentro dos plugs enquanto que o W em outros lugares da lâmina ainda não foi removido completamente [2.44]. Estes processos não são aceitáveis.

Em geral, a solução é aumentar o componente físico da corrosão. O efeito de bombardeamento iônico é o mesmo para pequenas áreas que para grandes áreas [2.45]. Portanto usa-se em geral plasmas tipo RIE e não plasmas do tipo apenas

químico. Muitas vezes adiciona-se um outro gás, como Ar, para aumentar o bombardeamento iônico [2.46].
Uma boa detecção do ponto final é sempre necessário. Em geral usa-se a linha de F a 704 nm.

Referências:

[2.1] B. Chapman, "Glow Discharge Plasmas", John Wiley and sons (1980).
[2.2] J. Coburn, "Plasma Etching and Reactive Ion Etching", IV Oficina Brasileira de Microeletronica, pp. 41-80, edt Mammana (1983)
[2.3] Mogab, "Dry Etching" in "VLSI Technology"pp 303-346, edt. Sze, Mc. Graw - Hill (1983)
[2.4] P. Verdonck, "Dry Etching for Integrated Circuit Fabrication", in "Processos de Microeletronica", edt. Baranauskas (1990)
[2.5] D. Hess, "Tungsten and Tungsten Silicide Etching in Halogenated Plasmas". Solid State Technology, April 1988, 97.
[2.6] Cook, "Downstream Plasma Etching and Stripping", Solid State Technology, vol 30 nr 4, 147 (April 1987)
[2.7] D. Flamm, J. Mucha in "Chemistry of the Semiconductor Industry", p 380.
[2.8] V. Mc Koy, private communications.
[2.9] CRC Handbook of Chemistry and Physics, 65th edition, edt: R. Weast, CRC Press Inc. (1984-1985)
[2.10] C. Tang, D. Hess, "Tungsten Etching in CF4 and SF6 Discharges", J. Electrochem. Soc. 131, 115 (1984)
[2.11] T. Bestwick, G. Oehrlein, "Tungsten Etching Mechanisms in CF4/O2 Reactive Ion Etching Plasmas", J. Appl. Phys. 66, 5034 (1989)
[2.12] W. Pan, A. Steckl, "Selective Reactive Ion Etching of Tungsten Films in CHF3 and other Flúorinated gases", J. Vac. Science Technol. B 6, 1073 (1988)
[2.13] K. Greenberg, T. Verdeyen, "Kinetic Processes of NF3 etchant gas discharges", J. Appl. Phys. 57, 1596 (1985)
[2.14] A. Richards, B. Thompson, K. Allen, H. Sawin, "Atomic Chlorine Concentration Measurements in a Plasma Etching Reactor", J. Appl. Phys. 62, 792 (1987)
[2.15] T. Daubenspeck, P.Sukanek, "Investigation and Modelling of mixed Halogen Freon/Oxygen Plasma Chemistries for Tungsten Etching", J. Electrochem. Soc. 136, 3779 (1989)
[2.16] A.C. Seabra, "Construção e caracterização de um equipamento de corrosão por plasma e sua aplicação na corrosão de SiO2 ", Tese de mestrado (1990)
[2.17] A. Durandet, Y. Arnal, J. Pelletier, G. Pomot, "Anisotropy and Kinetics of the Etching of Tungsten in SF6 Multipolar Microwave Plasma", J. Appl. Phys. 67, 2298 (1990)
[2.18] K.J. Laidler, "Chemical Kinetics", Tata-Mc.Graw-Hill.
[2.19] Vacuumtechniek - L. Wolterbeek Muller, Kluwer Technische boeken, (1989)
[2.20] D. Fischl, D. Hess, "Plasma Enhanced Etching of Tungsten and Tungsten Silicide in Chlorine Containing Plasmas", J. Electrochem. Soc. 134, 2265 (1987)

[2.21] M. Burba, E. Degenkolb, S. Henck, M. Tabassy, E. Jungbluth, R. Wilson, "Selective Dry Etching of Tungsten for VLSI Metallization", J. Electrochem Soc. 133, 2113 (1986)
[2.22] Susa, "Comparison of GaAs, tungsten and Photoresist Etch Rates and GaAs surfaces using RIE with CF4, CF4 + N2 and SF6 + N2 Mixtures", J. Electrochem. Soc. 132, 2762 (1985)
[2.23] F. Fracassi, J. Coburn, "Plasma-assisted Etching of Tungsten Films: a quartz-crystal Microbalance Study", J. Appl. Phys. 63, 1758 (1988)
[2.24] Mutsukura, Turban, "Reactive Ion Etching of Tungsten in SF6-N2 plasmas", J. Electrochem. Soc, 137, 225 (1990)
[2.25] Collumeau e.a., "RIE of a T-shape refractory ohmic contact for a self-aligned heterojunction bipolar transistor", J. Electrochem. Soc. 137, 671 (1990)
[2.26] Whetten e.a., "Reactive Ion Etching of submicrometer size features in Tungsten Thin Films", in "Tungsten and other Reafractory Metals for VLSI Applications, II", eds. Brewer, Mc. Conica, MRS 1987.
[2.27] S. Murarka,"Silicides for VLSI Applications", Academic Press, 1983.
[2.28] Adachi, Susa, "Reactive Ion Etching of Tungsten Films Sputter Deposited on GaAs", J. Electrochem. Soc. 132, 2980 (1985)
[2.29] W. Greene, D. Hess, W. Oldham, "Ion-bombardment-enhanced Plasma Etching of Tungsten with NF3/O2", J. Vac. Science Technol. B 6, 1570 (1988)
[2.30] A. Bensouala, J. Strozler, A. Ignatiev, J. Yu, J.Wolfe, "Ion Enhanced Reactive Etching of Tungsten Single Crystals and Films with XeF2", J. Vac Science Technol. A 5, 1921 (1987)
[2.31] Bensaoula, Grossman, Ignatiev, "Etching of tungsten with XeF2: An X-ray photoelectron spectroscopy Study", J. Appl. Phys. 62, 4587 (1987)
[2.32] J. Coburn, H. Winters, "Plasma-etching, a Discussion of Mechanisms", J. Vac. Sci. & Techn. 16, 391, (1979)
[2.33] P. Verdonck, G. Brasseur, J. Swart, "Chemical Plasma Etching of Tungsten", to be published in the Proceedings of Microcircuit Engineering 92.
[2.34] Fischl e.a., "Etching of Tungsten and Tungsten Silicide Films by Chlorine Atoms", J. Electrochem Soc. 135, 2016 (1988)
[2.35]. S. Tandon, G. Jones, "Reactive Ion Etching of Tungsten in SF6 and CF4", in "Tungsten and other refractory Metals for VLSI Applicationsd IV", Eds. Blewer & Mc. Conica (MRS Proceedings of the 1988 Workshop).
[2.36] J. Coburn, Chen, J. Appl. Phys. 51, 3134 (1980)
[2.37] P. Verdonck, P. Degeyter, J. Swart, "Actinometry and its Application on Polysilicon Etching in a Magnetically Confined Reactor", Proceedings of the VII Congresso da Sociedade Brasileira de Microeletronica (1992)
[2.38] W. Ostrout, S. Hunkler, S. Ward,"Enhanced Process Control for Submicron Contact Definition", Proceedings of SPIE Vol. 1392, eds. Bondur, Turner (1991), 151.
[2.39] M. Jenkins, M. Mocella, K. Allen, H. Sawin,"The Modelling of Plasma Etching Processes using Response Surface Methodology", SST, April 1986, 175.

[2.40] G. Box, W Hunter, J. Hunter,"Statistics for Experimenters: an Introduction to Design, Data Analysis and Model Building", John Wiley & Sons, 1978.
[2.41] G. Box, N. Draper, "Empirical Model Building and Response Surfaces", John Wiley & Sons, 1987.
[2.42] G. Taguchi, "Introduction to Quality Engineering", Asian Productivity Organization, Tokyo 1986.
[2.43] P.J. Ross, "Taguchi Techniques for Quality Engineering", Mc. Graw - Hill, 1988
[2.44] Saia, Gorowitz, Woodruff, Brown, "Plasma etching methods for the formation of planarized tungsten plugs used in multilevel VLSI metallizations", J. Electrochem. Soc, 135, 936 (1988)
[2.45] Miller, Frazier, Su,"Controlling tungsten etchback on submicron devices", MMT, January 1992,28
[2.46] Riley, Clark,"Integrated chemical vapor deposition and plasma etchback of tungsten in a multichamber, single-wafer system",J. Electrochem. Soc. 138, 3008 (1991)

Capítulo 3 : Desenvolvimento experimental.

Introdução

O uso de tungstênio na fabricação de circuitos integrados está se tornando cada vez mais importante. Novos processos de deposição e corrosão estão sendo desenvolvidos diariamente.
Um dos grandes problemas encontrados com sistemas tradicionais de corrosão por plasma é a baixa seletividade do tungstênio para o resiste. Um outro problema é o efeito de carregamento durante a corrosão para a obtenção de "plugs".
Para melhorar estes dois aspectos, corrosões por plasma foram feitas em dois equipamentos não tradicionais : o Cobrain SWAFER e o Tegal 15xx.
Para confirmar alguns mecanismos que ocorreram no SWAFER foram feitos alguns testes no Matrix 303.

3.1) Processos de corrosão por plasma no SWAFER.

3.1.1) Equipamento.

Uma vista esquemática é mostrada na figura 3.1.
A grande diferença entre este equipamento e outros equipamentos tradicionais é o fato que a potência é aplicada a uma freqüência de 25 kHz (AF) , ao invés da tradicional 13,56 MHz (RF). A potência pode ser aplicada nos dois eletrodos, deixando o outro eletrodo aterrado ou flutuante.
Os modos de corrosão usados foram modo RIE, quando a potência está sendo aplicada no eletrodo inferior e o eletrodo superior está aterrado, e o modo PF (Plasma Float) quando a potência está sendo aplicada no eletrodo superior e o eletrodo inferior está flutuante.
Uma descrição mais detalhada acha-se no anexo II e na ref [3.1].

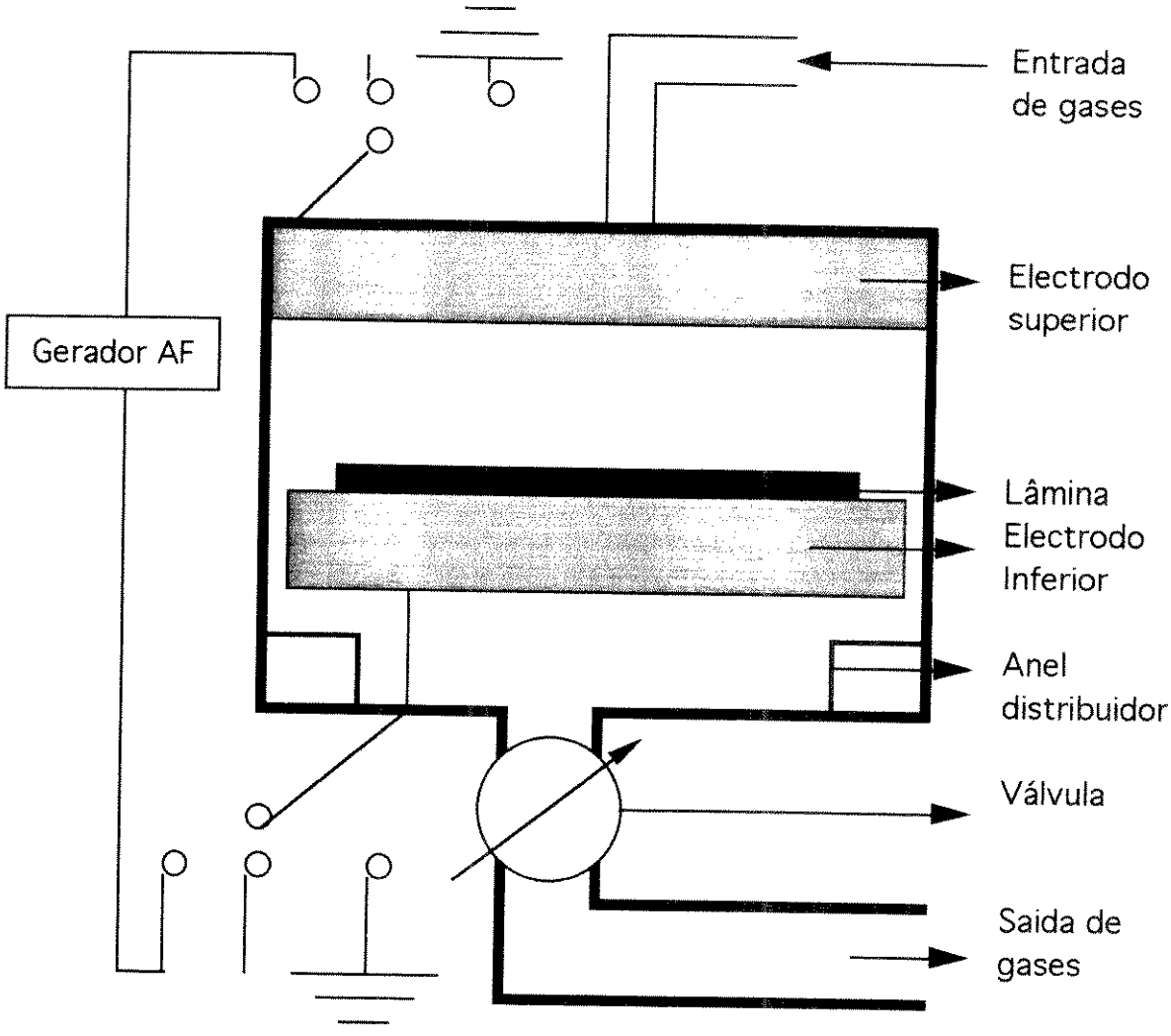

Figura 3.1 : Vista esquemática do SWAFER.

3.1.2) Resultados experimentais.

3.1.2.1) Objetivos - preparações.

O objetivo dos testes era em primeiro lugar determinar as características de processos de corrosão neste equipamento, para depois desenvolver 2 tipos de processos : uma corrosão anisotrópica, para obter estruturas em tungstênio que possam ser usadas como porta ou metal 1, e um processo para fazer o "back-etch", para fazer "plugs".
Para fazer a caracterização, taxas de corrosão, uniformidades, seletividades e perfis de paredes foram determinados para tungstênio e também para silício policristalino. A influência dos seguintes parâmetros foi investigada : gases usados (NF_3, O_2, SF_6), fluxos dos gases (20 até 125 sccm), pressão (40 até 400 mTorr), potência (50 até 200 W) e modo (RIE ou PF).

Várias corridas de lâminas de 125 mm foram preparadas. A seqüência era a seguinte : deposição de óxido ou oxidação, deposição de uma camada de barreira : TiW ou TiN, deposição de 1 µm de W. Várias lâminas não receberam a aplicação de uma máscara; a maioria das lâminas recebeu a aplicação de uma máscara de resiste, campo claro; algumas lâminas receberam uma máscara de resiste, campo escuro; algumas lâminas receberam uma máscara de óxido PECVD com resiste acima, campo claro; e algumas lâminas receberam uma máscara de óxido PECVD com resiste acima, campo escuro. A influência das máscaras é grande, como explicado adiante.
A definição da uniformidade usada aqui é a taxa mínima da lâmina dividida pela taxa máxima da lâmina.

3.1.2.2) Misturas de NF_3 e O_2 em modo RIE.

O efeito do fluxo de O_2 nas taxas de corrosão de tungstênio e de silício policristalino é mostrado na figura 3.2.

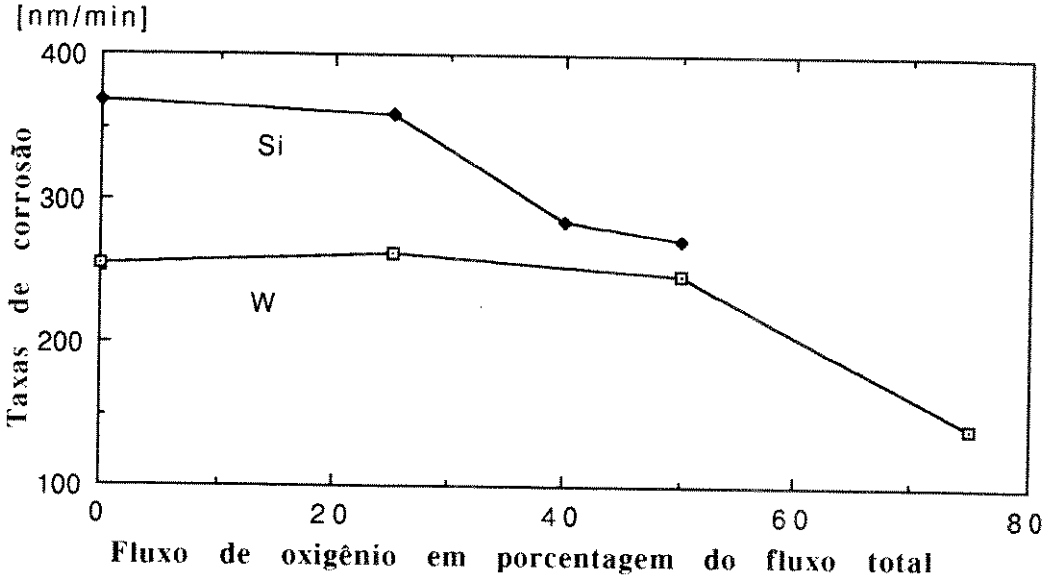

Figura 3.2 : Taxas de corrosão de tungstênio e silício policristalino em função do fluxo de oxigênio, para plasmas de NF_3-O_2 em modo RIE, a 150 mTorr e 50 W.

A taxa de corrosão não aumenta muito com o fluxo de oxigênio a baixos fluxos, contrariando o que foi reportado na literatura para CF_4 e SF_6. Este fato pode ser explicado pela grande decomposição do NF_3, pois as ligações N-F são muito menos estáveis que S-F por exemplo.
Observamos também que as taxas de corrosão sempre aumentam com o aumento de potência. Quando a pressão diminui abaixo de 100 mTorr, a taxa de corrosão diminui (veja anexo 2).
A uniformidade da corrosão de tungstênio aumenta quando diminui a pressão, mas é independente de potência ou dos fluxos dos gases.
Sobre um diâmetro de 105 mm, obtém-se valores de 96 % a 40 mTorr e 90 % a 150 mTorr. A taxa de corrosão máxima ocorre

sempre na borda da lâmina, a mínima sempre no centro : é do tipo olho de boi (bull's eye) tradicional. A uniformidade não muda muito com o tipo de máscara.
A seletividade de tungstênio para resiste e óxido de silício diminui quando aumenta a potência e/ou diminui a pressão. A 150 mTorr e 50 W, seletividade para o resiste é de 1:1 para NF_3 puro, mas diminui com fluxo de O_2. A seletividade para o óxido fica, para esta pressão e potência, ao redor de 2:1, independente dos fluxos.
O efeito de área depende muito do tipo de máscara. Com uma máscara de resiste, quase não há efeito de área : as taxas de corrosão são quase as mesmas com campo claro quanto com campo escuro. Com máscara de óxido, a taxa de corrosão com campo claro é a mesma do que com máscara de resiste, mas com campo escuro a taxa aumenta em mais de 100 %. Isto indica que há um grande efeito de área. Portanto este tipo de processo não pode ser usado para um processo de "back-etch".
O perfil da parede de tungstênio é sempre vertical, para todas as corrosões investigadas.
Quando se use uma máscara de resiste, não se observa "undercut".
Usando uma máscara de óxido PECVD, observa-se um pequeno "undercut" de aproximadamente 100 nm, como mostrado na figura 3.3. Este "undercut" já ocorre durante a corrosão, pois pode ser observado também para estruturas que não foram corroídas completamente.

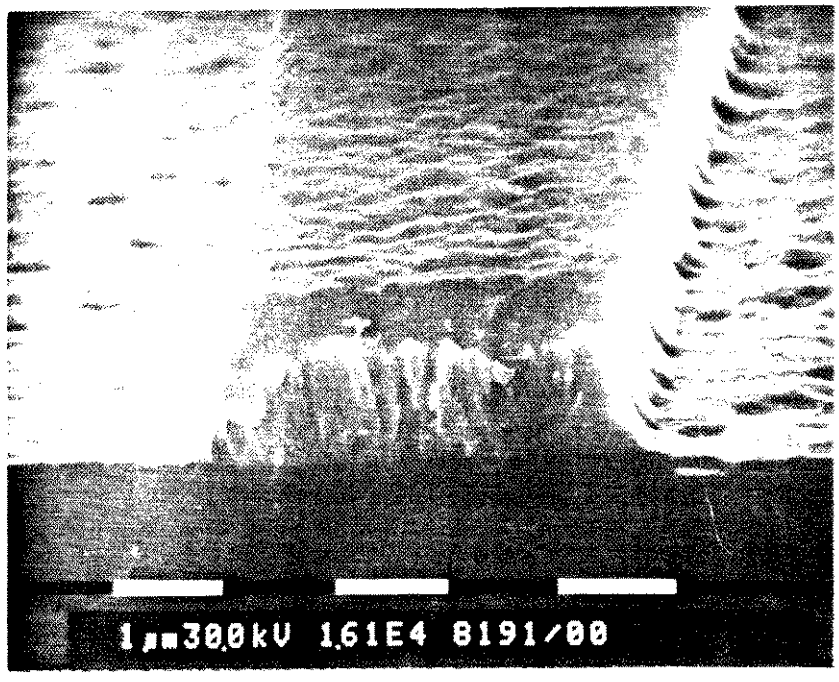

Figura 3.3 : Corrosão anisotrópica com plasma de NF_3 - O_2 em modo RIE, máscara de óxido.

O ponto final pode ser detectado pela variação das voltagens DC e AC ou por espectrometria de emissão.
A maioria dos testes foram feitas com camada intermediária de TiN. Quando o tungstênio é removido e se alcança esta camada de TiN, as voltagens AC e DC diminuem tipicamente com 10 %. No mesmo momento pode-se observar com o espectrômetro de emissão um aumento da intensidade do espectro inteiro, portanto também das linhas de Flúor (por exemplo de 704 nm) e nitrogênio (por exemplo de 334 nm). Depois da remoção da camada de TiN, a intensidade das linhas de F permanece alta enquanto que a intensidade das linhas de N diminui, como mostrado na figura 3.4.

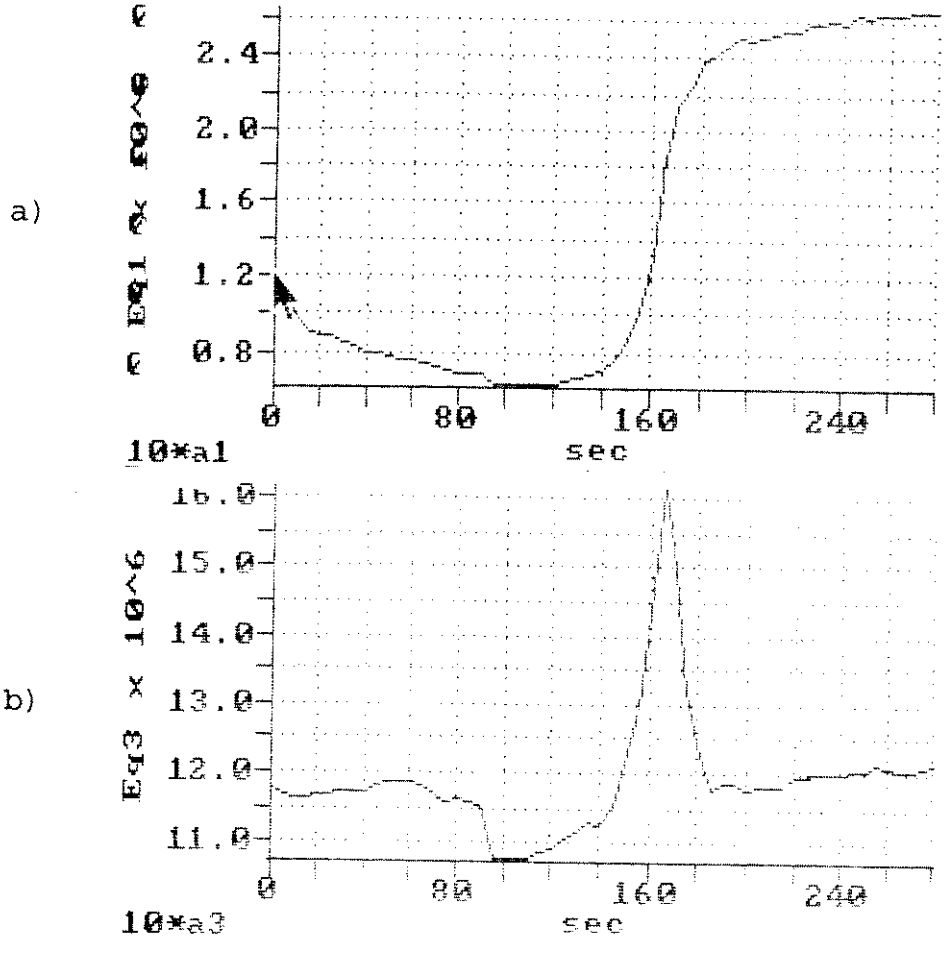

Figura 3.4 : Intensidade das linhas de a: F, 704 nm, e b: N, 334 nm, no final de uma corrosão de W e TiN.

3.1.2.3) Misturas de SF_6 e O_2 em modo RIE.

O efeito do fluxo de O_2 nas taxas de corrosão de tungstênio e de silício policristalino é mostrado na figura 3.5.

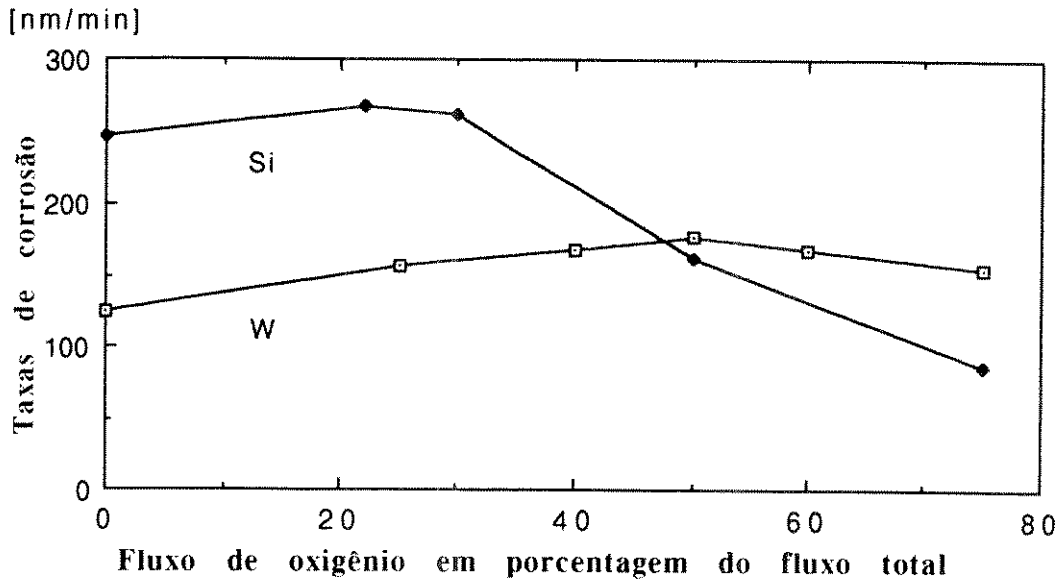

Figura 3.5 : Taxas de corrosão de tungstênio e silício policristalino em função do fluxo de oxigênio, para plasmas de SF_6-O_2, pressão de 150 mTorr, potência de 50 W em modo RIE.

A seletividade de tungstênio para resiste comporta-se como para misturas de NF_3 e O_2, mas fica tipicamente 20 % mais alta, seletividade para óxido é também de aproximadamente 2:1 e para TiW é 1:1.
Com esta mistura foram feitos vários testes para verificar se uma cura de resiste, junto com um tratamento de luz ultravioleta (um "DUV curing") aumente a seletividade. Não houve um ganho expressivo, confirmando a mesma tendência para corrosão de silício policristalino [3.2].
Também foi verificado que não era possível fazer actinometria neste equipamento, confirmando ref [3.3] que relata que actinometria não funciona bem para plasmas AF.
O ponto final da corrosão pode ser observado pela mudança de voltagens AC e DC. Também é possível seguir a intensidade da linha de F a 704 nm.
Para determinação de perfis da parede do tungstênio, foram usadas apenas máscaras de resiste. Para nenhum processo observa-se "undercut", como mostrado na figura 3.6, onde o tungstênio não foi removido completamente. Esta figura mostra bem a rugosidade do tungstênio, por causa da deposição por CVD.

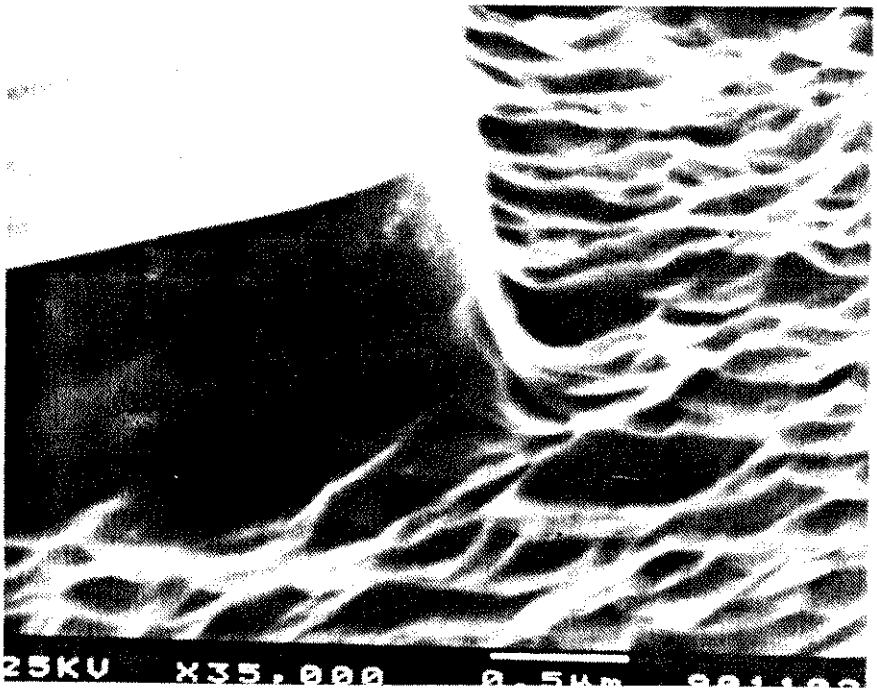

Figura 3.6 : Corrosão anisotrópica com plasma de SF_6 - O_2 em modo RIE, máscara de resiste.

Figura 3.7 mostra o resultado com um processo com SF_6 puro.

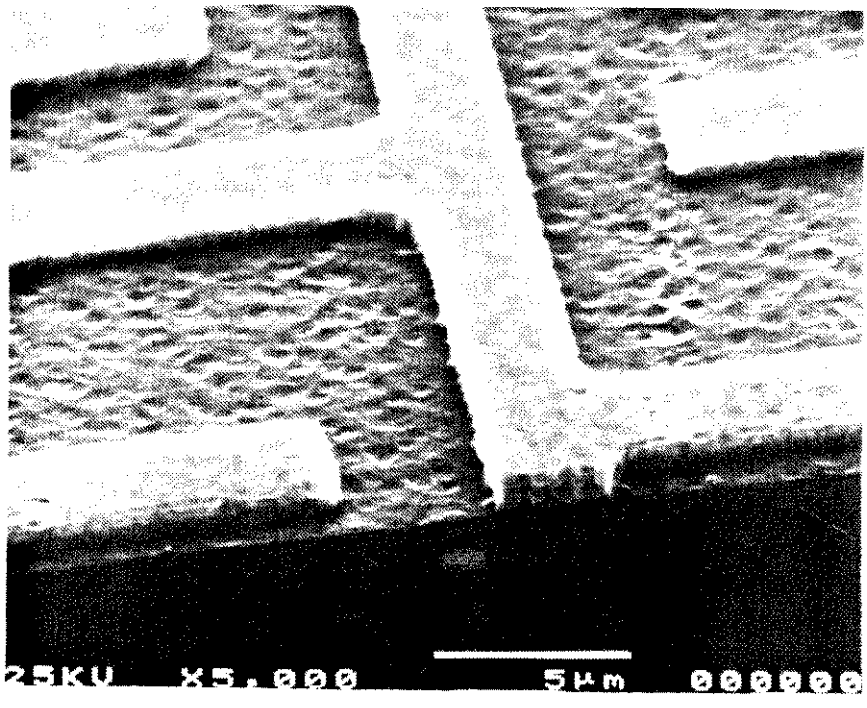

Figura 3.7 : Conjunto de linhas depois de uma corrosão anisotrópica com plasma de SF_6 - O_2 em modo RIE, máscara de resiste.

Pode-se observar que o resiste já foi removido completamente. Como a seletividade do tungstênio para o resiste é de aproximadamente 1:1, a superfície do resiste fica bem mais lisa do que a superfície do tungstênio como depositado. Como a seletividade do tungstênio para o óxido é de apenas 2:1, a rugosidade original do tungstênio foi transferida parcialmente para o óxido debaixo de tungstênio.

3.1.2.4) Misturas de NF_3-O_2 em modo PF.

Para estes plasmas deve-se fazer a distinção entre plasmas a pressões maiores que 100 mTorr e menores que 70 mTorr, A região intermediária não foi investigada.

A: Processos com pressões maiores que 100 mTorr.

O efeito do fluxo de O_2 nas taxas de corrosão de tungstênio e de silício policristalino é mostrado na figura 3.8.

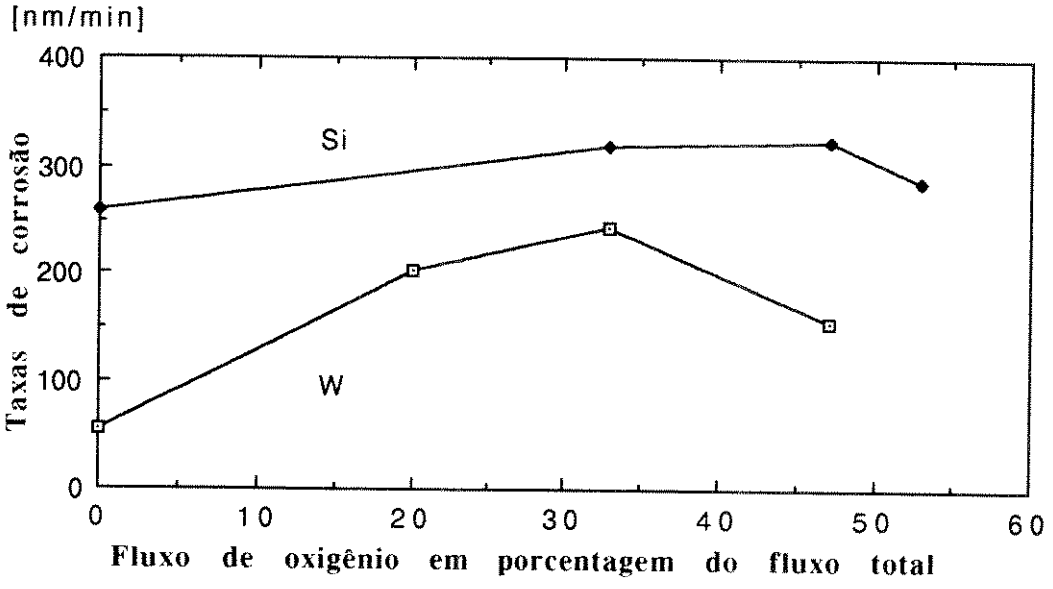

Figura 3.8 : Taxas de corrosão de tungstênio e silício policristalino em função do fluxo de oxigênio, para plasmas de NF_3-O_2, pressão de 200 mTorr, potência de 50 W em modo PF.

Verificou-se também que a presença do resiste é um fator de maior influência na taxa de corrosão.
Para uma lâmina sem resiste ou com máscara de óxido, a taxa de corrosão é sempre maior na borda da lâmina, tipicamente 15% maior do que no centro. Para lâminas com os 8 mm externos da lâmina cobertos por resiste, a taxa de corrosão perto desta área de resiste é sempre menor do que no centro, tipicamente 20 %. Neste caso, a taxa maior ocorre no meio entre o centro e a borda da lâmina. A taxa de corrosão da lâmina sem resiste é sempre maior.
Uma lâmina com 5 % de cobertura de resiste (máscara clara) tem uma taxa de corrosão (de tungstênio) 50 % maior que uma

lâmina com 95 % de cobertura (máscara escura). Este fenômeno é exatamente o inverso do que se observa em outros equipamentos (ou no modo RIE). Para uma máscara de óxido, as taxas de corrosão do tungstênio aumentam com a cobertura: de campo claro (5 % de cobertura) para campo escuro (95 % de cobertura) a taxa aumenta em 40 %. Este é um valor razoável para o uso em processos de "back-etch" [3.4].
Para uma lâmina com resiste e máscara com campo escuro a taxa de corrosão não aumenta com a potência, entretanto para uma lâmina com resiste e máscara clara a taxa de corrosão aumenta, mas menos do que em modo RIE.
Tudo isto indica que o resiste tem uma influência grande, diminuindo a taxa de corrosão.
A uniformidade dos processos é também determinada pela presença do resiste. As melhores uniformidades foram obtidas com máscara clara e remoção do resiste na borda ("edge bead removal") : 90 % é o melhor valor.
Para lâminas com um pouco ou nada de resiste, a uniformidade melhora bastante com a diminuição da pressão e um pouco com a diminuição da potência. Para lâminas sem resiste, a uniformidade melhora de 80% a 200 mTorr para 90% a 100 mTorr.
Para plasmas com fluxo de oxigênio de 5 % a 50 % do fluxo total, seletividades de tungstênio para resiste e óxido de silício são muito maiores do que em modo RIE. A seletividade aumenta com a pressão, mas é independente de potência e fluxos de gases. Para processos a 200 mTorr, as seletividades de tungstênio para resiste e óxido de silício são maiores que 10:1.
A camada de TiW é corroída com uma taxa de corrosão muito parecida com a da camada de W. A camada de TiN resiste muito bem a uma corrosão em modo PF. A seletividade de tungstênio para TiN a estas pressões é sempre superior a 10:1. Para uma pressão de 200 mTorr esta seletividade é maior que 50:1.
O perfil da parede de tungstênio depois de corrosão em modo PF é sempre isotrópico. O "undercut" depende do processo : em geral pode-se dizer que quanto maior a taxa de corrosão, maior o "undercut". Figura 3.9 mostra um perfil típico. As bolhas sobre o resiste serão discutidas mais adiante.
Quando usada uma máscara de óxido PECVD, o perfil não muda , como mostrado na figura 3.10. Não importa se a máscara seja de campo claro ou campo escuro : o "undercut" fica o mesmo.

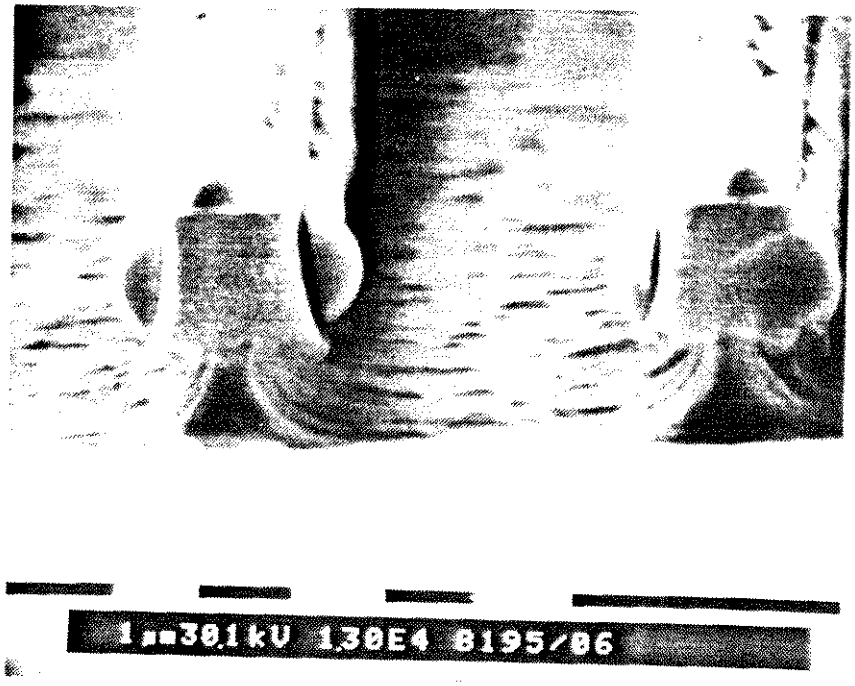

Figura 3.9 : Corrosão isotrópica com plasma de NF_3 - O_2 em modo PF, máscara de resiste.

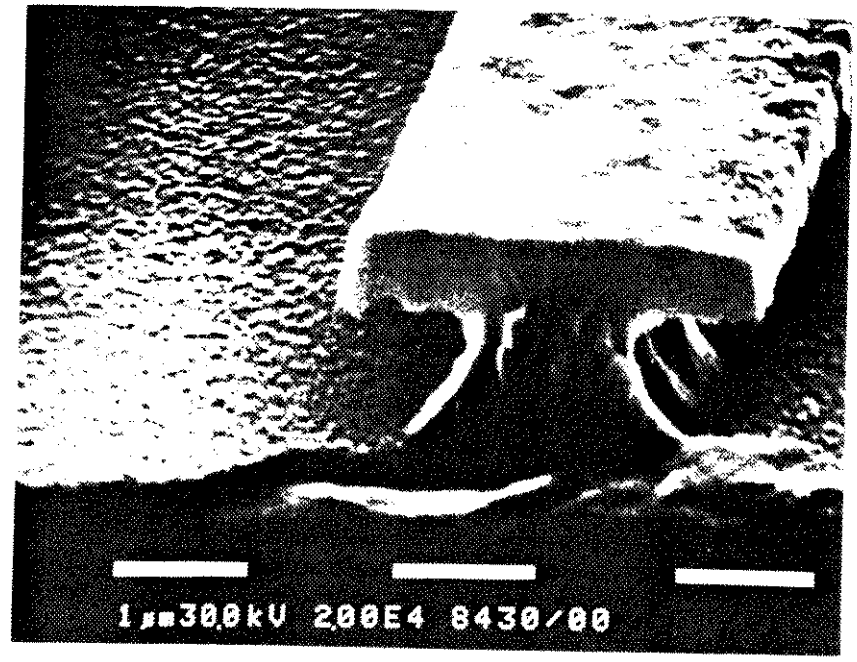

Figura 3.10 : Corrosão isotrópica com plasma de NF_3 - O_2 em modo PF, máscara de óxido.

Determinação de ponto final pode ser feito através da monitoração das voltagens DC ou AC ou através de espectrometria de emissão, observando por exemplo a linha de F a 704 nm.

Vários fenômenos estranhos ocorrem quando uma lâmina que foi exposto a estes tipos de plasma sai do reator e entra no ar:
1: forma-se uma camada colorida por cima do tungstênio;
2: formam-se bolhas por cima do resiste, como mostrado na figura 3.9 ("resist pops").
O filme colorido se forma no ar : deixando a lâmina num ambiente de nitrogênio durante 30 minutos não causa uma coloração, entrando no ar, a coloração acontece em menos que 5 segundos. Um plasma de oxigênio para remover o resiste também não causa coloração.
A formação desta camada e das bolhas pode ser evitada expondo as lâminas a um plasma do tipo RIE por alguns segundos, imediatamente antes que as lâminas saem do reator. Em alguns casos observou-se ainda bolhas nas paredes laterais do resiste, mas não na superfície superior.
Isto mostra que um processo com bastante bombardeamento remove as camadas que dão origem a estes fenômenos.
A camada colorida inibe uma corrosão posterior do tungstênio em modo PF. Esta camada pode ser removida por um plasma do tipo RIE, mas a taxa de corrosão é um fator 25 mais baixa do que do tungstênio. Depois pode-se corroer de novo o tungstênio que ficou em baixo desta camada colorida, mesmo em modo PF.
A composição da camada colorida foi investigada via análise Auger. Várias amostras foram preparadas para determinar qual o mecanismo da formação desta camada.
Houve duas cores predominantes nestas camadas : azul escuro e marrom. O azul escuro forma-se perto de grandes áreas de resiste enquanto que o marrom se forma a vários milímetros de distância de grandes áreas de resiste.
O sinal Auger de superfície é igual para as regiões das duas cores. Detectam-se os seguintes materiais : tungstênio : picos a 163, 169 e 174 eV, carbono : pico a 271 eV e oxigênio: pico a 503 eV. Não se detectou flúor ou nitrogênio. O perfil de profundidade da amostra com cor azul é mostrado na figura 3.11.
Pode-se concluir que o sinal de O cai para 50 % do valor na superfície depois de ter removido aproximadamente 25 nm de (óxido de) tungstênio. O perfil da amostra com cor marrom é similar mas o sinal de O cai mais rapidamente. O valor de 50% é alcançado depois de remover apenas 10 nm do material. Para ambas as amostras a razão O:W na superfície é de aproximadamente 3:1.
Isto mostra que a diferença nas cores é devida à diferença de espessura das camadas e não à diferença de composição.
O sinal de carbono cai imediatamente o que mostra que se trata apenas de carbono adsorvido na superfície, não de carbono ligado com tungstênio.

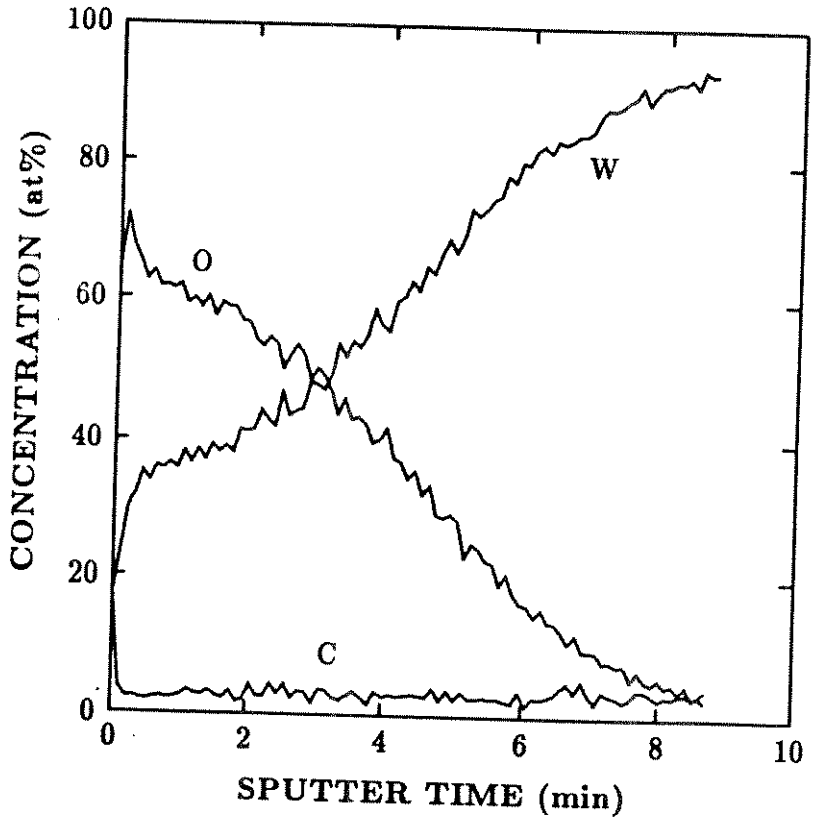

Figura 3.11 : Perfil de profundidade dos sinais Auger para a amostra com coloração azul.

Uma segunda amostra foi preparada e transportada do reator de corrosão para o espectrômetro Auger num ambiente de nitrogênio. Durante o carregamento da amostra dentro do espectrômetro, não era possível evitar totalmente o contato com o ar portanto entrou também oxigênio. O sinal diferencial da análise Auger é mostrado na figura 3.12.

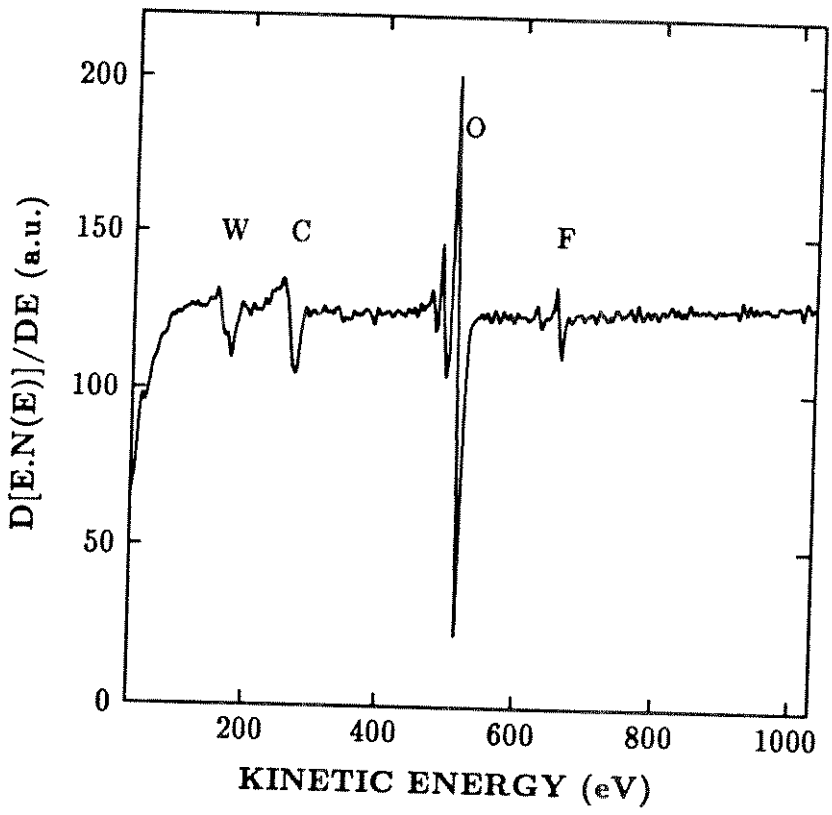

Figura 3.12 : Sinal diferencial da análise Auger para a amostra transportada em nitrogênio.

Fora dos materiais observados na amostra anterior acha-se também flúor (pico a 658 eV). O perfil de profundidade é mostrado na figura 3.13. A observação mais importante é que o sinal de F diminui da mesma maneira que o sinal de O. Isto mostra que eles estão relacionados um ao outro. O sinal de W aumenta da mesma maneira que para a amostra anterior.

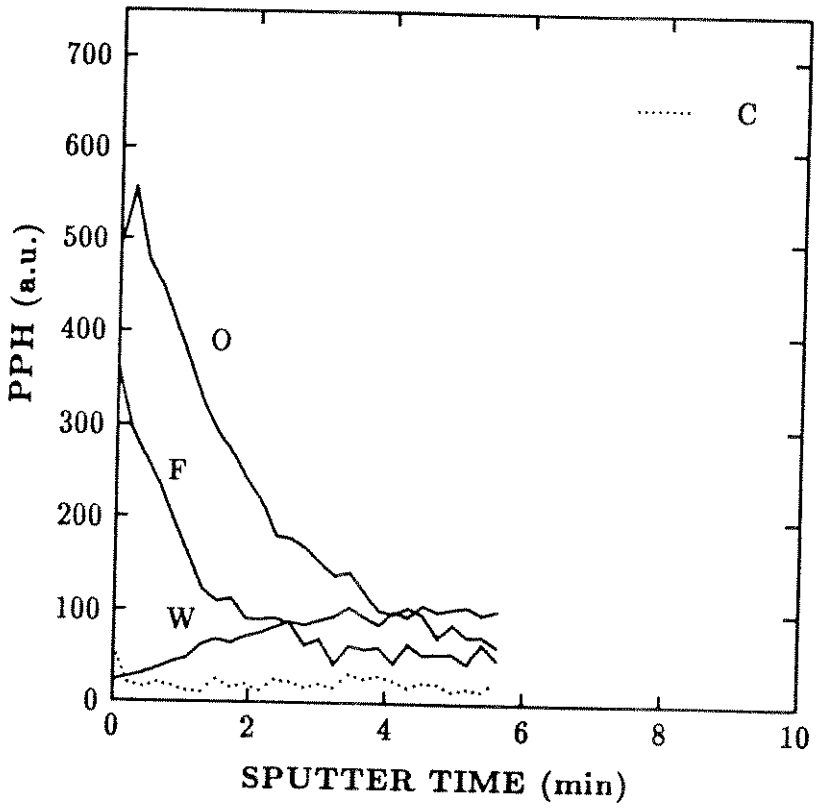

Figura 3.13 : Perfil de profundidade dos sinais Auger para a amostra transportada em nitrogênio.

Depois desta análise, foi analisada uma amostra da mesma lâmina que a amostra 2, só que esta nova amostra ficou no ar durante algumas horas. O resultado era que não houve mais flúor e que o sinal de O diminui da mesma maneira que na amostra anterior e que o sinal de W aumenta como na amostra anterior; a razão O:W é de novo 3:1.
Tudo isto indica que o F é substituído por O se deixar a amostra no ar.
Numa lâmina de referência não exposta ao plasma, acham-se W, O e C mas o C e o O desaparecem imediatamente depois de alguns segundos de sputtering. Nesta amostra a razão O:W é menor que 2:1.

B: Processos com pressões menores que 70 mTorr.

A estas pressões, o plasma comporta-se mais como um plasma do tipo RIE. Neste caso, as seletividades de tungstênio para resiste diminuem para 1:1, a uniformidade é melhor que 92 % para um diâmetro de 115 mm, não observa-se "undercut" para lâminas com resiste, não forma-se óxido de tungstênio, não observa-se bolhas no resiste. A taxa de corrosão é um fator 2 mais baixa do que para processos em modo RIE.

3.1.2.5) Misturas de SF_6-O_2 em modo PF.

Para obter taxas de corrosão da mesma ordem de grandeza do que para misturas de NF_3-O_2, a potência deve ser aumentado por um fator 3. Não se observa oxidação do tungstênio.

3.1.2.6) O processo "back-etch".

Com todos estes dados foi desenvolvido um processo de "back-etch". O processo consta de 3 etapas:
1 : 63 sccm NF_3, pressão 75 mTorr, potência : 50 W, RIE, tempo : 2 minutos.
2 : 50 sccm NF_3, 10 sccm O_2, pressão : 100 mTorr, potência : 100 W, PF, tempo determinado pelo ponto final pelo espectrômetro de emissão;
3 : 100 sccm NF_3, 20 sccm O_2, pressão : 100 mTorr, potência : 100 W, PF, tempo : tipicamente 25 % do tempo de etapa 2.

A primeira etapa serve para corroer metade da camada de tungstênio de 1 µm de espessura com um processo muito uniforme.
A segunda etapa é usado pois é um processo isotrópico e uniforme, com pequeno efeito de área.
A terceira etapa tem uma excelente seletividade de tungstênio para TiN e o efeito de área é pequeno.
O resultado final é mostrado em figura 3.14 : o "plug" ficou quase inteiro e não há mais tungstênio em cima do TiN. A superfície de TiN é muito lisa.

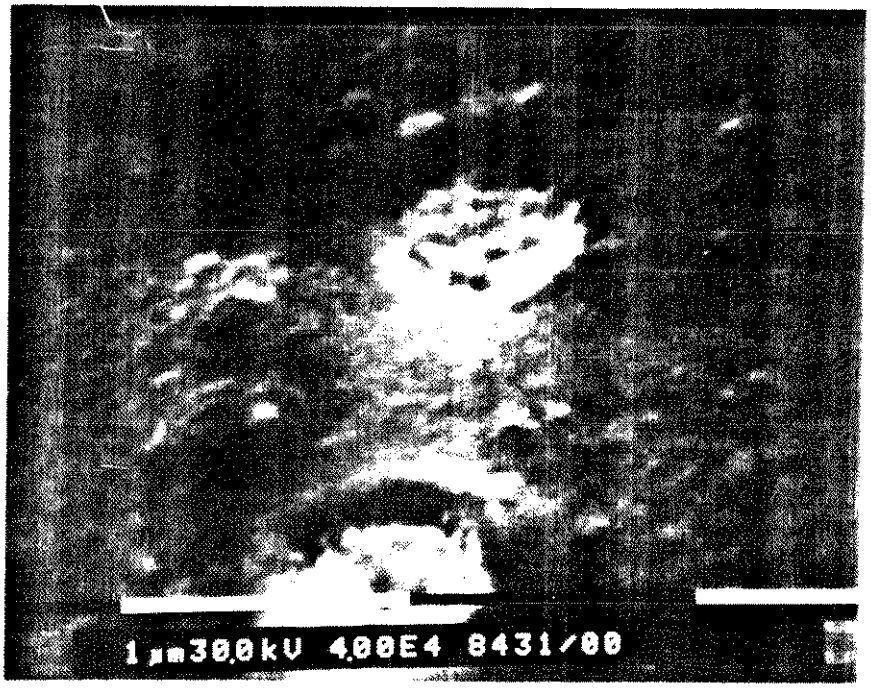

Figura 3.14 : Vista superior de um "plug" de boa qualidade.

3.1.3) Discussão sumária.

Estes resultados mostram que os processos no SWAFER têm em geral as mesmas características que os processos em equipamentos mais tradicionais, como descrito no capítulo 2. As divergências serão tratadas com mais detalhes no capítulo 4. Para estes testes foram feitas corrosões em camadas de tungstênio, depositadas em 3 diferentes tipos de equipamentos de deposição por CVD. Portanto as características observadas aqui são válidas em geral, não apenas para um determinado tipo de tungstênio. Além disso, os testes no Matrix 303, como descritos abaixo, mostram que a oxidação do tungstênio não é apenas uma característica de um equipamento, o SWAFER. Portanto pode-se dizer que é um fenômeno geral.

3.2) Processos de corrosão por plasma no Matrix 303.

3.2.1) Equipamento.

Este equipamento é um sistema de plasma remoto ou "afterglow", similar ao descrito na ref. [3.5] e mostrado na figura 3.15. A potência RF a 13,56 MHz é aplicada na parte superior do reator. A parte inferior é separada da parte superior por uma grade para impedir que a lâmina fique dentro do plasma. A temperatura do carregador da lâmina pode ser controlado até 200°C. Os gases disponíveis eram : NF_3, O_2 e He. Não houve disponibilidade de SF_6.

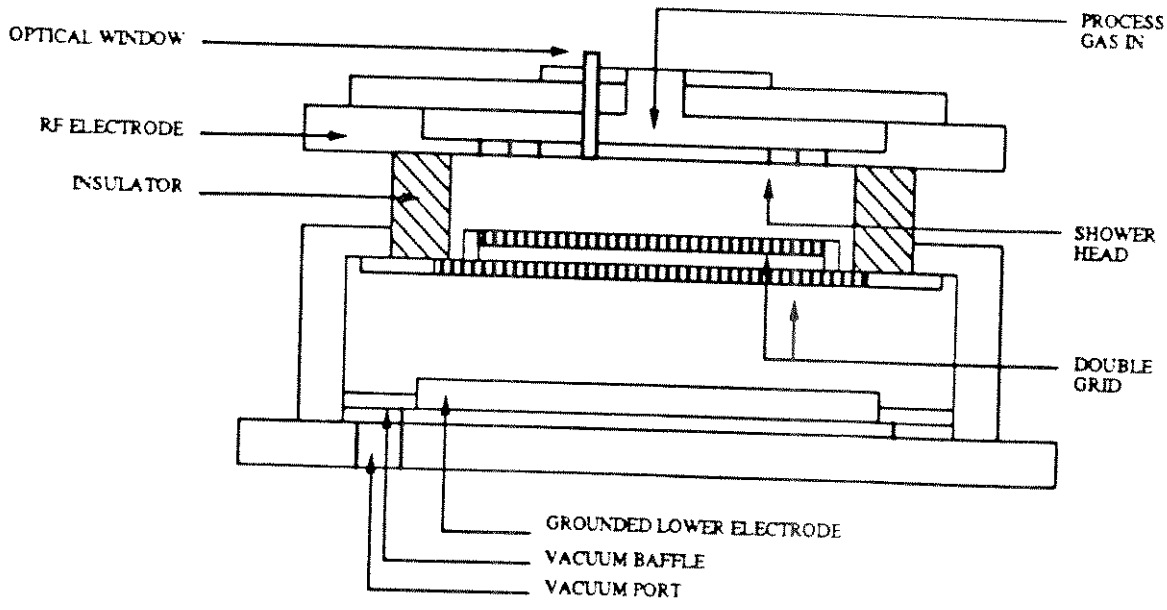

Figura 3.15 : Vista esquematizada de um reator do tipo Matrix 302 [3.5].

3.2.2) Resultados experimentais.

Sendo um sistema de plasma remoto, a corrosão é completamente química : não há bombardeamento iônico. Portanto as características dos processos devem ser um pouco similar com aquelas do SWAFER em modo PF. Testes foram feitos com NF3 para verificar se houvesse uma coloração como no SWAFER.
A lâmina foi removido do reator depois de cada 30 segundos de plasma para observar o que acontece.
Os processos são mostrados na tabela 3.1.

Tabela 3.1 : Parâmetros para os testes de coloração.

Teste nr.	Fluxo de NF_3 [sccm]	Fluxo de O_2 [sccm]	Fluxo de He [sccm]	Pressão [mTorr]	Potência [W]	Temp. [°C]
1	50	10	20	800	300	50
2	50	0	45	800	300	50
3	50	10	15	800	300	50

Observamos o seguinte :

Teste 1 : depois de 2 ciclos de 30 segundos de plasma, a coloração começa depois que a lâmina permanece 60 segundos no ar.

Teste 2 :
depois de 2 ciclos de 30 segundos de plasma, ocorre o início de coloração, localmente;
após mais 2 ciclos de 30 segundos de plasma, a borda fica completamente colorida.
Teste 3 : já há coloração depois de 30 segundos de plasma, se deixar a lâmina suficiente tempo no ar. Este fenômeno é bastante parecida ao que ocorre no teste 1.

3.2.3) Discussão.

Observamos que ocorre coloração também neste equipamento, não apenas no SWAFER. Nestes testes foi mostrado mais claramente ainda que a coloração ocorre fora do reator, no ar.
Teste 2 mostra que não é necessário ter oxigênio no plasma para ter coloração. A coloração é menos intensa, pois sem oxigênio no plasma há menos flúor atômico no plasma, portanto também na superfície da lâmina e há menos difusão para dentro do tungstênio. Esta é a razão da menor coloração.

3.3) Processos de corrosão por plasma no Tegal 15xx.

3.3.1) Equipamento.

O equipamento usado para estes testes é ainda um protótipo, embora haja uma descrição de um equipamento parecido na ref. [3.7].
A característica especial deste equipamento é que ele tem duas séries de ímãs permanentes : uma no eletrodo superior e uma na parede, como mostrado na figura 3.16. Graças a estes ímãs obtém-se um plasma muito intenso, chamado "Magnetically Confined Plasma" (MCP). Não há ímãs perto do eletrodo inferior.
O eletrodo superior é sempre aterrado.
Em modo Triodo I, a potência RF a 13,56 MHz é aplicada nas paredes do reator.
Em modo Triodo II, a potência RF a 13,56 MHz é aplicada no eletrodo inferior.
Em ambos os modos pode-se aplicar potência AF a 100 kHz no eletrodo inferior.
Quando não se aplica potência AF no eletrodo inferior no modo Triodo I, este eletrodo fica flutuante. Portanto pode ser comparado com o modo PF no SWAFER.
O controle da temperatura do eletrodo inferior é boa.
Normalmente o eletrodo era refrigerado a 20°C.
Os gases usados para estes testes foram : SF_6 e O_2.
Não houve disponibilidade de NF_3.

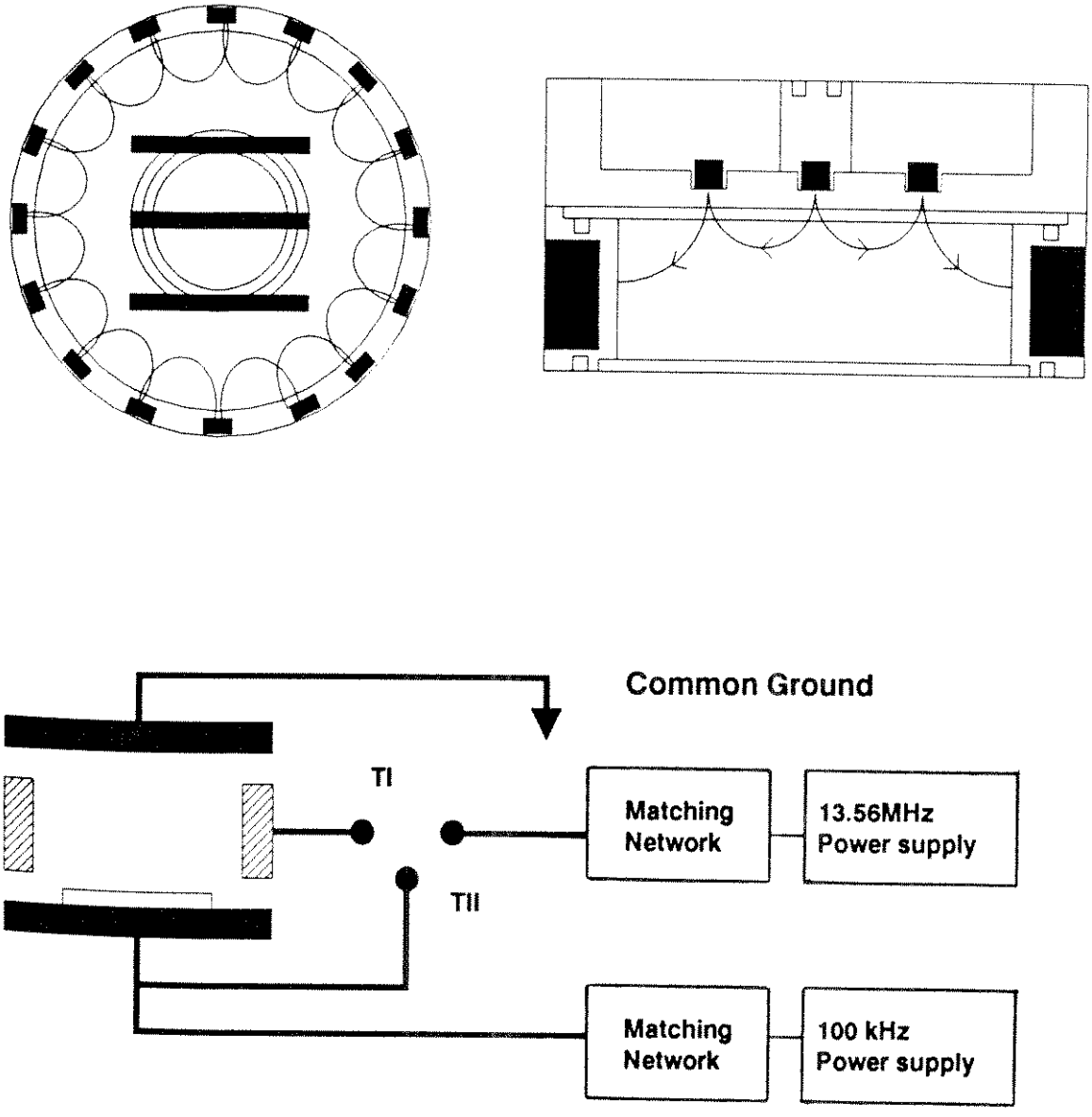

Figura 3.16 : vistas esquemáticas do reator do Tegal 15xx e dos sistemas de AF e RF [3.8].

Alguns testes foram feitos com misturas de SF_6 - Cl_2 mas os resultados não foram bons, veja anexo IV.

3.3.2) Resultados experimentais.

3.3.2.1) Objetivos - preparações.

O maior objetivo destes testes foi o desenvolvimento de um processo de "back-etch" para obter "plugs". Como este equipamento não foi caracterizado anteriormente, houve também

uma caracterização geral. Isto foi feito por actinometria e depois por corrosão de silício policristalino.

Portanto iniciamos com testes de actinometria numa grande faixa de valores dos parâmetros :
- fluxos de gases : SF_6 : 20 sccm a 80 sccm, O_2 : 0 sccm a 16 sccm;
- pressão : 10 mTorr a 25 mTorr;
- potência : a 13,56 MHz : 400 W a 700 W, em ambos os modos
  a 100 kHz : 0 W e 50 W

Usamos a técnica de projeto estatístico de experimentos para reduzir o número de testes. Alguns testes dedicados extra foram feitos para determinar certos mecanismos.
A preparação da lâminas é igual àquela para o SWAFER. Apenas usamos máscaras de resiste.

3.3.2.2) Resultados da actinometria.

Para obter os dados da tabela 3.2, medimos a intensidade das linhas de F a 704 nm e de Ar a 697 nm. O procedimento detalhado encontra-se no anexo IV.

Tabela 3.2 : Concentração de Flúor em Unidades Arbitrárias em função de vários parâmetros de processo.

Nr	Fluxos SF_6 [% de 100 sccm]	Fluxos O_2 [% de 20 sccm]	Press. [mTorr]	RF Pot. [W]	Concentração de F em [U.A.] a 0W AF TrI	0W AF TrII	50W AF TrI	50W AF TrII
1	80	80	25	750	64	50	62	45
2	80	40	18	575	54	36	59	32
3	80	0	25	400	53	28	48	27
4	20	80	10	750	18	19	17	19
5	20	40	18	575	35	24	40	22
6	20	0	25	400	64	30	52	39
7	80	0	10	750	46	25	51	20
8	20	0	10	750	25	25	22	22
9	20	80	25	750	26	34	26	30
10	50	40	18	575	33	37	34	29
11	20	80	10	400	16	14	16	13
12	80	0	10	400	40	17	34	17
13	50	0	18	575	47	31	41	26
14	50	80	18	575	40	30	47	26
15	50	40	18	575	35	29	35	30
16	50	40	18	400	39	26	35	26
17	20	0	10	400	25	22	23	22
18	50	40	10	575	24	18	26	19
19	80	80	10	400	27	17	33	17
20	50	40	18	750	37	38	33	35
21	20	0	25	750	56	65	51	54
22	20	80	25	400	55	40	51	38
23	50	40	25	575	52	40	44	41
24	80	80	10	750	34	21	42	20
25	80	80	25	400	66	37	52	39
26	80	0	25	750	83	50	84	41

As tendências gerais são as seguintes :
1) Quase não há diferença entre 0 W AF e 50 W AF.
2) Para esta faixa de potência RF, a concentração de F não muda com potência.
3) No modo Triodo I gera-se mais F do que em modo Triodo II.
4) A concentração de F aumenta com a pressão.
5) A influência dos fluxos de SF_6 e O_2 dependem do tipo de plasma e das faixas dos próprios fluxos. Em geral observa-se o mesmo fenômeno descrito no capítulo 2: a baixos fluxos de O_2 a concentração de F aumenta com o fluxo de O_2, por causa da maior decomposição de SF_6, até chegar a um máximo. Depois a concentração diminui por causa da diluição.
Para fluxos baixos de SF_6 este fenômeno não foi observado, mas sim para fluxos maiores. A razão é que um plasma MCP é muito mais eficiente que um plasma comum, portanto consegue decompor o SF_6 muito bem mesmo sem a ajuda de O_2.

3.3.2.3) Corrosão de silício policristalino e de tungstênio.

Na literatura encontram-se muitos dados sobre corrosão de silício policristalino e também comparações entre corrosão de silício policristalino e tungstênio. Portanto fizemos testes com estes dois materiais para determinar melhor os mecanismos.
Como os testes de actinometria indicaram que a potência RF e AF não influenciaram muito a concentração de flúor, fixamos ambas no valor mais baixo, respectivamente 400 W e 0 W. Nestes valores mais baixos, as seletividades são melhores. Usamos de novo a técnica de projeto estatístico. Os resultados são mostrados na tabela 3.3.

Tabela 3.3 : Taxa de corrosão de silício policristalino em função de vários parâmetros de processo.

Nr	fluxo de SF_6 [% de 100 sccm]	fluxo de O_2 [% de 20 sccm]	Pressão [mTorr]	Taxas de corrosão TrI [nm/min]	TrII [nm/min]
1	50	40	25	1169	802
2	20	0	25	592	476
3	50	40	10	1133	748
4	20	0	10	638	471
5	20	80	25	554	504
6	20	40	18	687	542
7	50	40	18	1201	802
8	20	80	10	574	445
9	50	80	18	1145	798
10	80	40	18	1402	927
11	50	0	18	1069	750
12	80	0	10	1362	811
13	80	80	10	1375	853
14	80	0	25	1250	803
15	50	40	18	1269	782
16	80	80	25	1540	904

As tendências gerais são os seguintes:
1) em modo Triodo I, o silício policristalino corrói mais rapidamente que em Triodo II;
2) a pressão não é importante para a taxa média da corrosão, mas é para a uniformidade. Em Triodo II a uniformidade diminui de 0.90 para 0.70 quando aumentamos a pressão de 10 para 25 mTorr. Os resultados para Triodo I são similares;
3) o fator mais importante para o aumento da taxa de corrosão é o fluxo de SF_6. A taxa de corrosão aumenta mais com o aumento de fluxo de SF_6 a baixos fluxos de SF_6;
4) a baixos fluxos de O_2 a taxa de corrosão aumenta com o fluxo de O2; a altos fluxos, a taxa diminui.

Alguns resultados são discutidos em mais detalhes aqui, veja também anexo IV.
As tendências gerais da taxa de corrosão em função dos vários parâmetros de processo para Triodo I são mostrados na figura 3.17.

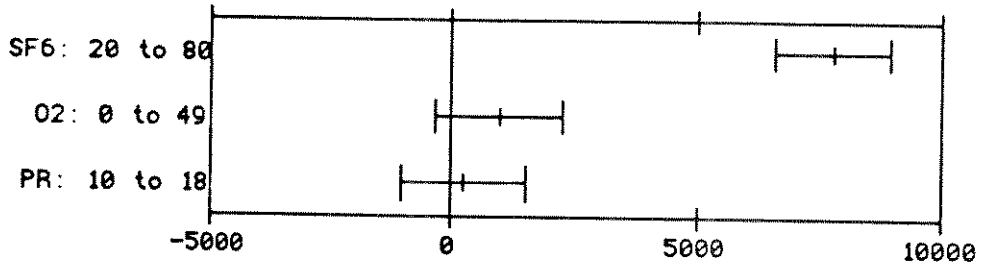

Figura 3.17 : Tendências gerais da taxa de corrosão de silício policristalino em função dos vários parâmetros de processo, para Triodo I. A abcissa indica o aumento da taxa de corrosão em Å/min; um valor negativo significa uma diminuição.

O fator dominante é o fluxo de SF_6 : aumento de 20 sccm para 80 sccm aumenta em mais de 100 % a taxa de corrosão. Nem o fluxo de oxigênio, nem a pressão influenciam muito a taxa de corrosão.
Mas a pressão influencia muito na uniformidade: a uniformidade aumenta em média de 0.50 a 25 mTorr para 0.73 a 10 mTorr.

As tendências gerais da taxa de corrosão em função dos vários parâmetros de processo para Triodo II são mostrados na figura 3.18.
Também neste modo, o fator mais importante é o fluxo de SF_6 : aumento de 20 sccm para 80 sccm aumenta em mais de 100 % a taxa de corrosão. A baixos fluxos de oxigênio, a taxa aumenta um pouco com o fluxo de oxigênio. A baixas pressões, a taxa aumenta um pouco com a pressão.

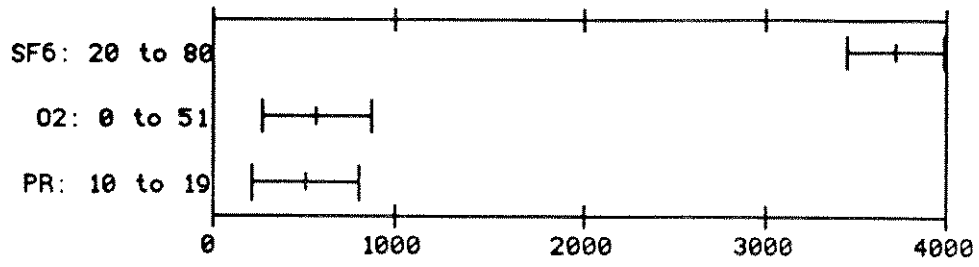

Figura 3.18 : Tendências gerais da taxa de corrosão de silício policristalino em função dos vários parâmetros de processo, para Triodo II. A abcissa indica o aumento da taxa de corrosão em Å/min.

Usamos a técnica de projeto estatístico também para a corrosão de tungstênio. O objetivo principal era de obter um processo "back-etch". Isto significa um processo com boa uniformidade, pequeno efeito de área e boa seletividade para a camada inferior. Por causa das primeiras 2 exigências usamos um processo em Triodo II : outros testes mostraram que neste modo o efeito de área é menor que em Triodo I. Testes com o silício policristalino mostraram que a uniformidade é também maior para Triodo II. A potência RF foi fixado em 400 W e a AF em 0 W, pelas mesmas razões que para o silício policristalino. Os resultados dos testes são mostrados na tabela 3.4.
Usamos os seguintes símbolos :
r_{cLF} : taxa de corrosão de tungstênio no centro de uma lâmina com máscara campo claro, em [nm/min]
r_{bLF} : taxa de corrosão de tungstênio na borda de uma lâmina com máscara campo claro, em [nm/min]
U_{LF} : uniformidade para uma lâmina com máscara campo claro, em [%]
r_{cDF} : taxa de corrosão de tungstênio no centro de uma lâmina com máscara campo escuro, em [nm/min]
r_{bDF} : taxa de corrosão de tungstênio na borda de uma lâmina com máscara campo escuro, em [nm/min]
U_{DF} : uniformidade para uma lâmina com máscara campo escuro, em [%]
LE_C : efeito de área no centro da lâmina, definido como o quociente da taxa de corrosão da lâmina com máscara campo claro pela taxa de corrosão da lâmina com máscara campo escuro, no centro da lâmina.
LE_b : efeito de área na borda da lâmina, definido como o quociente da taxa de corrosão da lâmina com máscara campo

claro pela taxa de corrosão da lâmina com máscara campo escuro, na borda da lâmina.

Tabela 3.4 : taxas de corrosão, uniformidades e efeitos de área em função de vários parâmetros de process para plasmas de SF_6 - O_2 em modo Triode II.

Nr	Fluxos SF_6 sccm	O_2 sccm	Press mTorr	r_{cLF} nm min	r_{bLF} nm min	U_{LF} %	r_{cDF} nm min	r_{bDF} nm min	U_{DF} %	LE_c %	LE_b %
1	80	80	25	542	623	87	736	808	91	74	77
2	20	80	10	386	381	99	557	575	97	69	66
3	80	80	10	525	559	94	652	651	99	81	86
4	20	0	10	304	327	93	462	506	91	66	65
5	80	0	25	467	537	87	668	737	91	70	73
6	80	0	10	495	544	91	632	646	98	78	84
7	50	40	18	469	521	90	740	767	96	63	68
8	50	40	18	487	524	93	733	775	94	67	68
9	20	80	25	442	451	98	738	772	96	60	58
10	80	0	25	278	305	91	475	534	89	59	57

As tendências gerais para estes processos são :

1) lâminas com máscara campo escuro sempre têm taxa de corrosão maior que lâminas com máscara campo claro;
2) a taxa de corrosão é (quase) sempre maior na borda da lâmina que no centro da lâmina;
3) a uniformidade em geral é maior para lâminas com máscara campo escuro do que para lâminas com máscara campo claro
4) a taxa de corrosão é principalmente determinada pelo fluxo de SF_6: quanto maior o fluxo, maior a taxa de corrosão;
5) a uniformidade aumenta com : diminuição de pressão, diminuição de fluxo de SF_6, aumento de fluxo de O_2; mas é sempre muito elevado;
6) O efeito de área melhora com o aumento de fluxo de SF_6 e a diminuição da pressão, enquanto o efeito do fluxo de O_2 é desprezível.
Um valor de LE de 0.81 no centro e de 0.86 na borda é muito bom. Além disso, a uniformidade deste processo é bom com um valor de 94%.

Analisamos 2 respostas com um pouco mais detalhes : a taxa de corrosão e o efeito de área no centro da lâmina.

As tendências gerais da taxa de corrosão no centro da lâmina, com máscara LF, em função dos vários parâmetros de processo são mostrados na figura 3.19.
O fator determinante para a taxa de corrosão é de novo o fluxo de SF_6 : aumentando este fluxo aumenta-se a taxa de corrosão. O fluxo de oxigênio aumenta a taxa de corrosão na mesma maneira, mas menos pronunciado. A influência da pressão é desprezível.

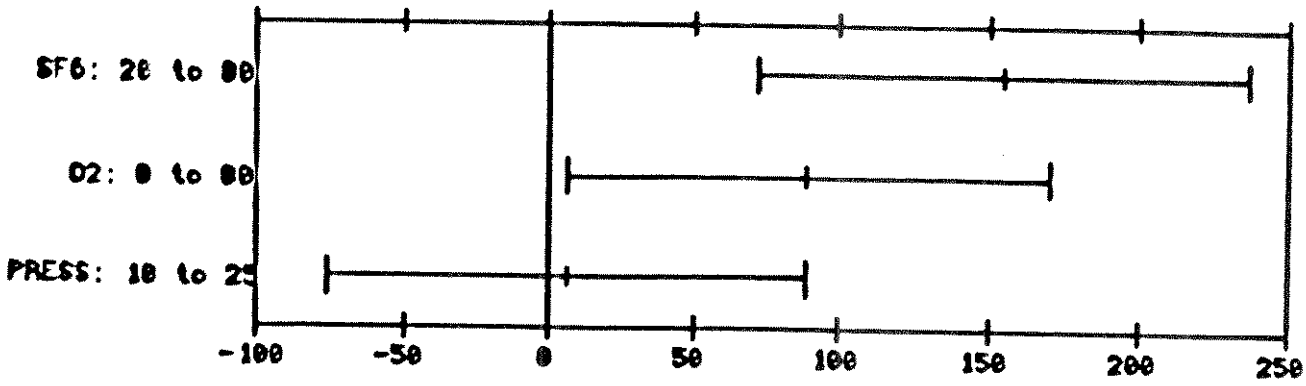

Figura 3.19 : Tendências gerais da taxa de corrosão em função dos vários parâmetros de processo. A abcissa indica o aumento da taxa de corrosão em nm/min; um valor negativo significa uma diminuição.

As tendências gerais para o efeito de área no centro da lâmina são mostrados na figura 3.20.

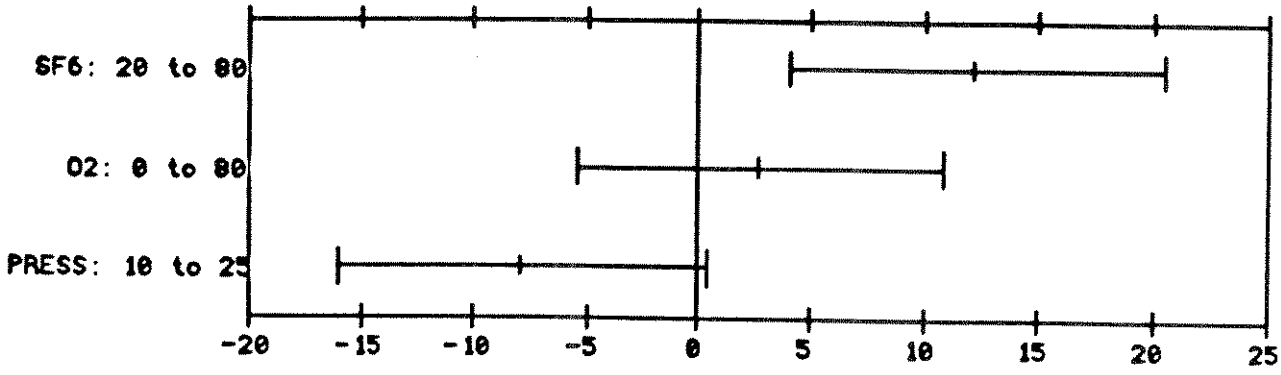

Figura 3.20 : Tendências gerais para o efeito de área no centro da lâmina; a abcissa indica a melhoria em porcento.

O fator mais importante é o fluxo de SF_6. Um aumento de 20 sccm para 80 sccm, melhora o efeito de área em 12 % (absoluto). A pressão também é importante : a diminuição de 25 mTorr para 10 mTorr causa um melhoramento de 8 %. A influência do fluxo de oxigênio não é importante.
Todos os resultados da tabela 3.4 são comentados no anexo IV.

A maior conclusão destes testes é :
o melhor processo, com a configuração atual do equipamento, para fazer "back-etch" para formar os "plugs" é o seguinte : fluxos : 80 sccm de SF_6, 16 sccm de O_2, pressão : 10 mTorr , potências : 400 W RF e 0 W AF, modo Triodo II.

Este processo tem uma taxa de corrosão de 530 nm/min, uniformidade de 94 % e uma diferença em taxas de corrosão entre campo claro e campo escuro menor que 20 %.

Além destes testes fizemos mais outros testes, principalmente para determinar mecanismos de corrosão por plasma de tungstênio.
Primeiramente fizemos vários testes em modo Triodo I. Os resultados são mostrados na tabela 3.5. As potências foram sempre : 400 W RF e 0 W AF.

Tabela 3.5 : taxas de corrosão e uniformidades de silício policristalino e tungstênio para vários parâmetros de processo em modo Triodo I.

Nr	Fluxo SF_6 [sccm]	Fluxo O_2 [sccm]	Pressão [mTorr]	Taxa Si [nm/min]	Uniform. Si [%]	Taxa W [nm/min]	Uniform. W [%]
1	96	0	10	1440	71	564	86
2	90	6	10	1482	69		
3	80	16	10	1374	74	752	88
4	70	26	10	1355	73	724	87
5	48	48	10	679	61	683	84
6	48	0	10	1109	73		
7	96	33	10	1349	72		
8	50	8	25	1169	54		
9	50	8	10	1133	76		
10	50	8	18	1201	69		
11	50	16	18	1145	70		
12	50	0	18	1069	68		

Os testes 1 até 7 mostram claramente a tendência tradicional da influência de oxigênio nas taxas de corrosão : a baixos fluxos a taxa aumenta, pois aumenta a concentração do flúor atômico, a altos fluxos a taxa diminui, pois há competição entre o O e o F para fazer ligações com o Si e há diluição, o que resulta em menor concentração de F atômico.. Estes fenômenos serão comentados em mais detalhes no capítulo 4.
Testes 10, 11 e 12 mostram o mesmo, para fluxos mais baixos.
A figura 3.21 mostra as taxas de corrosão em função do fluxo de oxigênio.
As tendências das corrosões de tungstênio são muito parecidas com as da corrosão no SWAFER em modo PF. As concordâncias mais importantes são :
- a taxa de corrosão mais baixa ocorre com 0 % de fluxo de oxigênio; mesmo quando metade do fluxo total é de oxigênio, a taxa fica muito alta;
- a seletividade de tungstênio para resiste não diminui com o aumento de fluxo de oxigênio; a seletividade é mais baixa quando não há oxigênio no plasma.

Há uma diferença no fato que no Tegal 15xx a taxa de corrosão do silício policristalino começa diminuir para fluxos muito pequenos de oxigênio, enquanto que a taxa de corrosão de tungstênio começa a diminuir a um fluxo maior. O inverso ocorre no SWAFER. Este fenômeno será comentado no capítulo 4.

A influência da pressão é confirmada para silício policristalino nos testes 8, 9, 10. A pressão não influencia muito na taxa de corrosão mas muito na uniformidade : a uniformidade é maior com a pressão menor. Este resultado é válido para ambos os materiais, pois todos os testes mostram este mesmo resultado.

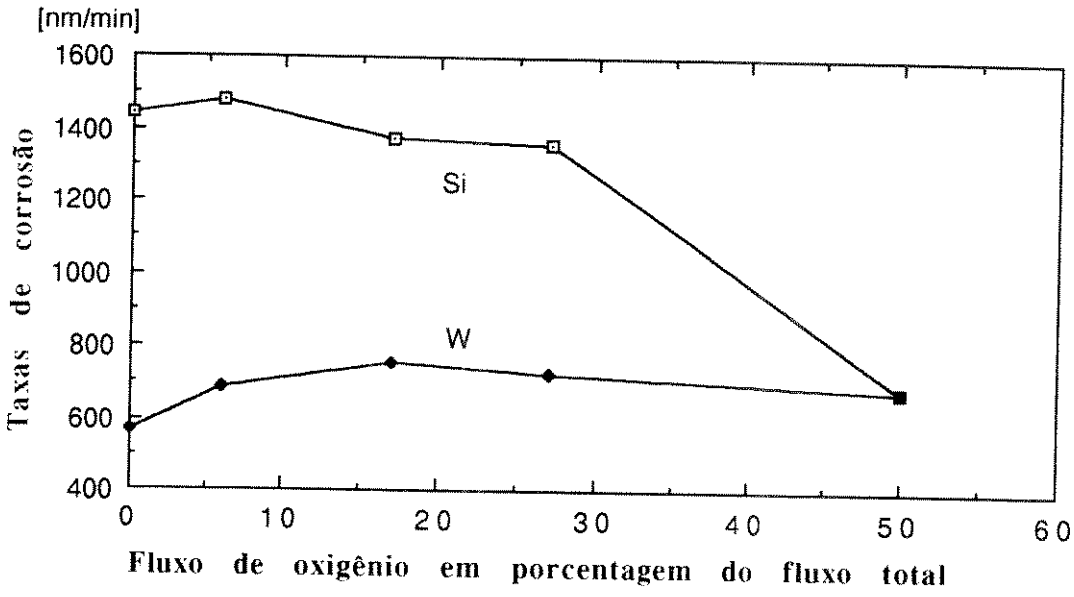

Figura 3.21 : Taxas de corrosão de silício policristalino e tungstênio em função do fluxo de oxigênio, em modo Triodo I, para 10 mTorr e 400 W de RF.

Os seguintes 3 testes mostram que a influência da potência na taxa de corrosão de silício policristalino é tão pouca como indicado pelos testes de actinometria.
Os fluxos eram para os 3 testes : 20 sccm de SF_6, 0 sccm de O_2; pressão : 10 mTorr:
1) 400 W RF, 0 W AF : r = 638 nm/min, U = 0.73
2) 600 W RF, 0 W AF : r = 750 nm/min, U = 0.77
3) 400 W RF,50 W AF : r = 702 nm/min, U = 0.82

Portanto um aumento de potência RF de 50% resulta num aumento de taxa de corrosão de menos de 20%. Isto é muito menos do que para processos tradicionais. A razão principal é que a decomposição da molécula de SF_6 já é bastante completa a 400W.
Colocando 50 W de AF extra resulta num aumento de taxa de corrosão de apenas 10 %. O que mostra que a influência da potência AF também não é importante, nem para processos em Triodo I. Portanto podemos concluir que para Triodo II também não é importante, uma vez que este já tem uma polarização aplicada ao seu eletrodo inferior.

Fizemos vários testes similares em modo Triodo II. Os principais resultados são mostrados na tabela 3.6. As potências foram sempre : 400 W RF e 0 W AF.

Tabela 3.6 : taxas de corrosão e uniformidades de silício policristalino e tungstênio para vários parâmetros de processo em modo Triodo II.

Nr	Fluxo de SF_6 [sccm]	Fluxo de O_2 [sccm]	Pressão [mTorr]	Taxa-Si [nm/min]	Taxa-W [nm/min]	Unif.W [%]
1	96	0	10	881	488	96
2	90	6	10	909	484	93
3	80	16	10	853	470	88
4	70	26	10	830	467	92
5	48	48	10	425		

A figura 3.22 mostra as taxas de corrosão em função do fluxo de oxigênio.

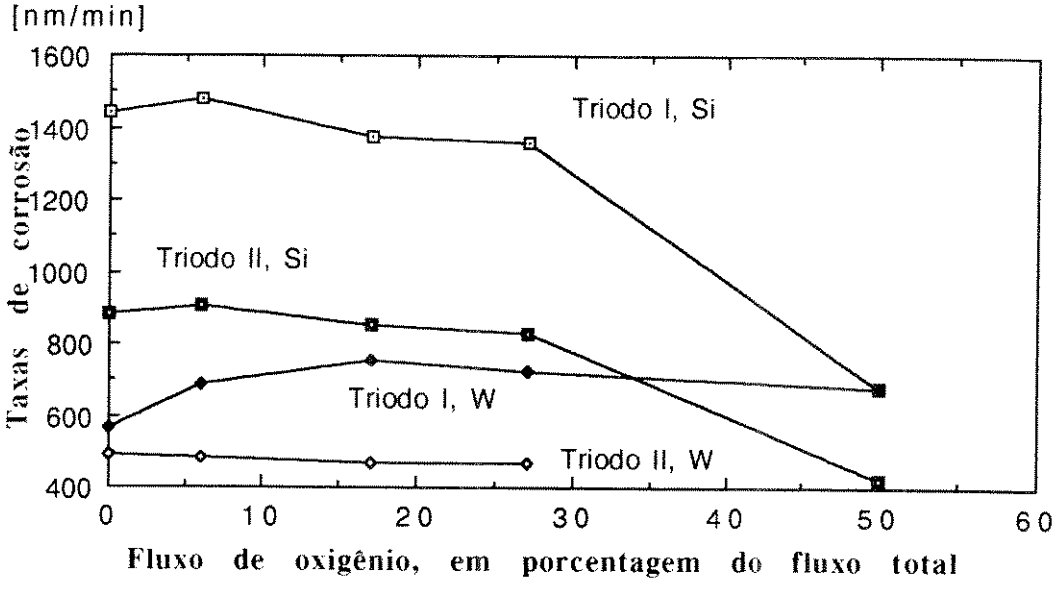

Figura 3.22 : Taxas de corrosão de silício policristalino e tungstênio em função do fluxo de oxigênio, em Triodo II e Triodo I.

Esta figura mostra as seguintes tendências para o modo Triodo II :
- a taxa de corrosão do tungstênio não e influenciada muito pelo fluxo de oxigênio, pelo menos não até 26 % do fluxo total. Este comportamento é muito parecido ao do SWAFER com NF_3 no modo RIE. No outro lado, a influência do fluxo de oxigênio na taxa de corrosão é tradicional, com a mesma explicação que para Triodo I;
- as taxas de corrosão (de W e de Si) são mais baixas que em modo Triodo I;
- a uniformidade é maior que em Triodo I;
- a taxa de corrosão do resiste é muito maior que em modo Triodo I.

A figura 3.20 mostra também taxas de corrosão em modo Triodo I para facilitar as comparações.

Alguns testes para investigar a influência da pressão deram o mesmo resultado de sempre : a pressão quase não influencia a taxa de corrosão, mas sim a uniformidade : quando menor a pressão, maior a uniformidade.
Apesar que os modos Triodo I e II são bem diferentes um do outro, os resultados, principalmente para o silício policristalino, têm tendências muito parecidas. Isto indica que os mesmos mecanismos determinam a corrosão nos dois modos.

3.3.3) Discussão sumária.

O comportamento da concentração de flúor atômico e das taxas de corrosão já foi comentado suficientemente. Mas há outros aspectos que merecem mais atenção.

3.3.3.1) A relação uniformidade - pressão.

Todos os testes mostram que com o aumento da pressão, diminui a uniformidade. Este fato pode ser explicado através do coeficiente de difusão. Sabe-se que a difusão é inversamente proporcional à pressão [3.7], como mostra também a formula (4.3) do capítulo 4. Portanto a pressões baixas o F atômico pode-se espalhar muito mais facilmente, assim aumentando a uniformidade.

3.3.3.2) Comparação dos resultados de actinometria com corrosão de silício policristalino.

A: Concordâncias.

1) As potências AF e RF influenciam muito pouco. A razão é que este MCP dissocia muito bem a molécula de SF_6. Portanto potência extra não dissocia mais.
2) As influências do fluxo de oxigênio também são as mesmas.

B: Paradoxos.

1) A concentração de F é proporcional com a pressão enquanto que a taxa de corrosão é independente dela. Este pode ser de novo explicado pelo coeficiente de difusão, que é inversamente proporcional com a pressão. A quantidade de flúor que chega na superfície da lâmina é função da concentração de flúor, mas também da difusão, como será mostrado no capítulo 4. Portanto os dois efeitos se cancelam, deixando a taxa de corrosão independente da pressão.
2) A influência do fluxo de SF_6 é predominante para a taxa de corrosão, mas pouco importante na concentração de flúor.
A corrosão é um processo dinâmico onde há consumo de flúor e precisa-se continuamente de novas moléculas de SF_6. A medida de concentração de flúor é um processo menos dinâmico, portanto o fluxo tem menos importância que a pressão.

3.3.3.3) Comparação dos resultados de corrosão de silício policristalino com corrosão de tungstênio.

Em geral a concordância entre as duas corrosões é grande :
- o fator dominante para a taxa de corrosão é o fluxo de SF_6;
- o fluxo de oxigênio é muito menos importante nos dois casos. As diferenças podem ser explicadas através da formação de WOF_4, como comentado no capítulo 2;
- a pressão não influencia a taxa de corrosão, mas sim a uniformidade : para os dois casos : quando maior a pressão, menor a uniformidade.

Referências :

[3.1] G. Brasseur, P. Bruneel, C. Jehoul, J. Vandersmissen, "Audio Frequency Plasma Generation Reactor Configuration for Dry Etch Processing", Proceedings of Microcircuit Engineering 90 eds. Coopmans, Van den hove, Declerck (1990).
[3.2] J. Vandersmissen, "Characterization of polysilicon and nitride processes in the SWAFER", internal Cobrain report, 1991.
[3.3] A. Richards, B. Thompsom K. Allen, H. Sawin, "Atomic Chlorine Concentration Measurements in a Plasma Etching Reactor", J. Appl. Phys. 62, 792 (1987)
[3.4] J. Berthold, C. Wieczorek, "CVD-W deposition and dry etch processes for planarized metallization and tungsten interconnect techniques", Proceedings of the European Workshop on Refractory Metals and Silicides, eds. De Keersmaecker, Maex, pp 506-516 (1989)
[3.5] W. Ostrout, S. Hunkler, S. Ward,"Enhanced Process Control of Submicron Contact Definition", Proceedings of SPIE, Vol 1392, eds. Bondur, Turner (1991), 151.
[3.6] Matrix Inc. : Operation and maintenance manual of the Matrix 302
[3.7] P. Laporte, L. Van den hove, Y. Melaku, "Dry Etching for sylilated resist development", Proceedings of the SPIE vol. 1392, eds. Bondur, Turner, 196 (1990)
[3.8] Tegal Corp. : Tegal 15xx : Operation and Maintenance Manual
[3.9] R.C. Reid, T.K. Sherwood, "The properties of gases and liquids", second edition, Mc.Graw - Hill, 1966

Capítulo 4 : Mecanismos de corrosão de tungstênio por plasma.

Introdução :

Capítulo 2 descreve os mecanismos gerais de corrosão por plasma, que são bem conhecidos e descritos na literatura. Modelamento de corrosão por plasma é muito mais difícil, pois é muito difícil quantizar os diferentes fenômenos que acontecem dentro do plasma e na interface lâmina - plasma. Neste capítulo usaremos os conhecimentos obtidos nos capítulos anteriores para fazer algumas análises quantitativas, determinar quais as etapas que limitam a taxa de corrosão e introduzir alguns mecanismos novos para corrosão de tungstênio.
O capítulo foi dividido em duas partes:

1: Cálculos básicos para a verificação de modelos de corrosão por plasma.

2: Modelamento qualitativo : Corrosão química versus corrosão induzida por bombardeamento e a influência de óxido de tungstênio.

4.1) Cálculos básicos para a verificação de modelos de corrosão por plasma, aplicado a corrosão de tungstênio.

O processo de corrosão por plasma pode ser dividido em vários subprocessos ou etapas. Pode-se distinguir as seguintes etapas:
- o plasma gera espécies reativas, para nosso caso flúor atômico, F.
- a espécies reativa chega no filme de tungstênio
- o reagente é absorvido na superfície
- forma-se uma ligação W-F : quimissorção
- outros átomos de flúor reagem com o átomo de W para formar um produto volátil, tipicamente WF_6
- o produto volátil dessorve e sai do reator para a bomba.

Como constantes físicas e químicas temos :
a : para tungstênio:
densidade ρ : 19.35 kg/dm^3 = 19.35 g/cm^3
peso atômico M: 184 g/mole
reação de corrosão: $W + 6\ F \rightarrow WF_6$
b : para silício:
densidade ρ = 2.33 kg/dm^3 = 2.33 g/cm^3
peso atômico M: 28 g/mole
reação de corrosão: $Si + 4\ F \rightarrow SiF_4$

No anexo I mostra-se que é possível calcular o consumo de F, J_F, através da seguinte fórmula (para uma lâmina sem máscara):

$J_F = 22400 \cdot \pi \cdot (d/2)^2 \cdot r \cdot \rho \cdot X / M$ (4.1)

com:

J_F : fluxo de átomos consumidos em [sccm]

d : diâmetro da lâmina em [cm]

r : taxa de corrosão em [cm/min] (em [nm/min] divida por 10^7)

ρ : densidade do material do filme em [kg/dm^3]

X : coeficiente da reação : Mat + X Hal -> $MatHal_X$

M : peso atômico do material do filme em [g/mol]

O fluxo J_F é proporcional à taxa de corrosão. Para lâminas de 125 mm, por nm/min de taxa de corrosão de tungstênio, consome-se um fluxo de F de 0,173 sccm e libera-se um fluxo de WF_6 de 0,029 sccm. Para silício, o consumo de F é de 0,092 sccm com liberação de SiF_4 de 0,023 sccm por nm/min, para o mesmo tipo de lâminas.

4.1.1) Geração de espécies reativas.

Como mostrado no capítulo 2, a geração de espécies reativas é muito difícil quantizar. Em seção 4.1.2 combinaremos a geração com a difusão e assim será possível obter dados quantitativos.

4.1.2) Fluxo de espécies reativas que chegam na superfície.

Para determinar o subprocesso que limita a taxa de corrosão é necessário saber o fluxo de espécies reativas que chegam na superfície. Este fluxo é determinado pela combinação de 2 mecanismos :

1: a geração de átomos de flúor dentro do plasma

2: o transporte destes átomos para a superfície da lâmina.

Em geral a fonte de flúor será depletada. O caso de uma fonte infinita de F é tratado em anexo V.

Durante a corrosão há consumo de flúor. Portanto cria-se um gradiente de átomos de F. Por difusão o F de dentro do reator pode chegar até a superfície da lâmina, como descrito pela equação (4.2).

$J = - A D dC/dx$ (4.2)

Com :

J : fluxo de espécies indo do plasma para a superfície em número de espécies por segundo [1/s]

A : área da lâmina em [cm^2]

D : constante de difusão em [cm^2/s]

dC/dx : gradiente da concentração de átomos de F em [$1/cm^4$]

A seguinte fórmula é utilizada para determinar a constante de difusão para gases binárias a baixa pressão [4.1]

$$D_{12} = 0.001858\ T^{3/2}\ [(M_1 + M_2)/M_1\ M_2]^{1/2}\ p\ \sigma_{12}^2\ \Omega_D \quad (4.3)$$

Com :
D_{12} : constante de difusão em [cm^2/s]
T : temperatura absoluta em [K]
M_1 , M_2 : pesos moleculares em [mol/g]
p : pressão em [atmosferas]
σ_{12} : a constante de força de Lennard-Jones que pode ser determinada através de fórmulas e tabelas na ref. [4.1]
Ω_D : o potencial de Lennard-Jones que pode ser determinada através de fórmulas e tabelas na ref. [4.1]

Para os cálculos abaixo, D é determinada para 2 exemplos: F em NF_3 a 200 mTorr e F em SF_6 a 10 mtorr, ambos a 20°C;
para exemplo 1: $\sigma_{12}^2 = 3.67$, $\Omega_D = 1.07$, D = 636 cm^2/s
para exemplo 2: $\sigma_{12}^2 = 4.14$, $\Omega_D = 1.105$, D = 9129 cm^2/s .
Para exemplo 2, D é muito maior pois a pressão é 20 vezes menor.
É muito mais difícil determinar o gradiente da concentração do F. A chegada de espécies reativas é a etapa que limita a taxa de corrosão se na superfície da lâmina a concentração de F for zero ou seja, se o F for imediatamente adsorvida/quimisorvida. A concentração de flúor dentro do plasma, C_F, é desconhecido em geral. Para determina-la é possível fazer medidas qualitativas, mas medidas quantitativas são extremamente difíceis, até impossíveis para a maioria dos reatores. Para uma primeira aproximação pode-se assumir que a concentração de flúor aumenta linearmente da superfície da lâmina em direção ao corpo do plasma, até uma certa distancia x_S dentro do plasma. Portanto dentro desta parte do plasma, que chamaremos de agora "a faixa depletada (ou a faixa) de plasma", o gradiente da concentração é constante. Portanto a concentração de flúor nesta faixa é exatamente a metade do que seria se não houvesse o gradiente, se não houvesse consumo de F, como mostra a figura 4.1.
Fora da faixa, a concentração C_F é constante, o gradiente é zero.
Portanto para este caso, a equação (4.2) é :

$$J_F = D\ A\ C_F/x_S \quad (4.4)$$

Para cada molécula mãe que entra no reator, (em nossos casos NF_3 ou SF_6), uma média de G átomos de F são gerados pelo plasma. Portanto a concentração de F é um fator G/(G+1) da concentração de todas as espécies, n, assumindo zero recombinação.

$$C_F = n\ (\ G/G+1\ ) \quad (4.5)$$

A densidade n é completamente determinada pela pressão do plasma.

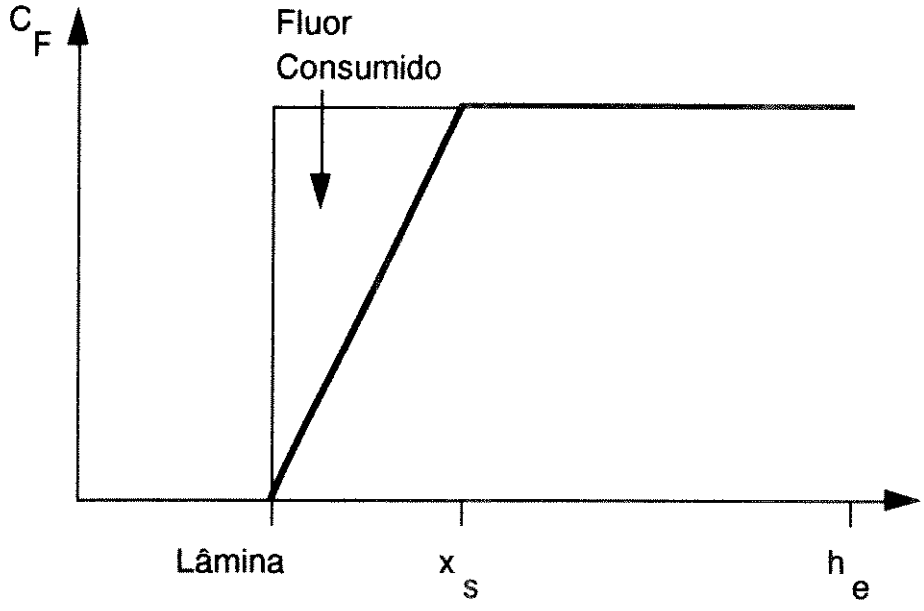

Figura 4.1 : Perfil de concentração de flúor no reator.

Para calcular a distancia x_S dentro do plasma, assume-se o seguinte :

1) o fluxo dos gases usados é homogêneo entre os dois eletrodos (assumindo um sistema de placas paralelas);
2) flúor atômico é consumido apenas dentro da faixa depletada, fora dele não há consumo. Esta hipótese é compatível com a hipótese que o gradiente fora da faixa seja zero. Se não houvesse um gradiente na faixa, não haveria difusão. Se os resultados dos cálculos a seguir forem compatíveis com as observações, consideraremos que o modelo linear do gradiente seja adequado.
O conteúdo total de F atômico por unidade de área na faixa é: $0.5\ C_F\ x_S$: metade do F é consumido, metade fica, como mostrado na figura 4.1 : o triângulo superior representa o flúor consumido.
3) De cada molécula mãe o plasma gera G átomos de F em média. Nos reatores comerciais, a pressão é regulado através de uma válvula automática, portanto no momento da geração do plasma a pressão fica constante, mas o fluxo de espécies aumenta. Com o plasma ligado o fluxo de espécies é um fator G+1 maior que o fluxo de entrada de moléculas mãe, f, enquanto que o fluxo de flúor é G f.

Como mostrado acima, é possível calcular o fluxo de F consumido, J_F, conhecendo a taxa de corrosão e as características da lâmina. Este fluxo é exatamente o fluxo de F que vem da faixa depletada.

Combinando hipóteses 1 e 3, pode-se concluir que se não houvesse consumo de F, o fluxo de F por unidade de distancia entre os eletrodos seria uma constante: $G\ f\ /\ h_e$
com : h_e a distancia entre os eletrodos.
O fluxo de F consumido, J_F, é metade do fluxo que passaria na faixa depletada com espessura x_S se não houvesse consumo de flúor livre.

$$J_F = 0.5\ G\ f\ x_S\ /\ h_e \qquad (4.6)$$

portanto :

$$x_S = 2\ J_F\ h_e\ /\ [G\ f] \qquad (4.7)$$

Temos 2 equações (4.4) e (4.6), com apenas x_S e G desconhecido. Combinando equações (4.4) e (4.5) :

$$J_F = A\ D\ n\ G\ /\ [(G+1)\ x_S]$$

Combinando com (4.7):

$$x_S = [\ A\ D\ n\ 2h_e\ /\ [(G+1)\ f]]^{1/2} \qquad (4.8)$$

Substituindo x_S em (4.5) :

$$G^2\ A\ D\ n\ f\ -\ G\ 2\ J_F^2\ h_e\ -\ 2\ J_F^2\ h_e = 0$$

portanto

$$G = (2J_F^2\ h_e + [4J_F^4\ h_e^2 + 8A\ D\ n\ f\ J_F^2\ h_e]^{1/2})/[2\ A\ D\ n\ f] \qquad (4.9)$$

Estas fórmulas são válidas para qualquer sistema de plasma para o qual as hipóteses acima sejam válidas.
Para ilustrar melhor a importância destas fórmulas, calculamos aqui 2 exemplos.
O primeiro exemplo sai da seção 3.1.2 : corrosão no SWAFER com o seguinte processo: 100 sccm de NF_3, pressão de 200 mTorr, potência AF de 50 W, o que resulta numa taxa de corrosão de 200 nm/min.
Pode-se calcular, através de fórmula (4.1) que o fluxo de F consumido é 34,7 sccm ou $9{,}323\ 10^{20}$ átomos por minuto : este é o fluxo J_F que deve chegar na superfície. Pode-se calcular que há $0{,}660\ 10^{16}$ espécies/cc a 200 mTorr e 20°C [4.2].
A distancia entre os dois eletrodos do SWAFER é 5 cm. A área de uma lâmina de 125 mm é 123 cm^2. A constante de difusão foi calculada acima. Os fluxos devem ser expressos em espécies por segundo :

$f = 4{,}48\ 10^{19}$ moléculas/s
$J_F = 1{,}55\ 10^{19}$ átomos/s

Substituindo estes valores nas equações (4.8) e (4.9) resulta em :

G = 0,378
x_S = 9,15 cm

O fato que x_S calculado ser maior que a distancia entre os eletrodos significa que a difusão não é a etapa limitante e sim a geração de espécies reativas. A difusão só seria a etapa limitante se a distancia x_S fosse menor que a distancia entre os eletrodos.
O segundo exemplo sai da seção 3.3.2 : corrosão no Tegal 15xx com o seguinte processo : fluxo de 80 sccm de SF_6, pressão de 10 mTorr, 400 W de potência RF em modo Triodo I, resultando numa taxa de corrosão de 750 nm/min.
A distancia entre eletrodo inferior e superior, he, é 10 cm. Pode-se calcular que há 0,033 10^{16} espécies/cc a 10 mTorr e 20°C [4.2]. O coeficiente de difusão foi calculado acima. Para este exemplo os fluxos são os seguintes :

f = 3,59 10^{19} moléculas/s
J_F = 5,81 10^{19} átomos/s

Isto resulta em :

G = 5,93
x_S = 5,76 cm

Este resultado significa que a taxa de corrosão é limitada pela combinação dos subprocessos, geração e difusão : se a geração de F fosse maior, C_F aumentaria, portanto J_F aumentaria, se a difusão fosse mais rápida, a taxa de corrosão também aumentaria : átomos de uma distancia maior também participariam da corrosão.
Pode-se observar que a taxa de geração é muito alto : quase todas as moléculas de SF_6 que entram, são completamente decompostas.
É muito difícil determinar os valores de C_F e x_S através de experimentos. Medidas de LIF podem dar indicações, mas para isso precisa-se de acesso a feixe de laser a várias alturas do reator. Portanto um projeto particular de janelas deve ser feito, o que não está disponível para sistemas comerciais.

4.1.3) Adsorção e quimissorção.

Neste capítulo não dedicamos muita atenção a estes subprocessos, pois achamos que eles não limitam a taxa de corrosão, o que será demostrado mais abaixo. Portanto a descrição no capítulo 2 é suficientemente adequada.

4.1.4) Formação do produto volátil.

Como no caso da quimisorção, a descrição como dado no capítulo 2 é suficiente, pois esta etapa também não limita a taxa de corrosão, em geral.

4.1.5) Dessorção

O produto volátil que no caso de tungstênio é WF_6, tem que sair da superfície. Este processo pode ser descrito pela equação (4.10) [4.3].

$$\tau = \tau_O \exp (Q/RT_S) \qquad (4.10)$$

Com τ_O: período de vibração : tipicamente 10^{-13} s
T_S : temperatura da superfície em [K]
R : constante universal: 8.31 J/mol K
Q : energia de ativação em [J/mol]
τ : tempo de residência de uma molécula adsorvida em [s]

Q pode ser determinado através de testes dedicados de dessorção programado de temperatura ("Temperature Programmed Desorption" (TPD)) [4.4]
Pode-se calcular que o pico gama, mostrado na figura 4.2 representa uma energia de ativação de 41 kJ/mol.

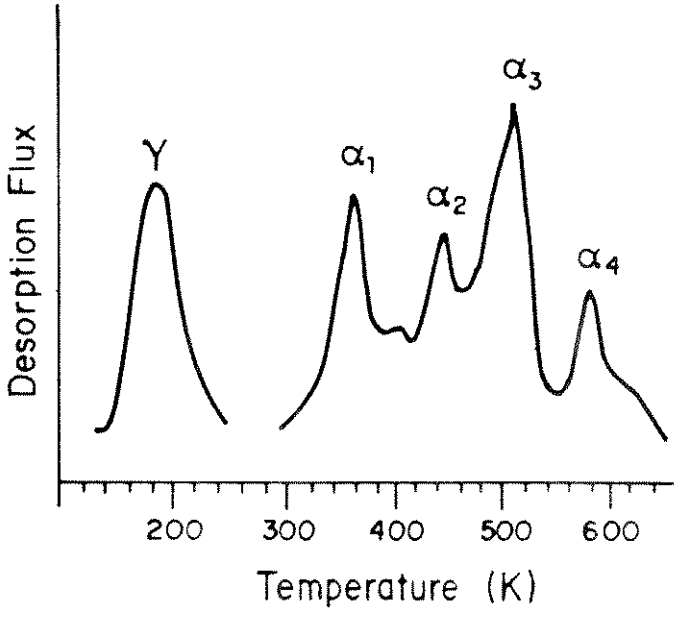

Figura 4.2 : fluxos de dessorção de WF_6 em função da temperatura em testes TPD [4.4].

Usando equação (4.10) a 300 K :
$\tau = 10^{-13} \exp (41000/8.31 \times 300) = 1.44\ 10^{-6}$ s
Uma monocamada de W consiste de aproximadamente 10^{15} átomo por cm^2 [4.5].
Portanto é possível calcular o número de moléculas dessorvidas por segundo por cm^2 , se dessorção fosse a etapa limitante :

$N_S = 10^{15} / 1.44\ 10^{-6} = 6.97\ 10^{20}$ moléculas/s cm^2.

Para uma lâmina de 125 mm, este é o equivalente de um fluxo de WF_6, se a cobertura fosse de 100% :
$f = 123 \times 60 \times N_S = 5.13\ 10^{24}$ moléculas/min = 191000 sccm .
Portanto dessorção de WF_6 do pico gama não limita a taxa de corrosão. Para os picos alfa, veja anexo V.

4.1.6) Conclusão.

Introduzimos um modelo simples que permite fazer alguns cálculos para determinar a geração de flúor atômico e sua difusão para a lâmina. Como será mostrado na seção seguinte, a chegada de F é em geral a etapa que limita a taxa de corrosão. Este novo modelo ajuda na determinação se a geração ou a difusão for a etapa limitante.

4.2) Modelamento qualitativo : corrosão química versus corrosão induzida por bombardeamento e a influência de óxido de tungstênio.

Como comentado no capítulo 2, há declarações contrárias na literatura sobre os seguintes dois itens :
- corrosão química de tungstênio é possível, e como é acelerada por bombardeamento iônico;
- a formação de óxido de tungstênio inibe a corrosão de tungstênio.
Para determinar qual mecanismo é válido, pelo menos nos sistemas usados neste trabalho, foram feitos os testes descritos no capítulo 3.

4.2.1) Corrosão química contra corrosão induzida por bombardeamento iônico.

Num sistema de corrosão tipo "afterglow", a corrosão é certamente puramente química, mas em sistemas onde a lâmina está num ambiente de plasma, sempre se forma uma bainha e acontece um pouco de bombardeamento. A voltagem sobre a bainha pode ser minimizada deixando a lâmina num potencial flutuante. Se a lâmina fica num eletrodo, este eletrodo deve ser deixado num potencial flutuante, portanto deve existir uma impedância grande entre o eletrodo e a terra.

4.2.1.1) Corrosão no SWAFER.

4.2.1.1.1) Plasmas de SF_6.

Em mode RIE, as características da corrosão como descritas no capítulo 3 e ref. [4.6] são as seguintes :
- alta taxa de corrosão para os filmes de tungstênio, silício policristalino, resiste, nitreto e óxido de silício, com baixa seletividade do tungstênio para resiste e óxido;
- paredes verticais para tungstênio, silício policristalino e nitreto de silício.
Estas características mostram que há bastante bombardeamento iônico, como esperado em modo RIE com a potência aplicada a 25 kHz.
Em modo PF, as taxas de corrosão são extremamente baixas, para todos os filmes. Ref. [4.6] menciona que taxas de corrosão de silício policristalino são um fator 3 mais baixas que em RIE, com 50 W de potência. Para este material foi observado um efeito de área muito grande: uma lâmina com resiste corrói 50% mais rapidamente que uma lâmina sem resiste. Há "undercut" para filmes de silício policristalino e nitreto : os processos são puramente isotrópicos.
A taxa de corrosão de tungstênio é tão baixa que não foram feitos muitos testes.
A conclusão geral é que neste equipamento silício policristalino e tungstênio corrõem por um processo químico mas com taxas muito baixas.

4.2.1.1.2) Plasmas de NF_3.

Em modo RIE, os resultados são similares aos dos processos com SF_6 :
- as taxas de corrosão são em geral maiores que para SF_6, mas as seletividades são da mesma ordem de grandeza, em geral um pouco menor que para SF_6;
- os perfis das paredes também são verticais, tanto para tungstênio com máscara de resiste que com máscara de óxido PECVD. Não houve "undercut" com máscara de resiste. Houve "undercut" de 100 nm com uma máscara de óxido. Isto indica que há corrosão química, mas muito pouco;
- Ref. [4.6] relata tendências similares para corrosão de silício policristalino e nitreto.
Isto mostra que corrosão em modo RIE com plasmas de NF_3 é induzida por bombardeamento iônico.
Em modo PF, os resultados são muito diferentes dos resultados com plasmas de SF_6. A taxa de corrosão de um plasma de NF_3 é um fator 20 maior que a taxa de corrosão com SF_6, com uma potência de 50 W. Para silício policristalino este fator é 5. Taxas de corrosão são em geral 50 % mais baixas que em modo RIE, mas este fator depende muito dos parâmetros do processo. É necessário distinguir processos com pressão maior que 100 mTorr e menor que 70 mTorr (a região intermediária não foi investigada).

Para processos com pressão maior que 100 mTorr, as características gerais são :
- "altas" taxas de corrosão para tungstênio, silício policristalino e nitreto. Taxas muito mais baixas para resiste e óxido. Isto resulta em boas seletividades. Seletividade de tungstênio para TiN também é excelente;
- os processos são puramente isotrópicos para tungstênio, silício policristalino e nitreto. "Undercut" de tungstênio não depende se a máscara é de resiste ou de óxido. "Undercut" não para no tempo, é possível de tirar vários micrometros de tungstênio debaixo da máscara. Isto é a melhor prova que corrosão de tungstênio não precisa de bombardeamento iônico!
Todas estas características mostram que a corrosão é puramente química. Portanto podemos concluir que é possível ter uma corrosão puramente química de tungstênio, se houver suficiente flúor atômico, como comentado mais adiante.
O efeito de área destes plasmas tem um comportamento estranho: para lâminas cobertas com resiste, a taxa de corrosão do tungstênio diminui com a cobertura do resiste. Para lâminas cobertas com óxido, a taxa aumenta com a cobertura. Este fenômeno será comentado em mais detalhes mais adiante.
Para processos com pressões mais baixas que 70 mTorr, as características são muito diferentes :
- a taxa de corrosão do resiste aumenta muito : a seletividade do tungstênio para o resiste diminui até aproximadamente 1:1;
- não observa-se "undercut" para camadas de tungstênio, cobertas com resiste.
Além disso há mais 2 características que são mais comum para modo RIE : alta uniformidade e ausência de bolhas no resiste. Estas características indicam que estes plasmas se comportam com bastante similaridade aos plasmas em modo RIE.
Em geral observa-se que quanto maior a pressão, maior o comportamento químico de plasmas em modo PF.

4.2.1.2) Corrosão no Tegal 15xx

Somente plasmas de SF_6 foram investigados, pois não houve disponibilidade de NF_3 neste equipamento.
O modo Triodo I é muito parecido com o modo PF no SWAFER, se não for aplicado potência AF. Portanto é de se esperar que as características sejam similares :
- taxas de corrosão de tungstênio e silício policristalino são altas, enquanto as taxas de corrosão de resiste são baixas, resultando em boas seletividades;
- há "undercut" para processos de tungstênio e silício policristalino.
Estas características indicam que a corrosão é química.
Quando aplicado uma potência AF no eletrodo inferior, mesmo que seja apenas 10 W, as características mudam completamente : paredes verticais podem ser obtidos em silício e tungstênio e a taxa de corrosão do resiste aumenta bastante.

Em modo Triodo II, a configuração é tipicamente RIE. As características dos processos são :
- as taxas de corrosão para tungstênio e silício policristalino ainda são altas, mas mais baixas do que em Triodo I. As taxas de corrosão de resiste são maiores, as seletividades são muito menores que em Triodo I;
- paredes verticais.
Isto mostra que a corrosão é induzida por bombardeamento iônico.

4.2.1.3) Conclusões gerais

É possível corroer tungstênio induzido por bombardeamento iônico, mas também por via química, se houver suficiente flúor atômico disponível. Até é possível dentro do mesmo equipamento, no caso um Tegal 15xx, obter taxas maiores de corrosão química do que por corrosão induzida por plasma, ambos para tungstênio e para silício policristalino.

4.2.2) Determinação da etapa limitante da corrosão.

O último comentário na seção anterior é uma forte indicação que a taxa de corrosão é principalmente limitada pela chegada de espécies ativas.
Comparando as taxas de corrosão e o consumo de flúor de processos de corrosão de tungstênio com de processos de corrosão de silício policristalino podemos tirar conclusões mais exatas.
Nesta seção explicamos também o papel de oxigênio nestes plasmas.

4.2.2.1) O papel de oxigênio nos processos no SWAFER.

4.2.2.1.1) Plasmas de SF_6.

Para estes plasmas só foi investigado o modo RIE.
A influência do oxigênio na taxa de corrosão é mostrado na figura 4.3. Esta influência é a mesma do que relatada na literatura para plasmas de 13,56 MHz e descrita no capítulo II e anexo V.

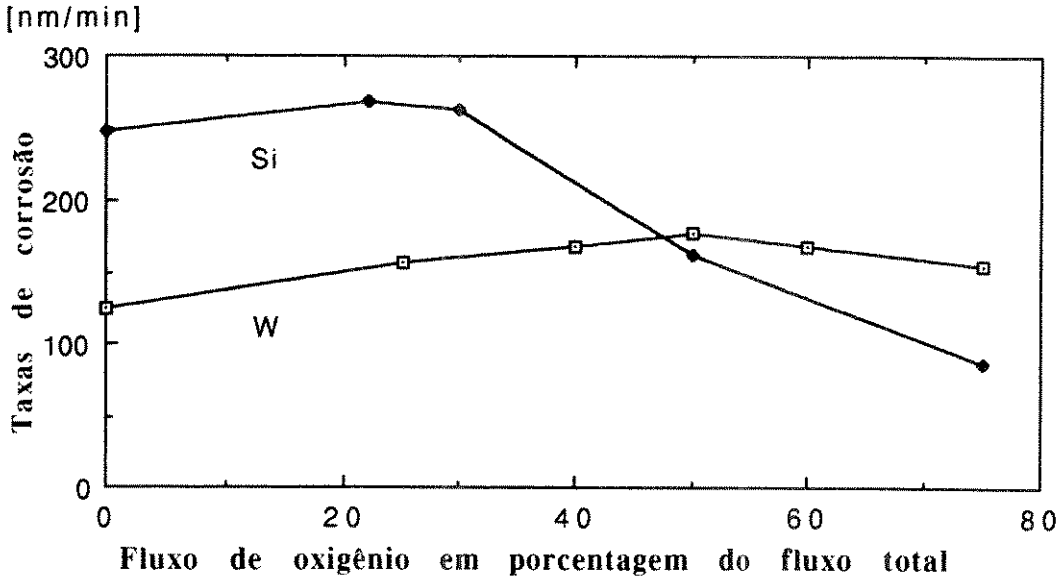

Figura 4.3 : Taxa de corrosão de tungstênio e silício policristalino em função do fluxo de oxigênio, para plasmas com SF_6, modo RIE.

4.2.2.1.2) Plasmas de NF_3.

Para o modo RIE, a influência do oxigênio na taxa de corrosão é mostrado na figura 4.4.

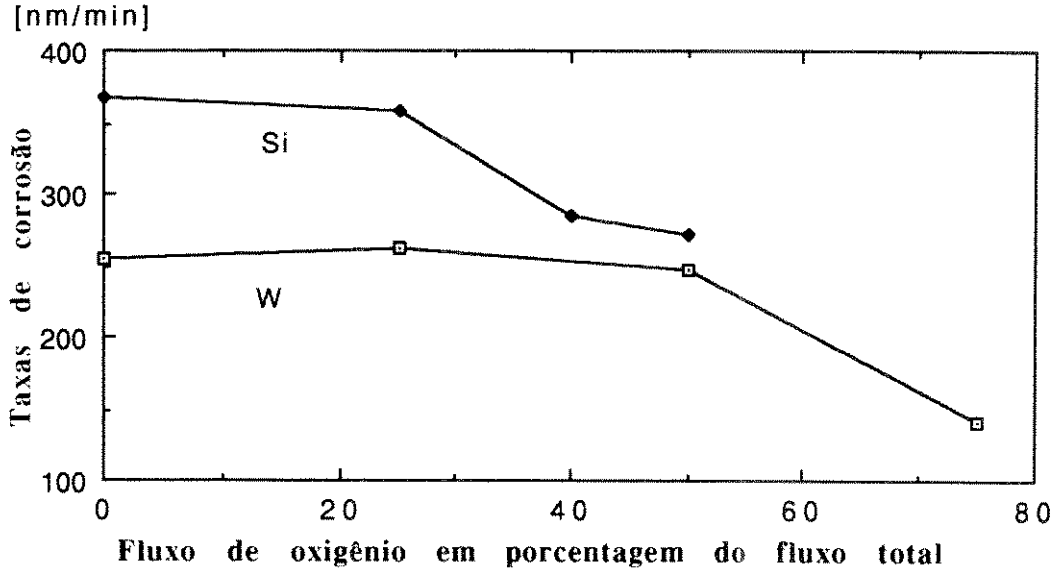

Figura 4.4 : Taxa de corrosão de tungstênio e silício policristalino em função do fluxo de oxigênio, para plasmas com NF_3, modo RIE.

As taxas de corrosão são bem maiores do que para plasmas de SF_6. Isto pode ser explicado pela decomposição mais rápida da molécula NF_3, devida às ligações N-F serem mais fracas que

as ligações S-F. Isto também explica porque não há incremento na taxa de corrosão com a adição de oxigênio (a fração de decomposição das moléculas já é muito elevada sem oxigênio). Para fluxos maiores de oxigênio, a diminuição das taxas de corrosão é a mesma que para SF_6 como relatado no capítulo 2 e anexo V.
Para o modo PF, mecanismos completamente diferentes ocorrem, como mostrado na figura 4.5. Ambas as taxas de corrosão de tungstênio e de silício policristalino aumentam com o aumento de oxigênio, até alcançar um máximo e depois ambas diminuem. A diferença com os outros casos é que o máximo para a corrosão de tungstênio fica a um fluxo de oxigênio muito menor : a 30 %, que é menor mesmo que para a máximo da taxa de corrosão do silício policristalino.
O fato de observarmos um forte incremento da taxa de corrosão de W com a porcentagem de oxigênio no modo PF e que não era observado no modo RIE pode ser explicado da seguinte maneira:
- há uma interação entre carbono, proveniente do fotorresiste, com a superfície de W, formando ligações W-C, que inibem a corrosão do W;
- o carbono é removido da superfície do W com auxílio de oxigênio, quando adicionado ao gás de entrada;
- no caso de RIE o carbono é removido pela ação do bombardeio e o efeito não é observado.
Este hipótese é reforçada por outras observações como discutido no item 4.2.4.2.

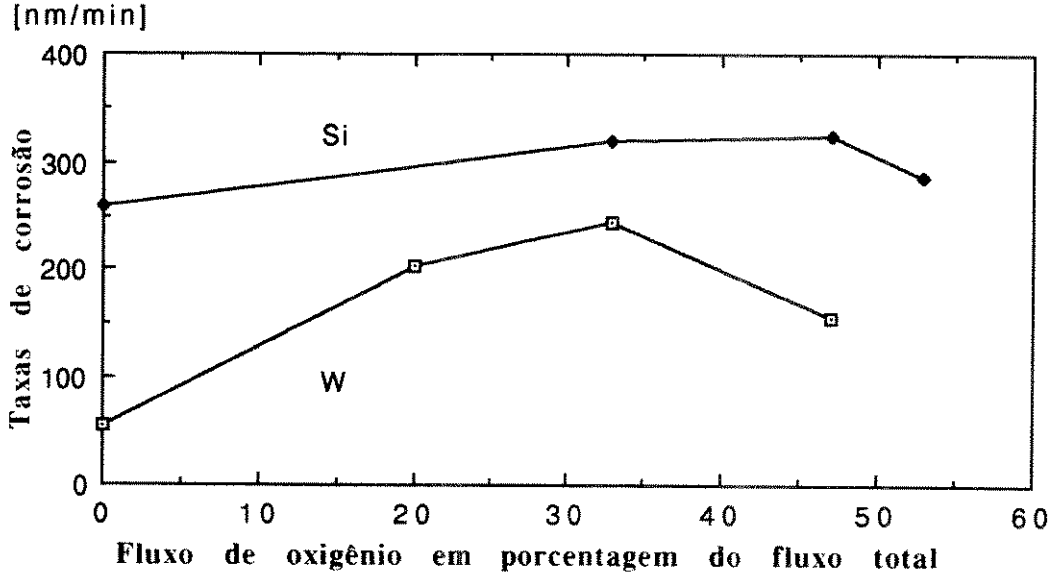

Figura 4.5 : Taxa de corrosão de tungstênio e silício policristalino em função do fluxo de oxigênio, para plasmas com NF_3, modo PF.

O mecanismo para a corrosão de silício policristalino é provavelmente o mesmo que nos outros casos : diminuição de taxa de corrosão por causa da competição entre o F e o O para fazer uma ligação com o átomo de Si. Para a corrosão de tungstênio um outro mecanismo, ainda não relatado na

literatura, deve acontecer para os fluxos maiores de oxigênio. Uma possível explicação pode ser achado no ponto de ebulição alto de WOF_4 : 188°C. Esta temperatura alta indica ser necessário adicionar energia para retirar esta molécula da superfície. No modo RIE, há suficiente bombardeamento que possa fazer este papel, mas isto não é o caso em modo PF. Portanto é possível que esta molécula fique na superfície, assim diminuindo a taxa de corrosão ao invés de aumenta-la. Para uma molécula WOF_4, a razão de O para F é 25 %, enquanto que para $SiOF_2$, esta razão é 50%. Portanto o efeito inibidor de WOF_4 ocorre a fluxos de oxigênio mais baixos do que para $SiOF_2$, o que explica o máximo da taxa de corrosão de tungstênio a um fluxo de oxigênio mais baixa do que para o máximo da taxa de corrosão de silício policristalino.

4.2.2.2) Consumo de flúor para processos no SWAFER.

Através da fórmula (4.1) é possível calcular o consumo de flúor durante a corrosão. Figuras 4.6-4.8 mostram os resultados para alguns processos descritos no capítulo 3. Nesta seção daremos apenas as conclusões gerais, para mais detalhes, veja anexo V.

4.2.2.2.1) Para plasma de SF_6 em modo RIE.

A figura 4.6 mostra o consumo de F para este caso.

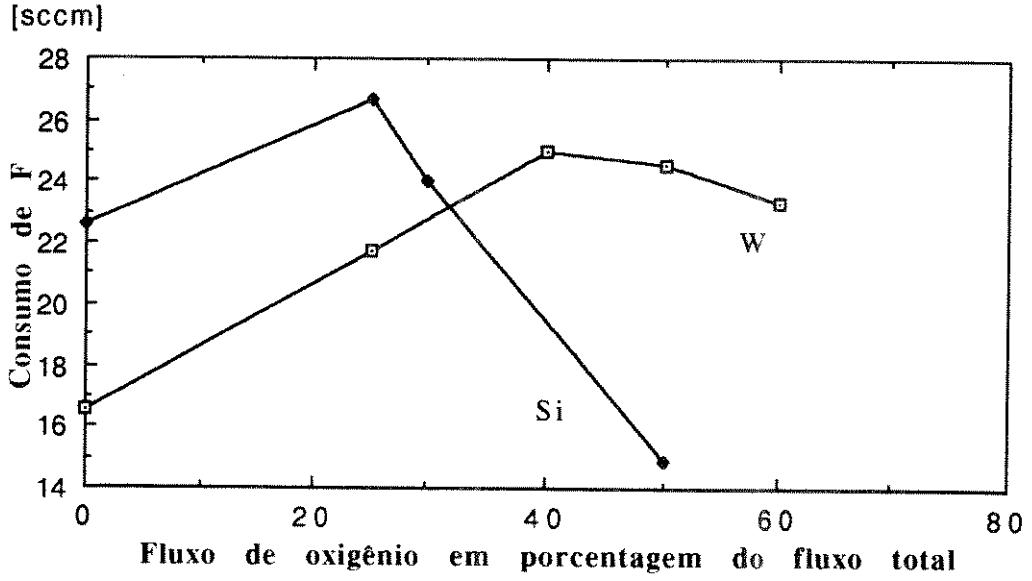

Figura 4.6 : Consumo de flúor durante a corrosão de tungstênio e de silício policristalino em função do fluxo de oxigênio, para plasmas com SF_6, modo RIE.

Há 3 regiões :
- na primeira, sem ou com pouco oxigênio, o consumo pelo silício policristalino é maior. Este comportamento pode

estar associado a fenômeno similar à da hipótese proposta no item 4.2.2.1.2. Neste caso podemos ter um efeito mais complexo tendo em vista a possibilidade do enxofre participar da formação de polímero o que não ocorre com o nitrogênio;
- na segunda região com fluxos de oxigênio, os consumos para os dois materiais são (quase) iguais. Isto indica que para ambos os materiais a chegada de F atômico é a etapa limitante;
- na terceira região, o consumo pelo tungstênio é maior. Isto indica que para silício policristalino um outro mecanismo limita a taxa de corrosão. Como descrito na literatura e no capítulo 2, este mecanismo é a competição entre os átomos de F e de O para o Si, formando produtos não voláteis como SiO_2 e $SiOF_2$.
Usando fórmulas (4.7) e (4.9) podem-se calcular os valores para G e x_s, como feito no anexo V.
Os resultados mostram que a etapa limitante (para região 2) é a geração do flúor atômico, não a difusão.

4.2.2.2.2) Para plasmas de NF_3.

Figura 4.7 mostra que o consumo de flúor para o modo RIE é o mesmo para corrosão de tungstênio e para corrosão de silício policristalino para fluxos de oxigênio baixos. De novo, isto mostra que a taxa de corrosão é limitada pela chegada de átomos de flúor.

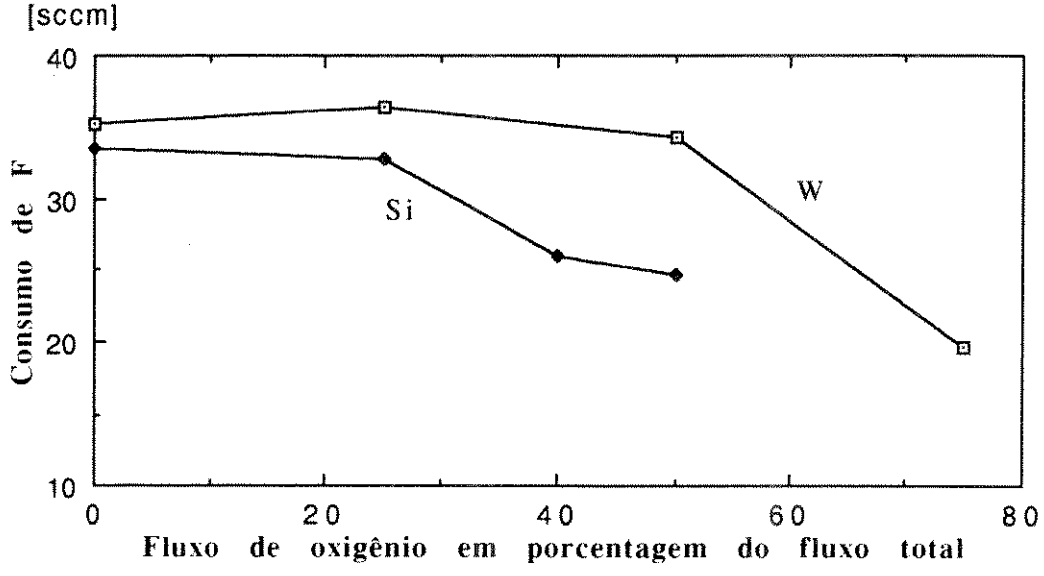

Figura 4.7 : Consumo de flúor durante a corrosão de tungstênio e de silício policristalino em função do fluxo de oxigênio, para plasmas com NF_3, modo RIE.

Usando fórmulas (4.7) e (4.9) podemos calcular os valores para G e x_s.
Estes resultados mostram que a etapa limitante é a geração do flúor atômico, não a difusão, veja anexo V.

Figura 4.8 mostra o consumo de flúor no modo PF.

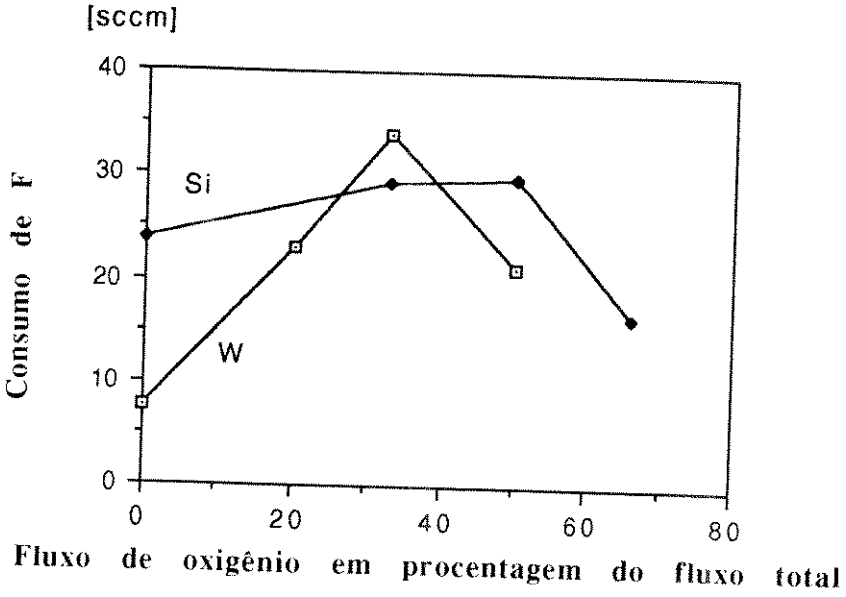

Figura 4.8 : Consumo de flúor durante a corrosão de tungstênio e de silício policristalino em função do fluxo de oxigênio, para plasmas com NF_3, modo PF.

Figura 4.8 mostra que para o modo PF há de novo 3 regiões:
- na primeira região ocorre um fenômeno similar que na figura 4.6 e explicado pela mesma hipótese da interação W-C (ver item 4.2.4.2);
- na segunda região o consumo é o mesmo para os 2 materiais, indicando que a chegada de flúor atômico é a etapa limitante para a corrosão;
- na terceira região, o consumo de flúor é menor para o tungstênio. Este fenômeno pode ser explicado pela formação de WOF_4, como também explicado acima.

Usando fórmulas (4.7) e (4.9) podem-se calcular os valores para G e x_S.
Estes resultados mostram que a etapa limitante (para região 2) é a geração do flúor atômico, não a difusão, também para modo RIE, veja anexo V.

4.2.2.3) O papel de oxigênio nos processos no Tegal 15xx.

A influência de oxigênio na taxa de corrosão em modo Triodo I está mostrada na figura 4.9.

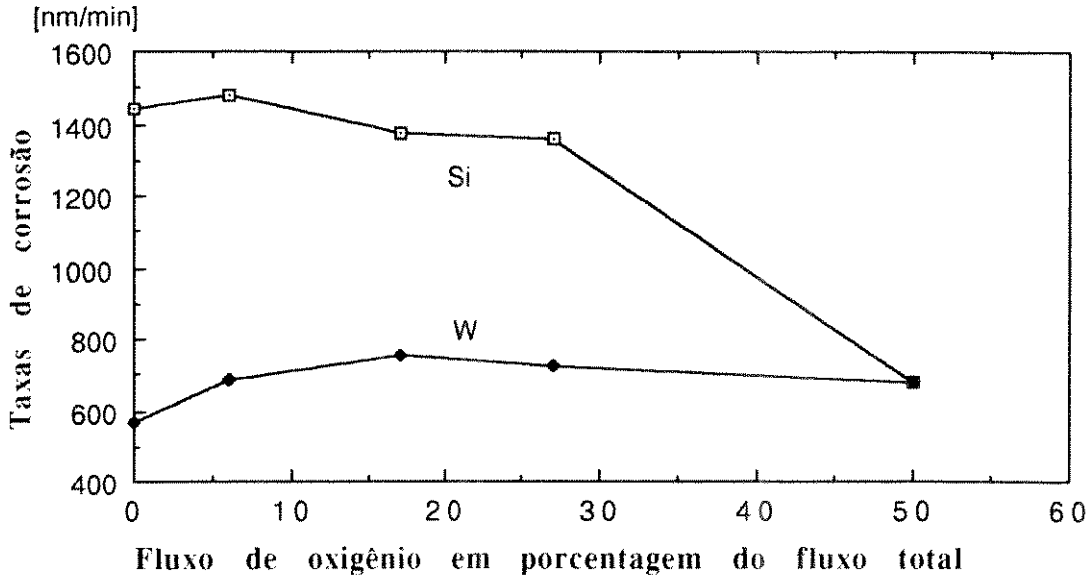

Figura 4.9 : Taxa de corrosão de tungstênio e silício policristalino em função do fluxo de oxigênio, para plasmas modo Triodo I.

O resultado é muito similar ao resultado no SWAFER em modo PF:
os principais pontos de concordância são :
- a taxa de corrosão de tungstênio é mais baixa sem oxigênio : mesmo com um fluxo de 50 % de oxigênio, a taxa é maior do que com 0 %;
- a seletividade de tungstênio para resiste não diminui com fluxo de oxigênio : ela é mais baixa com zero oxigênio no plasma.

Há também dois pontos de diferença entre os resultados no SWAFER e no Tegal 15xx :
- no Tegal 15xx a taxa de corrosão do silício policristalino não aumenta significativamente com aumento de oxigênio;
- o máximo da taxa de corrosão de tungstênio ocorre a um fluxo maior de oxigênio do que o máximo da taxa de corrosão do silício policristalino (no Tegal 15xx).

Esta primeira diferença pode ser explicada pela alta densidade do plasma, portanto mesmo sem a ajuda do oxigênio há muito flúor atômico no plasma. Isto também foi verificado nas medidas de actinometria, como mostrado no capítulo 3 e usado para explicar o comportamento do silício policristalino. Da segunda diferença podemos concluir que neste caso não temos inibição de corrosão pela formação do composto WOF_4 e portanto devemos ter maior bombardeamento que no caso do SWAFER em modo PF.
O mecanismo que explica a baixa taxa de corrosão de tungstênio a 0% de oxigênio é explicado pela hipótese do item 4.2.2.1.2.
A influência de oxigênio na taxa de corrosão em modo Triodo II está mostrada na figura 4.10.

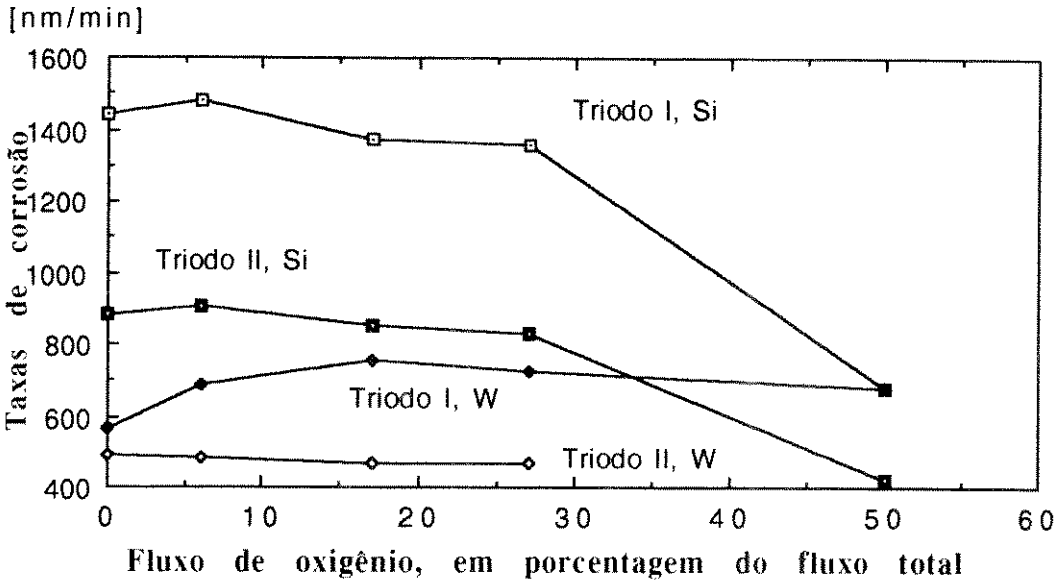

Figura 4.10 : Taxa de corrosão de tungstênio e silício policristalino em função do fluxo de oxigênio, para plasmas modo Triodo I e II.

Neste caso há uma boa concordância com o comportamento de corrosão com misturas de NF_3-O_2 em modo RIE no SWAFER. Os mecanismos devem ser parecidos.
Outras características dos processos de corrosão, como também comentadas em capítulo 3 e anexo IV :
- as taxas de corrosão de tungstênio e de silício policristalino são menores que no modo Triodo I;
- a uniformidade é muito maior que no modo Triodo I;
- a taxa de corrosão do resiste é muito maior que no modo Triodo I.

4.2.2.4) Consumo de flúor para processos no Tegal 15xx.

Através da fórmula (4.1) é possível calcular o consumo de flúor durante a corrosão. Figura 4.11 mostra os resultados para alguns processos descritos no capítulo 3. Nesta seção daremos apenas as conclusões gerais, para mais detalhes, veja anexo V.
Para modo Triodo II, a figura 4.11 mostra que na região investigada a concordância de consumo do tungstênio com o consumo do silício policristalino e muito boa. Isto significa que a etapa limitante deve ser a chegada do flúor atômico.
Usando fórmulas (4.7) e (4.9) podem-se calcular os valores para G e x_S. Estes resultados mostram que a combinação da geração do flúor junto com a difusão, limita a taxa de corrosão, veja anexo V.

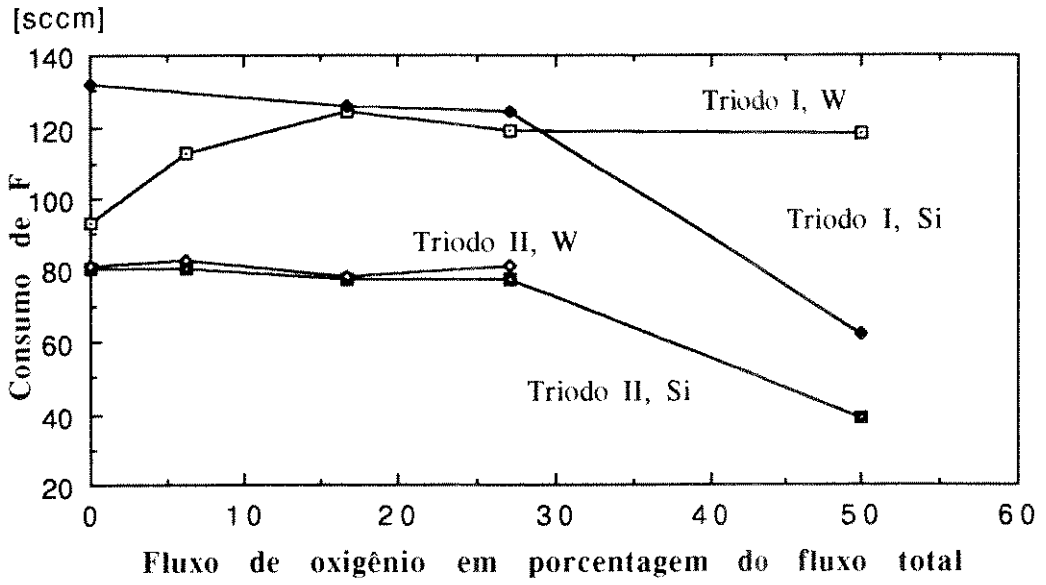

Figura 4.11 : Consumo de flúor durante a corrosão de tungstênio e de silício policristalino em função do fluxo de oxigênio para Triodo I e Triodo II.

Para o modo Triodo I há de novo 3 regiões, como nas figuras 4.6 e 4.8 :
- na primeira região ocorre um fenômeno similar do que nas figuras 4.6 e 4.8 e explicado pela hipótese do item 4.2.2.1.2;
- na segunda região o consumo é o mesmo para os 2 materiais, indicando que a chegada de flúor atômico seja a etapa limitante para a corrosão;
- na terceira região, o consumo pelo tungstênio é maior. Isto indica que para silício policristalino um outro mecanismo limita a taxa de corrosão. Como descrito na literatura e no capítulo 2, este mecanismo é a competição entre os átomos de F e de O para o Si, formando produtos não voláteis como SiO_2 e $SiOF_2$.

4.2.3) Formação de óxido de tungstênio por oxidação de uma camada fluorada.

Como descrito no capítulo 3, forma-se uma camada de óxido de tungstênio quando uma lâmina contendo uma camada de tungstênio parcialmente corroída por um processo químico rico em flúor, sai do reator. O fato que este fenômeno ocorre tanto no SWAFER quanto no Matrix 303 indica que este fenômeno não está ligado a um equipamento específico, mas que é um fenômeno geral.
Para explicar o mecanismo atrás desta oxidação, usamos os resultados das análises Auger, como descritos no capítulo 3 :
- a lâmina oxida no momento que ela chega no ar, ela não oxida num ambiente de nitrogênio;
- os perfis de profundidade das concentrações de F e de O são muito similares;

- não houve mais F na lâmina que ficou no ar durante algumas horas.
assim, propomos o seguinte mecanismo para a formação destes óxidos. Em plasmas de NF_3-O_2 forma-se muito flúor atômico. Parte deste flúor é usado para corroer o tungstênio por um processo chamado de dessorção associativo [4.5], uma parte do flúor difunde para dentro do tungstênio. Quando uma lâmina chega no ar, que sempre contém vapor de água, assumimos que a seguinte reação ocorre :

W-F + H-H-O -> W-O + H-F + H .

O HF evapora no ar e ficam as ligações W-O, formando a camada de óxido.
Para maiores detalhes, veja anexo V.

4.2.4) Formação de óxido de tungstênio em geral e suas influências.

4.2.4.1) : Influência de pré-tratamentos.

Na literatura encontram-se dados contraditórios sobre a formação de óxido de tungstênio e suas influências [4.7,4.8]. Vários testes foram feitos e as conclusões são as seguintes :
- deixando uma lâmina no ar ou colocando-a num plasma de oxigênio a uma temperatura menor que 200°C, não se forma um óxido de tungstênio que impede uma posterior corrosão;
- colocando a lâmina num plasma de oxigênio a uma temperatura maior que 250°C, forma-se uma camada de óxido de tungstênio que diminui a taxa de corrosão;
- um óxido formado por oxidação de uma camada fluorada, como descrito em 4.2.3, diminui a taxa de corrosão.
Os espectros Auger, mostrados no capítulo 3, indicam que se houver formação de um composto do tipo WO_3 na superfície, o óxido é formado por ligações químicas e diminui a taxa de corrosão.
Lâminas com W, não corroídas em plasma e deixadas no ar por semanas tiveram um composto WO_x na superfície, com x menor que 2. Neste caso o oxigênio era apenas adsorvido e o composto não forma uma impedância para a corrosão.

4.2.4.2) Influência do resiste.

O fato que a taxa de corrosão de tungstênio diminui com a cobertura de resiste para processos em PF no SWAFER, mostra que a influência do resiste é bem diferente que para outros filmes. O fato que há um efeito de área tradicional para silício policristalino coberto com resiste [4.6] e para tungstênio coberto por óxido PECVD, veja capítulo 3, mostra ainda mais que o conjunto tungstênio - resiste comporta-se bem diferente do que qualquer outro conjunto de materiais. Outros fatos, comentados no anexo V, indicam no mesmo sentido.
Figuras 4.6,4.8 e 4.11 mostram que com 0 % de oxigênio o consumo de flúor é menor para tungstênio do que para silício

policristalino. Assumimos que este fenômeno é causado pela diminuição da taxa de corrosão pelo resiste ou pelo carbono que faz parte do resiste. Quando houver oxigênio, formam-se produtos CO e CO_2 que tiram a influência do carbono.
Porém não foi possível determinar exatamente qual é o mecanismo que faz com que o complexo W - C diminui a taxa de corrosão.
Os dois mecanismos mais prováveis, que podem até ocorrer simultaneamente são :
- formação de ligações W-C na superfície da lâmina, que impede a corrosão; o C é removido facilmente pelo O nos plasmas que contém oxigênio;
- com a adição de oxigênio aumenta a voltagem sobre a bainha, portanto há mais bombardeamento iônico que possa quebrar as ligações W-C.
Para mais detalhes, veja anexo V.

Referências

[4.1] R.C. Reid, T.K. Sherwood, "The properties of gases and liquids", second edition, Mc.Graw - Hill, 1966
[4.2] B. Chapman, "Glow Discharge Plasmas", John Wiley and sons (1980).
[4.3] Vacuumtechniek - L. Wolterbeek Muller, Kluwer Technische boeken, 1989
[4.4] Hindmann and Raupp, "Coadsorption of WF_6 and H_2 on polycrystalline tungsten: implications for the hydrogen reduction reaction", Advanced Metallization for ULSI Applications, October 1991, extended abstracts.
[4.5] A. Durandet, Y. Arnal, J. Pelletier, G. Pomot, "Anisotropy and Kinetics of the Etching of Tungsten in SF6 Multipolar Microwave Plasma", J. Appl. Phys. 67, 2298 (1990)
[4.6] J. Vandersmissen, "Characterization of polysilicon and nitride processes in the SWAFER", internal Cobrain report, 1991.
[4.7] T. Bestwick, G. Oehrlein, "Tungsten Etching Mechanisms in CF4/O2 Reactive Ion Etching Plasmas", J. Appl. Phys. 66, 5034 (1989)
[4.8] Adachi, Susa, "Reactive Ion Etching of Tungsten Films Sputter Deposited on GaAs", J. Electrochem. Soc. 132, 2980 (1985)

Capítulo 5 : Conclusões gerais do trabalho.

5.1) Desenvolvimento de processos.

Foram desenvolvidos processos para obter "plugs" nos dois equipamentos investigados. Ambos os processos têm boas caractrísticas : boa uniformidade, pequeno efeito de área, boa seletividade para o material em baixo e uma razoável taxa de corrosão.
Conseguimos obter processos para corrosão anisotrópica de tungstênio. Infelizmente, não conseguimos obter seletividades de tungstênio para resiste reprodutíveis maiores que 1,1:1. Esta baixa seletividade implica que não se pode usar um resiste tradicional de 1 μm de espessura para corroer um filme de tungstênio da mesma espessura. Portanto é necessário usar um sistema de mascaramento alternativo, ou uma camada de tungstênio mais fina. No entanto, este processo pode ser utilizado com sucesso na corrosão de policeto de tungstênio, onde a seletividade é bem maior.

5.2) Determinação de mecanismos de corrosão por plasma de tungstênio.

Foi confirmada a maioria dos mecanismos descritos na literatura, para os dois equipamentos investigados. Portanto a maioria dos mecanismos que valem para plasma tradicionais a 13.56 MHz, valem também para plasmas de 25 kHz e plasmas com confinamento magnetico. Estas confirmações incluem :
1: o papel de oxigênio é quase sempre o mesmo : a baixos fluxos, ajuda na formação de flúor atômico; a altos fluxos, ele dilui e/ou faz com que haja competição entre F e O para fazer a ligação com o Si ou o W.
2: no caso de W há formação de WOF_4 que na maioria dos casos é volátil; no caso de Si forma-se SiO_2 e/ou $SiOF_2$ que não são voláteis;
3: bombardeamento iônico aumenta a taxa de corrosão
4: é possível obter corrosão anisotrópica.

No caso das contradições encontradas na literatura, tiramos os seguintes conclusões :
1: é possível remover tungstênio por corrosão meramente química, se houver suficiente flúor atômico disponível;
2: uma corrosão anisotrópica ocorre se houver suficiente bombardeamento iônico; não há necessidade de criar uma proteção na parede;
3: deixando as lâminas em ar ou colocando-as num plasma de oxigênio a baixas temperaturas, não se forma um óxido que inibe a corrosão de tungstênio.
4: quando o tungstênio entra em contato com oxigênio a temperaturas altas, tipicamente maiores que 250°C, ou quando entra em contato com ar depois de uma corrosão parcial por plasma em modo químico com uma mistura contendo NF_3, forma-se um óxido que diminui a taxa de corrosão do tungstênio.

5: a presença do resiste diminui a taxa de corrosão para um processo químico com NF_3. O complexo tungstênio - resiste - plasma causa fenômenos não compreendidos ainda.

Além disso determinamos mais alguns mecanismos:
1: para a grande maioria dos processos, a etapa que limita a taxa de corrosão é a chegada do flúor atômico na superfície da lâmina;
2: para taxas de corrosão baixas, a geração do flúor é a etapa limitante; para taxas de corrosão altas, a difusão também limita a taxa;
Sugerimos mais os seguintes mecanismos :
3: se não houver suficiente bombardeamento iônico, o WOF_4 inibe a corrosão ao invés de promover a corrosão;
4: o carbono do resiste forma junto com o tungstênio e o fluor do plasma um composto W-C-F que inibe a corrosão se não houver suficiente oxigênio e/ou bombardeamento para remove-lo da superfície de tungstênio.

5.3) Sugestões para futuros trabalhos.

Para elucidar dúvidas deixados em aberto no trabalho sugerimos os seguintes experimentos :

1) Determinação de taxas de corrosão e consumo de flúor para lâminas com tungstênio sem resiste no Tegal 15xx em modo Triodo I, principalmente para o processo sem oxigênio. Por este teste poderíamos verificar se o carbono do resiste é realmente o fator importante na limitação da taxa de corrosão. Por outro lado não se pode esquecer que sempre há carbono no reator por causa do material do sistema de "clamping" da lâmina: os dedos são feitos de um polímero.
2) Determinação de taxas de corrosão e consumo de flúor para lâminas com tungstênio sem resiste no SWAFER em modo PF, principalmente para o processo sem oxigênio. Por este teste poderíamos verificar se o carbono do resiste é o fator importante na limitação da taxa de corrosão. No SWAFER porém uma parte do eletrodo é feito de grafite. Portanto para eliminar completamente o carbono, deve-se remover este anel.
3) Fazer testes com SF_6 no Matrix 303 para verificar se há oxidação do tungstênio.
4) Depois de fazer corrosão química de tungstênio com flúor, deixar a lâmina durante um tempo dentro de um ambiente de oxigênio a pressão atmosférica para verificar se o oxigênio puro pode oxidar o tungstênio.
5) Fazer um estudo mais extensivo da influência de pré-tratamentos na taxa de corrosão de tungstênio, principalmente em modo PF no SWAFER, mas também no modo Triodo I no Tegal 15xx.

Como continuidade do trabalho sugerimos :

1) investigar o uso de outras misturas de gases, por exemplo adicionar HBr;
2) combinar os conhecimentos da corrosão de silício policristalino e de tungstênio para desenvolver processos de corrosão de silicetos de tungstênio;
3) um estudo especial sobre a formação de particulados e a passivação de reatores em função do número de lâminas e os processos específicos de corrosão de tungstênio por plasma.

Appendix I : Plasma etching of tungsten: existing models and auxiliary techniques.

Index

Appendix I : Plasma etching of tungsten: existing models and auxiliary techniques.

Introduction:

General principles of plasma etching are well described in the literature [1-4]. Some etch mechanisms are known and models have been proposed, mainly for silicon etching. Papers on tungsten etching are rather scarce, certainly in comparison with silicon etching or tungsten deposition. As tungsten is a relatively new material in the fabrication of integrated circuits, its etching is not described in publications on etching in general. Ref [5] is the most comprehensive compilation article, but far from complete and up to date.
The main objectives of this appendix are:
1) to describe qualitatively the different mechanisms involved in plasma etching of tungsten, (starting from general plasma etching knowledge, applied to tungsten etching).
2) to make an overview of the mechanisms and models of tungsten plasma etching in the literature
3) to describe two techniques which were used in the experimental part of this work: actinometry and statistical design of experiments.
4) to describe the application of tungsten most used in the industry : the formation of plugs.

This report was divided in six parts:

1: Overview of the overall mechanisms of plasma etching.

2: Existing models for the etching of tungsten with fluorine containing gases - a brief overview of the existing literature.

3: Overview of the reports on tungsten etching with non fluorine containing gases.

4: Actinometry.

5: Statistical design of experiments.

6: An important application : tungsten plugs.

1) Overview of the overall mechanisms of plasma etching.

The plasma etch process can be divided in several subprocesses. A traditional division is as follows [1-3]:
- the active etch reagent particle reaches the surface to be etched
- the reagent adsorbs at the surface
- the reagent chemisorbs: a chemical bond is formed

- other reagent particles react with the surface atom, so that the volatile product molecule is formed
- the product molecule desorbs from the surface, and is pumped away.

One should observe that an extra step should be added at the start of this process:
- active etch reagent particles are formed.

Each step will be described briefly, with tungsten etching as application in mind.
We will investigate how these steps affect the etching of tungsten using a fluorine gas. These principles can easily be transposed to the etching of other films with other gases.

1.1) Formation of the active species.

In general the gas molecules entering the etch chamber do not spontaneously react with the film to be etched. For most of the films used in silicon technology, atoms from the halide group, like F, Cl and Br, form chemical bonds with the atoms of the material which is being etched. Even in the case of polymer etching with oxygen, it are the O atoms that form the bonds with C and H atoms and not the O_2 molecules [6]. The formation of atoms is not always necessary, as for chlorine etching of aluminium: Cl_2 is sufficiently reactive [7].
But when spontaneous etching does not occur, the main role of the plasma is often to deliver the extra energy to form the atoms from their original molecules and it are these atoms that then will adsorb-chemisorb and form the volatile product [2,3,5]. The binding energy between the non-fluorine atom and the fluorine atom is therefore an important parameter: table I shows the binding energies for some important gases [9]. From these values one can conclude that under fixed conditions more free fluorine will be formed with NF_3 than with SF_6, while CF_4 will yield the least free fluorine. As will be shown later, the formation of free fluorine very often is the etch rate limiting step. In these cases etching will be faster with NF_3, then with SF_6 and slowest with CF_4.

Table I : Binding energies for important etch molecules.

CF_3 - F : 128 kcal/mol	C - F : 128 kcal/mol
SF_5 - F : 90 kcal/mol	S - F : 82 kcal/mol
NF_2 - F : 55 kcal/mol	N - F : 63 kcal/mol
	W - F : 131 kcal/mol

Determining absolute values for the formation or concentration of free fluorine is extremely difficult - at this moment even impossible - with the actual knowledge. However there are techniques such as mass spectroscopy, Laser Induced Fluorescence (LIF) and actinometry which can yield relative concentrations, while comparing different plasma processes.[5,10-15].

The formation of free fluorine can also be influenced by the addition of other gases. The best known systems are those of CF_4 + O_2 and CF_4 + H_2. [1-4,16]
For the first mixture the following (amongst other) reactions occur:

$CF_4 + O_2 \rightarrow CO_2 + 4F.$ (1)
$2\ CF_4 + O_2 \rightarrow 2\ COF_2 + 4F$ (2)

Through these reactions, the density of free fluorine increases, often increasing the etch rate, as is shown in the literature and also in this work.
The presence of carbon, in the form of an electrode, but even as a composing element of photoresist, will also influence the free fluorine as it will scavenge oxygen atoms and molecules through the following reactions:

$C + O_2 \rightarrow CO_2$ (3)
$2\ C + O_2 \rightarrow 2\ CO$ (4)

Therefore reactions (1) and (2) will occur less, decreasing the density of free fluorine.
Similar reactions occur when adding oxygen to NF_3 and SF_6.
The presence of hydrogen influences directly the density of free fluorine as the following reaction occurs in the plasma:

$2\ F + H_2 \rightarrow 2\ HF$ (5)

Hydrogen scavenges fluorine, decreasing its concentration and decreasing the etch rate. This kind of chemistry is often used for the etching of silicon dioxide, to obtain selectivity towards silicon.
When a somewhat adequate model of generation of atomic species in a reactor is to be determined, all these factors have to be taken into account.
Traditional fluorine containing etch gases are CF_4, SF_6 and NF_3. Unless their fluorine atoms are liberated, these gases will not etch films used in the semiconductor industry. The generation of free fluorine is one of the most important functions of the plasma. The generation rate of this free fluorine is a function of the "macro plasma parameters" such as : halide gas used, additional gas(es) used, flows, pressure, applied power, power frequency, etch mode, interelectrode distance and materials of the etch reactor - mainly the electrode - etc. These macro parameters will determine the "micro plasma parameters" such as : density of ions and electrons, energies of these ions and electrons, plasma potentials etc [1,2]. It is clear that modelling of plasma kinetics as a function of all these parameters is extremely difficult, though it is being tried [8]. In this report we shall try to determine qualitatively and quantitatively some parameters and their influences on the etch process.

1.2) Flow of reactive particles reaching the surface of the wafer.

What needs to be known to determine the etch rate is the flow of free fluorine atoms that reach the surface. This flow is determined by two mechanisms:
1: the generation of free fluorine atoms.
2: the transport of these atoms to the surface.
As discussed above, a numerical determination of the first factor is nearly impossible.
The second factor can be calculated making some assumptions, as will be shown in appendix V.

It is very hard to quantitatively determine through experiments the free fluorine concentration, C_F, which varies in space. Spatially resolved LIF measurements could give some indications, but a special reactor would be necessary, with access of the laser beam to several heights above the wafer. So a special design of windows in the reactor would be needed, which is normally not available in commercial systems.

1.3) Adsorption and chemisorption.

Not all fluorine atoms that reach the surface will react with the tungsten to form eventually the volatile WF_6 product. Part of the incoming atoms will return into the plasma without reacting with the surface at all. E.g. part of the impinging atoms will adsorb for some time, but desorb before chemisorption occurs.
A part of the incoming atoms however will form a bond with the tungsten atom to form a WF_x compound, with x = 1,2,3 or 4 [17]. These WF_x compounds will interact as discussed below in 1.4.
A sticking coefficient s can be defined as:
s = ratio of the chemisorbed atoms to the impinging atoms.
The sticking coefficient depends on the type of atom, the nature of the surface (e.g. surface roughness is an important parameter) and the available area to adsorb (e.g. if the total surface area is already covered with F, no new incoming atom will stick).
As the initial energy needed for an atom to adsorb is less than the energy needed to chemisorb, adsorption is not the rate limiting step. It can be observed that the enthalpy of the system of the chemisorbed atoms (e.g. N-F) is lower than the enthalpy of the system where all atoms are separate (N and F separate), but a potential barrier has to be overcome before reaching the overall more stable situation [18].
The rate of chemisorption will depend on the concentration of adsorbed free fluorine and on the energy input in the system. The energy can be delivered in the form of heat or in the form of kinetic energy from the impinging ions.
It is well known that pure chemical etching follows Arrhenius' law when chemisorption is the limiting process.

This is e.g. the case for photoresist removal in afterglow strippers: a lot of atomic oxygen is formed and the temperature of the wafers can be controlled. It is then easy to determine the activation energy, E_a, through the measurement of the etch rate at several temperatures, from:

$$r = r_o \exp(-E_a/kT) \qquad (6)$$

with k the Boltzmann factor, T absolute temperature in Kelvin and r_o a proportionality factor.
E_a has been determined for resist-oxygen systems [6] but also for tungsten - halide systems [10].
For RIE plasmas however, most energy will come from the impinging ions: the etching will be bombardment enhanced. Curves of the type ln r as a function of 1/T are not straight lines then. In this case it is very hard to quantify this type of process mechanism.

1.4) Formation of the volatile product.

It is not sufficient to form 1 W-F bond : WF is not a volatile product. WF_6 on the other hand is a volatile product. This product formation is not fully understood yet, but studies have shown that certain models are more acceptable than others (see item 2 below). The model of associative desorption [17] assumes the formation of WF_x (x = 1->4) compounds over the wafer, which eventually form WF_6 at certain sites through the following reactions:

$$WF_2 + WF_4 \rightarrow WF_6 + W \qquad (7)$$
$$WF_3 + WF_3 \rightarrow WF_6 + W \qquad (8)$$
$$WF_3 + WF_4 \rightarrow WF_6 + WF \qquad (9)$$

This is the case when very orderly chemical etching takes place. In the case of bombarding ions, the model is much more chaotic: the energy of the incoming ion can be sufficient to dislocate F from several sites and bind them to 1 W-atom, in this way forming the volatile product, without having to cover the whole area with WF_3 and WF_4 complexes. It is also possible to remove non-volatile WF_x molecules from the surface, which are then fluorinated into WF_6 in the plasma.

1.5) Desorption

The volatile product, for tungsten : WF_6, must leave the surface and be removed from the reactor through the pump. This process is described in more detail in ref [19] and in appendix V, where some calculations will be made.

1.6) Summary

The etch rate can be limited by whatever subprocess described above. A huge part of the studies in the literature is dedicated to the determination of the etch rate limiting step for the etch processes of a certain material in a certain reactor with certain etch process parameters. In appendices II, III and V the investigations to determine the etch rate limiting step for the etching of tungsten with fluorine containing gases will be described, for 2 types of equipment: a low frequency plasma etch system and a magnetically confined plasma etch system.

2) Existing models for the etching of tungsten with fluorine containing gases - a brief overview of the existing literature.

In this item a short overview is given of reports published on tungsten etching which are relevant for our work. Reports confirmed by our work receive a (!) sign, reports in contradiction are indicated by the (*) sign.

2.1) General observations.

Table II shows the boiling points of possible volatile etch products of W and Si:

Table II : Boiling points of possible volatile etch products.

SiF_4	-86°C	WBr_5	333°C
$SiCl_4$	57.6°C	WOF_4	188°C
WF_6	17.5°C	$WOCl_4$	228°C
WCl_5	276°C	$WOBr_4$	327°C
WCl_6	347°C		

These data indicate that fluorine is the most adequate halogen to remove silicon and tungsten layers quickly. By adding energy, e.g. by ion bombardment, it is also possible to etch tungsten with chlorine or bromine containing gases. [10,20,21]
It should be remarked that most published tests occurred in a 13.56 MHz system, some with microwave plasmas. No reports were found on Audio Frequency (AF) plasmas.

2.2) Influence of the used gases

Several tests have been reported on tungsten etching with SF_6 and CF_4 plasmas.
Small additions of O_2 (and N_2) increase the number of free fluorine, through reactions similar to (1) and (2), see section 1.1. This causes the etch rate of tungsten to increase [11,12,15,21-25]. However, if too much additional gas is added, other mechanisms become more important. A first factor is the dilution of the halogen gas by the added

gas, which becomes more important than the F generating factor, hence the F concentration decreases, with a decreasing etch rate as consequence. A second factor is the competition between the halogen atoms and the added gas atoms to form bonds with the surface atoms of the film to be etched, as is the case for etching of silicon, with addition of O_2 .
Etch rates were plotted as a function of O_2 content. On the same plot the relative concentration of free fluorine and sometimes the etch rates of silicon or polysilicon in the same system were plotted, resulting in figures similar to fig. 1.

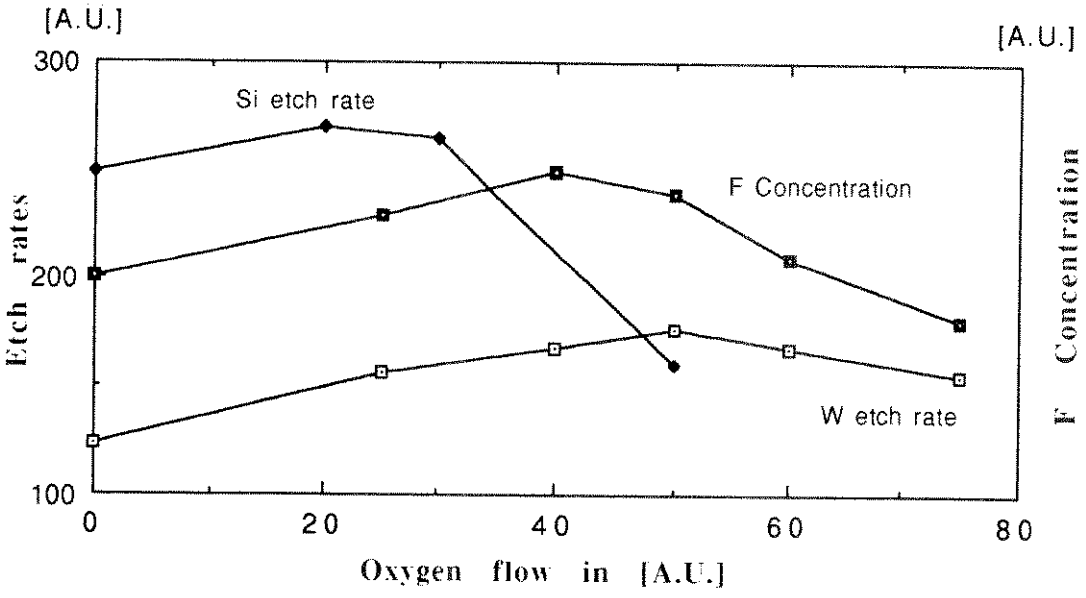

Figure 1 : General trends in polysilicon and tungsten etch rates and F concentration as a function of oxygen content, in this case all in arbitrary units.

From these curves, mass spectroscopy and XPS analysis [11,23-25] the following model has been proposed.
There are three significant regimes: the first with little oxygen addition, where the etch rate is determined by the F content and WF_6 is formed. At intermediate regimes the formation of WOF_4 helps to keep the etch rate high, although WOF_4 is less volatile than WF_6. When more oxygen is added there is competition in the formation of tungsten fluorides and tungsten oxydes [11] or the dilution is too large to form enough free fluorine to form one of the halogenated volatile etch products.
The difference with the model for silicon etching is that besides the formation of WF_6, also WOF_4 is formed when O_2 is added to the plasma. This is the reason that the maximum of the tungsten etch rate curve is located at a higher O_2 percentage than the maximum of the F curve. The maximum of the silicon etch rate curve is located at an even lower oxygen content for the following 2 reasons:

1: $SiOF_2$ (the equivalent of WOF_4) is not volatile at all. Therefore it does not contribute to the increase of the etch rate.
2: Oxygen will oxidize the silicon surface, hereby making the etching much more difficult, as SiO_2 is harder to etch than pure Si [17].
WO_3 is a stable but volatile molecule [27](*). In the literature one can find that the formation of a tungsten oxide layer inhibits the etching [28], but also that it does not influence the etching [11]. In this work we shall show that the influence of the tungsten oxide depends on the used etch mode (and the thickness of the oxide).
Addition of oxygen can also influence the anisotropy of the process: it can increase it, when mixed with SF_6, through the increase of the ion bombardment [25], or can decrease it by formation of more free fluorine, increasing the chemical etching [26] (depending on the other plasma process parameters).
Small nitrogen additions can increase the etch rate significantly by firstly creating more free fluorine and secondly increasing the ion bombardment [24,26].
For NF_3 + O_2 plasmas it was reported that no WOF_4 was found [29] (for etch processes in RIE mode). Also for these gases a damage induced etching has been proposed. No report was found on pure chemical etching using NF_3 as an etch gas, only on RIE mode etchings.

2.3) The influence of ion bombardment.

Ion bombardment can be a very important etch rate increasing factor in tungsten etching. It is possible to etch tungsten in a purely chemical way (!), but ion bombardment caused by electric fields, related to a difference in potential over the dark sheath as small as 25 V, increases the etch rate by a factor of 2 [23]. The increase of the DC bias voltage can result in considerable etch rate increase. Traditionally, this is done by increasing the RF power, but changes in pressure and in additional gases can be responsible for greater etch rate differences than expected on a chemical basis only.
Ion bombardment causes the formation of active W sites. On these sites the sticking coefficient of the impinging F is higher. In this way etch rates can be increased by a factor of 15 or more by traditionally available 100 V DC bias [29,30]. When using an ion beam it could be shown that the etch rate is proportional to the ion current, not to the ion energy [31]. A lot of these tests used XeF_2 as etching gas, without using a plasma. It has been shown [32] that this gas dissociates at the wafer surface when bombarded, in this way increasing the etch rate also. It is very hard to determine which mechanism is responsible for the larger part of the etch rate increase. In traditional plasma systems, using CF_4, SF_6 or NF_3, a lot of free fluorine arrives at the surface from the plasma, more than is generated by

dissociation of parent molecules at the surface. Therefore ion bombardment increases much less dramatic the etch rate than with XeF_2 gas, as occurred in the tests mentioned above. Reports on anisotropy show all kinds of results [23,25,26,35]. It is clear that anisotropy depends on a lot of factors, such as resist material, electrode material, oxygen addition, besides the traditional factors as pressure, power and (resulting) DC bias. It sometimes is assumed that a polymer has to be formed to protect sidewall etching. Other reports show that the formation of active W sites through ion bombardment, increases the vertical to horizontal etch rate so that anisotropy is obtained.

2.4) Chemical etching.

It is not obvious that pure chemical etching of W with fluorine should take place with a boiling point for WF_6 as high as 17.5°C. The following mechanism of associative desorption has been proposed [17]: enough free fluorine needs to be generated in order to form WF_x (x = 2-4) compounds over the whole surface by the following chemical reactions:

$W + F \rightarrow WF$ (10)
$WF + F \rightarrow WF_2$ (11)
$WF_2 + F \rightarrow WF_3$ (12)
$WF_3 + F \rightarrow WF_4$ (13)

The volatile WF_6 compounds are formed by the following 2 reactions:.

$WF_3 + WF_3 \rightarrow WF_6 + W$ (14)
$WF_4 + WF_2 \rightarrow WF_6 + W$ (15)
$WF_4 + WF_3 \rightarrow WF_6 + WF$ (16)

This mechanism is similar to the formation of SiF_4 by associative desorption of two SiF_2 molecules, formed at the fluorinated surface of a silicon film.
Few data are shown on the temperature influence: ref [10] shows that the tungsten etch rate has an Arrhenius dependence on temperature, with activation energies of 0.2 eV, both for CF_4 as for SF_6 gas. The experiments were done in Plasma Etch mode, so etching is presumably merely chemical.

2.5) Summary of the proposed models.

Though there are several contradictions in the literature, there exists agreement on the following topics:
- Tungsten can be etched by free fluorine, even without bombardment enhancement.
- Ion bombardment enhances the etch rate of tungsten, in some circumstances even dramatically.

- The etch rate follows quite well the free fluorine concentration. Both for CF_4 and SF_6 the formation of WOF_4 increases the etch rate of tungsten. For NF_3 no formation of WOF_4 was observed.

Contradictions were found mainly on the following two topics:
- addition of oxygen to a halide decreases the etch rate through formation of tungsten oxide.
- which mechanism is responsible for the formation of the vertical walls of the tungsten when having a bombardment enhanced etching : the formation of active sites or passivation of the sidewall by a carbon containing material.

The chemical etching of tungsten is also not very well modelled, but the existing model of associative desorption is well accepted.

2.6) Calculation of the fluorine flow consumed during etching.

In ref [1] a formula is found from which it is possible to calculate the quantity of consumed species. A more general result can be obtained, as deduced below. This calculation will be important to illustrate etch mechanisms and their influence on the etch rate. The following numerical example is used :
tungsten etching of a 125 mm wafer proceeds at a rate of 200 nm/min at a 200 mTorr pressure with a flow of 100 sccm of NF_3 (this is an example of an etch process in the Cobrain SWAFER equipment [33], also presented in appendix II).
The following well known data are necessary: density of the film, atomic weight of the material of the film, overall etch reaction, area of the wafer that is being etched. One can often assume that the density of the film is equal to the density of the material.
For tungsten this yields:

density ρ : 19.35 kg/dm^3 = 19.35 g/cm^3
atomic weight M: 184 g/mol
overall reaction: W + 6 F -> WF_6

For the above mentioned example we have:
Volume of W removed in 1 minute : V_{rem} = A x r =

$\pi \times (6.25)^2 \times 200 \times 10^{-7} = 2.45\ 10^{-3}$ cm^3
The number of atoms per volume n can be calculated from density and atomic weight, using the number of Avogadro NA.
For tungsten: $n = \rho / (M/NA) = 19.35 / (184/6.02\ 10^{23}) = 0.633\ 10^{23}$ atoms/cc
The number of W atoms removed per minute is : n x V_{rem} = $1.554\ 10^{20}$ atoms per minute
Assuming WF_6 as the sole etch product, 6 F atoms are needed to remove one W atom, its consumption is: $9.323\ 10^{20}$ atoms per min.

From the definition that 1 sccm = 1/22400 mol/min = 0.269 10^{20} atoms/min one can conclude that when etching a blanket 125 mm W wafer at 200 nm/min, 34.7 sccm of F is consumed. It must be observed that this flow has to reach the W surface of the wafer. At the same time a flow of 5.8 sccm WF_6 leaves the wafer. As these flows are proportional to the etch rate one can also state that per nm/min of W etch rate a F flow of 0.173 sccm is consumed and a WF_6 flow of 0.029 sccm comes free from the surface, for 125 mm wafers.

It is possible to calculate the flow J_F of consumed F directly from the general formula:

$$J_F = 2.24\ 10^{-3} . \pi . (d/2)^2 . \text{etch rate} . \rho . X / M \quad (17)$$

with:
J_F : flow of F atoms consumed in [sccm]
d : diameter of the wafer in [cm]
etch rate : of the film in [nm/min]
ρ : density of the film material in [kg/dm^3]
X : Coefficient of the reaction : Mat + X Hal -> $MatHal_X$
M : atomic weight of the film material in [g/mol].

For silicon with ρ = 2.33, M = 28 and X = 4, for a 125 mm wafer at 200 nm/min the consumption of F = 18.3 sccm.

It is also possible to obtain the efficiency of the used gas by dividing the flow J_F of consumed atoms by the total amount of available atoms. This amount is the flow of the mother molecule multiplied by the number of F atoms in this mother molecule. Most often this efficiency is between 1% and 10% for traditional RIE plasmas.
These data are independent of etch gas used, reactor type etc. as we made no use of dissociation rates, specific chemical reactions in the plasma state, etc.

3) Overview of the reports on tungsten etching with non fluorine gases.

Tungsten can be etched by chlorine atoms without any ion bombardment [5,20]. The overal reaction is :

$$W + 6\ Cl \rightarrow WCl_6 \quad (18)$$

It is shown that, even at high temperatures, Cl_2 molecules do not etch tungsten. In an afterglow plasma, Cl atoms are responsible for the tungsten etching [34]. But it is necessary to give the samples a diluted HF dip or a short plasma cycle, before introducing them in this reactor; if not, no etching takes place. This shows that a small inhibiting layer is normally formed (probably tungsten oxide). These results show on the other hand that chemical etching by Cl atoms is more important than the high boiling temperature of WCl_6 suggests.

W etch rate increases with pressure, at least if the flows are high enough, i.e. at low residence times. It is even possible to increase the etch rate till pressures of 1200 mTorr for residence times of half a second [20]. This phenomenon shows that chemical etching can be very important. Temperature effects are more important in afterglow plasmas than in RIE plasmas [34].
BCl_3 additions can have dramatic influences. As little as 3% addition of BCl_3 to Cl_2 can increase the etch rate with a factor of 2. But addition of 10% decreases etch rate with a factor of 2. BCl_3 is believed to remove water vapour or a tungsten oxide at the surface, but when added too much, it reduces the Cl atom density (dilution effect) [34].

4) Actinometry

A relatively simple technique to analyse the plasmas is actinometry. This technique is based on optical emission spectroscopy.
Optical emission spectroscopy on itself is widely used in plasma analysis, because of its simplicity [5,10-15,36,37]. The various species in a plasma emit light at different, well known wavelengths. However one has to be careful when trying to perform a quantitative analysis of these species. The light intensity at the wavelength of a particular specie is not only a function of the concentration of the specie, but also of the electron density and electron energy distribution of the applied plasma. It is possible to make a correction by introducing an inert gas which must have similar excitation characteristics as the specie to be characterized. It is well known that Ar is suitable as a reference gas for the monitoring of free fluorine concentration [36,37].
Comparing optical emission spectroscopy with mass spectroscopy, its drawback is that only excited species can be measured. Therefore the following reaction has to occur:

$$e^- + S \rightarrow S^* + e^- \qquad (19)$$

The intensity of the light is proportional to the number of excited species that relax by photoemission. If one wants to compare the free fluorine content of different process a constant fraction of the excited S^* species must relax by photoemission for these processes. When comparing processes e.g. at different pressures, this is not always the case.

$$S^* \rightarrow S + h\nu \qquad (20)$$

If relaxation by photoemission is constant, then the intensity of the emission, I_S, is proportional to the generation rate of S^*.

$$I_S \propto k_S [e^-] [S] \qquad (21)$$

The constant k_S is proportional to the excitation efficiency. The excitation efficiency E_S can be expressed as:

$$E_S = \int v(E)\ \sigma_S(E)\ f(E)\ dE \qquad (22)$$

In this equation : $v(E)$ is the electron velocity, $\sigma_S(E)$ is the collision cross section for excitation and $f(E)$ is the electron energy distribution function. It is well known that $v(E)$ and $\sigma_S(E)$ are functions of the electron energy E. Applying these equations to the specie X to be monitored and the reference gas A:

$$\frac{I_X}{I_A} = \frac{k_X\ [X]}{k_A\ [A]} = \frac{E_{SX}\ [X]}{E_{SA}\ [A]} \qquad (23)$$

If the reference gas A is chosen so that σ_X and σ_A are similar functions of electron energy, then E_{SX} and E_{SA} will also be similar functions of the electron energy. In this case k_X/k_A can be considered a constant.

To determine the concentration of the specie X, one has to take care that the concentration of the monitor gas A is a constant. Therefore the flow of the gas A must always be a constant fraction of the total flow that enters the reactor. At different pressures, the total density of the gas is also different. Therefore to obtain a measure of the absolute concentration of the specie X, the pressure has to be taken into account. This results in the formula:

$$[X] \propto p''\ I_X\ /\ I_A \qquad (24)$$

p" is a factor proportional to the total pressure in the reactor. The validity of this technique has been shown for various combinations of gases [5,10-15,36,37]. On the other hand, this technique does not work for all plasmas [14]. For the plasmas used in this work, it is the free fluorine concentration [F] that has to be determined. The peak most often used is the one at 704 nm.
As a reference gas Ar is in general used. Ar has an excitation energy of 13.5 eV, while F has an excitation energy of 14.5 eV: therefore one can assume that their excitation efficiency is very similar. For Ar the peak at 750 nm is most often used. In some plasmas however, the intensity at this wavelentgh is rather low, so that the signal to noise ratio is very low. In this case, the peak at 697 nm can be used. For this peak the drawback exists that with no Ar flow, its intensity is not equal to zero. In this case one can perform tests with several Ar flows and through interpolation determine the correct value of I_{Ar}. This technique is well described in ref [37].

5) Statistical design of experiments.

Statistical design of experiments is a technique to obtain a maximum of information from a certain set of tests in an efficient way [38-43]. As a consequence, the number of tests to optimize the characteristics of a process is minimized. This technique is used frequently in several industries, since a few years also in the semiconductor industry. US plasma etch equipment manufacturers rely heavily on statistical design of experiments to develop etch processes on their equipment or for finetuning existing processes, e.g. to specific layers [38,39].
To obtain the parameter set for the optimal process or to study mechanisms of a certain process, a number of tests have to be performed. It is very important to choose the parameter settings of these tests wisely as to obtain significant results with as few test runs as possible. Each extra etch test is expensive in the plasma etch business as both machine time and wafer preparation are expensive.
If a completely new process has to be developed and very little is known about it, first tests are typically performed to screen a probably useful parameter range. Most often a parameter matrix is set up. E.g. for a process with 3 variable parameters, such as gas flow, pressure and power for a plasma etching, typically 3 numerical values per parameter are determined and 3 x 3 x 3 = 27 tests are performed. However, by carefully determining the test points and applying a mathematical analysis on the test results, the same (or nearly the same) information can be obtained by less tests, e.g. only 18 tests are necessary for the example above if a quadratic model is found adequate. (The number of tests is determined by the number of parameters and the used model.) The final result is often given in the form of a formula where the result (e.g. an etch rate) is given as a sum of linear terms of the variable parameters, sometimes of quadratic terms or even terms of higher orders. The higher the order of the model, the better the agreement between model and process, but the higher the number of tests. Therefore a compromise has to be made. One of the drawbacks of statistical design of experiments is that one does not know before which order will give the best compromise.
Another big drawback of statistical design of experiments is that the analysis of the data can be wrong. Even steep decreases in the process results outside the optimal point region can lead to wrong optimization.
As for these studies the Response Surface Method (RSM) method was used, we shall dwell somewhat more on it.
The RSM method combines an experimental strategy to determine the complete test set with data analysis to generate an empirical equation which represents the results (in this context the test results are called : the reponses) of the process. The method can be applied to whatever type of process as long as the responses can be quantified and behave as a continuous function and as the parameters (often called

factors here) can be manipulated independently of one another.
Regions of abrupt changes in the behaviour of the response have to be avoided, because of their instable nature. In general, in the regions of interest the responses should behave as continuous, smooth functions to be represented by polynomial functions [39-41].
The design of an experiment to obtain the surface of the response is a fractional factorial design with three or more levels for each factor.
Most often a quadratic model is used : this model has the general form :

$$Y = b_o + \sum_{i=1}^{f} b_i X_i + \sum_{i=1}^{f-1} \sum_{j=2}^{f} b_{ij} X_i X_j + \sum_{i=1}^{f} b_{ii} X_i^2 \quad (j>i) \qquad (25)$$

in which :
Y : the response
X_i : the parameters of the process
b_{ix} : the coefficients of the polynomial
f : the total number of factors.

The most used design for processes with three parameters is of the Box Behnken type as shown in fig. 2.

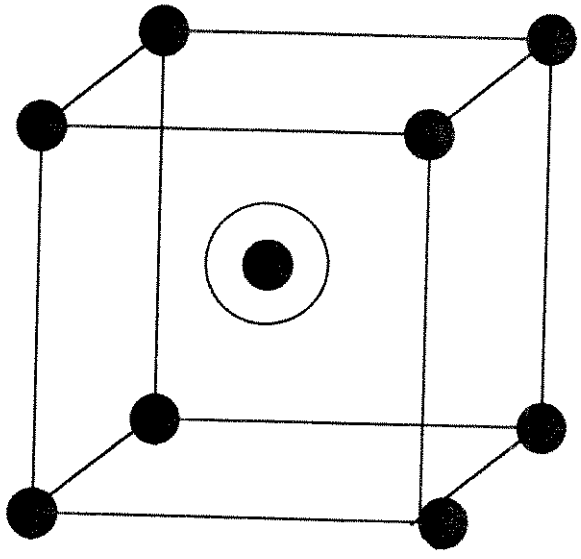

Figure 2 : Geometric Representation of Box-Behnken design [39]

These designs have repetitions of the central point to estimate the experimental error.
The coefficients b_{ix} are determined by the method of the minimal squares.

The validity of the model can be verified by evaluating the correlation factor R^2 and/or performing an analysis of variances.
The correlation factor R^2 is determined as follows :

$$R^2 = \Sigma (y_{ci} - y)^2 / \Sigma (y_i - y)^2 \qquad (26)$$

with y the average value, y_{ci} the calculated result and y_i the experimental result, therefore $0 < R^2 < 1$.
As explained in ref [40] the nearer R^2 approximates to 1, the better the model.
Analysis of variances gives a statistical indication if the difference between the observed value and the calculated value (of the fitted model) is caused by the experimental error or by a lack of fit of the model. The experimental error can be estimated through repetition of experiments for a certain parameter set. The differences between the results of these repeated tests result in a distribution (with an average and a standard deviation) of the experimental error. The error induced by the lack of fit can be calculated in the following way. One has to perform more tests than strictly necessary to determine the coefficients b_i of the equation of the model. The remaining test results can be used to calculate the average and the standard deviation of the difference between model and process.
To determine if a model is valid, the distribution of the differences between model and experiment is compared with the distribution of the experimental error. In this way one can predict with a certain probability if the error induced by the lack of fit is larger or smaller than the experimental error. A larger error induced by the lack of fit, indicates that the model is not adequate.
One must be very cautious with these results: one should also verify if the repeated test results show good reproducibility or bad reproducibility.
A first case happens when the results of the repeated tests are very similar, e.g. for plasma processes with differences < 1 %. Reproducibility of etch rates is typically ± 5 %. If e.g. an experimental result differs 3 % from the result of the fit, this error is probably an experimental error, not a lack of fit. However, because of the small difference for the repeated test, analysis of variances will probably indicate a lack of fit. The inverse can also happen : in this case the repeated test results have big differences, e.g. > 5 %. It is then well possible that the analysis of variances indicates that the fit is good, though in reality it is not so good. When one has doubt about the result of the analysis of variances, an extra reproducibility test can be performed to give more information.
Most commercially available programmes deliver the worksheet to perform the test set. After entering the test results the programme delivers the function, an analysis of variances, the correlation factor and graphical representations of the function.

One should distinguish between finetuning of a process and the development of a new process.
In the first case the parameter range to be optimized is quite small and immediately outside this small parameter range the behaviour of the process is already known. Only small excursions around a central point will be made. In this case a linear model is in general adequate. The Taguchi method is often the best technique for these cases [42,43].
In the second case, one starts in general with a screening test of a wide parameter range. Besides, the behaviour of the process is not known, or in the best case only general trends can be assumed. In this case the Response Surface Method (RSM) is often the most adequate technique. The results must always be evaluated critically, as already indicated above on the topic of analysis of variances.

6) Tungsten plug etching, a special application.

The most common application of tungsten etching is the back etching to form plugs in the via holes. The deposition of the tungsten is well reported in literature, while etching not as much. Some reports, mainly in cooperation with equipment manufacturers, describe the used processes and the problem of microloading.[44-46]
Fig. 3 shows the purpose of the etching. A tungsten layer is deposited in the via holes and on top of the insulating oxide to form a planar layer. This layer has to be etched back so that only the plugs in the via holes remain.
To obtain a good plug process, it is necessary to have a uniformly deposited tungsten layer on top of a glue layer, often TiW or TiN. It is not within the spectrum of this work to discuss this part of the processing.
The etch process must have the following characteristics:
- Good uniformity.
- Good selectivity towards oxide or glue layer.
- Good endpoint detection.
- No problems with microloading.

It is quite easy to develop processes which have the first three characteristics, but with enormous problems with the fourth.
The problem of the microloading is the following: at the moment the tungsten - oxide (or tungsten - glue layer) interface is reached, the area of material which is rapidly etched away by the process decreases dramatically: from 100% to a few % of the area. For most processes the concentration of the free fluorine (or halogen) remains the same, but as there is much less free area, the vertical etch rate will increase considerably (while in fact, the number of removed tungsten atoms per second will decrease). The small tungsten plugs etch at much higher etch rates than the blanket tungsten layer. For some processes it occurs that the tungsten is already completely removed from the plugs in one region, while in another region the blanket tungsten has not been removed completely, even for processes with good uniformities of deposition and etching [44].

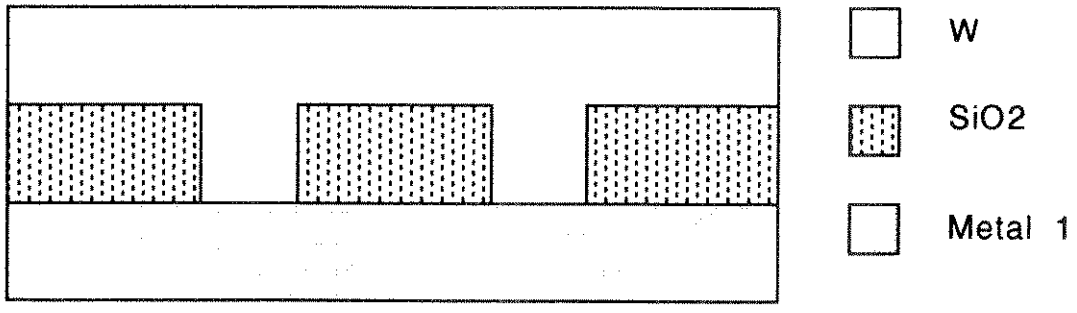

Fig 3.a : Plug formation: structure after WCVD deposition

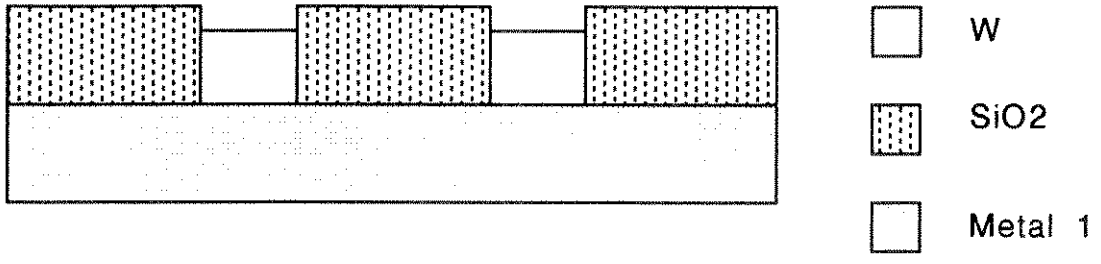

Fig. 3.b : Plug formation : structure after W back etch

Figure 3 : Tungsten back etch process to form plugs.

The solution is in general to use plasmas which etch more physically than chemically: the influence of the ion bombardment is the same on large as on small areas [45]. Therefore in general RIE plasmas are used and not PE plasmas. Often an additional gas such as argon is used to increase the ion bombardment factor [46]. Good endpoint detection is always necessary. Traditionally the F line at 704 nm is used to determine when the tungsten blanket layer has been removed.
A new technique to obtain tungsten plugs without using "chemical etching", is wafer polishing, as described in references [47,48].

References:

[1] B. Chapman, "Glow Discharge Plasmas", John Wiley and sons (1980).
[2] J. Coburn, "Plasma Etching and Reactive Ion Etching", IV Oficina Brasileira de Microeletronica, pp. 41-80, edt Mammana (1983)
[3] Mogab, "Dry Etching" in "VLSI Technology"pp 303-346, edt. Sze, Mc. Graw - Hill (1983)
[4] P. Verdonck, "Dry Etching for Integrated Circuit Fabrication", in "Processos de Microeletronica", edt. Baranauskas (1990)
[5] D. Hess, "Tungsten and Tungsten Silicide Etching in Halogenated Plasmas". Solid State Technology, April 1988, 97.
[6] Cook, "Downstream Plasma Etching and Stripping", Solid State Technology, vol 30 nr 4, 147 (April 1987)
[7] D. Flamm, J. Mucha in "Chemistry of the Semiconductor Industry", p 380.
[8] V. Mc Koy, private communications.
[9] CRC Handbook of Chemistry and Physics, 65th edition, edt: R. Weast, CRC Press Inc. (1984-1985)
[10] C. Tang, D. Hess, "Tungsten Etching in CF4 and SF6 Discharges", J. Electrochem. Soc. 131, 115 (1984)
[11] T. Bestwick, G. Oehrlein, "Tungsten Etching Mechanisms in CF4/O2 Reactive Ion Etching Plasmas", J. Appl. Phys. 66, 5034 (1989)
[12] W. Pan, A. Steckl, "Selective Reactive Ion Etching of Tungsten Films in CHF3 and other Fluorinated gases", J. Vac. Science Technol. B 6, 1073 (1988)
[13] K. Greenberg, T. Verdeyen, "Kinetic Processes of NF3 etchant gas discharges", J. Appl. Phys. 57, 1596 (1985)
[14] A. Richards, B. Thompson, K. Allen, H. Sawin, "Atomic Chlorine Concentration Measurements in a Plasma Etching Reactor", J. Appl. Phys. 62, 792 (1987)
[15] T. Daubenspeck, P.Sukanek, "Investigation and Modelling of mixed Halogen Freon/Oxygen Plasma Chemistries for Tungsten Etching", J. Electrochem. Soc. 136, 3779 (1989)
[16] A.C. Seabra, "Construção e caracterização de um equipamento de corrosão por plasma e sua aplicação na corrosão de SiO2 ", M. Sc. Thesis (1990)
[17] A. Durandet, Y. Arnal, J. Pelletier, G. Pomot, "Anisotropy and Kinetics of the Etching of Tungsten in SF6 Multipolar Microwave Plasma", J. Appl. Phys. 67, 2298 (1990)
[18] K.J. Laidler, "Chemical Kinetics", Tata-Mc.Graw-Hill.
[19] Vacuumtechniek - L. Wolterbeek Muller, Kluwer Technische boeken, (1989)
[20] D. Fischl, D. Hess, "Plasma Enhanced Etching of Tungsten and Tungsten Silicide in Chlorine Containing Plasmas", J. Electrochem. Soc. 134, 2265 (1987)
[21] M. Burba, E. Degenkolb, S. Henck, M. Tabassy, E. Jungbluth, R. Wilson, "Selective Dry Etching of Tungsten for VLSI Metallization", J. Electrochem Soc. 133, 2113 (1986)
[22] Susa, "Comparison of GaAs, tungsten and Photoresist Etch Rates and GaAs surfaces using RIE with CF4, CF4 + N2 and SF6 + N2 Mixtures", J. Electrochem. Soc. 132, 2762 (1985)

[23] F. Fracassi, J. Coburn, "Plasma-assisted Etching of Tungsten Films: a quartz-crystal Microbalance Study", J. Appl. Phys. 63, 1758 (1988)
[24] Mutsukura, Turban, "Reactive Ion Etching of Tungsten in SF6-N2 plasmas", J. Electrochem. Soc, 137, 225 (1990)
[25] Collumeau e.a., "RIE of a T-shape refractory ohmic contact for a self-aligned heterojunction bipolar transistor", J. Electrochem. Soc. 137, 671 (1990)
[26] Whetten e.a., "Reactive Ion Etching of submicrometer size features in Tungsten Thin Films", in "Tungsten and other Reafractory Metals for VLSI Applications, II", eds. Brewer, Mc. Conica, MRS 1987.
[27] S. Murarka,"Silicides for VLSI Applications", Academic Press, 1983.
[28] Adachi, Susa, "Reactive Ion Etching of Tungsten Films Sputter Deposited on GaAs", J. Electrochem. Soc. 132, 2980 (1985)
[29] W. Greene, D. Hess, W. Oldham, "Ion-bombardment-enhanced Plasma Etching of Tungsten with NF3/O2", J. Vac. Science Technol. B 6, 1570 (1988)
[30] A. Bensouala, J. Strozler, A. Ignatiev, J. Yu, J.Wolfe, "Ion Enhanced Reactive Etching of Tungsten Single Crystals and Films with XeF2", J. Vac Science Technol. A 5, 1921 (1987)
[31] Bensaoula, Grossman, Ignatiev, "Etching of tungsten with XeF2: An X-ray photoelectron spectroscopy Study", J. Appl. Phys. 62, 4587 (1987)
[32] J. Coburn, H. Winters, "Plasma-etching, a Discussion of Mechanisms", J. Vac. Sci. & Techn. 16, 391, (1979)
[33] P. Verdonck, G. Brasseur, J. Swart, "Chemical Plasma Etching of Tungsten", to be published in the Proceedings of Microcircuit Engineering 92.
[34] Fischl e.a., "Etching of Tungsten and Tungsten Silicide Films by Chlorine Atoms", J. Electrochem Soc. 135, 2016 (1988)
[35]. S. Tandon, G. Jones, "Reactive Ion Etching of Tungsten in SF6 and CF4", in "Tungsten and other refractory Metals for VLSI Applicationsd IV", Eds. Blewer & Mc. Conica (MRS Proceedings of the 1988 Workshop).
[36] J. Coburn, Chen, J. Appl. Phys. 51, 3134 (1980)
[37] P. Verdonck, P. Degeyter, J. Swart, "Actinometry and its Application on Polysilicon Etching in a Magnetically Confined Reactor", Proceedings of the VII Congresso da Sociedade Brasileira de Microeletronica (1992)
[38] W. Ostrout, S. Hunkler, S. Ward,"Enhanced Process Control for Submicron Contact Definition", Proceedings of SPIE Vol. 1392, eds. Bondur, Turner (1991), 151.
[39] M. Jenkins, M. Mocella, K. Allen, H. Sawin,"The Modelling of Plasma Etching Processes using Response Surface Methodology", SST, April 1986, 175.
[40] G. Box, W Hunter, J. Hunter,"Statistics for Experimenters: an Introduction to Design, Data Analysis and Model Building", John Wiley & Sons, 1978.
[41] G. Box, N. Draper, "Empirical Model Building and Response Surfaces", John Wiley & Sons, 1987.

[42] G. Taguchi, "Introduction to Quality Engineering", Asian Productivity Organization, Tokyo 1986.
[43] P.J. Ross, "Taguchi Techniques for Quality Engineering", Mc. Graw - Hill, 1988
[44] Saia, Gorowitz, Woodruff, Brown, "Plasma etching methods for the formation of planarized tungsten plugs used in multilevel VLSI metallizations", J. Electrochem. Soc, 135, 936 (1988)
[45] Miller, Frazier, Su,"Controlling tungsten etchback on submicron devices", MMT, January 1992,28
[46] Riley, Clark,"Integrated chemical vapor deposition and plasma etchback of tungsten in a multichamber, single-wafer system",J. Electrochem. Soc. 138, 3008 (1991)
[47] C.W. Kaantu et.al. in the Proceedings of the VLSI Multilevel Interconnect Conference (VMIC), New York 1991, 199; IEEE (1991).
[48] R. Kolenkow, R. Nagahara,"Chemical-Mechanical Wafer Polishing and Planarization in Batch Systems", SST 35, June 1992, 112.

Appendix II : Etch Processes in the SWAFER.

INDEX

Appendix II : Etch Processes in the SWAFER.

Introduction.

The use of tungsten as material in Integrated Circuit fabrication is becoming more and more important. The main application at the moment is the use of tungsten plugs. To obtain these structures, in general an etch back step is used, as explained in appendix I. Another potential application is tungsten as interconnect or gate material. One of the problems is the relatively low selectivity of tungsten to resist for anisotropic processes.
In the SWAFER anisotropic profiles were obtained for polysilicon, with good selectivities towards silicon dioxide and resist. Therefore, it was only natural to try to obtain a process with vertical tungsten walls and good selectivity towards resist (and towards oxide).
As tungsten back etching is the most applied etching of tungsten, a process for this application was developed. During these developments, several phenomena were observed and studied to model the plasma etching of tungsten and to reduce the contradictions found in the literature, as reported in appendix I.

1) Equipment.

A schematic drawing of the SWAFER is shown in fig. 1. Etch processes were performed in three versions of this equipment: a manually loaded system and two automatically loaded systems.
The special characteristic of this equipment is the applied power. Power is applied at 25 kHz, it is an audio-frequency (AF) plasma that is formed, and not a radio-frequency (RF) plasma, typically at 13.56 MHz, which is used in most etch equipment.
Power can be applied at both electrodes, while leaving the other electrode floating or grounded. It is even possible to apply power simultaneously at both electrodes in a controlled rate.
The matching network of this system is extremely simple: a transformer with several taps is placed between the generator and the blocking capacitor. The optimum tap was found by maximizing the load power to forward power ratio. The impedance of the plasmas turned out to be in the range of 1000 to 1600 Ohm.
The lower electrode is formed by a central aluminium disc, with a carbon ring around it. When a wafer is placed on the electrode, it rests only on the aluminium part, covering it completely, so the plasma will not sputter aluminium away from the lower electrode. There is no contact between the carbon ring and the wafer.
The temperature of the lower electrode can be controlled. Unless mentioned otherwise, the temperature of the coolant is 15°C.

The upper electrode is made of aluminium. The walls are formed by non-conductive material: quartz in the manual and the third system, anodized aluminium in the second system.

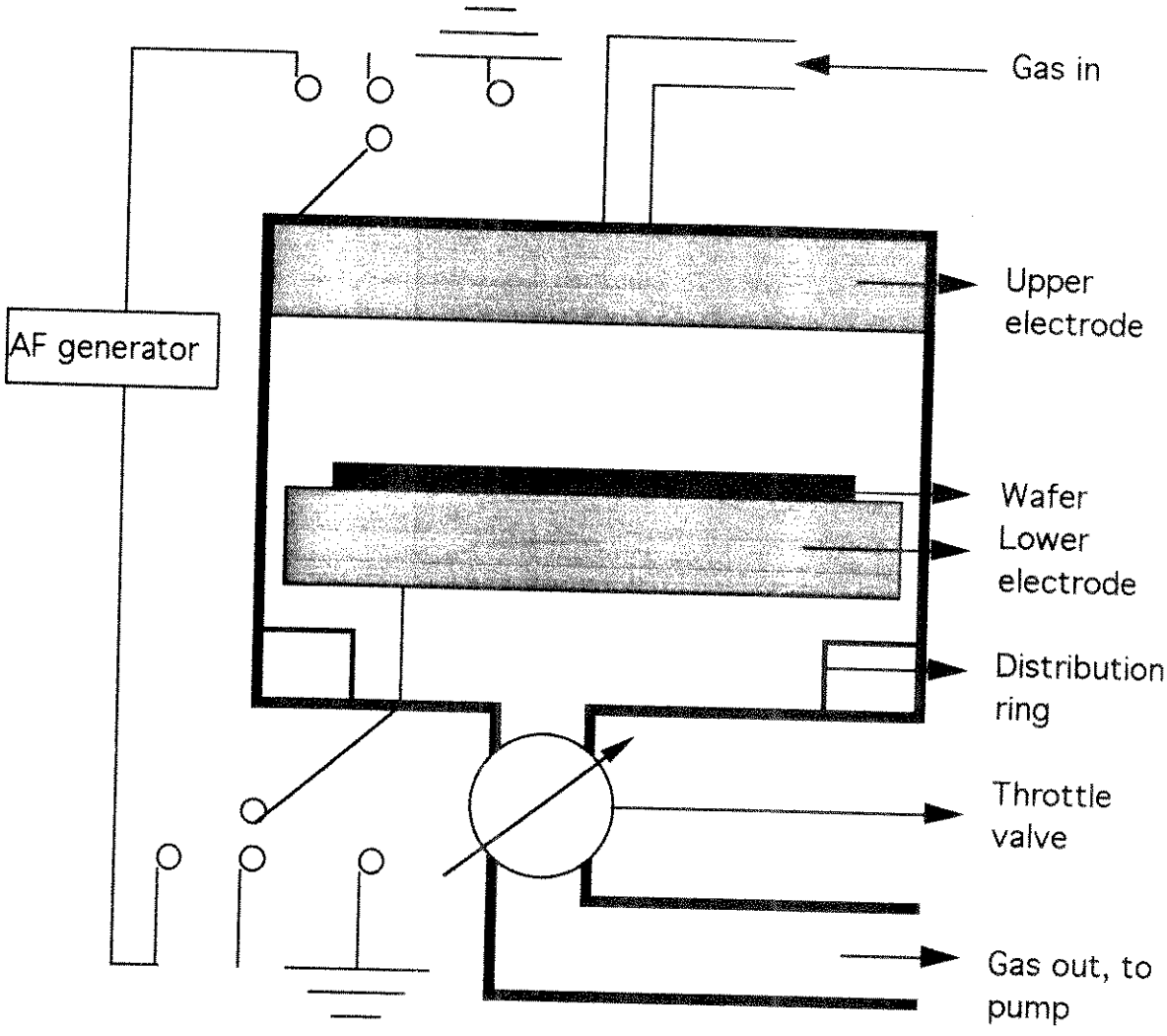

Figure 1 : Schematic drawing of the SWAFER.

Both DC and AC voltages are constantly monitored on the powered electrode. For these tests only two etch modes were investigated: Reactive Ion Etch (RIE) mode, when the lower electrode is powered and the upper grounded and Plasma Float (PF) mode, when the upper electrode is powered and the lower electrode is left floating.
The use of 25 kHz is not very common. There are not much investigations done for these plasmas.
The main drawback is that the plasma is not a continuous plasma: it is extinguished each time the AC voltage crosses the zero volt level. So, in a certain way it can be considered an intermittent DC plasma. While an RF plasma is mainly a capacitive plasma, an AF plasma is mainly resistive.

As a consequence, coupling through highly resistive (e.g. non conducting) samples is very difficult. Therefore one must not cover the powered electrode completely.
The main advantage is that the energy of the ions will also be enhanced by the AC voltages, not only by the DC bias voltage. Therefore also negative ions can play an important role in these etchings. This explains the high etch rates of polymers in oxygen plasmas in these equipment. In RIE mode, this enhanced bombardment has 3 main consequences on the process characteristics : the profiles are vertical, but the etch rates of oxide and photoresist are rather high [1], resulting in low selectivities.
Radiation damage is expected to be higher than in RF systems, but CV measurements done on devices etched in the SWAFER showed none of this. The influence of plasmas on radiation damage is not very clear. A new theory says that the energy of the incoming ions is not the most important cause of radiation damage, but rather the current of the incoming electrons [2]. This explains why in Magnetically Enhanced systems, the radiation damage is much higher. For most practical purposes the radiation damage is not very important because in the processing of an integrated circuit, etch steps are always followed by high temperature steps : the sintering step being often the last step in an IC production process.
Another advantage of AF plasmas is the use of a simple transformer as matching network. The plasma impedance of AF plasmas does not change much with the process parameters, only the etch mode has considerable influence. Therefore, a fixed transformation value can be chosen for each etch mode, no other changes are necessary. So only a few taps on the transformer must be accessible, no continous change is needed, unlike the continuous change of the capacitances in RF plasma matching networks.

2) Etch tests on other films.

The equipment has been developed for etching of polymer, silicon nitride and polysilicon films.
As the etch mechanisms of tungsten and polysilicon etching are quite similar, as reported in the literature [3-15], data from polysilicon etching are also important for tungsten etching.
The investigated parameter range is: gases : SF_6 and NF_3, and several mixtures with O_2, 10 - 200 sccm total gas flow, pressure : 100 - 200 mTorr, Power : 50 - 150 W, etch modes : RIE and PF.
The following characteristics were investigated: polysilicon etch rate, selectivity of polysilicon towards photoresist, selectivity of polysilicon towards oxide, wall profile.
General trends are the following.
In RIE mode, the etch rate has a maximum at an intermediate oxygen flow. When etching with pure SF_6, the etching has an inverse Bull's eye non-uniformity (etch rate higher in the center of the wafer than at the border), when adding oxygen

the non-uniformity is of the Bull's eye type (etch rate at the center lower than at the border).
Selectivities towards photoresist are of the order of 1:1 and decreasing with increasing oxygen flow.
Selectivities towards thermal oxide are of the order of 2.5:1.
The etch rate of a NF_3-O_2 plasma is in general 50% higher than that of a SF_6-O_2 plasma.
The wall profile is anisotropic.
In PF mode, a maximum of the etch rate exists at an intermediate oxygen flow. The maximum selectivity towards oxide is also around this maximum and is of the order 30:1.
Selectivities towards photoresist are also extremely high, often more than 50:1 and increase with increasing pressure.
The etch profile is purely isotropic.
From these tests it is clear that in RIE mode, polysilicon etching is considerably ion bombardment enhanced, while in PF mode, the etching is chemical.
Polysilicon etch tests were performed in the same parameter range as for the tungsten etchings described below, both for SF_6-O_2 and NF_3-O_2 mixtures. In this way the etch rates can be compared, the type of non-uniformity and the mechanisms of the model as proposed in appendix I can be controlled.
Results and discussion are reported in appendix V.

3) Etch tests on tungsten films.

For these tests tungsten films deposited in four different equipment were used: 3 CVD equipment (of different manufacturers) 1 sputtering equipment. Wafer preparation was also different:
For the first CVD equipment, tests were performed on 125 mm (100) wafers which received the following treatment:
- deposition of 500 nm of PECVD oxide
- sputter deposition of 150 nm of TiW
- CVD deposition of 1000 nm of tungsten: the tungsten was deposited at 420°C, its density is 19.35 kg/dm^3 and its resistivity is 10 µOhmcm;
- etching of the back side of the wafer to remove the tungsten.
When distinction is necessary, this tungsten will be called W_I;
- patterning with Shipley 1713 photoresist, using a wafer stepper, followed by a 30 minutes 95°C post bake.
Specific processes, such as DUV hardening, were added for some samples and will be mentioned when used.

For the second CVD equipment tests were performed on 125 mm (100) wafers which received the following treatment:
- thermal oxidation of 190 nm of oxide;
- sputter deposition of 80 nm of TiN;
- CVD deposition of 1000 nm of W : deposition temperature 445°C, the density of the W is 16 kg/dm^3, the resistivity is 10µOhmcm.

When distinction is necessary, this tungsten will be called W_{II}. The deposition proved not to be very reproducible : thicknesses between 1000 nm and 1100 nm were measured;
- lithography process: JSR i-line IX resist was patterned by a projection printer exposure system, with light field mask with 5% coverage. A 1 minute 95°C hot plate postbake was applied. The main difference with the former lithography process is that the resist walls are not very steep in this case, an angle of typically 75° is obtained. Two series were prepared: 1 with 1.1 µm thickness, which is used for most processes, and 1 with 1.4 µm thickness.

For the third CVD equipment tests were performed on 125 mm (100) wafers which received the following treatment:
- thermal oxidation of 190 nm of oxide;
- sputter deposition of 100 nm of Ti;
- sputter deposition of 80 nm of TiN;
- CVD deposition of 1000 nm of W; the deposition of W ocurred at 425°C, the density of the W is 19.35 kg/dm^3, the resistivity is 10µOhmcm.
When distinction is necessary, this tungsten will be called W_{III};
- lithography process: 1.1 µm of JSR i-line IX resist was patterned by a projection printer exposure system. A 1 minute 95°C hot plate postbake was applied. There has also been an edge bead removal; therefore, very little resist remains at the border of the wafer.

For the sputtered tungsten, tests were performed on 125 mm (100) wafers, which received the following treatment:
- thermal oxidation;
- sputter deposition of 150 nm of TiW;
- sputter deposition of 200 nm of W;
- patterning with Shipley 1713 photoresist, using a wafer stepper, followed by a 30 minutes 95°C post bake.

The following descum process was used for some wafers: equipment : magnetron enhanced etcher MRC MIE 720, oxygen flow : 40 sccm, what results in a pressure of approximately 5 mTorr, RF power: 500 W, time : 10 seconds.

Stripping of the wafers after etching was in general done in an Emergent Technologies NORD afterglow plasma stripping equipment. Gas used: only oxygen, flow : 1000 sccm, pressure: 1 Torr, microwave power : 900 W, temperature : 250°C, time: endpoint + 20% overetch time.
For some tests the SWAFER itself was used as a stripper.
To determine the etch rates of tungsten (r_W) and photoresist (r_{PR}), step heights were measured before etching, after etching and after stripping of the resist. A SLOAN DEKTAK II was used to determine the step heights. For the wafers patterned with a wafer stepper (wafers of tungsten type W_I) the step heights were always measured at the same structure : the second line of an array of 15 um line-spaces. In this way the possible error induced by

the influence of "internal loading effects" (the dependence of etch rate on the line-space dimensions of the pattern) was avoided. For wafers patterned with the projection printer (wafers of tungsten type W_{II} and W_{III}), we used a large square of 150 um by 150 um for step height measurement as shown in fig. 2.

a)

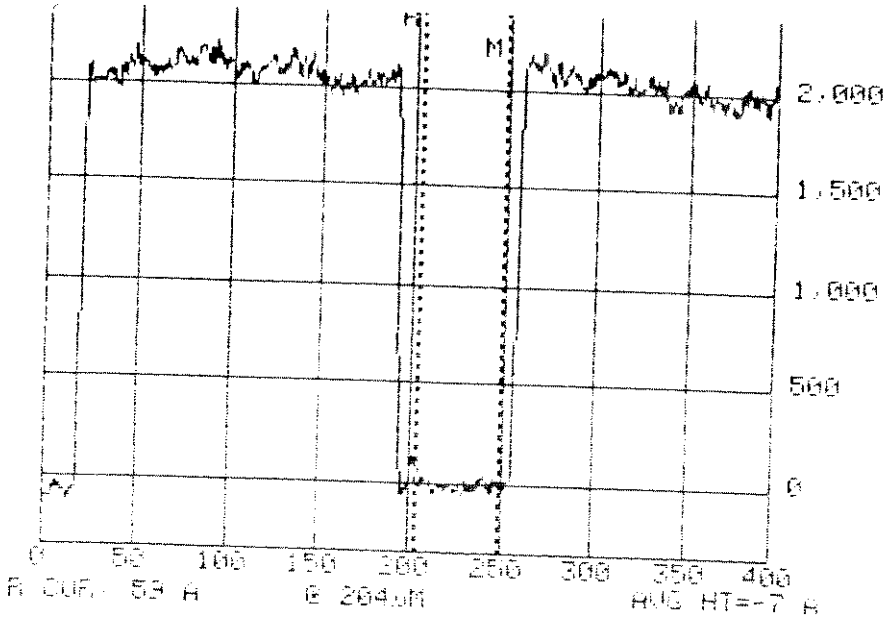

b)

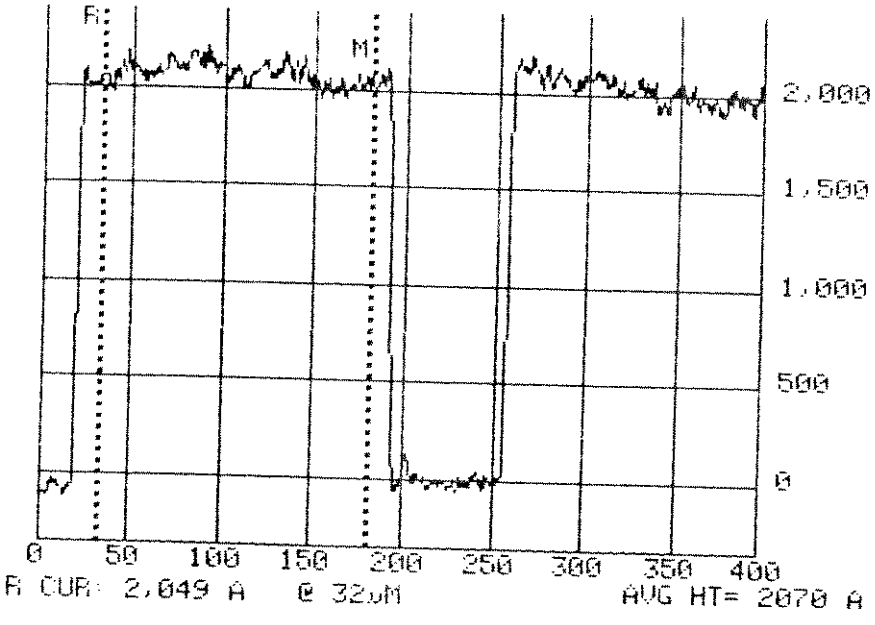

Figure 2 : Step height meter profiles, after levelling; determination of height of bottomline (a) and top (b).

After levelling, the average height outside the square is automatically measured as shown in fig. 2.a, then the averaged height inside the square is measured as shown in fig. 2.b and then the difference between both values is calculated. In this way, the surface roughness influence is decreased very much, decreasing the error of the measurement to less than 10 nm. By measuring twice at each point, we assume that the final error will be less than 7 nm.

There are two ways to determine the etch rate of the W of a non patterned wafer:
1) by the difference of weight dw of the wafer.
$dw = w_1 - w_2 = \rho\ A\ r_W\ t \Rightarrow r_W = (w_1 - w_2)\ \rho\ A\ /\ t$
with w_1, w_2 : weight of the wafer repectively before and after etching; a microbalance with resolution of 0.0001 g was used to weigh the wafers.
ρ : density of the tungsten.
For W of the W_I and W_{III} type wafers : $\rho = 19.35\ kg/dm^3$,
for W of the W_{II} type wafers $\rho = 16.0\ kg/dm^3$
A : area of 125 mm wafer = 123 cm^2, t : etch time.
2) by the difference in sheath resistance of the layer.
With a four point measurement probe, it is possible to measure the sheath resistance of a layer.
$R_{sq} = R_{sp} / t_1$
with R_{sq} : the sheath resistance of the layer, which is measured;
t_1 = thickness of the layer.
R_{sp} is the resistivity of the material. For our tests a value of 10 µOhmcm was used, based on data furnished by the equipment manufacturers and by measurements performed together with researchers at IMEC.
Therefore :

$t_{11} - t_{12} = R_{sp}\ (\ 1/R_{sq1} - 1/R_{sq2}\ )$ or
$r_W = [R_{sp}\ (\ 1/R_{sq1} - 1/R_{sq2}\ )\ ]\ /\ t$

with t the etch time.
On the contrary of the density, the resistance of a thin film is quite different from the bulk resistivity. It is dependent on the deposition equipment and process and can even change within the film. Therefore one has to be careful in using this measurement methode.
A 4 point spreading resistance measurement probe, with automatic wafermapping was used. Test diameter was 115 mm, with 45 test points. The system itself calculates the average value of Rsq, excluding values which differ more than 3 σ from the average (these were mainly values at the border of the wafer). This average value was used to calculate the average etch rates, as they are reported further on in this report. For the calculation of the

uniformities of the processes, the values which differed more than 3 σ were not excluded.

The definition of the uniformity (U) of the etch rate of a certain film is the following : lowest etch rate measured on the wafer divided by the highest etch rate measured on the wafer.
The selectivity of the etching of one film to another film is defined by the ratio of the average etch rate of the first film, in our case always tungsten, to the etch rate of the second film, most often photoresist or oxide.

3.1) Processes with SF_6-O_2 mixtures

As no tungsten etching in a 25 kHz plasma was reported, the first tests served to obtain data to verify if the proposed mechanisms of formation of WF_6 and WOF_4 for 13.56 MHz plasmas, as described in appendix I and refs [3,6-9], are also valid for this equipment. These data will be analysed and discussed in appendix V. At the same time the possibility of an anisotropic process with good resist selectivity was investigated to obtain an etching with vertical walls. It is also important to determine if the reproducibility of tungsten etchings in this equipment is good enough and if preliminary processes influence the etch rate. As in the literature the influence of an oxide is reported to inhibit the etching [16], this must be investigated. All tests were performed on W_I type wafers.

3.1.1) Determination of etch rates, uniformities and selectivities in RIE mode.

Some wafers suffered an oxygen plasma descum process as described above.
Some wafers received a DUV curing step, standard IMEC procedure, followed by a hard bake of 140°C, 30 minutes. As the wafers had received already a post bake step of 95°C, 30 minutes, the DUV step step will be less efficient to increase the resist resistance for these wafers than for wafers which did not receive a post bake step before DUV curing.
As the resist covered the outer 10 mm of the wafers, step height measurements were done only at 2 points at approximately 12 mm from the edge of the wafer and in the center of the wafer. Therefore the uniformity of the tungsten etch rate (U) and the photoresist etch rate (U_{PR}) given below is only valid as an indication, not as the exact value.
The values for the etch rates are the averages of the etch rates at these three points, expressed in nm/min.
The grains of the CVD deposited tungsten are large, therefore, the surface is rather rough. This makes step height measurements difficult and less accurate. For wafers of the W_I type, the estimated error of step height measurements at these surfaces is ± 20 nm. For etch tests

with 2 minutes duration, the error on the tungsten etch rate is ± 10 nm/min, and on the resist etch rate ± 30 nm/min. These are large errors, which accumulate when determining the uniformity. Also for this reason, the values of the uniformities as mentioned below must be considered as qualitative.

The first tests were all done at 150 mTorr, pressure used for optimal polysilicon processes, 50W AF power in RIE mode, during 2 minutes. Total flow is always 100 sccm.
The results of these tests, with their process conditions, are shown in table I:

Table I: results of tests to determine etch rates, uniformity and selectivity for SF_6-O_2 mixtures in RIE mode.

Resist treatment	Test series	SF_6 flow [sccm]	O_2 flow [sccm]	r_W [nm/min]	U	r_{PR} [nm/min]	U_{PR}	S
A	I	100	0	146	0.89	115	0.75	1.20
B	I	100	0	140	0.79	133	0.81	1.05
C	I	100	0	142	0.97	132	0.66	1.10
D	I	100	0	130	0.79	125	0.87	1.04
A	II	100	0	124	0.83	101		1.10
A	III	100	0	119	0.82	137		0.87
E	III	100	0	104		116		0.90
E	III*	100	0	120	0.82	118		1.02
A	I	75	25	157	0.75	175	0.69	0.90
A	II	75	25	157	0.71			
A	I	70	30	171	0.77	199	0.94	0.86
A	II	60	40	168	0.80	180		0.83
A	I	50	50	190	0.88	253	0.88	0.75
C	I	50	50	185	0.79	251	0.87	0.74
D	I	50	50	174	0.75	151	0.84	1.20
A	II	50	50	177	0.84	199		0.79
A	II	40	60	168	0.89	235		0.66
A	I	25	50	166	0.78	323	0.81	0.50
A	II	25	75	155	0.89	286		0.49

Where :
A : the standard resist treatment, as descibed above;
B : the standard resist treatment with an extra descum step just before etching;
C : the standard resist treatment with an extra DUV curing step just before etching;
D : the standard resist treatment with extra DUV curing step and descum step just before etching.
E : the standard resist treatment, without post bake, followed by DUV curing and post bake of 30 minutes at 140°C.

The influence of the oxygen content on the etch rate for wafers of the first test series (I) with standard resist treatment is shown in fig. 3.

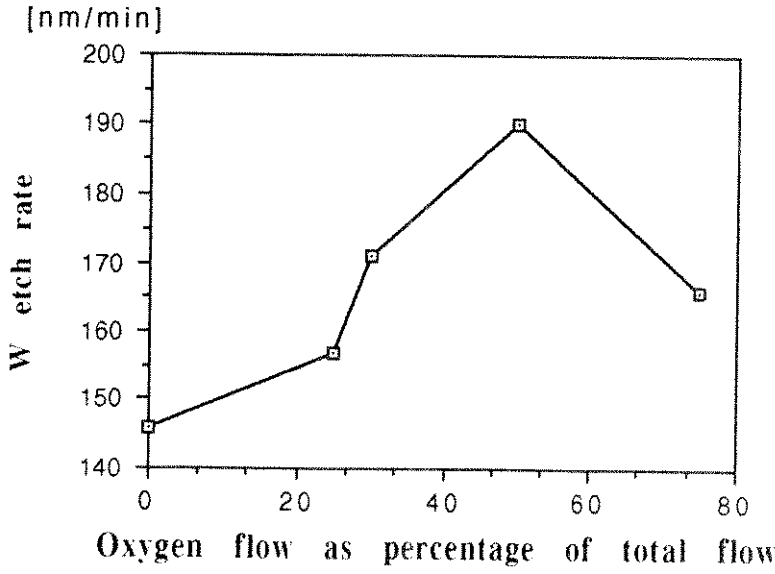

Figure 3 : Tungsten etch rate as a function of oxygen flow for SF_6-O_2 mixtures in RIE mode, series I.

The nonuniformity of the tungsten etching is always in the form of a Bull's eye.
These tests show firstly that there is no influence of the preliminary processes of plasma flashing and DUV curing on the etch rates and secondly that the reproducibility of the etchings is good. The differences in etch rate between the equal processes are always within the estimated error, as calculated above. Only for the test with 50 sccm SF_6 and 50 sccm O_2, treatment D, test series I, the resist etch rate is much lower than for other processes. Other tests showed that this result was not reproducible (see below 3.1.2).
We must remark that the fact that DUV curing has no effect on the resist etch rate in these experiments, is not conclusive as it has to be performed before any post bake.
But we can certainly conclude that the plasma flash does not form a tungsten oxide layer which could inhibit the etching, at least in this etch mode and for these processes.
The tungsten etch rate as a function of the oxygen content behaves in the same way as for 13.56 MHz plasmas. (Further tests to confirm this statement were done later and are reported below.)

For test series II, process and measurement procedures are the same as for test series I, only the etch rate of the photoresist was measured only in the center of the wafer as earlier processes showed that selectivity was lowest at that location. (Therefore it is normal that in this table the indicated S is lower than the average tungsten etch rate divided by the resist etch rate in the center, as etch tungsten etch rate in the center is lower than in the rest of the wafer.)

The tungsten etch rate as a function of O_2 flow for test series II is shown in fig. 4.

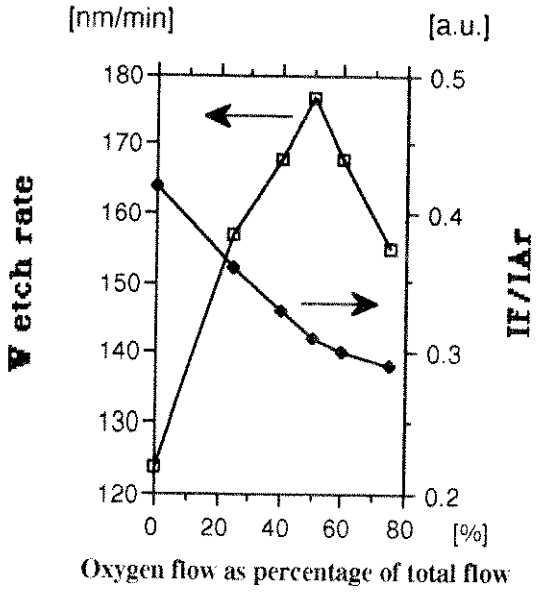

Figure 4 : Tungsten etch rate and I_F/I_{Ar} ratio as a function of oxygen flow for SF_6-O_2 mixtures in RIE mode, series II.

In comparison with the results of test series I, the absolute etch rates are lower. The W etch rates decrease continuously in time, from run to run, albeit at a very slow rate. We think that a passivation effect occurs which has as a consequence a decrease in etch rates. But the results of the selectivity tungsten to resist are surprisingly corresponding. In this way the reproducibility of these etchings is good.
At the same time actinometry meassurements were performed: the monitored emission lines were : 704 nm for F and 697 nm for Ar. The I_F/I_{Ar} ratio is also shown in fig. 5. The intensity of the spectrum is very low, the signal to noise ratio of the spectral lines is therefore also rather bad. But even so, one can observe that the I_F/I_{Ar} ratio does not behave at all as the etch rate. It has been reported [17] that actinometry can for some systems not be applied at low frequency plasmas. It is our belief that this is also the case for this system and these plasmas. No further actinometry measurements were done on the SWAFER. This does not mean that emission spectroscopy can not be used as an endpoint monitoring technique in this equipment as shown further on in this appendix.

For test series III the lithography process was different: standard patterning with Shipley 1713 photoresist, except post bake.

Split the lot in 2 groups:
- group 1: receives the standard post bake of 95°C during 30 minutes.
- group 2 receives a DUV curing and a postbake of 140°C during 30 minutes.

In these tests the influence of the DUV curing and extra hard bake step was investigated. The results are shown in table I. For the test marked with III*, the etch time was 4 minutes, instead of the normal 2 minutes.
The main conclusion is that DUV curing does not have much influence on the selectivity. During the preliminary investigations on polysilicon etching, the same conclusion had been drawn. Therefore, DUV curing has been discarted as a solution for increasing selectivity in this etch equipment.

3.1.2) Tests determining the tungsten wall profile in RIE mode.

Once the etch rates of several processes are determined, it is possible to investigate the profile of the etched tungsten walls.

The following tests used the same parameters as above: 150 mTorr pressure and 50 W AF power in RIE mode. Table II shows the additional process conditions for these wafers.

Table II : Process conditions for tests for the determination of the wall profile.

Wafer nr	SF_6 flow [sccm]	O_2 flow [sccm]	time
1	100	0	5'
2	100	0	6'45"
3	70	30	4'30"
4	50	50	5'30"

All wafers showed profiles with angles well over 80 degrees. No undercut was observed, also not of the TiW, when it was removed. Linewidth loss is always less than 0.2 um.
The specific results of these etchings are:
Wafer 1 (fig. 5): at the edge of the wafer the tungsten was completely removed. In the center the remaining tungsten has a rough surface. It is also possible to see the interface between the tungsten and the photoresist at the cleaved lines. The roughness of this interface, which is the original roughness of the deposited tungsten film is the same as the roughness of the etched film. As expected of an anisotropic etching, it does not smooth the film.
Wafer 2 (fig. 6): the tungsten is removed all over the wafer, remainders of the thicker tungsten grains still cover approximately 5% of the PEOX surface in the center of the wafer. An extra step of 1'30"removed all remaining tungsten. All the resist was also removed. As the selectivity towards the resist is around 1:1, the process is expected to

planarize well the surface of the tungsten lines: this is also what is observed: the surface of the tungsten lines is flat and smooth.

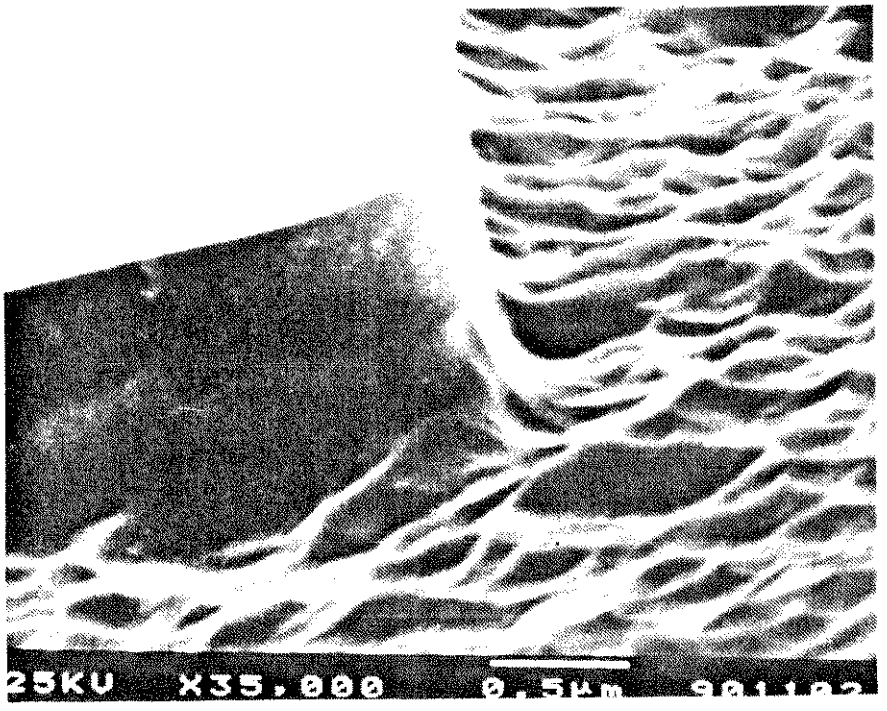

Figure 5 : Tungsten surface and wall profile for partial etching with a pure SF_6 plasma.

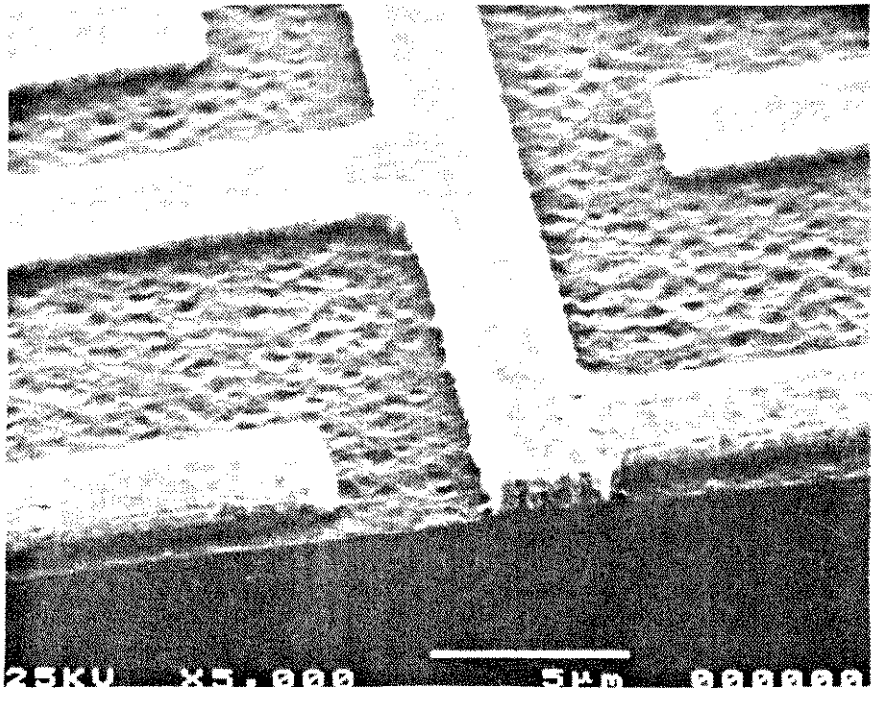

Figure 6 : Tungsten structures upon a PECVD oxide for complete etching with a pure SF_6 plasma.

The tungsten to PECVD oxide selectivity proves to be rather low: therefore the surface roughness of the tungsten film is transferred, though less pronounced in the underlying oxide. Comparing roughness in the original tungsten film and now in the PECVD oxide film, a selectivity of 2:1 can be estimated. One can observe that a slight negative angle is formed in the tungsten with this etch process.
Wafer 3 (fig. 7): the etching through the tungsten is not complete: a rough surface, very similar to wafer 1 remains. As could be expected from the lower resist selectivity of this process, more photoresist has been removed.

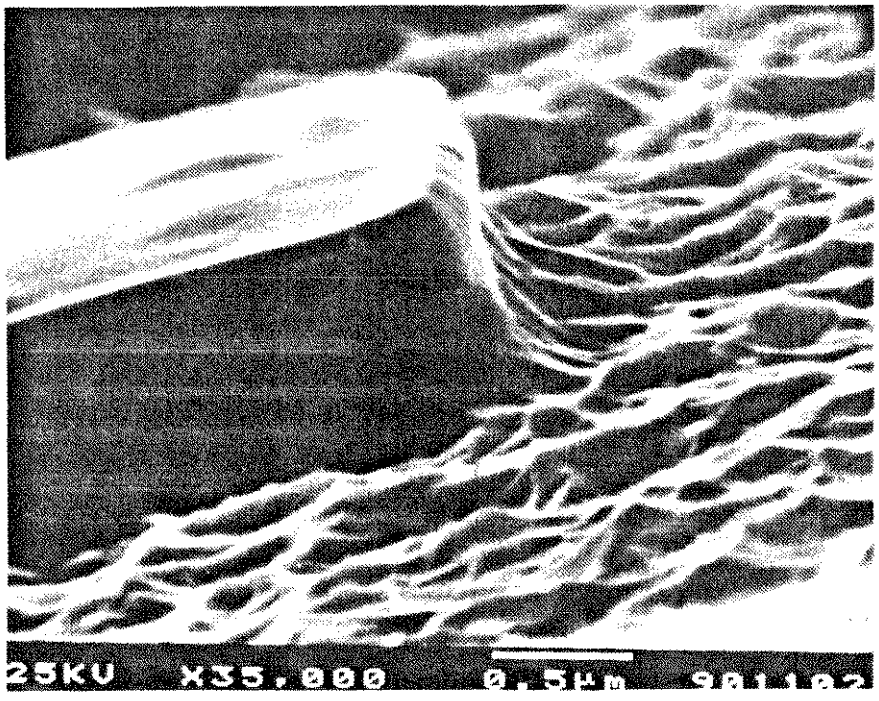

Figure 7 : Tungsten surface and wall profile for partial etching with a SF_6 - 30% O_2 plasma.

Wafer 4 (fig. 8): the etching through the tungsten is not complete: a rough surface as for wafers 1 and 3 is observed. At the edge of the wafer, the tungsten has nearly been cleared completely. Because of the high resist etch rate, the resist has been removed completely.
The resulting lines have vertical walls, very close to 90 degrees and the surface is quite smooth, though a little bit less than wafer 2: the 100% SF_6 process has a selectivity towards photoresist much closer to 1 than the 50% SF_6 - 50% O_2 process.
These results show that it is possible to obtain an anisotropic etching with SF_6 based mixtures, even with a 100% SF_6 plasma. This shows that it is not necessary to form a tungsten oxide as a protective layer against undercut at the sidewalls. As we knew already that SF_6 based plasmas etch polysilicon anisotropically in this equipment and tungsten is considered to etch more easily in an anisotropic way than

polysilicon, this result is not surprising. On the other hand, it is different from the results reported at 13.56 MHz [5]. It is clear that with this 25 kHz plasmas the ion bombardment factor is much more important than in 13.56 MHz systems. The ion bombardment enhances the etch rate so much that no undercut is observed.

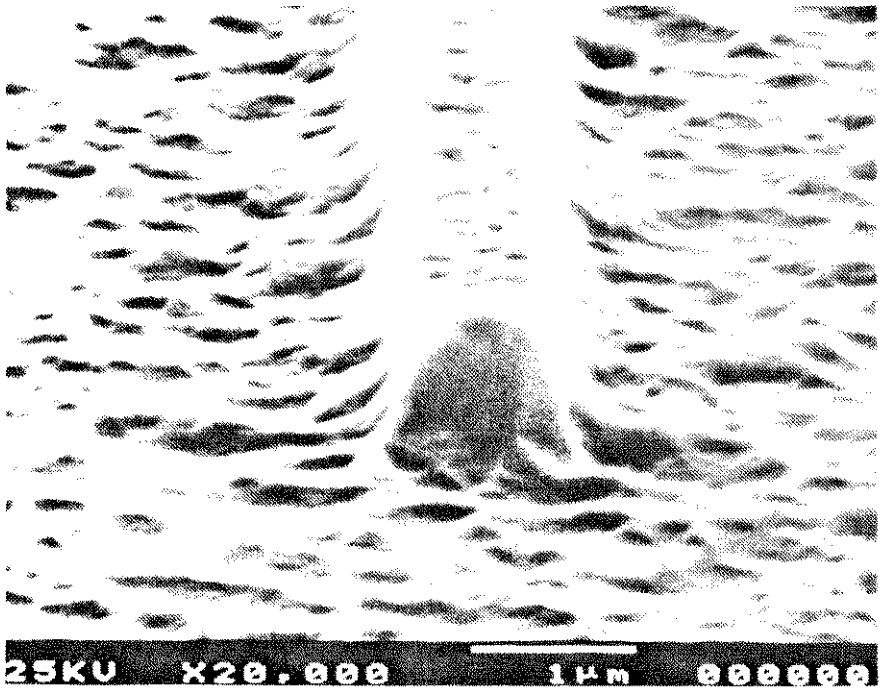

Figure 8 : Tungsten surface and wall profile for partial etching with a SF_6 - 50% O_2 plasma.

For the use of tungsten as metal 1, there is a fundamental problem with the photoresist erosion during the etching. As photoresist thickness is of the same order of magnitude as the tungsten thickness, the selectivity of the process has to be higher than 1. In practical applications, because of topography in the underlying layers, it has to be higher than 2. This value could not be reached with the etch processes and photoresist processes used until now. As neither a DUV curing step did help to increase the selectivity of the tungsten to the resist, this is a serious problem. It means that another type of mask, or a thicker resist layer has to be used to obtain vertical wall profiles in 1 µm thick tungsten layers over topography.
However these processes can be used for the etching of tungsten gates, for which the thickness is typically 0.5 µm.

3.1.3) Etch tests in PF mode.

The following process was performed : 50 sccm SF_6, 25 sccm O_2, pressure : 200 mTorr, power : 50W in PF mode, time: 4 minutes.

The etch rate is less than 7.5 nm/min all over the wafer. It was very hard to measure the step heights of the grooves, as they were of the same order of magnitude as the grain size. Therefore, this result is not very accurate. The main conclusion is that the etch rate of tungsten in PF with SF_6 gas is very low.
After having obtained several results with NF_3-O_2 plasmas in PF mode, a new test was done with an SF_6-O_2 plasma in the second SWAFER. The power was increased to 150W, leaving the other etch parameters the same. There was no resist on the wafer.
Process: 50 sccm of SF_6, 25 sccm of O_2, pressure: 200 mTorr, power: 150W in PF mode.
1) Time : approximately 2 minutes
2) Extra 4 minutes etching
3) Extra 10 minutes etching
Between the processes, the wafer was measured with an automatic 4 point resistance probe. These measurements indicate a constant etch rate of approximately 30 nm/min. (For the NF_3-O_2 process with 50W in PF mode, the etch rate is 40 nm/min in the second SWAFER equipment.)

3.2) Processes using NF_3 - O_2 mixtures in RIE mode.

3.2.1) Determination of etch rates, uniformities and selectivities in RIE mode.

The same W_I type of wafers were used as in test series I and test series II with SF_6-O_2 mixtures and also the same measurement procedures were used. Pressure was always 150 mTorr, AF power 50 W and etch time 2 minutes. The results are shown in table III.

Table III: Results of tests to determine etch rates, uniformity and selectivity for NF_3-O_2 mixtures in RIE mode, for tungsten of the W_I type, in the manual SWAFER.

NF_3 flow [sccm]	O_2 flow [sccm]	r_W [nm/min]	U	r_{PR} nm/min]	S
100	0	254	0.85	299	0.85
75	25	262	0.89	364	0.72
50	50	247	0.87	380	0.65
25	75	141	0.80		

The influence of the oxygen content on the etch rate is shown in fig. 9.
The etch rate of NF_3 is much higher than the etch rate of SF_6. This can be explained by the fact that the dissociation of the NF_3, molecule into free fluorine atoms is much faster than of the SF_6 molecule (see appendix I). Fig. 9 shows also clearly that the effect of the oxygen content is quite different than for SF_6. As NF_3 dissociates more easily, the effect of the oxygen addition is certainly much less. It

could be very well possible that because of the higher fluorine generation in NF_3 plasmas, the fluorine generation is not anymore the etch rate limiting mechanism. This will be discussed in more detail in appendix V.

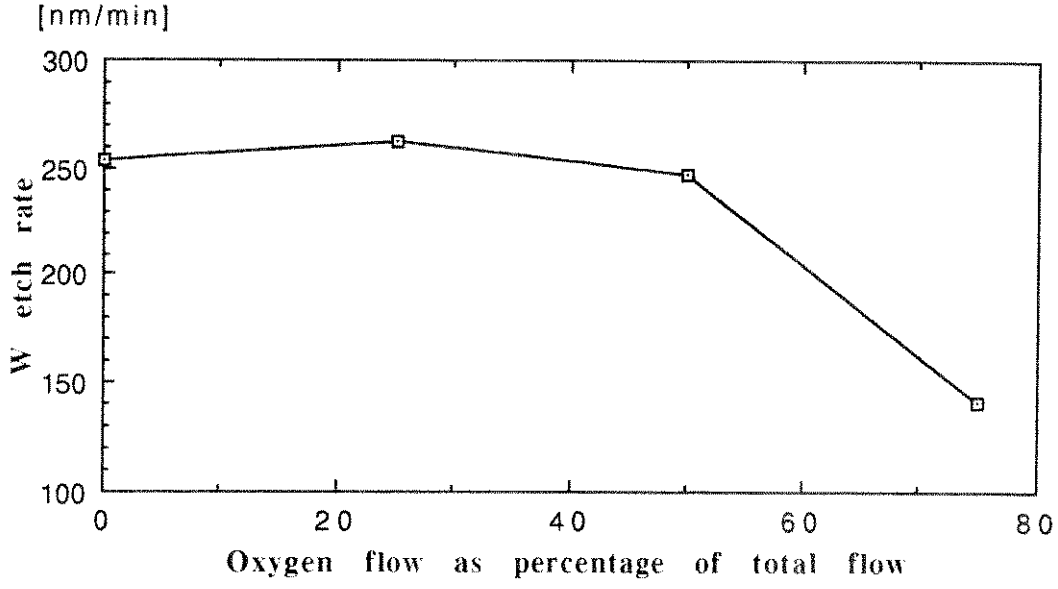

Figure 9 : Tungsten etch rate a function of oxygen flow for NF_3-O_2 mixtures in RIE mode, for tungsten of the W_I type, in the manual SWAFER.

Only in the RIE mode, the addition of oxygen does not dramatically increase the free fluorine concentration.
At higher oxygen contents, the dilution effect has its effect and decreases the etch rate.
The etch rate limiting mechanisms are described in appendix V, section 2.2.2.2.
The etch rate of the photoresist is much higher in these plasmas than for SF_6 plasmas, it increases more than the tungsten etch rate, therefore the selectivity of tungsten to photoresist drops with more than 20%. This can be explained by the increase of the AC voltages. The AC voltages as a function of oxygen content are shown for both SF_6 and NF_3 plasmas in fig. 10. For NF_3, more oxygen addition decreases the AC voltages and also the difference between AC voltages generated by NF_3 and SF_6 plasmas. The difference in the selectivity between the two gases decreases in the same way as the difference between the AC voltages. This indicates that the AC voltages are also a factor for resist erosion.
The main factor which determines the resist etch rate, is of course the oxygen content: oxygen will chemically remove the photoresist through the reactions [20]:

$C + O \rightarrow CO$
$CO + O \rightarrow CO_2$
$2\,H + O \rightarrow H_2O$

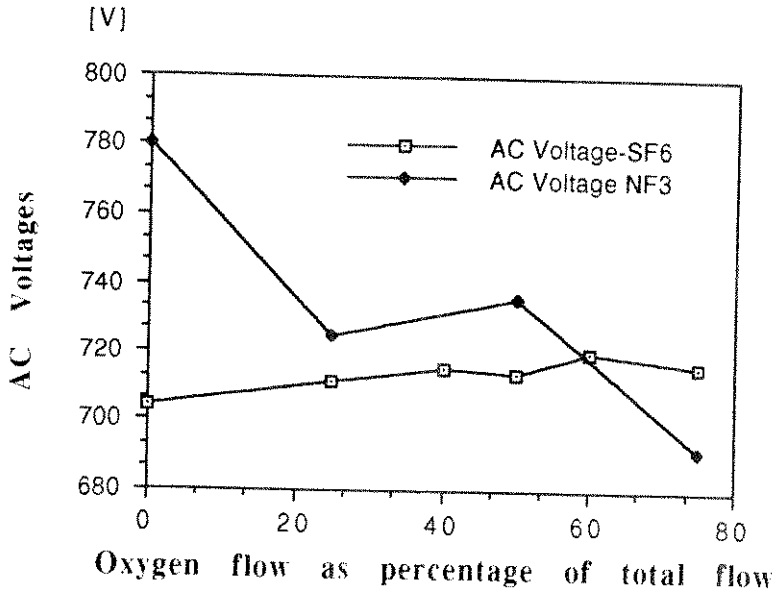

Figure 10 : AC voltages of plasmas of mixtures of oxygen with NF_3 and SF_6 as a function of oxygen flow.

The following tests were performed to determine the etch characteristics of tungsten of type W_{II}, etched in the second automatic SWAFER machine. The results are shown in table IV. Etch rate are always these at the center of the wafer.

Table IV: results of tests to determine etch rates, uniformity and selectivity for NF_3-O_2 mixtures in RIE mode, for tungsten of the W_{II} type, in the second automatic SWAFER.

Test nr.	NF_3 flow [sccm]	O_2 flow [sccm]	Press. [mTorr]	Pow. [W]	Time	r_W [nm/min]	U	r_{PR} [nm/min]	S	Wafer type
1	125	0	150	50	2'	206	0.86	241	0.86	W_{II}
2	105	20	150	50	2'	203	0.81	260	0.78	W_{II}
3	85	40	150	50	2'	220	0.85	387	0.57	W_{II}
4	85	40	200	50	2'	210	0.77	312	0.67	W_{II}
5	85	40	200	50	2'	205	0.79			W_I
6	125	0	150	100	1'	320	0.87	477	0.67	W_{II}
7	125	0	150	150	1'	387	0.89	1000	0.39	W_{II}

The influence of oxygen content on etch rate is shown in fig. 11 for a constant pressure of 150 mTorr and a constant power of 50 W. The influence of power on etch rate is shown in fig. 12, for a constant flow of 125 sccm of NF_3 and pressure of 150 mtorr.

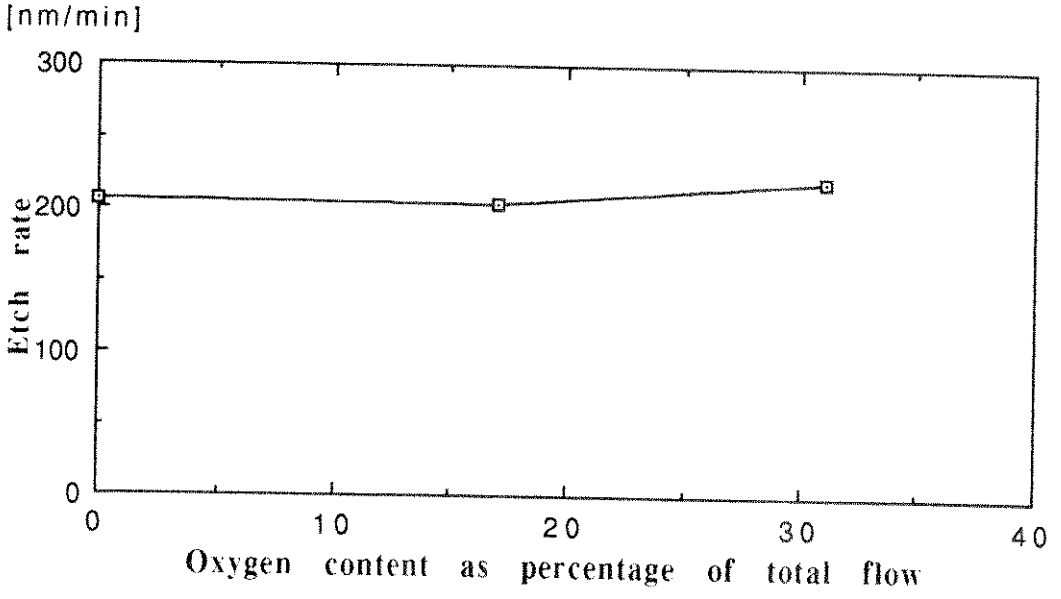

Figure 11 : Tungsten etch rate as a function of oxygen flow for NF_3-O_2 mixtures in RIE mode, for tungsten of the W_{II} type, in the second automatic SWAFER.

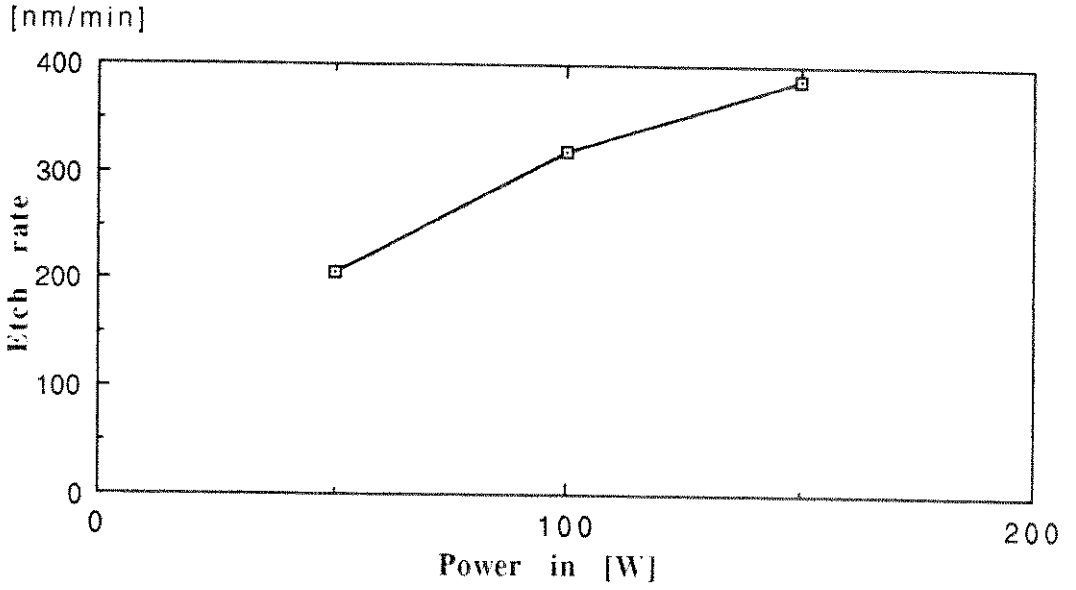

Figure 12 : Tungsten etch rate as a function of power for NF_3-O_2 mixtures in RIE mode, for tungsten of the W_{II} type, in the second automatic SWAFER.

Conclusions:

These tests show that the tendencies are the same as with former systems and type of tungsten layer W_I : the addition of oxygen increases only slightly the tungsten etch rate, while the resist etch rate increases considerably. The uniformity of the tungsten etching is very good within the central 100 mm of the wafers, but decreases in the outer 12 mm. Non-uniformity is always of the bull's eye type. Etch

rates are always measured halfway the center and the border, but they are very similar to the etch rate at the center of the wafer.
An increase of pressure does not change the average etch rate, but decreases the uniformity and increases the selectivity, as expected.
Tungsten etch rate increases with power, but not at all linearly. The resist etch rate increases linearly with power, therefore the selectivity is best at low power.
The wafer of test 6 was etched again after stripping, with the same process for another minute. The step heights remained the same, within an error of 5 nm. This indicates that the etch rate of the process is independent of the former treatment (unlike processes in PF mode, as will be described below).
Tests 4 and 5 show that the etch rate of tungsten types W_I and W_{II} are approximately the same, with W_I etching slightly slower than W_{II}.

3.2.2) Determination of wall profiles.

No tests were performed on wafers of the type W_I.
A test was done with a wafer of type W_{II}, with a 1.4 µm thick resist on top, patterned as described above.
The process used was : flows: 125 NF_3; pressure : 150 mTorr; power : 50 W, total etch time 5 minutes.
End point could be detected after 4'15" by a slight decrease of (the absolute value of) DC and AC voltages.
The TiN layer underneath the tungsten was completely removed and measurements of the PECVD oxide (with a Leitz MVP optical layer thickness measuring system) showed that in the center 32 nm and at the border 66 nm was removed.
SEM analysis shows that no undercut occurs. The tungsten wall is not vertical because of the resist erosion (and the poor wall profile of the resist).

3.3) Processes using NF_3 - O_2 mixtures in PF mode.

3.3.1) Determination of etch rates, uniformities and selectivities in PF mode.

The same wafers were used as in test series I and test series II with SF_6-O_2 mixtures and also the same measurement procedures were used. Pressure was always 200 mTorr, AF power 50W and etch time 2 minutes. The results are shown in table V; in this table r_W is the average etch rate.
The tungsten etch rate as a function of O_2 flow is shown in fig. 13. For these processes, the etch rates follow the general trends as explained in appendix I.

Table V: results of tests to determine etch rates, uniformity and selectivity for NF_3-O_2 mixtures in PF mode, at 200 mTorr and 50 W.

NF_3 flow [sccm]	O_2 flow [sccm]	r_W [nm/min]	U	r_{PR} [nm/min]	S
75	0	55	0.66	22	2.5
100	25	166	0.73	(<0)	
50	25	245	0.66	15	16
37	37	155	0.77	5	34

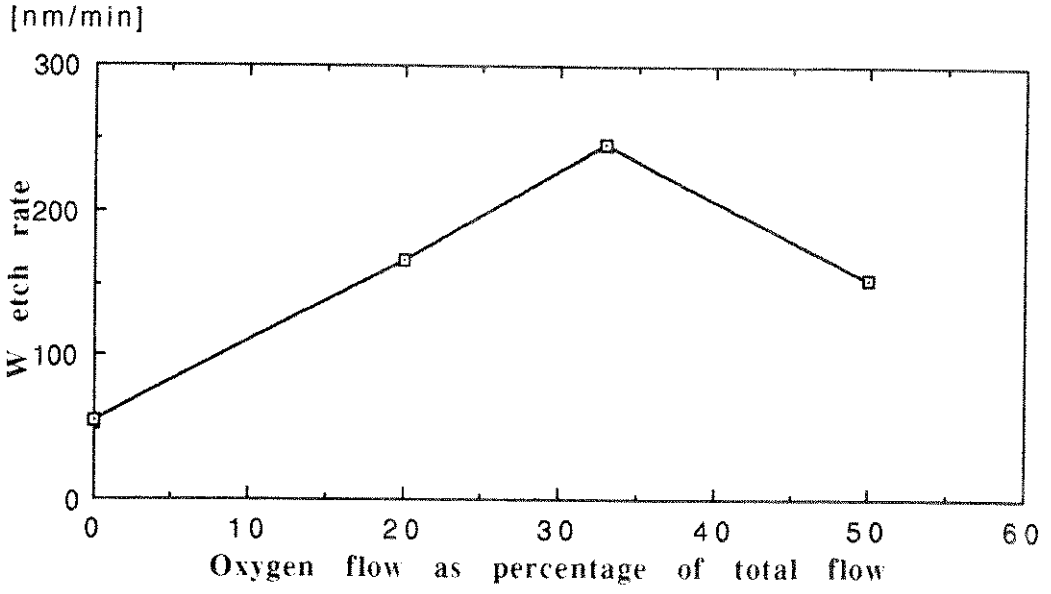

Figure 13 : Tungsten etch rate as a function of oxygen flow for NF_3-O_2 mixtures in PF mode.

The non-uniformity is of the inverse Bull's Eye type. Uniformity is better than 0.90 over the inner 90 mm of the wafer. Etch rate decreases dramatically over the outer 10 mm of the free tungsten area. The total etch depth as a function of the place on the wafer is shown in fig. 14 for the 4 etchings of this series.
The result of the measurements of the sample with the 100% NF_3 flow is rather uncertain, as the etch depth is only twice the surface roughness.
As the photoresist removal rate is also very low, for the 4 etchings, the accuracy of its rate, and therefore the selectivity is very low. The measurement cyclus is the following: measure resist thickness before etching (h_1), after etching (h_2) and after stripping (h_3). The removed photoresist thickness Δt_{PR} is then: h_1-h_2+h_3.
The resist thickness is typically 1100 nm. Accuracy of the measurement of this thickness is typically 50 nm. If the selectivity of the etching towards the photoresist is higher than 1, then $h_2 > h_1$, and the accuracy of the measurement is

of the same order of magnitude. Therefore if less than 100 nm of photoresist is removed, the error on Δt_{PR} can be 100%! This error is reduced by measuring several times the step heights, but even so the selectivities indicated above show only that the selectivity is really high, but the quantitative results are very doubtful, as the result for the 20% O_2 test shows.

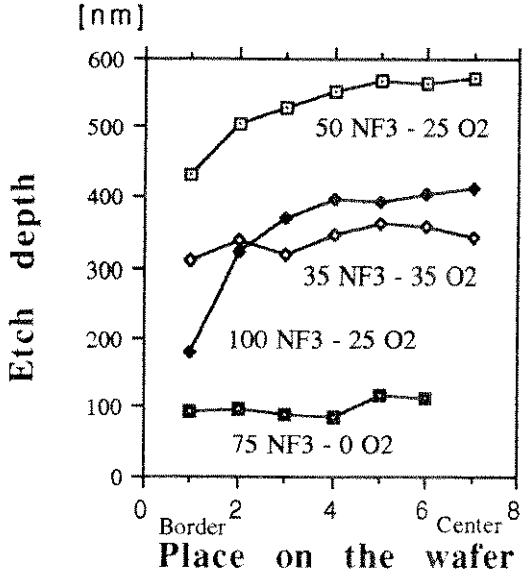

Figure 14 : Etch depth as a function of the place on the wafer and oxygen flow for NF_3-O_2 mixtures in PF mode, etch time was 2 minutes.

The reason that a total flow of 125 sccm was used for the second test is that for O_2 only a 500 sccm mass flow controller was available, limiting the minimum (controlable) flow to 25 sccm.
Examination under the optical microscope showed that resist popping had occurred. It could be observed that the wafers had changed of colour when they arrived back in the cassette. Later we shall discuss these phenomena in much more detail. During the study of the colouration of the tungsten wafers, as presented in section 3.3.3.1, the following processes were performed: pressure always 200 mTorr, AF power 50W, varying flows, as shown in table VI.
In this table r_W is the etch rate at the center of the wafer (which is higher than the average etch rate).
As explained before, it is not very accurate to determine the resist etch rate by measuring step heights. Therefore etch tests were performed on completely coated resist wafers, which suffered only a standard post bake. The resist etch rate r_{PR} is the average resist etch rate of the wafer. Thickness was measured before and after etching with an optical thickness measurement system: the Prometrix Spectramap.

Etch time was 2 minutes for the tungsten tests, 5 minutes for the resist tests.

Table VI: results of tests to determine etch rates, uniformity and selectivity for NF_3-O_2 mixtures in PF mode, at 200 mTorr and 50 W.

NF_3 flow [sccm]	O_2 flow [sccm]	r_W [nm/min]	r_{PR} [nm/min]
100	25	197	10
80	40	253	12
60	60	165	15
0	125		35

The tungsten etch rates are in good agreement with the ones reported in table V.
To control the reproducibility of the resist etch rate, process one was also performed on a completely coated resist wafer during 2 minutes, resulting in a 11 nm/min etch rate. Thus reproducibility is good; the etch rate is independent of etch time.
When increasing the pressure to 300 mTorr, the resist etch rate for the pure oxygen plasma halves, decreasing it to 100 mTorr, the etch rate doubles.
The first three plasmas had bull's eye non-uniformities for the resist etching, the pure oxygen plasma had an inverse bull's eye non-uniformity. This indicates that the etch mechanisms are somewhat different. The type of non-uniformity seems to be different between the tungsten etching and the resist etching, but later tests will show that the non-uniformity is dependent on the resist coverage of the wafer, therefore no conclusion should be drawn. Later tests show that the etch non-uniformity of blanket W wafers is of the bull's eye type.

Table VII shows the results of the first etch tests with the second automatic SWAFER machine. Gas flows are constant : 85 sccm of NF_3, 40 sccm of O_2, pressure is constant at 200 mTorr, power varies as shown in the table, etch time is 2 minutes. The resist pattern is either light field (LF), as usual, or dark field (DF). Etch rate r_W is as measured in the center of the wafer.

Table VII : etch rates and uniformities as function of power and resist pattern, at 200 mTorr, 85 sccm of NF_3 flow, 40 sccm of O_2 flow and 2 minutes etch time.

Power [W]	Pattern	r_W [nm/min]	U	Special remark
50	LF	180	0.93	
50	DF	120	0.95	
100	DF	120	0.93	
100	DF	130	0.95	lower electrode temperature increased to 35°C

These tests show that a W wafer patterned with a dark field mask etches slower than with a light field mask, contrary to most other experiments reported in the literature [18-20].
Even an increase by a factor of 2 in power does not increase the etch rate of a DF patterned wafer. For a LF wafer, the etch rate increases with power, as will be shown in later tests. An increase of temperature does not significantly increase the etch rate of a DF wafer. It is clear that the influence of photoresist is tremendous for tungsten etching in this etch mode.

Then several processes were investigated for wafers with tungsten type W_{II}.
The following process was firstly investigated:
flows: 85 sccm NF_3, 40 sccm O_2, pressure : 200 mTorr, AF power : 50 W or 100 W; varying etch times.
The following phenomena were observed:
- etch rate is not constant in time: for both power levels, etch rate remains constant until approximately 600 nm of tungsten is removed. Then the etch rate suddenly decreases very rapidly until etching eventually stops. With this process and type of tungsten W_{II}, it was not possible to remove the last remainders of the tungsten film at the border of LF resist patterned wafers.
- SEM analysis shows that the undercut is extremely high: several microns: there were several lines where the tungsten was just completely removed and the resist fell on the TiN layer.
- The DC plasmas in these plasmas do change in a rather abrupt way after some time. They become more negative, for the 50 W plasmas typically after 4 minutes, for the 100 W plasmas typically after 2 minutes and 20 seconds (i.e. for both plasmas, after having etched away approximately 600 nm of tungsten). At the same time, the AC voltage decreases.
- Furthermore, when the plasma with a low AC voltage is turned off, a large pressure drop occurs, what is not the case for a plasma with a high AC voltage.
This indicates that two types of plasma occur for these processes. Confirming the removed W thicknesses, it can be concluded that nearly all of the etching occurs only in the first type of plasma, and very little in the second type of plasma. Similar phenomena were observed for wafers of the W_I and W_{III} types.
For these tests, also blanket tungsten wafers were used. The tests always show that without resist the etching non-uniformity is of the bull's eye type, while with resist at the border of the wafer, an inverse bull's eye non-uniformity occurs. But the same 2 types of plasma occur with the same consequences as for resist patterned wafers.

Tests with other oxygen concentrations were performed: always with total flows of 125 sccm at 200 mTorr. Table VIII gives an overview of the results. Etch rates are

always these at the center of the wafer. Type of wafer: R: with resist, B: blanket tungsten layer, no resist. To determine the SiO_2 etch rates, 125 mm wafers with thermally grown oxide were etched during 2 minutes.

Table VIII : results of tests to determine etch rates, uniformity and selectivity to SiO_2 for NF_3-O_2 mixtures, at 200 mTorr.

Test nr.- wafer type	NF_3 flow [sccm]	O_2 flow [sccm]	Power [W]	Time	r_W [nm/min]	U	r_{SiO2} [nm/min]	S	Remarks
1-R	105	20	100	4'			30		IBE, 1,2
2-R	105	20	100	2'	302	0.76	29	10	3
3-R	105	20	50	4'	165	0.80	16	10	BE
4-R	125	0	100	2'	70	0.90	14	5.0	3
5-B	105	20	100	4'					4

Remarks:
1) The central 110 mm are completely free of tungsten. It can be observed that in the resist structures, at the border of the TiN-W region, more tungsten remains than outside these structures. This indicates, once more, the etch rate decreasing influence of the photoresist.
2) SEM analysis shows that the TiN surface is very smooth and that the undercut is of the same order of magnitude as the vertical etching.
Where tungsten was not completely removed, the surface is rough and there is also undercut of the same order of magnitude as the vertical etching.
3) For this process, the etch rate is highest halfway between the center and the border of the wafer. The non-uniformity is a combination of 2 mechanisms: etching of bare tungsten has a bull's eye non-uniformity, whereas the resist (at the border of the wafer) causes an inverse bull's eye non-uniformity.
4) The tungsten was completely removed.
After 3 minutes 15 seconds the DC voltage started to increase (i.e. become more negative) and the AC voltage to decrease, until stabilizing after 3 minutes and 30 seconds.
This could indicate end point at 3'30".

Conclusions:
1) Tests 1 and 2 show that the etch rate for this plasma is independent on etch time. No sudden voltage change nor pressure drop at the end of the plasma were observed.
2) Etching with pure NF_3 remains extremely slow, also for processes with 100 W power.
3) Etch rates of silicon dioxide are very low in PF mode. In this way, good selectivities of tungsten to oxide can be obtained.
4) Test 5 indicates that a blanket tungsten layer etches faster than a patterned layer.

A new series of tests was performed to investigate the influence of varying pressure and power. The results are shown in table IX.

Table IX : results of tests to determine etch rates and uniformity for NF_3-O_2 mixtures.

Test nr.- wafer type	NF_3 flow [sccm]	O_2 flow [sccm]	Press. [mTorr]	Power [W]	Time	r_W	U [nm/min]	$S_{W/PR}$	Remarks
1-R	52	10	140	100	2'	222	0.91	2.6	1,2
2-R	105	20	200	150	2'	375	0.75	>15	IBE; 1,3

Remarks :

1) After etching no colouration of the wafer was observed and no popping of the resist was seen under the optical microscope.
2) For these processes, the same remark as remark 3 for table VIII is valid.
3) A preliminary test with 200 W showed that the plasma is not stable.
The influence of the applied power on etch rate for these processes is shown in fig. 15, for constant flows of 105 sccm of NF_3, 20 sscm of O_2 and pressure of 200 mTorr.

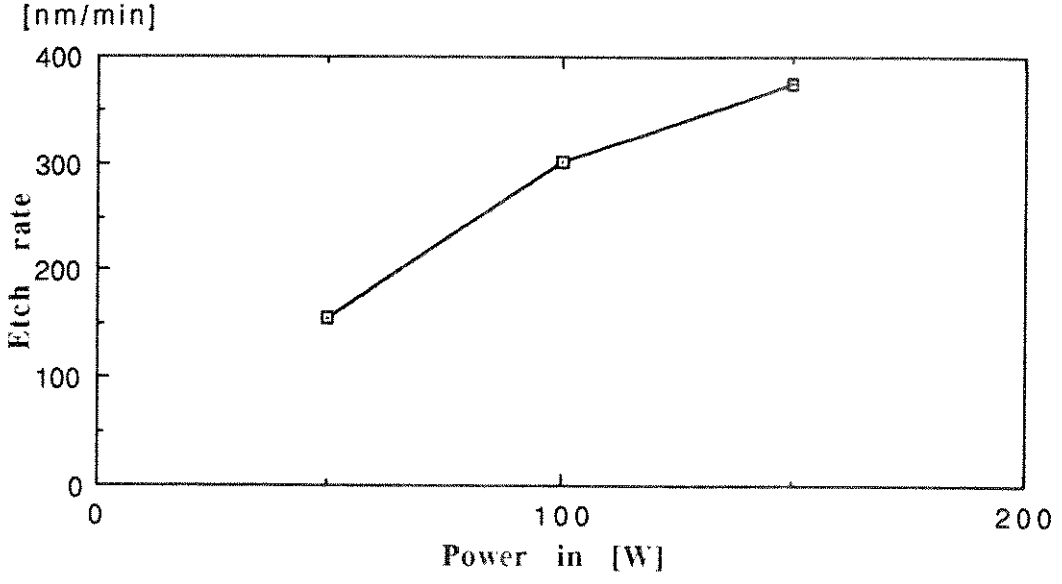

Figure 15 : Tungsten etch rate as a function of power for NF_3-O_2 mixtures in PF mode.

Conclusions:
All these data indicate that at lower pressure, the typical PF characteristics have been lost somewhat and that some bombardment enhanced etching occurs.

The increase of the power has a similar effect, but in a lesser extend : the selectivity of the tungsten to the resist remains high, but the colouration and popping of the resist disappear.

The influence of the resist on etch rate was investigated for the following process:
105 sccm NF_3, 20 sccm O_2, pressure : 200 mTorr, power : 100 W.
For a wafer patterned with a standard resist process, it took 3'30" before DC and AC voltages indicated end point. On the other hand, for a blanket tungsten layer, after 3 minutes of etching, the W was completely removed at the outer 50 mm of the wafer, only in the center 25 mm W was still found.
SRP measurements resulted in resistances from 1 to 6 Ohm per square at the center till 72 to 98 Ohm per square at the border, where we had bare TiN (specific resistivity of TiN is typically 80μOhmcm, therefore the thickness of the remaining TiN ranges from 82 to 111 nm).
This test shows that the etch rate of a bare wafer is much higher than for a wafer with a photoresist pattern on it. The uniformity also changes completely: with a bare tungsten film, the border etches faster than the center, while this is the inverse for a wafer patterned with resist at the border of the wafer. (When there had been edge bead removal, the non-uniformity can be of the normal bull's eye type.)
The same process was performed on a blanket tungsten layer but etch time = 2'30".
At the outer 2 mm the W was completely etched away.
The difference in thickness of the layer was measured through the weight method and the SRP method, both described above.

$w_1 - w_2 = 0.1813$ g => $\Delta t_W = 929$ nm

Through SRP : mean R before = 0.08634 Ω/sqr, after etch = 0.54944 Ω/sqr

=> Δt_W = 1158 nm - 182 nm = 976 nm

At the center : through SRP : Δt_W = 1158 - 360 = 798 nm
To verify which of the two measurement methods is the most adequate, the wafer was patterned with the standard mask used in the former tests, etched with the same plasma and stripped.
The remaining tungsten thickness could be determined: center : 370 nm, halfway : 290 nm, border : 185 nm, second chip from the border: 233 nm.
This result shows that the SRP method is very reliable. But a difference of less than 5% between the two measurement methods is quite acceptable.
The etch rates, as determined by SRP measurements, are: center : 319 nm/min, at 96 mm : 347 nm/min, at 105 mm : 389 nm/min, U = 0.80, at 115 mm : 463 nm/min, U_2 = 0.69.

This test shows mainly that the etch rate increases mainly at the outer 20 mm of the wafer, while in the inner 85 mm the uniformity is quite good.

3.3.2) Determination of wall profiles.

After determining etch rates, it is possible to etch through the complete tungsten layer to determine the wall profile. For this test the following process parameters were used : gas flows : 100 sccm NF_3 and 25 sccm O_2, pressure : 200 mTorr, power : 50W. Photoresist process used for a first wafer included DUV curing and 140°C hard bake.

It was possible to determine the etch time by following the DC voltage. Fig 16 shows how the DC voltage changes in the last minute of the etching : its absolute value increases initially, presumably when part of the wafer gets cleared and drops at the end. In this way the etch time was determined, which was for the first wafer 5 minutes and 5 seconds.

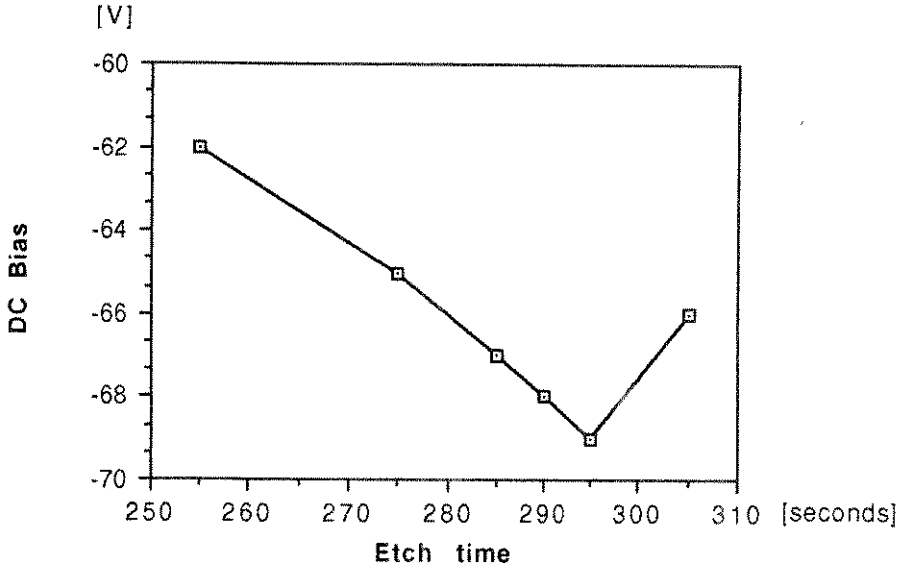

Figure 16 : Change in DC bias voltage when reaching end point of the tungsten etching.

The photoresist did "explode" completely in the large patterns. There only remained photoresist on the borders of the bonding pads and on the small lines.

Another wafer was etched with the same process, but this time a standard photoresist process was used.
End point detection was performed in the same way as for the first wafer, total etch time was 5 minutes and 15 seconds.

The photoresist withstood this time better than on the first wafer: under the optical microscope all the patterns were still on the wafer, only some popping was visible.

The wafer was then inspected in the SEM. Fig. 17 shows a structure.
It can be observed that the etching is completely isotropic: there is severe undercut. The resist itself has not eroded: the thickness is still approximately the same as the original thickness. A lot of bubbles are formed on all the resist surfaces: as well on the horizontal as on the vertical. These bubbles seemed to be dependent on the photoresist process used. Later tests with the same wafers showed the same bubbles, but when a new batch of wafers was patterned with a well controlled lithography process, these bubbles were not observed anymore with an optical microscope. For tests with the second and third machine for W deposition, these bubbles were always observed during SEM analysis. Both resist and lithography process were different from the processes used for the tests with the first type of tungsten: due to special circumstances post bake was always performed hours after development. This delay can cause problems such as resist popping.

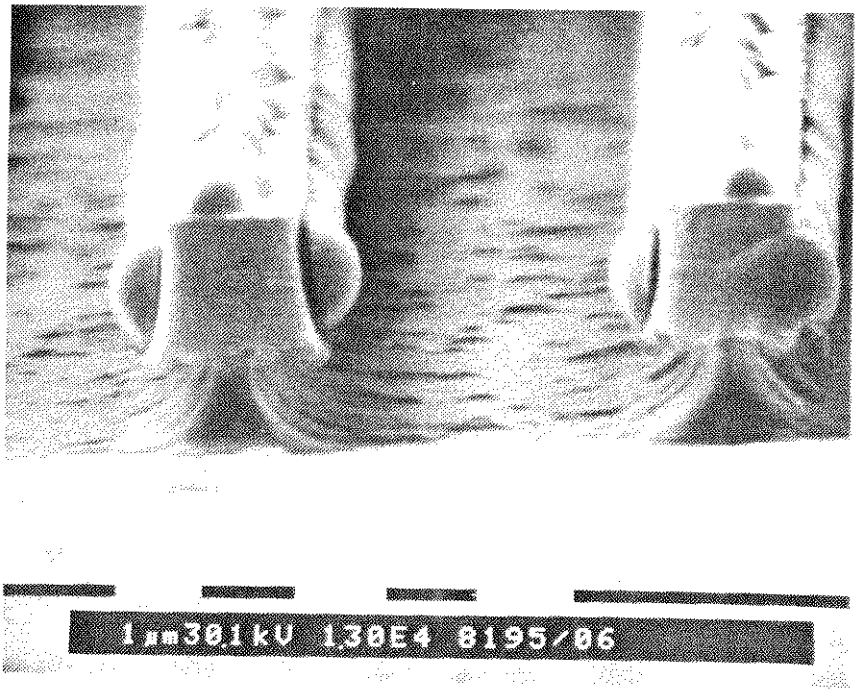

Figure 17 : Tungsten profile, resist and bubbles after PF mode etching with NF_3 - O_2 plasmas.

The characteristics of etching through of a wafer of type W_{II} in the second SWAFER machine with a PF process followed by a 5 seconds RIE process, were determined.
The following sequence was applied:
1) gas flows : 105 sccm NF_3, 20 sccm O_2, pressure : 200 mTorr, power : 100 W, PF, total time : 4 minutes. After 3 minures 30 seconds, decrease of the voltages, stabilizing after 3 minutes 45 seconds, indicating end point.

2) gas flow : 125 sccm NF_3, pressure : 150 mTorr, power : 50 W, RIE, time : 5 seconds.
The center 75 mm was etched free, stop on TiN.
SEM observations show that the undercut at the center of the wafer is much less sever than the 85 sccm NF_3, 40 sccm O_2, pressure : 200 mTorr, power : 100 W, PF, process.
Undercut at center and border are of the same order of magnitude.
The TiN surface is very smooth, whereas where the W had not been removed, the surface is rough.

3.3.3) Special effects occurring with etch processes in PF mode.

3.3.3.1) Colouration.

The colouration of the wafers by the PF etching with NF_3-O_2 plasmas, as observed before in the tests to determine etch rates, was further investigated.

Etch tests were performed at : pressure: 200 mTorr, power : 50 W in PF mode and flows, wafers of the W_I type:
1) 100 sccm NF_3, 25 sccm O_2.
2) 80 sccm NF_3, 40 sccm O_2.
3) 60 sccm NF_3, 65 sccm O_2.

By examining the wafers thoroughly under the optical microscope, the following general tendencies could be observed: the tungsten which was not etched (because it was protected by resist during the etching) has the original brown-yellow tungsten colour. In the central 100 mm of the wafer, the colour of the etched tungsten is more dark, brown, except in smaller structures, where the colour goes to yellow-blue and more to the border dark blue. This dark blue colour is also the colour at the border of the wafer in larger structures.
At approximately 20 mm from the border there is a rectangle of resist of approximately 20 mm by 10 mm (it are 2 chips which are not exposed by the stepper, therefore we shall call this structure the "double chip"). Near this resist area the colour after etching becomes also dark blue, 4 to 5 mm from the area the colour turns gradually into dark brown, the "normal" colour after etching in this region. This is a first indication that the presence of the resist alters something in the process.
(Auger tests, discussed later in 3.3.3.2, will show that the region which has a brown colour is an oxygen rich region with a depth of approximately 20 nm, and where the blue colour is dominant, an oxygen rich layer of 50 nm thick can be found.)
To determine the cause of the colouration, the following sequence of process steps was performed on a wafer:

1) 125 sccm NF_3, 200 mTorr, 50 W PF, 15 seconds
2) 125 sccm O_2, 200 mTorr, 50 W, PF, 30 seconds.

This sequence was done 8 times in a row, but the wafer always leaves the reactor after the second step.. After the eighth sequence, step height measurement indicated that the step has decreased by 250 nm, due to resist etching.
The same sequence was done another 8 times, which results in a total etch time of 4 minutes in the NF_3 plasma.
The wafer showed the same colour pattern as the wafers of the former tests.
After stripping, the tungsten was measured again and less than 50 nm was removed!
This means that with the pure NF_3 process, the oxidized tungsten is not removed anymore, at least when the etch time is only 15 seconds.

A simpler sequence was done in the following way:

80 sccm NF_3, 40 sccm O_2, pressure : 200 mTorr, power : 50W in PF mode, first test: 4 minutes.

During this test it became clear that the colouration occurred when the wafer left the reactor: it means that the oxidation occurs in the air, not during the etching.
The step height was measured, with resist still on the wafer, and it had increased with approximately 450 nm.

The same plasma was applied to the same wafer during 4 more minutes. Measuring the step height again, with resist still on the wafer, it was found that it was increased by only 100 nm this time.
Stripping the wafer and measuring the etch depth in the tungsten yielded: 605 nm of tungsten removed.

A new wafer was etched with the same plasma during 4 minutes. Half of the wafer was stripped and the etch depth in the tungsten was measured: 530 nm.
This means that after oxidation the etching is completely different: the etching in PF mode of this tungsten oxide is much slower than of pure tungsten.

It was easy to observe on the border between the stripped and the not stripped part of the wafer, that the strip itself does not influence the colouration of the wafer.

As the Dektak stylus of our equipment has a diameter of 12 micrometer, it was not possible to detect in this way whether smaller spaces etched more rapidly than larger ones.
Therefore, the stripped part of the wafer was cleaved and examined in the SEM. Next to structures of 1.25 µm wide lines-spaces a large open area of over 100 µm can be found.
It was easy to observe there that small spaces where etched as deep as the large spaces.
The wafers of this series had received a different photoresist pattern: the used reticle was the same, but much more fields were exposed, so that even the border of the

wafer was free of resist. There were 2 main differences with the results of former tests:
1) The (time) average tungsten etch rate decreases dramatically, by nearly a factor of 2 in the center of the wafer. This etch rate decrease is due to the non-reproducibility of the etching with this type of plasma (as has been shown in 3.3.1).
2) The non-uniformity seems to be rather of the bull's eye type than of the inverse bull's eye type. On the border of the wafer the difference in etch rate is much less. There the etch rates are : 165 nm/min for the wafer with much resist, 134 nm/min for the wafer with no resist at the border. For the first wafer, the local high density of the resist decreased the etch rate at the border, a decrease which is not observed when no resist at the border.
This indicates that the presence of the resist modifies the etching characteristics quite a lot (as it also influences the depth of the oxide layer).

A wafer was prepared to be analysed by Auger spectrometry: half of the wafer was free of resist, in the center there was 1 row of IC patterns, and the rest of the wafer was covered with resist. In this way we were sure to obtain the brown as well as the blue coloured oxide. The processs used, was the following: 80 sccm NF_3, 40 sccm O_2, pressure : 200 mTorr, power : 50W in PF mode, etch time : 4 minutes. The AES analysis will be described in section 3.3.3.2 below, as the results of the first sample.

After this test the manually loaded system was removed from the clean room and an automatically loaded system was connected. Unfortunately, the etch characteristcs of both systems were not the same.
A lot of etch tests were done on the new machine, but results of all the etching processes were rather different than for the manual machine and another system that had been characterized before.
The overall results were:
1) In PF mode the etch rate of the tungsten was a factor of 5 lower now, while the etch rate of the resist was a factor of 3 higher.
2) The measured AC voltages on the lower, floating electrode are higher. The DC voltages on the upper electrode are higher.
3) There is still colouration, but much more uniform than in the manual system. There is no difference in colour in the neighbourhood of large resist areas.
All these results indicate that less free fluorine is formed. This explains that the etch rate of the tungsten decreases. The etch rate increase of the photoresist can be explained by the higher voltages at the floating electrode.
4) There are large non-uniformities in the etchings of polysilicon, resist and tungsten in all etch modes. Separate regions could be identified, which had e.g. different colouration.

Later we found out that the lower electrode was not really floating, but remained at a fixed potential. In this way a plasma mode between plasma float and plasma ground was created.
A first phenomenom is the fact that the plasma in this pseudo PF mode was much less intense than for the real PF mode. The reason is that in the pseudo PF mode, the lower electrode (probably) acts as the counterelectrode, but with a smaller area than the grounded gas distribution ring, which acts as the counterelectrode for the real PF mode.
The etch rate results show that a second phenomenom occurs: more bombardment in this pseudo PF mode. This explains why resist etch rates are higher and why less tungsten oxide is formed, as will be discussed in more detail in appendix V.

A special process sequence was performed to investigate if the oxide layer has still the same characteristics as in the manual SWAFER. A wafer without photoresist was used.

1) 50 sccm of NF_3, 25 sccm of O_2, pressure : 200 mTorr, power: 50W in PF mode, time : 30 seconds.
Result: a brownish oxide was formed.
2) Same process: extra 2 minutes.
Result: the colour changed to blue-brown. (The influence of time on the colour, which is an indication of the depth of the oxide layer had not been observed in the manual SWAFER.)

Then the carbon ring of the SWAFER was removed to investigate if its presence changes the formation of the oxide layer.
The same processes 1) and 2) were performed on a new resistless wafer.
The results were approximately the same, only the extra colouration in the second step was less expressive.
Extra steps were now done on the same wafer:
3) 50 sccm of NF_3, 25 sccm of O_2, pressure: 150 mTorr, power: 50W in RIE mode, time: 2 minutes.
Result: the wafer shows a brown of a lighter shade, indicating a thinner oxide.
4) Extra 30 seconds of the same RIE process.
Result: there is still a very light brown shade, if it is an oxide, it will be very thin.
5) Same PF etch process as 1) and 2) during 2 minutes.
The colour has changed into dark brown to blue.
6) Extra 2 minutes of PF process.
Result: the whole wafer has a blue oxide layer.

Conclusion: a PF process forms a tungsten oxide layer, an RIE process removes the tungsten oxide layer.

Etching with SF_6-O_2 processes in PF does not result in the formation of a tungsten oxide.
It is clear that the etch mechanisms of SF_6-O_2 processes are different from NF_3-O_2 processes. It should be remarked that

the voltages on the lower electrode for the 150W SF_6 process are approximately twice as large as for the 50W NF_3 process. The consequence of this can be that the etching with SF_6 is much less chemical than with NF_3: more ion bombardment will occur with SF_6 than with NF_3. And it is shown in former tests that no oxide layer is formed with RIE NF_3 plasmas.

3.3.3.2) Auger analysis of the etched samples.

Auger analyses were performed to investigate the nature of the layers formed when leaving the SWAFER reactor after NF_3-O_2 etching in PF, and how they are generated. The equipment used was a Perkin Elmer PHI600 Auger Electron Spectrometer.

A. First sample.

The first sample was of the wafer as described in 3.3.3.1.
Results:
1) Six equidistant points were analysed : the first point was at 0.6 mm from the border of the resist area, the last point at 5.6 mm from this border. In this way there were investigated regions where the colour was brown and other where the colour was blue. The surface signal, as shown in fig. 18, was the same for all the points.

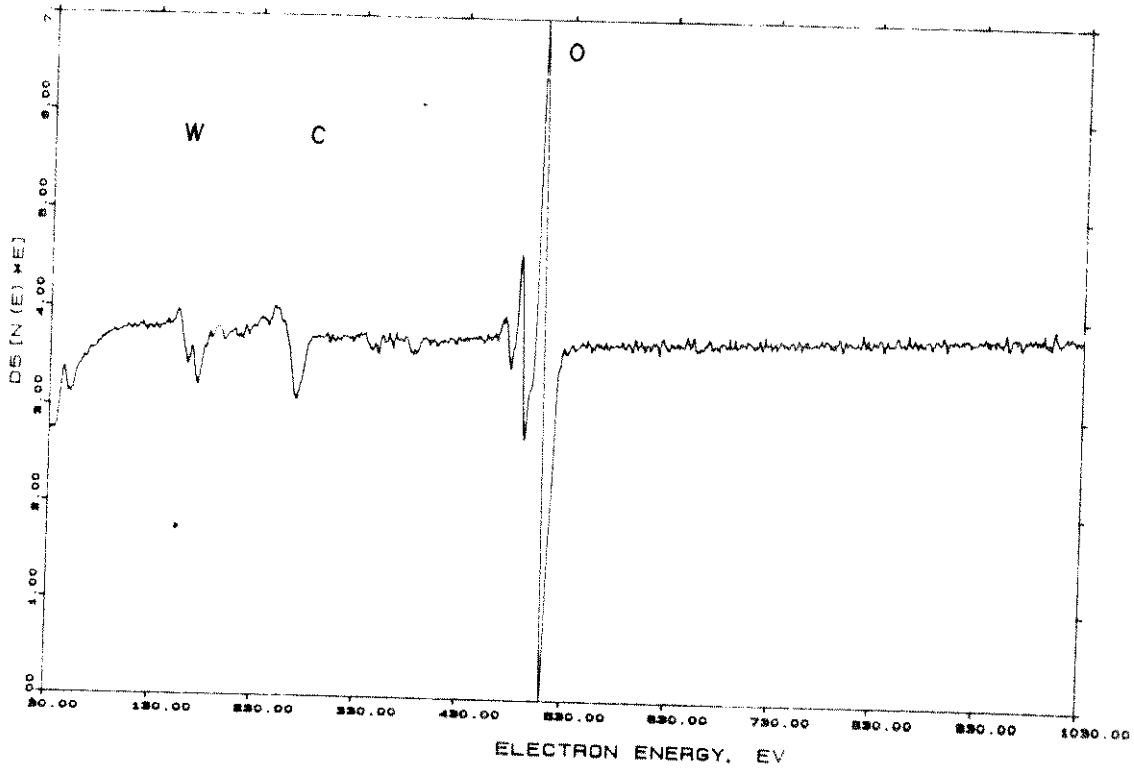

Figure 18 : Auger spectrum of the surface of the tungsten where a blue colouration took place.

At the surface we can observe tungsten peaks at 163, 169 and 174 eV, a carbon peak at 271 eV and a large oxygen peak at 503 eV. No fluorine and no nitrogen were found.
2) At 3 mm of the border of the large resist area a depth profile was made, as shown in fig. 19. This was in a region where a blue colouration had taken place.
The carbon signal dissappears immediately when the AES Ar sputtering starts. We can conclude that the carbon is adsorbed at the surface, but does not diffuse into the tungsten bulk.
The oxygen signal decreases and reaches 50% of its value at the surface after sputtering time of 5 minutes. It can be estimated that 5 minutes of sputtering in the used Auger system removes about 25 nm of tungsten.
The tungsten to oxygen ratio is 1 to 3, so that we can presume that at the surface a WO_3 compound has been formed.

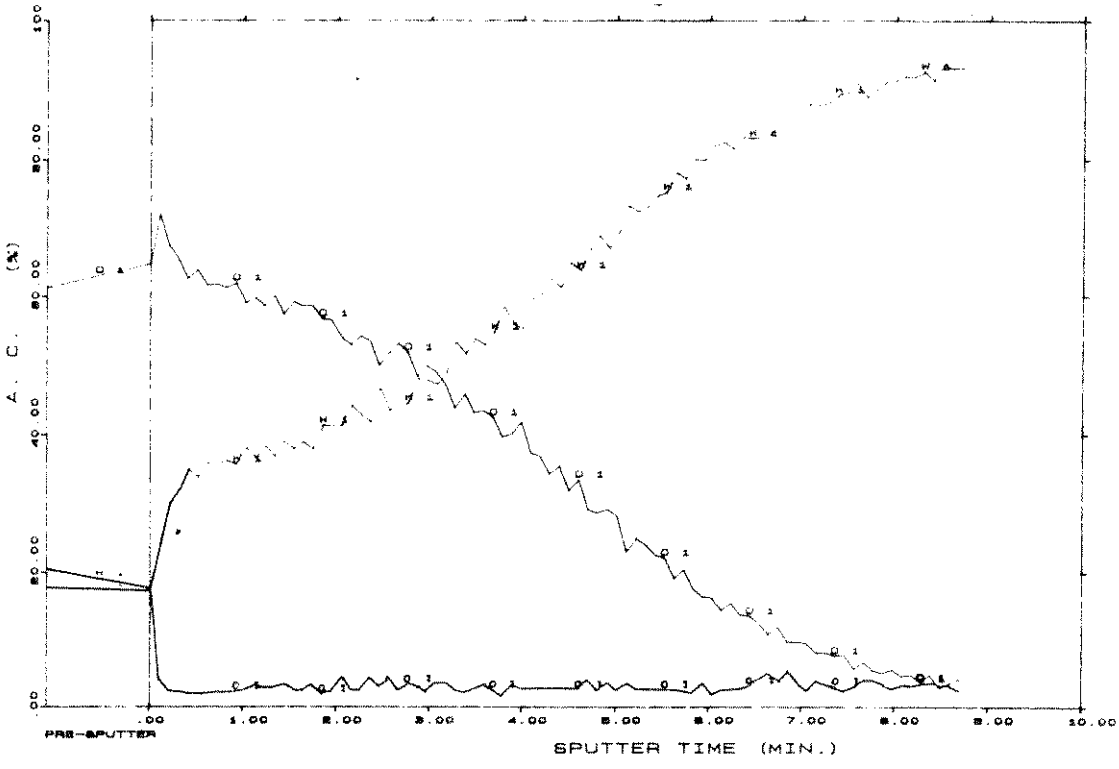

Figure 19 : In depth Auger profiles of the tungsten where a blue colouration took place.

3) At 6 mm of the border of the resist area a depth profile was made, as shown in fig. 20. This was in a region where a brown colouration had taken place.
For this sample, the carbon signal also dissappears immediately. The surface W to O ratio is also 1 to 3. The oxygen signal decreases and reaches 50% after sputtering approximately 2 minutes. It can be estimated that approximately 10 nm of tungsten was removed after 2 minutes.

These results show that the chemical composition of the oxides is the same for the blue and brown colours. At the

surface we find WO_3 in both cases. The difference in colour is caused by the difference in thickness of the oxide layer and not by the difference in W-O composition.

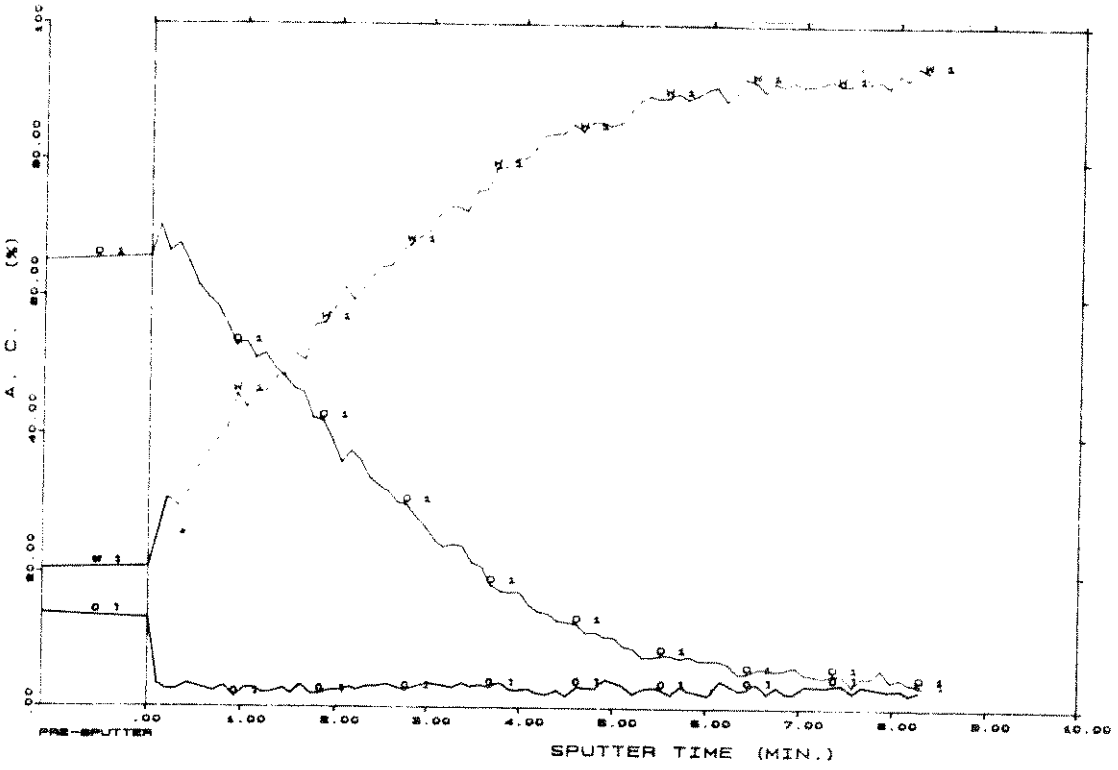

Figure 20 : In depth Auger profiles of the tungsten layer where a brown colouration took place.

B Second, third and fourth sample.

It was tried to leave the sample as much as possible in a nitrogen ambient and verify what kind of structure was formed, as it was observed that the colouration took place in air, and 20 minutes in nitrogen at 1 atmosphere of pressure in the reactor did not change the colour of the tungsten. A (not completely airtight) load-lock was made around the automatic SWAFER and filled with nitrogen. The wafers were cleaved in this load-lock, mounted on the AES holder and transported in a box, which was wrapped in a plastic bag, which was filled by nitrogen. It is possible to flush the entrance port of the Auger system with nitrogen and let it flow through the open entrance valve. The holder was taken out of the box and inserted into the port. During this operation it was impossible to avoid that the sample came in contact with the air. Then the port was closed and pumped to vacuum. It was not possible to see if the sample was coloured before making the Auger analysis. When the sample left the Auger system, a colouration was observed, but this could have happened upon opening the system after the analysis.
All samples were etched with the following process:
50 sccm of NF_3, 25 sccm of O_2, pressure : 200 mTorr, power : 50W in PF mode, etch time: 2 minutes.

The cleaving of the first wafer, the mounting of the sample to the holder and transfer to the Auger system took over 20 minutes time (second sample).
The same procedure took less than 10 minutes for the second wafer (third sample). A sample of this second wafer which remained in air for four hours was also investigated (fourth sample).
A reference wafer which contains a non etched CVD tungsten film, was also analysed.
Results:
The second and the third sample showed the same results, only the fluorine content of the second sample was approximately 30% less than that of the third sample. The analysis of the second sample will not be commented anymore.
The surface signal of the third sample is shown in fig. 21.
The following peaks can be observed: tungsten, carbon, oxygen (as in fig 18) and fluorine at 658 eV.

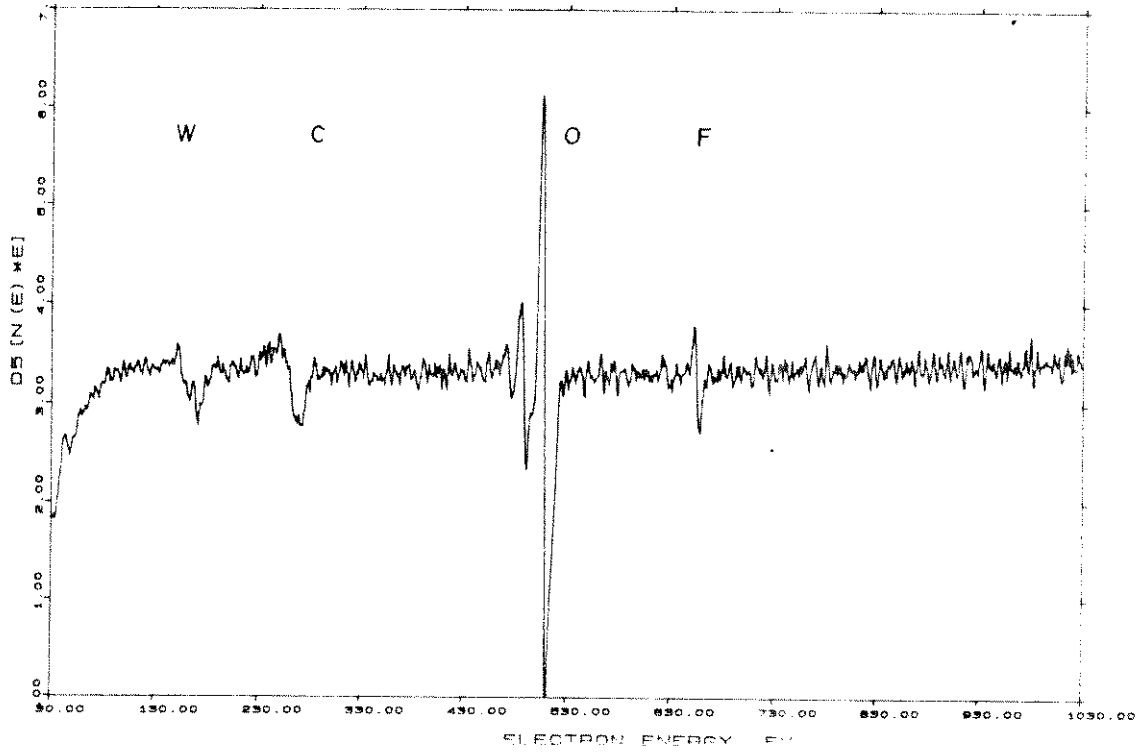

Figure 21 : Auger spectrum of the surface of the tungsten moved to the Auger electron spectrometer in a nitrogen ambient.

The depth profiles are shown in fig. 22.
The carbon signal dissappears immediately when the sputtering starts. As in the first sample it is just adsorbed carbon. The fluorine and the oxygen signals decrease in a similar way. This indicates that the presence of F and of O is linked to each other. The sputter time to 50% of the surface value is again approximately 2 minutes. The colour of the oxide formed when coming into air was the same brown as for the second region investigated in sample 1. Therefore we can conclude that the colour reproducibly indicates the thickness of the oxide layer.

The tungsten signal increases as oxygen and fluorine signals decrease.

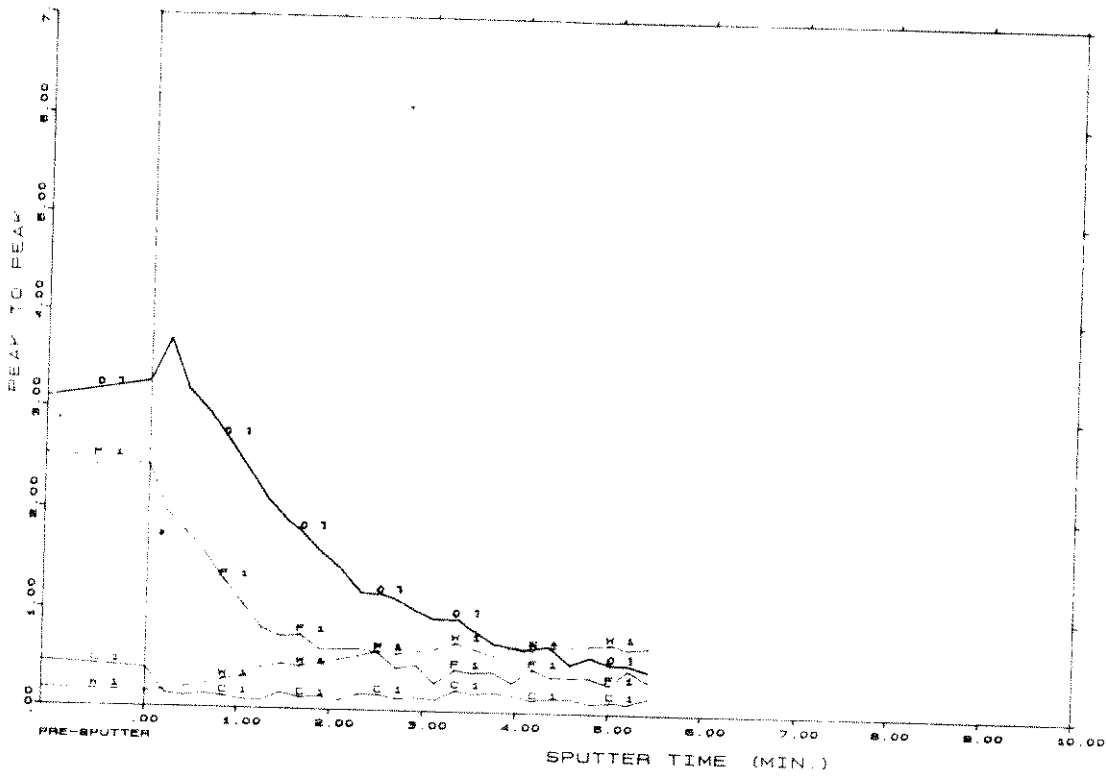

Figure 22 : In depth Auger profiles of the tungsten moved to the Auger electron spectrometer in a nitrogen ambient.

Even in these samples with fluorine present, the W to O ratio at the surface is still approximately 1 to 3. The F concentration in the sample is only a few %, whereas the O concentration is approximately 60% of the atoms found at the surface. Therefore it is normal that the differences are small.
As it is known that the electron beam causes desorption of the fluorine [21], fluorine was always investigated first in these depth profiles.
Then the sample which remained in air for approximately 4 hours was analysed.
The surface signal is shown in fig. 23. The tungsten, carbon and oxygen peaks can clearly be observed. It is very hard to say if the peak at 658 eV, which indicates the fluorine atom, is real or just noise.
Looking at the depth profile in fig. 24, one is inclined to state that very little fluorine still remained at the surface, but none in the bulk of the tungsten. Carbon disappears as in all former samples. The oxygen content decreases as in the former samples to 50% of its surface value in approximately 2 minutes. And W to O ratio at the surface is again 1 to 3.
The colour of the sample, before entering was the standard brown.

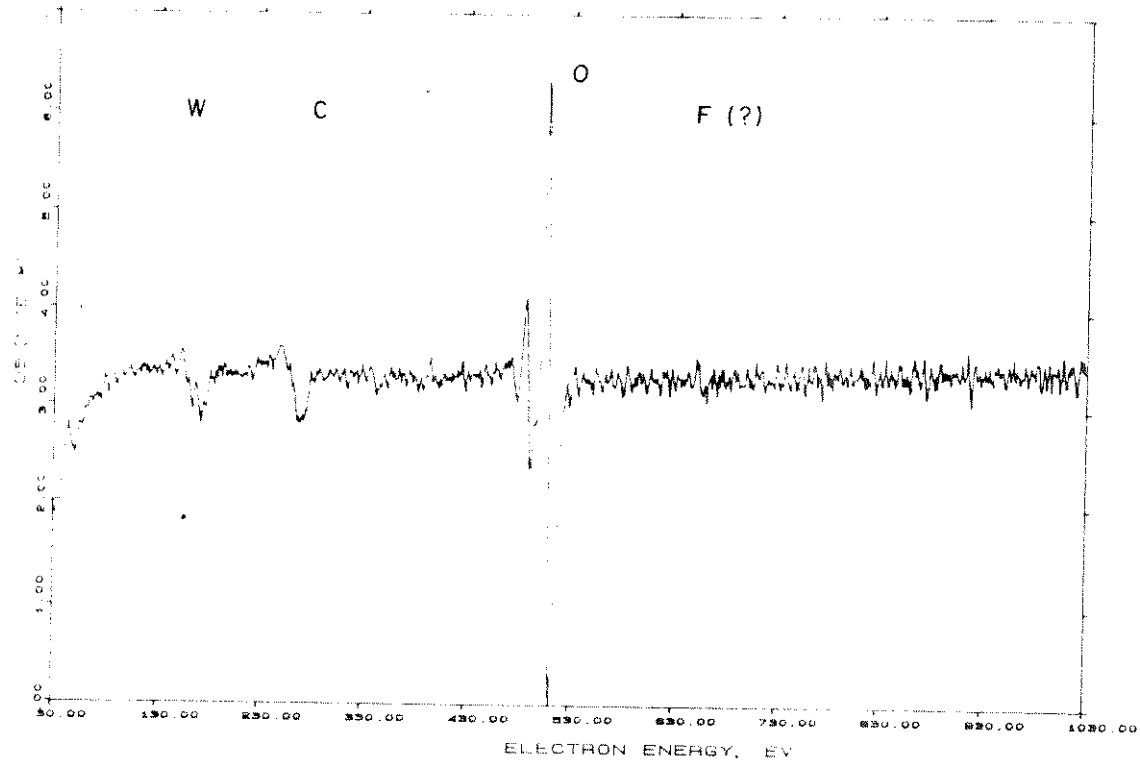

Figure 23 : Auger spectrum of the surface of the tungsten which remained in an air ambient for approximately 4 hours before being analysed.

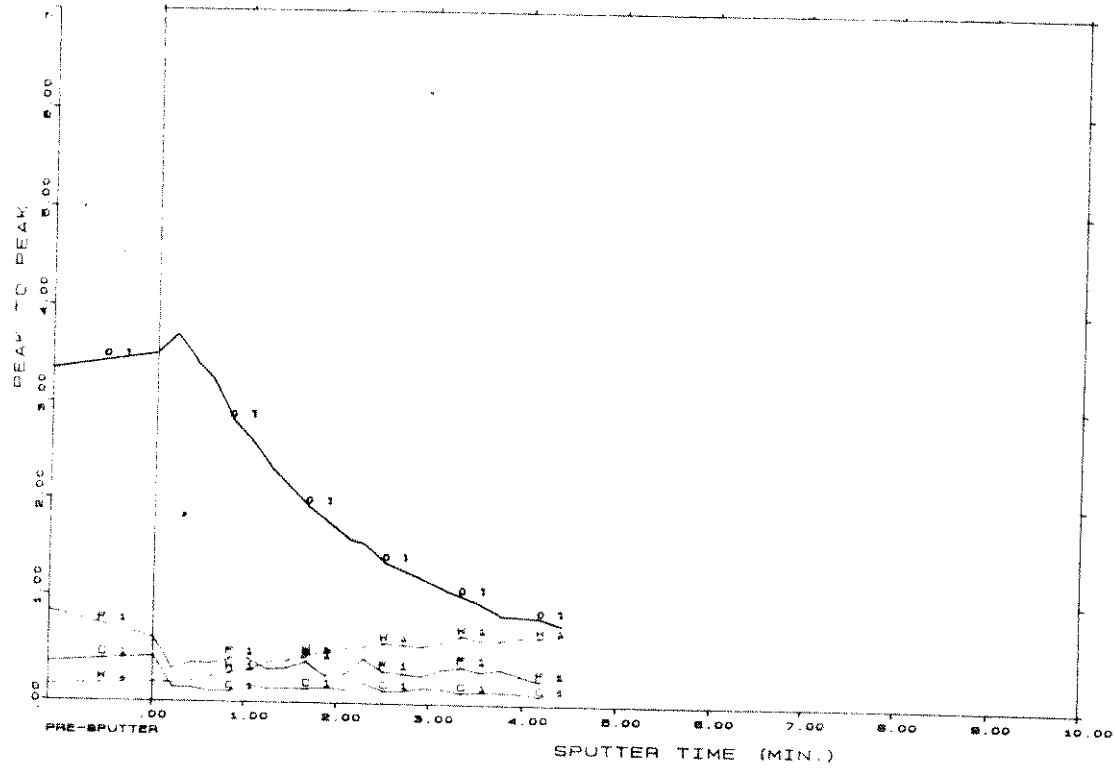

Figure 24 : In depth Auger profiles of the tungsten layer which remained in an air ambient for approximately 4 hours before being analysed.

The surface signal of the reference sample is shown in fig. 25. It is possible to observe the same tungsten, carbon and large oxygen peaks.

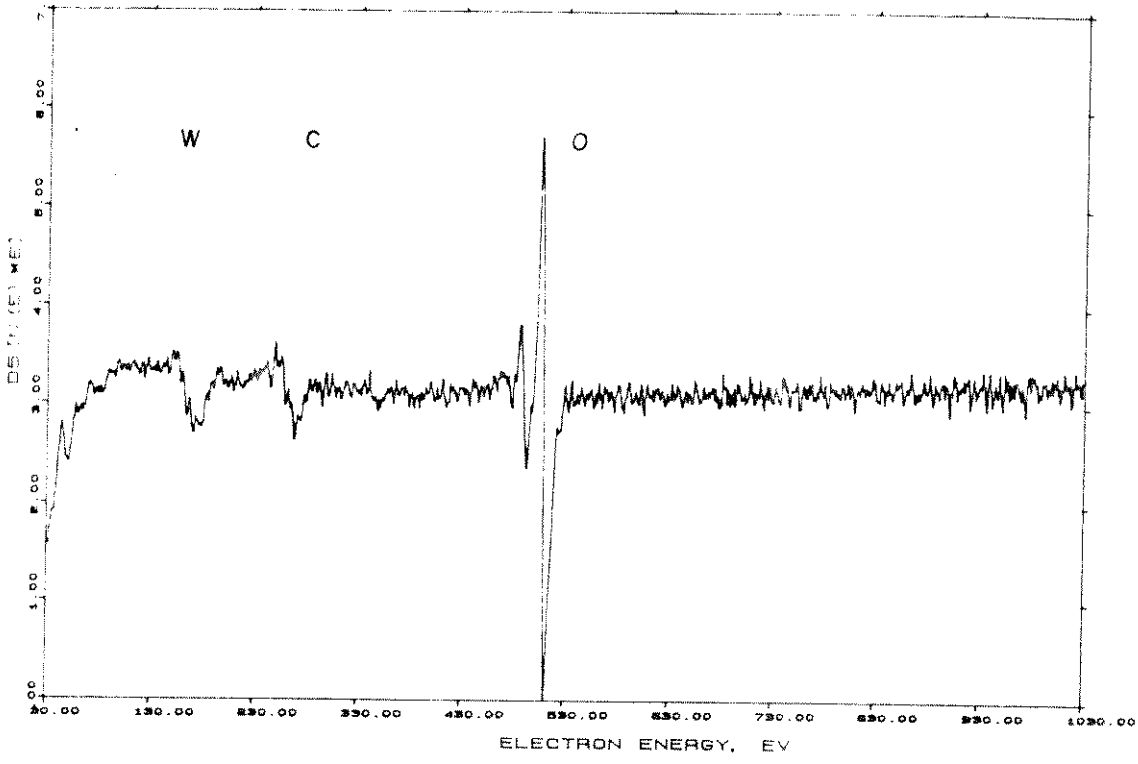

Figure 25 : Auger spectrum of the surface of the tungsten of the reference sample.

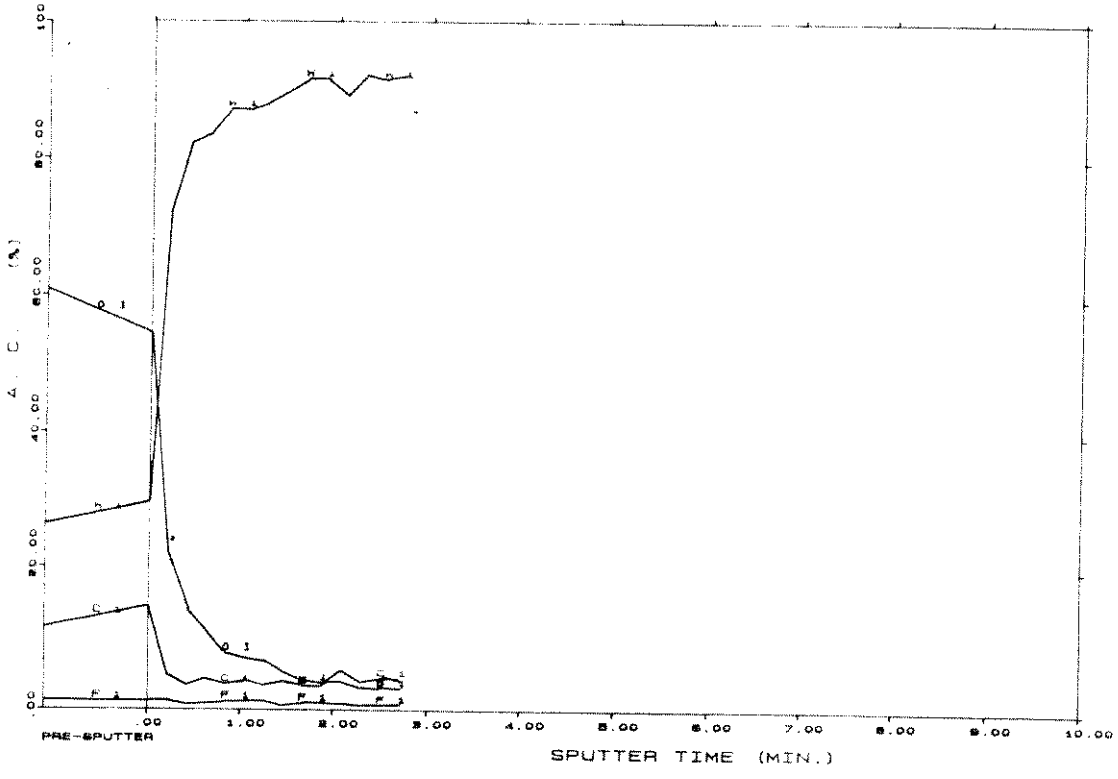

Figure 26 : In depth Auger profiles of the tungsten layer of the reference sample.

Figure 26 shows the depth profile of the reference sample. When sputtering starts, both carbon and oxygen peaks disappear immediately. It can also be observed that the oxygen to tungsten ratio at the surface is less than 2. This indicates that the oxygen is rather adsorbed than chemisorbed.

Conclusions.

The fluorine and the oxygen signal are linked very much together: they decrease in the same way in the bulk of the tungsten.
The oxygen content of a sample which still contained fluorine, decreases in the same way as a sample which does not contain any fluorine anymore.
Samples prepared in different equipment, but with the same colour, show the same oxygen and tungsten profile.
If the colours are different, the surface signal, therefore the surface content, is the same, but the concentrations in depth are different: oxygen can be found at greater depth in one sample than in the other.
The fluorine and oxygen contents decrease steadily in depth.
The reference sample shows that no tungsten oxide compound is formed on a non etched tungsten wafer.

3.3.3.3) Effects of treatments before and after the etching of tungsten.

The characteristics of an etch process for etching completely through the tungsten layer of a wafer of type W_{II} in the second SWAFER machine with a PF process followed by a 5 seconds RIE process, were determined.
The following sequence was applied:
1) 105 sccm NF_3, 20 sccm O_2, pressure : 200 mTorr, power : 100 W, PF, total time : 4 minutes. After 3 minutes 30 seconds, decrease of the voltages, stabilizing after 3 minutes 45 seconds, indicating end point.
2) 125 sccm NF_3, pressure : 150 mTorr, power : 50 W, RIE, time : 5 seconds.
In the central 75 mm the tungsten was completely removed.
The etching had not removed the TiN layer.
No oxidation was observed when the wafer left the reactor.
Resist popping could not be observed under the optical microscope, some "bubbles" were seen in the SEM, but much less severe than for wafers which had not suffered a RIE plasma. Besides, most of the bubbles are located at the sidewalls of the resist, not as much on the top.
This indicates that a short RIE step removes the fluorine containing layer on top of the tungsten and a layer on top of the resist also.
A possible explanation for the formation of the bubbles is that during the PF processes a C_xF_y layer is formed at the top of the resist, also depending on the treatment the resist received before. When applying an RIE plasma, this layer is removed. When the wafer leaves the reactor

without an RIE treatment, this layer pops when it arrives in the air.

Wafers which had been etched before were submitted to a PF etch process to see how the oxide layer formed when coming out of the SWAFER influenced the etching.
The process used was always: 100 sccm NF_3, 25 sccm O_2, pressure : 200 mTorr, power: 50W in PF mode.
Conclusions:
1) The tungsten which had been etched in a PF NF_3-O_2 plasma does not etch anymore.
2) Tungsten that had been protected by resist, but the resist had been stripped 6 months ago, do not etch in these PF mode.
3) Tungsten that had been etched in an RIE plasma and where the resist pattern had remained on the wafer, etches in the same way as tungsten on a new wafer.
4) Tungsten which had been protected by a resist pattern which is removed just before the etching etches as tungsten on a new wafer, including the formation of the oxide after the etching.
5) The oxide can be used as a mask to etch the tungsten which had been protected before by the resist.
6) The etch rate of the tungsten in the center of the wafer is independent of the mask material : resist or tungsten oxide.

A wafer which had suffered a RIE process was stripped and the following process was performed:
flows: 105 sccm NF_3, 20 sccm O_2, pressure : 200 mTorr, power : 100 W, PF, time : 2 minutes.
By measuring with a step height meter, a strange phenomenom was discovered.
In the center of the wafer, the step height was reduced with 200 nm to 176 nm, halfway the step height was zero and at the border, the step had become a valley of 100 nm deep, what means that 530 nm was etched more at the place that had been protected by the resist in the former RIE process, than at the place where the RIE etching had occured.
All this indicates that PF etching of tungsten is very sensitive to former treatments.

3.3.3.4) Special process : influence of the resist.

A wafer was etched completely through with a combined PF-RIE process.
1) 35 sccm of NF_3, 35 sccm of O_2, pressure : 200 mTorr, power: 50W in PF mode, time : 3 minutes.
2) 100 sccm of NF_3, pressure: 150 mTorr, power : 50W in RIE mode, time : 3 minutes.

Results:
1) The photoresist has been removed completely.

2) The profile of the tungsten wall is not of the form of a champaign glass, but rather there was a general undercut.
3) The tungsten surface was smooth.
4) The silicon dioxide surface was smooth, no rests of tungsten could be observed.
5) By measuring the remaining thickness of the PECVD oxide, one can conclude that the non-uniformity was of the bull's eye type. This can be considered normal, as this wafer did not have resist at its border.
The remaining PECVD oxide thickness was also measured near the "double chip": a teststructure which does not receive exposure in this mask level. Fig. 27 shows this thickness as a function of the distance to the resist border of the double chip. It is clear that a large area of resist decreases the etch rate, even as far as 2 mm away from it. This means that the etch rate (of the tungsten) is lower where a blue colouration occurs, while it is higher where the brown colouration takes place.

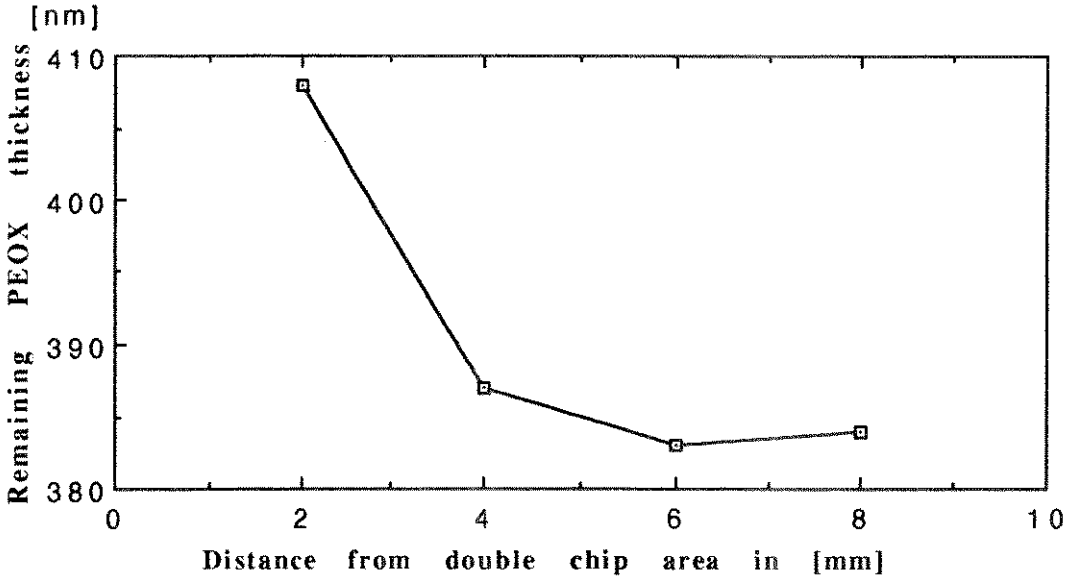

Figure 27 : Remaining PECVD oxide thickness as a function of distance from the double chip resist area after a PF mode etching with a NF_3 - O_2 plasma

3.4) Specific process development to obtain a tungsten back etch process.

The tests performed in 3.1 till 3.3 served mainly to obtain data to study the etch mechanisms and to investigate if it is possible to obtain a process with vertical walls in the tungsten.
In this chapter, the process development to obtain a tungsten back etch process is described. Of course, the results of the tests can also be added to the previous results to study etch mechanisms.

From earlier tests, we know the following general trends:
- in RIE mode, etching is anisotropic, uniform but not selective
- in PF mode, etching is isotropic, not as uniform as in RIE mode, with good selectivity towards oxide (and resist).
Therefore, it is logical to use a two step process:
- a first step in RIE mode, with uniformity as high as possible, but still high etch rates;
- a second step in PF mode, which will remove stringers, because of the isotropic nature of the etching, and which will stop on the underlying layer.
For some tests, we used special wafers which received a PECVD oxide mask : wafers with the same preparation as W_{III}, received a 500 nm thick PECVD oxide on top of the tungsten layer. On top of this a traditional 1.1 µm thick resist was patterned in both LF and DF, with 5% resist coverage and open areas respectively.
This wafers received an oxide etching, with an overetch step of 20%. Some of the wafers were stripped before tungsten etching, others were not, and retained approximately 0.8 µm of resist. These wafers are used for tests in both RIE and PF mode.

3.4.1) Determination of etch rates, uniformities, selectivities and wall profiles.

For a good back etch process, uniformity has to be as high as possible. The processes studied before do not have a good enough uniformity for a back etch process. As it is known that processes at lower pressure have in general better uniformities (because of the higher diffusion constant) some tests at lower pressure and reduced flows, with the same residence times as before, were performed, both in RIE as in PF mode.
For a commercial process, the number of gases should be reduced. In PF mode, SF_6 does not serve as an etch gas. Therefore, we reduced the development in RIE mode also to NF_3 alone.
In some back-etch processes one applies a resist layer on top of the tungsten layer to planarize the structure. For these cases a process with 1:1 selectivity is most useful. Therefore no oxygen was added for etch processes in RIE mode, as the tungsten etch rate is more or less independent on oxygen content, as shown in figures 9 and 11.

Table X shows the tests performed in RIE mode. Etch rates are these at the center of the wafer (C in column remarks) or are the average etch rates (A in column remarks), etch time is 2 minutes unless mentioned otherwise.
Non-uniformity is always of the bull's eye type.
The reproducibility of the processes is good, uniformity is higher than for processes at higher pressure. The etch rate of process 4 is too low to be used as a commercial process. The decrease of the selectivity shows that at lower pressure, the ion bombardment effect is much larger.

Table X: results of tests to determine etch rates, uniformity and selectivity for NF_3-O_2 mixtures in RIE mode for wafers with (R) and without (B) resist mask.

Test nr.- wafer type	NF_3 flow [sccm]	O_2 flow [sccm]	Press. [mTorr]	Power [W]	r_W [nm/min]	U	r_{PR} [nm/min]	S	Remarks
1-R	62	0	75	50	158	0.92	262	0.60	C
2-R	62	0	75	100	306			0.38	A
3-B	62	0	75	100	305	0.88			A
4-R	31	0	40	50	112	0.96	237	0.47	C

Table XI shows the results for processes in PF mode. The conventions are the same as for table X.

Table XI: results of tests to determine etch rates, uniformity and selectivity for NF_3-O_2 mixtures in PF mode for wafers with (R) and without (B) resist mask.

Test nr. - wafer type	NF_3 flow [sccm]	O_2 flow [sccm]	Press. [mTorr]	Power [W]	r_W [nm/min]	U	r_{PR} [nm/min]	S	Remarks
1-R	52	10	100	100	287	0.84	137	2.1	C
2-B	52	10	100	100	279	0.80			A, t = 1'
3-R	25	7	50	100	207	0.97	71	2.9	C
4-B	25	7	50	100	224	0.85			A, t = 3'

Non-uniformity is always of the inverse bull's eye type for wafers with resist, of the bull's eye type for blanket tungsten layers.
Resist patterned wafers are measured with a step height meter, blanket wafers with an SRP, which measures much more points. Therefore thye calculated uniformity of tests 2 and 4 are lower than of tests 1 and 3.
There was oxidation observed on the wafer of test 1, as usual for etch processes in PF mode, but there was no oxidation observed on the wafers of tests 3 and 4.
For test 2, after the PF process a 10 seconds 25 W RIE plasma was applied before the wafer left the reactor and no oxidation was observed. This once again shows that even a weak RIE plasma removes the F rich layer created in the PF plasma.
Comparing these tests with the results of processes at 200 mTorr, one can conclude that at lower pressures the PF plasma behaves more like a RIE plasma, with more ion bombardment: higher uniformity, lower selectivity and at 50 mTorr the tungsten oxide is not formed anymore.

As the last process has the best uniformity of all the PF plasmas, some tests were performed to evaluate etch rates of TiN and oxide with this last process. The main conclusions of these tests are :

- the selectivity W/TiN is much lower than for processes at higher pressures;
- TiN which was partially etched and then exposed to air, does not etch anymore by this process.
With this process, a thermal oxide etches with an average rate of 19 nm/min and uniformity of 0.72, with inverse bull's eye.

These results indicate that some ion bombardment enhanced etching is taking place, not only mere chemical etching. On the other hand, the facts that air exposed TiN remains on the wafer and that SiO_2 etches still very slow, indicate that much less ion bombardment occurs for this process than for any RIE process.

Therefore an extra test was done: etching through the W layer with the same process during 6 minutes. The voltages dropped after 4'10" and stabilized after 4'25".
The W and the TiN were etched away all over the wafer.
Measurement with the Leitz MVP show that there is 141 nm (at the center) to 155 nm (at the border) of oxide left, from the original 180 nm.
SEM analysis, see fig. 28, shows that the resist has been removed nearly completely on most of the fine lines (not on the larger pads).

Figure 28 : Profile etched with the 50 mTorr process (nr 4 in table XI). Observe the large undercut of the TiN between tungsten and oxide.

The walls are lightly sloped, due to the resist erosion rather than to undercut. But enormous undercut of the TiN

layer can be observed. This indicates that the TiN etches much faster, with a loading effect, than the W. This is completely unacceptable for a tungsten back etch process.

From now on, only wafers of the type W_{III} were etched. New tests were performed to investigate the etch characteristics of the new type of tungsten and to develop a tungsten back etch process. Results of etching in RIE mode are shown in table XII. The same conventions are used as in table X.

Table XII: results of tests to determine etch rates, uniformity and selectivity for NF_3-O_2 mixtures in RIE mode.

Test nr. - wafer type	NF_3 flow [sccm]	O_2 flow [sccm]	Press. [mTorr]	Power [W]	r_W [nm/min]	U	r_{PR} [nm/min]	S	Remarks
1-R	62	0	75	50	170	0.98	289	0.60	C
2-B	62	0	75	50	169	0.89			A
3-B	125	0	150	50	237	0.86			A, t = 3'
4-B	125	0	150	50	234	0.87			A, t = 3'

These results are similar to the ones obtained for W_{II}. The tests also show that the etching is very reproducible and that influence of the presence of resist is not important (for a LF pattern).
Etch rate of blanket tungsten layers was determined both by SRP and weight method, and the error was always less than 5%, showing good agreement.
Then several tests were performed to determine the profile of the tungsten wall for a tungsten layer covered with a PECVD oxide mask. The first tests showed that the selectivity of tungsten to oxide is only 1.6 for process 1 of table XII and 1.9 for process 3. Therefore the following process was used to etch through the tungsten layer:
flow : 125 sccm NF_3, pressure : 150 mTorr, power : 50 W, RIE, 4 step process to follow the etching visually : time : 30" + 1'30"+ 1'30"+ 30". The wafer had originally a resist layer on top of the PECVD layer, but the resist was completly removed after the etching.
In the central 90 mm there was still some W, around it was TiN.
Where the TiN was free, a SEM analysis was performed. There was a very slight undercut, over the whole wall, of approximately 100 nm. This is shown in fig. 29.
This test (combined with former tests with resist masks) shows that:
- the etching of the tungsten in RIE mode is really anisotropic although there is a slight isotropic component;
- the presence of resist forms a masking layer at the sidewall of the tungsten to impede completely the isotropic etching.

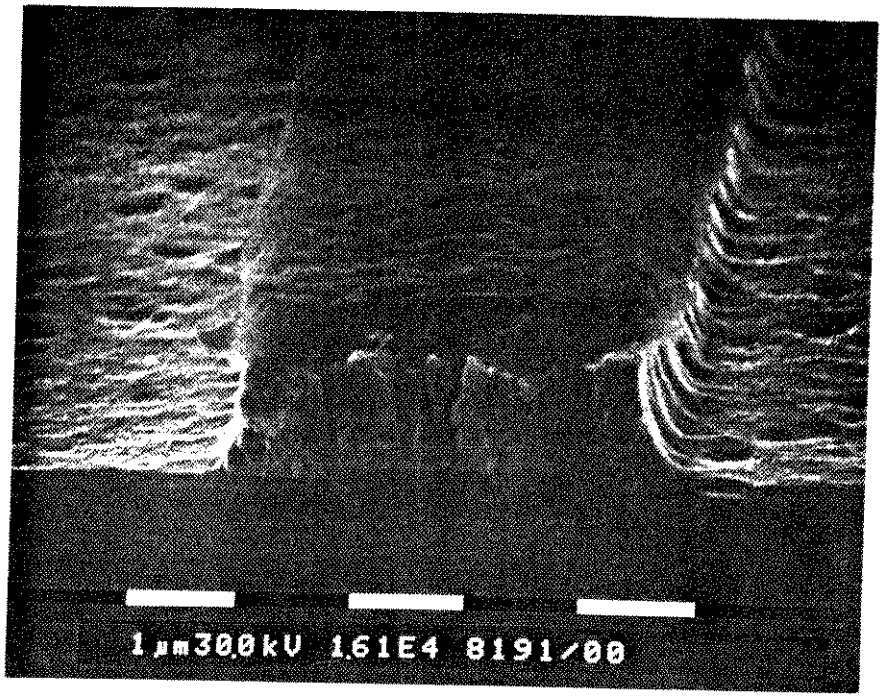

Figure 29 : tungsten profile after RIE mode etching with a pure NF_3 plasma, using a PECVD oxide mask.

Results of etching in PF mode are shown in table XIII. The same conventions are used as in table X.

Table XIII: results of tests to determine etch rates, uniformity and selectivity for NF_3-O_2 mixtures in PF mode.

Test nr. - wafer type	NF_3 flow [sccm]	O_2 flow [sccm]	Press. [mTorr]	Power [W]	r_W [nm/min]	U	r_{PR} [nm/min]	S	Remarks
1-R	50	10	100	100	243	0.94	96	2.5	C
2-B	85	40	200	100	28				A
3-B	50	10	100	100	316	0.83			A

Test 2 shows that this process is not stable for tungsten type W_{III}, just as for types W_{II} and W_I, as described before. Therefore, the instability is not a function of the tungsten type, but of the process.
The etch rates of test 1 are a bit lower than for W_{II}. This is probably due to a passivation effect, as described already before in 3.3.1. The influence of the resist (or better the lack of it at the border) is clearly visible : a traditional bull's eye non-uniformity is observed. Also for test 3 a bull's eye non uniformity was observed.
The first tentative to etch through the W layer of a wafer masked with only 500 nm of PECVD oxide was not succesful.

The used process was : flows : 50 sccm NF_3, 10 sccm O_2, pressure : 100 mTorr, power 100 W, time : 3'30".
When leaving the reactor, no colouration occurred, the tungsten looks the same as before the etching. Measurements with the step height measurement and SRP systems confirm that no W etching has occurred: the sheath resistance is still 0.117 ohm per square and the step height is 450 nm (so only approximately 40 nm of PECVD oxide has been etched away).
We attribute the lack of etching to the formation of an etch inhibiting layer formed during the PECVD oxide etching, during the 20% overetch step. In RIE mode this layer will immediately be removed through bombardment. But in PF mode the etch rate of this teflon like film is extremely low.
Before performing tests for PF processes, it is necessary to give a short RIE plasma step to remove the teflon layer. The following process was used :
flow : 63 sccm NF_3, pressure : 75 mTorr, power : 50 W, RIE mode, time : 6 seconds.
This process removes typically 22 nm of tungsten.

3.4.2) Comparison of processes with light field (LF) and dark field (DF) masks.

As explained in appendix 1, the loading effect is very important for a back etch process. A traditional way to determine how severe the loading effect is, is comparing etch rates of LF patterned layers with DF patterned layers.
Normally the masking material is a resist. We already know that in PF mode, the presence of resist decreases the etch rate. Therefore wafers with a PECVD oxide mask were prepared. Instead of using a resist as mask, wafers with the same preparation as W_{III}, received a 500 nm thick PECVD oxide on top of the tungsten layer. On top of this, a traditional 1.1 µm thick resist was patterned in both LF and DF, with 5% resist coverage and open areas respectively.
These wafers received an oxide etching, with an overetch step of 20%. Some of the wafers were stripped before tungsten etching, others were not, and retained approximately 0.8 µm of resist. These wafers are used for tests in both RIE and PF mode.

The first four tests of table XIV compare etch rates of wafers patterned with resist through a DF mask, with former processes with LF masked wafers, in RIE mode. Tests 5 and 6 compare etch rates between LF and DF oxide masked tungsten.
The results are shown in table XIV. In the first column, RLF stands for a resist light field pattern, RDF stands for a resist dark field pattern, OLF stands for an oxide light field pattern, ODF stands for an oxide dark field pattern.
For tests 5 and 6 S is the selectivity of tungsten to oxide.
Etch time is 2 minutes unless mentioned otherwise.

Table XIV: results of tests to determine etch rates, loading effect, uniformity and selectivity for NF_3-O_2 mixtures in RIE mode.

Test nr. - wafer type	NF_3 flow [sccm]	O_2 flow [sccm]	Press. [mTorr]	Power [W]	r_W [nm/min]	U	r_{PR} [nm/min]	S	Remarks
1-RDF	125	0	150	50	196	0.95	320	0.63	C
2-RLF	125	0	150	50	206	0.86			W_{II} type
2bis	125	0	150	50	234	0.87			blanket layer
3-RDF	62	0	75	50	160	0.92	299	0.54	C, t = 3'
4-RLF	62	0	75	50	170	0.98	289	0.60	table XII,1
5-ODF	125	0	150	50	572	0.95		3.25	C, t=1'30"
6-OLF	125	0	150	50	224	0.82		1.82	C, t=1'30"

Tests 1 to 4 indicate that for these plasma processes in RIE mode W etch rates do not change very much with the coverage of resist, or that two effects happen that cancel each other: an etch rate increase due to the decrease of free tungsten area and an etch rate decrease due to the influence of the resist, a phenomenom similar to processes in PF mode, or due to extra fluorine consumption because of the resist etching. Therefore tests 5 and 6 with a PECVD mask were executed; the resist was stripped before etching. These tests show the results as expected and reported in the literature : an increase in tungsten etch rate when the wafer is masked by a DF mask.
The etch rate of the tungsten increases by a factor of 2.5 which indicates a strong loading effect. At the same time the 704 nm F line intensity was measured and it showed a difference by the same factor 2.5 . When 95% of the wafer is covered by slow etching PECVD oxide, the consumption of fluor through etching of tungsten is much less than for the LF patterned wafer.
Though both DC and AC voltages are lower for the DF than for the LF patterned wafer, the oxide etch rate is higher: this can also be explained by the larger content of free fluorine in the former case. Because of the results of tests 5 and 6, processes in the SWAFER in RIE mode do not seem to be adequate as a last step for an etch back process : the loading effect is too large.

Then several tests were performed in PF mode to investigate the loading effect.
Table XV compares etch rates between LF and DF oxide masked tungsten layers in PF mode, which received first a 6 second RIE step as mentioned above. Etch time is always 2 minutes.

Table XV: results of tests to determine etch rates, loading effect, uniformity and selectivity for NF_3-O_2 mixtures in PF mode.

Test nr. - wafer type	NF_3 flow [sccm]	O_2 flow [sccm]	Press. [mTorr]	Power [W]	r_W [nm/min]	U	r_{SiO2} [nm/min]	S	Remarks
1-OLF	52	10	100	100	329	0.89	31	>10	C
2-ODF	52	10	100	100	510	0.94	67	7.5	C
3-OLF	105	20	200	100	329	0.87		>20	C
4-ODF	105	20	200	100	480	0.90		>20	C

Tests 1 and 2 show very different results from similar tests with DF and LF resist patterned wafers. In this case the expected loading effect occurs. The effect is not as outspoken as for the RIE tests before : here an etch rate increase by a factor of 1.5 against 2.5 in RIE mode. The fact that more free fluorine is available in PF mode than in RIE mode is probably responsible for this effect, though the F-line intensity is also for these tests a factor of 2.5 higher for the DF masked wafer than for the LF masked wafer. The difference in the oxide etch rate can also be explained by the difference in free fluorine content. Also in this case the etch rate of the LF wafer, masked with PECVD oxide is higher than when masked with resist, even in the center of the wafer.
The non-uniformity of the tungsten is always of the bull's eye type.
For tests 3 and 4 the oxide etch rates are so low that it is not possible to measure them adequately with the step height meter. Selectivities are over 20.
Also for tests 3 and 4 the traditional loading effect occurs: the etch rate increases by a factor of 1.4. Etch rates are very similar between the 100 mTorr and 200 mTorr process. The higher pressure process has a lower oxide etch rate as can be expected, probably due to less ion bombardment.
An increase of 40% of the etch rate when changing from a LF pattern to a DF pattern is good enough for an back etch process : in the literature an increase with 100% has been called "acceptable" [22] and "standard processes" are run with an etch increase of 45% in industry.

3.4.3) End point detection and wall profile determination of PF processes.

A series of tests was performed to obtain endpoint detection by optical emission spectroscopy. Additional results were obtained on the TiN etching.
At first some tests were done to determine the complete spectra (from 300 nm to 750 nm) of the etching of bare silicon and blank wafers of tungsten till reaching the TiN layer with process: 100 sccm NF_3, 20 sccm O_2, pressure : 200 mTorr, power : 100 W, PF mode.

When reaching the TiN layer, the intensity of the whole spectrum increases.
Then more specific tests were done with blank wafers of the W_{III} type.
1) The first test used the following process :
flows : 52 sccm NF_3, 10 sccm O_2, pressure : 100 mTorr, power: 100 W, total etch time : 5 minutes.
The TiN layer had also been removed completely.
The complete spectrum was measured and two kind of spectral lines were discovered: lines whose intensity increases after approximately 3 minutes of the process and retain their high intensity and lines whose intensity also increases after 3 minutes but after 20 seconds of increase it drops suddenly and remains afterwards at a low level.
Examples of the first case are the fluorine lines, fig. 30.a shows the 704 nm line, the second case occurs only for nitrogen lines, fig. 30.b shows the 334 nm line, the strongest line of the spectrum.

a)

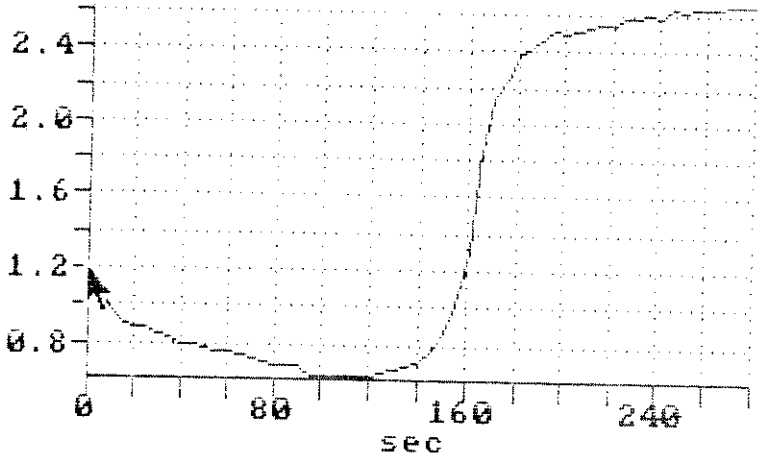

b)

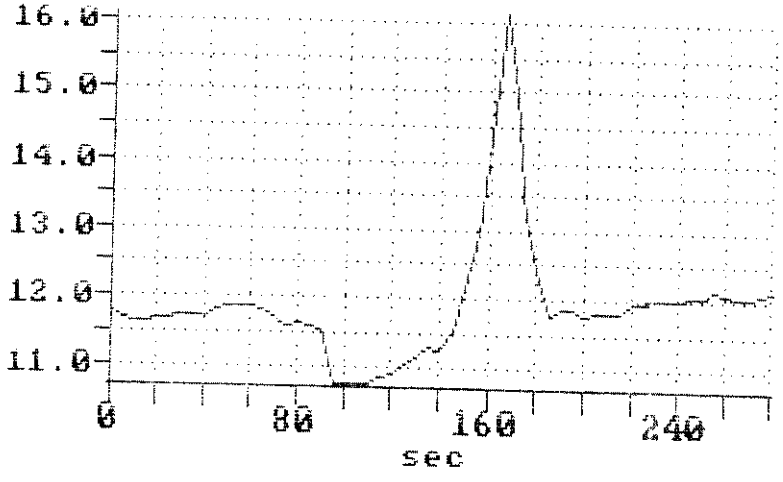

Figure 30 : Intensity of the 704 nm line (a) and the 334 nm line (b) when reaching the end of the tungsten and TiN etching for the 100 mTorr process in PF mode.

These intensity changes can be explained in the following way: during tungsten etching there is a large consumption of fluorine, which finishes when the TiN layer is reached. When this layer is reached, the complete spectrum increases but the N lines increase even more due to the extra N proceeding form the etching TiN layer. When this layer has been removed, the N line intensity decreases again.

2) The second test had the following process parameters : flows: 105 sccm NF_3, 20 sccm O_2, pressure: 200 mTorr, power: 100 W, total etch time: 5 minutes.

The TiN layer has not been removed.

The complete spectrum was measured and in this case all the lines increase in intensity after 2 minutes and 30 seconds; but afterwards, no line is found whose intensity drops.

Figures 31.a and b show the 704 nm F line and 334 nm N line. After the removal of the tungsten, all the lines of the spectrum increase in intensity. As the etching of the TiN is much slower than for the former process, the increase of the N intensity is much less: compare figures 30.b and 31.b, but beware of the scales: for the latter process the increase of the N intensity is a factor 1.3, for the former process it was a factor of 1.5.

a)

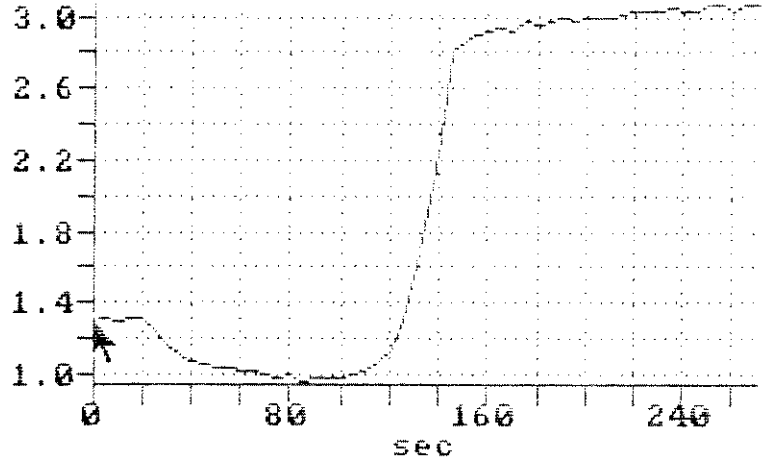

b)

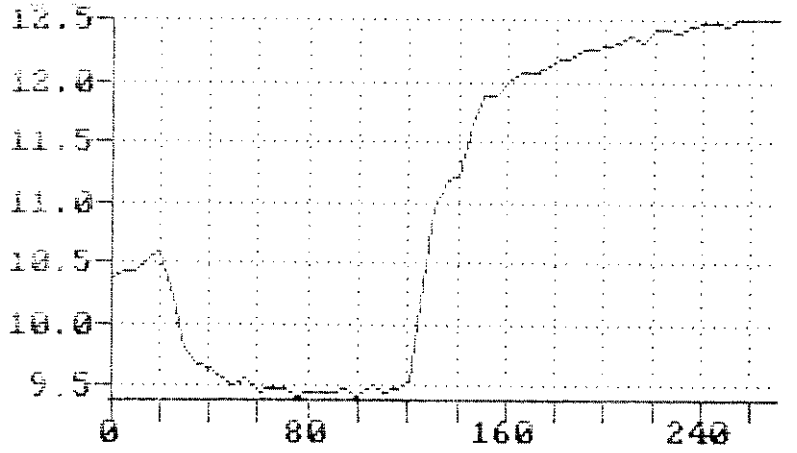

Figure 31 : Intensity of the 704 nm line (a) and the 334 nm line (b) when reaching the end of the tungsten and TiN etching for the 200 mTorr process in PF mode.

During the etching, the voltages were also observed: their changes, as reported before, occur during the same time intervals as the changes of the intensities of the emission spectrum.
These tests indicate it is very well possible to determine end point detection both by using emission spectroscopy and measuring the AC and DC voltages. At the same time it is possible to have an idea of the etch rate of the TiN by monitoring the peak in the N line.
This technique is now used to determine the etch rate of TiN for the following process:
flows: 105 sccm NF_3, 20 sccm O_2, pressure: 200 mTorr, power: 100 W.
We know already that the TiN etch rate is low, but it would be interesting to determine it somewhat more precise. During this test the intensities of the 704 nm line and the 334 nm line were followed to determine the beginning and the end of the etching of the TiN layer. After 2 minutes and 30 seconds the F and N intensities increase and the absolute values of the DC voltage increases.
After 16 minutes and 45 seconds the N intensity is still at the same level. The etch process was stopped and the wafer removed from the reactor: there still was TiN on it. This means that the etch rate is less than 6 nm/min, and therefore the selectivity W to TiN is over 50:1.
This is just excellent.

Then we performed two extra tests to determine what the wall profiles are when using a PECVD oxide mask, both for LF and DF patterned tungsten layers. This test simulates much better the situation during back etching than when using a resist mask.
For both tests the following process was used:
flows: 52 sccm NF_3, 10 sccm O_2, pressure: 100 mTorr, power: 100 W.

For the LF wafer the total etch time determined by end point detection was 3 minutes.
The intensity curves of the 704 nm and 334 nm line are similar to the ones shown in fig. 30.
At the border of the wafer, the TiN was already completely removed, in the center of the wafer still W could be found. SEM analysis was performed. At the center of the wafer there is the traditional undercut, which had been observed already for resist patterned wafers. As shown in fig. 32, at the border of the wafer, there is also undercut, even whem still some W is present. This means that this process will remove stringers during a back etch process.

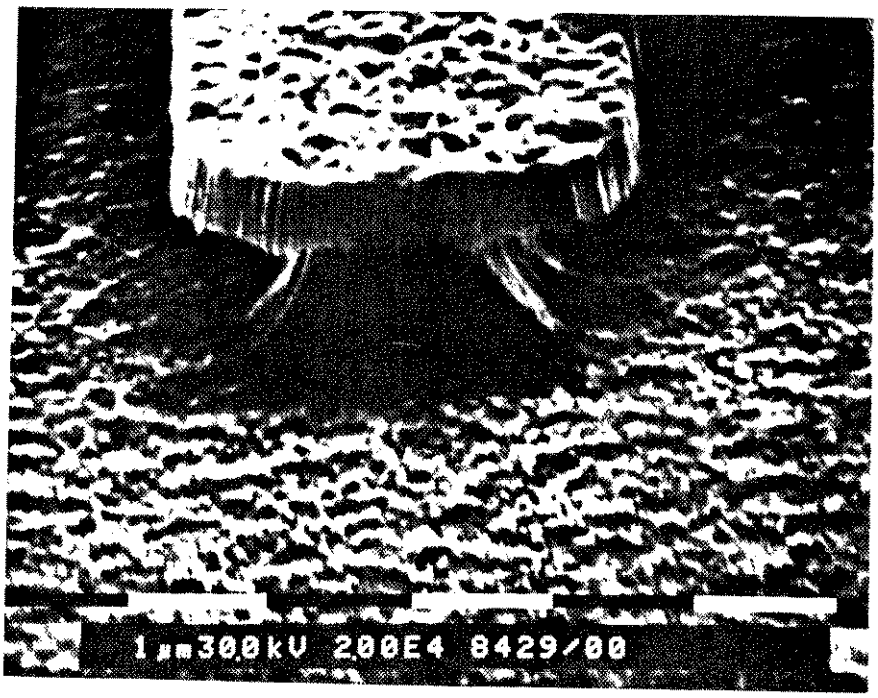

Figure 32 : Tungsten profile after PF mode etching with a NF_3 - O_2 plasma, using a PECVD oxide LF mask.

For the DF wafer the total etch time determined by end point detection was 2 minutes and 25 seconds.
The last 2 minutes of the intensity curves of the 704 nm and 334 nm line are shown in fig. 33. As there is much less free area for this DF masked wafer, it is normal that the signals are much less intense and that end point detection is harder to perform. However, the fluorine line indicates the endpoint quite well, the N line does not show an abrupt change. Analyses with optical microscope and SEM indicate that the tungsten and even the TiN were removed from the whole wafer.

a)

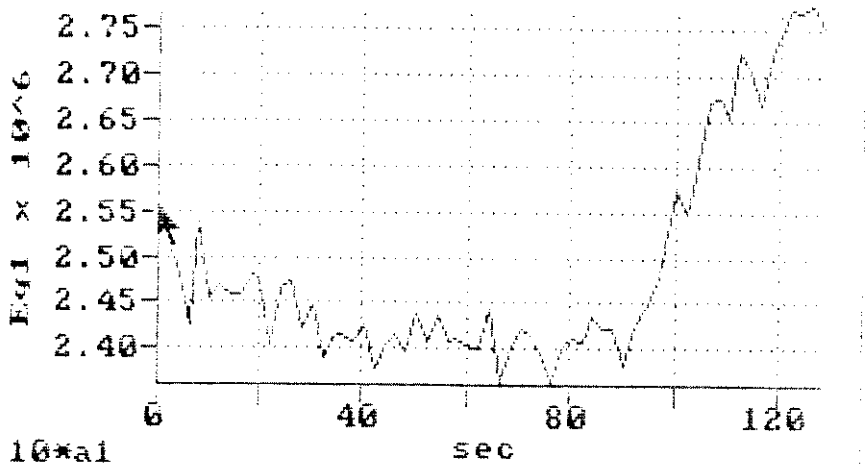

b)

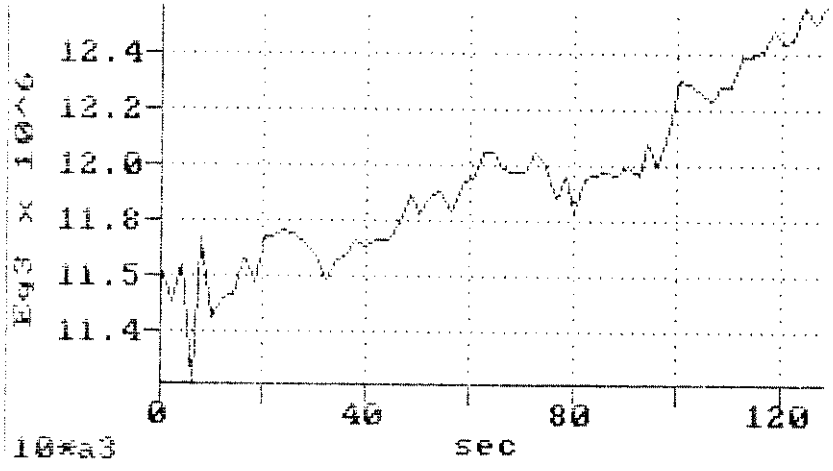

Figure 33 : Intensity of the 704 nm line (a) and the 334 nm line (b) when reaching the end of the tungsten and TiN etching for the 100 mTorr process in PF mode.

The profile of the tungsten wall is shown in fig. 34. It shows that the undercut is similar as for a BF masked wafer. Very often it occurs that for a DF masked wafer the undercut is much more severe than for a BF masked wafer, and in those cases this indicates a severe loading effect. The fact that undercut for BF wafers is similar to undercut for DF wafers indicates that the loading effect is not pronounced for this process.

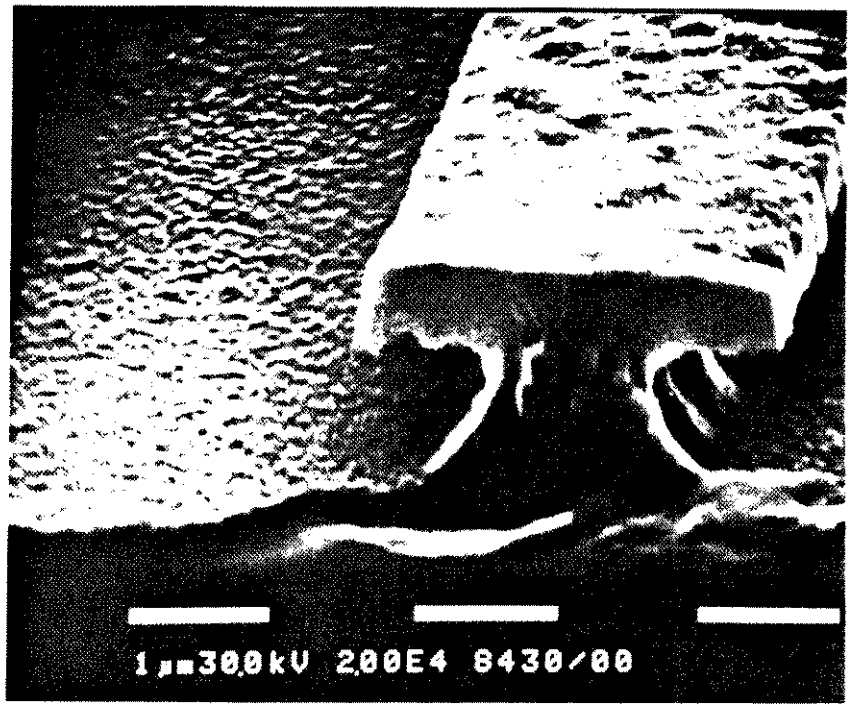

Figure 34 : Tungsten profile after PF mode etching with a NF_3 - O_2 plasma, using a PECVD oxide DF mask. (One can still observe the original roughness of the tungsten film at the down side of the PECVD oxide mask.)

3.4.4) The back etch process.

From all these tests we can synthesize a complete back etch process.
The following 3 step process was tested:
1: flow: 63 sccm NF_3, pressure: 75 mTorr, power: 50 W, RIE, time: 2 minutes
2: flows: 50 sccm NF_3, 10 sccm O_2, pressure: 100 mTorr, power: 100W, PF, time determined by end point detection
3: flows: 100 sccm NF_3, 20 sccm O_2, pressure: 200 mTorr, power: 100W, PF, overetching: typically 25% of step 2.

The first step is used because it is a very uniform process. Half of the tungsten layer is removed by this process.
The second step is used because it is an isotropic process, therefore the tungsten will be removed also at steps in the

underlying layers, without any overetching at the end. Furthermore the process is more uniform than other PF processes.
Step three is used because of its excellent selectivity of tungsten to TiN.
Besides, processes 2 and 3 have a reasonably low loading effect, therefore we expect that the plugs will not be removed.
Three wafers were etched by this sequence: a blank wafer with no topography, a blank wafer with topography under the tungsten and a plug wafer, with plugs at two (height) levels.

1) Blank wafer:
step 2 : 1'30", step 3: 30", the W was removed completely, the TiN remained all over the wafer.
2) Wafer with topography:
step 2 : 1'43", step 3: 24".
The W was completely removed, but the TiN was also etched away at the border of the wafer: this indicates that step 2 was a little bit too long.
Analysis on the optical microscope indicates that no W is left anymore, also not on the sides of the steps.
3) Plug wafer:
step 2 : 1'24", step 3 : 24".
The W was completely removed and the TiN remained all over the wafer, as shown in fig. 35.

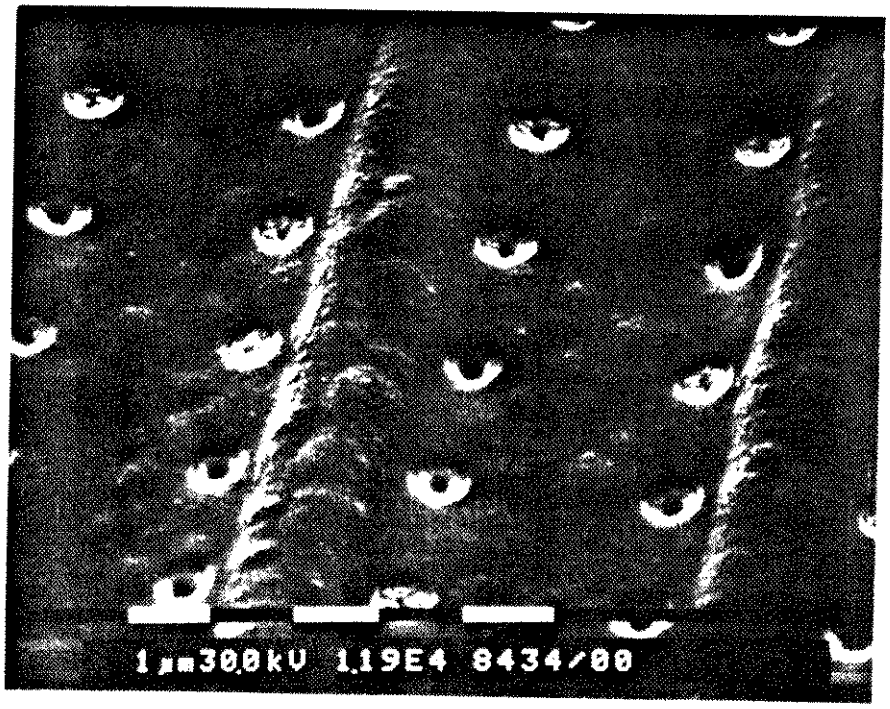

Figure 35 : Overview of several plug structures, at different heights.

SEM analysis shows that the W is removed completely, except perhaps some small spots of the order of 200 nm, in the center of the wafer. No stringers are observed at the steps. Most plugs show etching at the seam. Several plugs are still

complete, as shown in figures 35 and 36. Less than 100 nm of tungsten has been removed at the top of the plug, even for plugs at the highest level.
No plugs are completely removed.
Therefore it is hard to conclude if the opening in the plug at the seam is caused by the etching or rather by the deposition. These seams are often visible after back etch processes, as e.g. in fig. 9 of ref [22].
We can conclude that this process sequence can be succesfully used for back etching of tungsten.
One must observe that an extra step is necessary to avoid a tungsten oxide layer on top of the plug. This step can be an extra etch step in RIE mode in the SWAFER, before removing the wafer, or the process to remove the TiN layer (which can be an Ar sputtering process) can be used to remove the tungsten oxide layer.

Figure 36 : Detailed view of a plug.

3.5) Etching of sputtered tungsten.

Some tests were done on the etching of sputtered tungsten in the manual SWAFER.

The tungsten had to be etched with as little linewidth loss as possible. Therefore tests concentrated on the process with the highest selectivity in RIE: pure SF_6.
The main results are:
Etch rate is 50% higher than for CVD deposited tungsten.
Sputtered W and TiW etch at approximately the same etch rate.
From these we calculated the etch time to clear the 350 nm to be 1 minute and 15 seconds.
Uniformity of the etch rate is 90% or better.

The tungsten surface is very smooth. (This facilitates the step height measurements very much and it is possible that the better uniformity result for sputtered tungsten than for CVD tungsten is only caused by the more precise measurements of the tungsten etch rate.)
When etching was performed until the surface was cleared, without any overetching, the tungsten and TiW walls are perfectly vertical, but a small foot of approximately 0.1 µm can be found at the TiW-SiO_2 interface.
An overetch of 20% cleared this foot completely and did not cause any linewidth loss.
Linewidth measurements in a low voltage linewidth measurement SEM showed a linewidth loss of less than 0.05 µm.

3.6) General overview and conclusions.

In the SWAFER, etch rates, selectivities and uniformities of tungsten etch processes have been investigated as a function of used gases (NF_3, O_2, SF_6), flows (20 to 125 sccm), pressure (40 to 400 mTorr), applied power (50 to 200 W) and etch modes. The influences of the used gases and etch modes are the following:

1. SF_6-O_2 in RIE mode.
The effect of the O_2 content on the tungsten etch rate is shown in figures 3 and 4.
The uniformity of the tungsten etch rate increases with decreasing pressure but is not dependent on power or gas flows. Maximum etch rate is always at the border, minimum etch rate is always at the center of the wafer.
The selectivity of tungsten etch rate towards photoresist and silicon dioxide etch rates decreases with increasing power and decreasing pressure. At 150 mTorr and 50 W power, selectivity towards resist is 1.1:1 with pure SF_6, but decreases with O_2 content, selectivity towards silicon dioxide is of the order of 2:1, independent of gas flows.
The tungsten side wall is vertical. For some process conditions a negative slope can be observed.
End point can be detected by observing the voltages and the F-line, similar to the NF_3-O_2 processes.
The results indicate that some effect occurs in time : the etch rate (nearly) always decreases, for all the processes. This can be due to the formation of a passivation layer in the reactor.

2. NF_3-O_2 in RIE mode.
The effect of the O_2 content on the tungsten etch rate is shown in fig. 9. The etch rate always increases with applied power. When the pressure decreases below 100 mTorr, the etch rate also starts to decrease.
Trends for selectivities and uniformity are similar as for SF_6-O_2 plasmas, but selectivities toward photoresist are typically 20% lower. Selectivity towards TiW and TiN is of the order of 1:1.

The tungsten sidewall is vertical for all the investigated etchings. When a photoresist mask is used, no undercut occurs. When a silicon dioxide mask is used, a slight undercut of approximately 100 nm is observed, as shown in fig. 29. This undercut occurs already during the etching, as it can be observed also when the W film is not yet completely etched.
End point can be detected through the observation of AC and DC voltages and through optical emission spectroscopy. When the TiN layer is reached, both AC and DC voltages decrease significantly, typically with 10%. With an optical spectrometer, it can be observed that both F lines (e.g. at 704 nm) and N lines (e.g. at 334 nm) increase in intensity. When the TiN layer is removed, the voltages and the F line intensity remain constant but the N lines intensity decreases sharply, as shown in fig. 30.

3. NF_3-O_2 in PF mode.
A: Processes with pressures higher than 100 mTorr.
The effect of the O_2 content on the polysilicon and tungsten etch rate is shown in fig. 13.
The presence of photoresist is of major influence for the etch rate. A light field patterned wafer with 5% resist coverage etches 50% faster than a dark field patterned wafer with 95% resist coverage. This is the inverse of what is observed in most other systems.
For a blank wafer, the tungsten etch rate is always higher at the border than in the center of the wafer, typically 15%. When the outer 8 mm of the wafer were covered with resist, the etch rate near this resist area is typically 20% lower than at the center of the wafer. In this case the maximum etch rate is found halfway between the center and the border of the wafer.
For a dark field wafer, the etch rate does not increase with power; for a light field it does, but less than for RIE plasmas. The influence of changing pressure is similar to the change of power.
As indicated above, the main factor that determines the uniformity of the tungsten etch rate is the presence of resist. Uniformities better than 90 % are obtained for several process conditions for wafers patterned with a light field mask and with edge bead removal.
For wafers with light field resist pattern or no resist, the uniformity ameliorates somewhat with decreasing power but strongly with decreasing pressure. For blank wafers, uniformities range from 90 % at 100 mTorr to 80 % at 200 mTorr for a diameter of 115 mm.
For plasmas with oxygen flow from 5% to 50% of the total flow, selectivities towards photoresist and silicon dioxide are much higher than for RIE plasmas. They decrease with decreasing pressure, but are rather independent of power and gas flows. For 200 mTorr pressure processes, selectivities towards resist and silicon dioxide are over 15:1.
The TiW barrier etches in a similar way as the W layer. The TiN barrier layer resists the PF etching extremely well:

selectivities of W to TiN etching are always over 10:1. For 200 mTorr processes selectivity is over 50:1.
The tungsten etching is always isotropic. When overetching for longer times, undercut decreases, eventually leading to a vertical tungsten wall. Undercut is strongly dependent on the gas flows, pressure and power. In general, undercut is more severe for processes with higher etch rates.
Some tests were performed on wafers with a PECVD oxide mask. With a light field oxide mask, etch rates are similar to the etch rates of wafers with a light field resist mask. With a dark field oxide mask (95 % coverage), the etch rates are typically 50 % higher.
Undercut is the same for all these masks: the horizontal etch rate is not faster with a dark field oxide mask.
End point detection can be performed in the same way as for RIE plasmas.
When wafers which have been exposed to these plasmas leave the reactor and come into air, several phenomena occur:
- a tungsten oxide layer is formed on top of the tungsten
- on top of the resist occurs popping of a polymer which was deposited during the etching.

The formation of all these layers can be avoided by applying a RIE plasma of a few seconds to the wafer, just before it leaves the reactor.
The layer on top of the W film inhibits (or at least delays) further etching of these films in PF mode.
These layers can be removed by a RIE plasma, but at a 25 times lower rate than their original films.
Auger analysis was performed on wafers which received a PF etching. No fluorine is detected in wafers which remained in air ambient during several minutes after the etching. On the other hand, oxygen is detected as shown in figures 18 and 19. Oxygen content decreases with depth within the tungsten film, while the tungsten content increases. The oxygen concentration decreases to 50% of its surface concentration at a depth of approximately 15 nm.
When the etched wafer was moved from etch reactor to the Auger Electron Spectrometer (AES) in a nitrogen ambient, fluorine was detected as shown in figures 21 and 22. When loading the sample into the AES, contact with air could not be avoided. Therefore O entered also in the upper tungsten layers. The F concentration decreases in a similar way as the O concentration in this sample and also as in the sample which was exposed to air for several minutes. The W concentration increases in the same way as the W concentrations in the sample that remained into air.

B: Processes with pressures lower than 70 mTorr:
At these pressures, the plasma behaves somewhat similar to an RIE plasma: the selectivities towards resist are of the order of 1:1, the uniformity is better than 92 % for a 115 mm diameter, no undercut is observed for resist coated wafers, no tungsten oxide is formed, no popping can be observed on top of the resist layer. The tungsten etch rate is however a factor of 2 lower than for RIE plasmas.

4. SF_6-O_2 in PF mode.
To obtain tungsten etch rates of the same order of magnitude as for NF_3-O_2 plasmas in the PF mode, the applied AF power has to be increased by a factor of three. No oxidation of the wafer was observed, even after the etched wafer came in contact with air.

A back etch process for obtaining tungsten plugs was developed, with good results, as shown in figures 35 and 36.

In the SWAFER, wafers were etched with CVD tungsten deposited in equipment from three different manufacturers. All the trends were similar. Etch rates differ maximally 10%. The main influence is the tungsten deposition temperature: the higher this temperature, the lower the etch rate.
A few sputter deposited wafers were etched: the trends were also similar, but the etch rates are typically 50% higher than for CVD deposited tungsten films.

References

[1] G. Brasseur, P. Bruneel, C. Jehoul, J. Vandersmissen, "Audio Frequency Plasma Generation Reactor Configuration for Dry Etch Processing", Proceedings of Microcircuit Engineering 90 eds. Coopmans, Van den hove (1990).
[2] D. Pramanik, private conversations.
[3] D. Hess, "Tungsten and Tungsten Silicide Etching in Halogenated Plasmas". Solid State Technology, April 1988, 97.
[4] C. Tang, D. Hess, "Tungsten Etching in CF4 and SF6 Discharges", J. Electrochem. Soc. 131, 115 (1984)
[5]3. S. Tandon, G. Jones, "Reactive Ion Etching of Tungsten in SF6 and CF4", in "Tungsten and other refractory Metals for VLSI Applicationsd IV", Eds. Blewer & Mc. Conica (MRS Proceedings of the 1988 Workshop).
[6] T. Bestwick, G. Oehrlein, "Tungsten Etching Mechanisms in CF4/O2 Reactive Ion Etching Plasmas", J. Appl. Phys. 66, 5034 (1989)
[7] Mutsukura, Turban, "Reactive Ion Etching of Tungsten in SF6-N2 plasmas", J. Electrochem. Soc, 137, 225 (1990)
[8] Collumeau e.a., "RIE of a T-shape refractory ohmic contact for a self-aligned heterojunction bipolar transistor", J. Electrochem. Soc. 137, 671 (1990)
[9] F. Fracassi, J. Coburn, "Plasma-assisted Etching of Tungsten Films: a quartz-crystal Microbalance Study", J. Appl. Phys. 63, 1758 (1988)
[10] A. Bensouala, J. Strozler, A. Ignatiev, J. Yu, J.Wolfe, "Ion Enhanced Reactive Etching of Tungsten Single Crystals and Films with XeF2", J. Vac Science Technol. A 5, 1921 (1987)
[11] A. Durandet, Y. Arnal, J. Pelletier, G. Pomot, "Anisotropy and Kinetics of the Etching of Tungsten in SF6 Multipolar Microwave Plasma", J. Appl. Phys. 67, 2298 (1990)

[12] W. Greene, D. Hess, W. Oldham, "Ion-bombardment-enhanced Plasma Etching of Tungsten with NF3/O2", J. Vac. Science Technol. B 6, 1570 (1988)
[13] K. Greenberg, T. Verdeyen, "Kinetic Processes of NF3 etchant gas discharges", J. Appl. Phys. 57, 1596 (1985)
[14] T. Daubenspeck, P.Sukanek, "Investigation and Modelling of mixed Halogen Freon/Oxygen Plasma Chemistries for Tungsten Etching", J. Electrochem. Soc. 136, 3779 (1989)
[15] W. Pan, A. Steckl, "Selective Reactive Ion Etching of Tungsten Films in CHF3 and other Fluorinated gases", J. Vac. Science Technol. B 6, 1073 (1988)
[16] Adachi, Susa, "Reactive Ion Etching of Tungsten Films Sputter Deposited on GaAs", J. Electrochem. Soc. 132, 2980 (1985)
[17] A. Richards, B. Thompson, K. Allen, H. Sawin, "Atomic Chlorine Concentration Measurements in a Plasma Etching Reactor", J. Appl. Phys. 62, 792 (1987)
[18] Saia, Gorowitz, Woodruff, Brown, "Plasma etching methods for the formation of planarized tungsten plugs used in multilevel VLSI metallizations", J. Electrochem. Soc, 135, 936 (1988)
[19] Miller, Frazier, Su,"Controlling tungsten etchback on submicron devices", MMT, January 1992,28
[20] J. Coburn, "Plasma Etching and Reactive Ion Etching", IV Oficina Brasileira de Microeletronica, pp. 41-80, edt Mammana (1983)
[21] H. Bender, private conversations
[22] J. Berthold, C. Wieczorek, "CVD-W deposition and dry etch processes for planarized metallization and tungsten interconnect techniques", Proceedings of the European Workshop on Refractory Metals and Silicides, eds. De Keersmaecker, Maex, pp 506-516 (1989)

Appendix III : Etch processes in the Matrix 303.

Index

Appendix III : Etch Processes in the Matrix 303.

A few tests were done in a Matrix 303 etcher.

1) Equipment.

This equipment is an afterglow system, similar to the one described in ref [1] and schematically depicted in fig. 1. The RF power (at 13.56 MHz) is capacitively applied at the upper part of the reactor. The lower part of the reactor is separated from the upper part by a grid so that the wafer is not imbedded in the plasma. Temperature of the chuck on which the wafer rests can be controlled, up to 200°C. The main application of this equipment is in the isotropic etching of oxides.

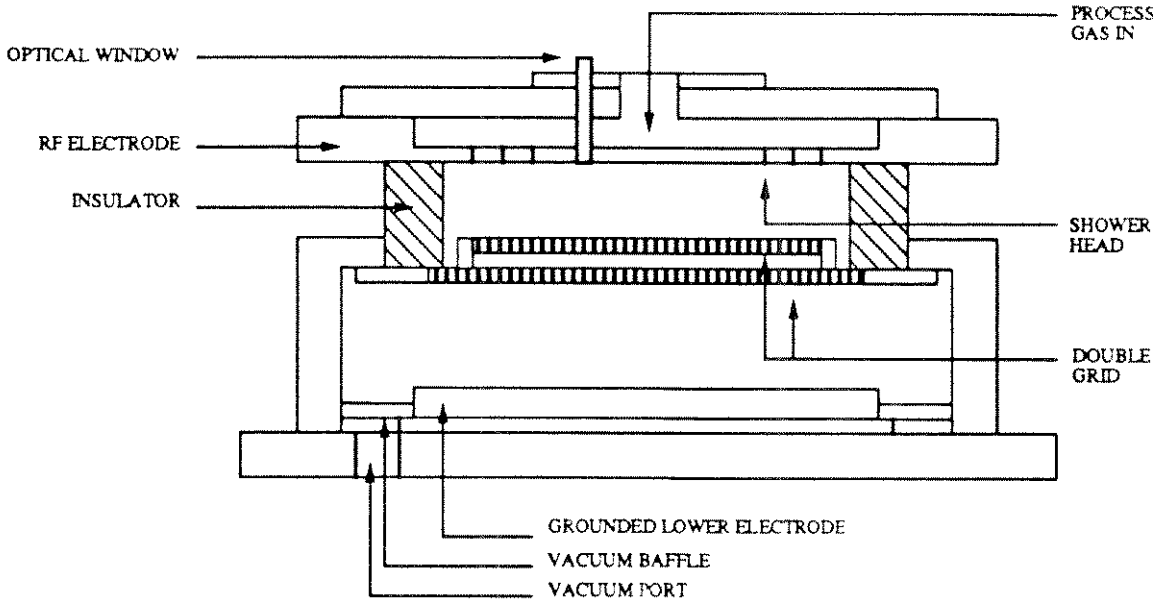

Figure 1 : Schematic presentation of the Matrix 302 model.

2) Etch tests

As this equipment is some kind of an afterglow plasma etcher, etching is purely chemical. Therefore the etch characteristics should be somewhat similar to the ones obtained in PF mode in the SWAFER. Etch tests were done with NF_3 containing mixtures to verify the colouration effects, as shown in table I. The wafer was removed after steps of 30 seconds of plasma from the reactor, to observe better what happens.

Table I : Process parameters for colouration tests

Test	NF_3 Flow [sccm]	O_2 Flow [sccm]	He Flow [sccm]	Pressure [mTorr]	Power [W]	Temp [°C]
1	50	10	20	800	300	50
2	50	0	45	800	300	50
3	50	10	15	800	300	50

The observations of the colouration after each etch step of 30 seconds are the following :
Test 1 :
- 30 seconds: no colouration, but the wafer remained little time in air.
- extra 30 seconds: colouration starts when the wafer is 60 seconds in air.
Two regions could be observed : the center region obtains a blue colour, while the outer region becomes rather brownish.
Test 2 :
- after 2 steps of 30 seconds : only some local colouration
- after 2 extra steps of 30 seconds, the whole border becomes coloured, when left a few tens of seconds in the air.
Test 3 :
- one step of 30 seconds : there is colouration already, in the same way as in process 1, when the wafer is left long enough in the air.

3) Conclusions

Oxidation of the tungsten layer happens also after etching in this equipment, not only in the SWAFER. The colouration clearly occurs outside the reactor, in the air ambient. The presence of oxygen in the plasma is not necessary for obtaining an oxide. As plasmas from tests 1 and 3 generate probably much more F than the plasma of process 2, there will be more F diffusion into the tungsten and therefore a thicker oxide is formed.
On the contrary of the SWAFER, where oxidation occurs very quickly once the wafer arrives in the air, here it takes more time. It is possible that the little bombardment, caused by the plasma sheath in the SWAFER makes the upper layers of the tungsten a bit more porous, therefore permitting the oxygen, or the water vapour, to diffuse faster into the tungsten, as explained in more detail in appendix V.

Reference :

[1] W. Ostrout, S. Hunkler, S. Ward,"Enhanced Process Control of Submicron Contact Definition", Proceedings of SPIE, Vol 1392, eds. Bondur, Turner (1991), 151.

Appendix IV : Etch Processes in the TEGAL 15XX.

Index.

Appendix IV : Etch Processes in the TEGAL 15XX.

Introduction

The use of tungsten as material in Integrated Circuit fabrication is becoming more and more important. The main application at the moment is the use of tungsten plugs. To obtain these structures, in general an etch back step is used, as explained in appendix I.
Tungsten etch back processes had been developed on the precursor of the 15xx, the Tegal 1500. The main change is that this new equipment has a magnetically confined plasma, therefore, one expects higher etch rates and better selectivities towards the underlying layers. It is necessary to characterize first this new reactor, before developing tungsten etch processes. In this chapter, characterization of SF_6-O_2 plasmas was done first by actinometry, then through analysis of polysilicon etch processes and then specific tests were performed on tungsten layers, to obtain a good etch back process.

1) Equipment.

The Tegal 15xx etch equipment used for these etchings is a prototype of a future commercially available equipment. It is for the moment sort of one of a kind, though in ref. [1] a description of a similar equipment is given.
In fact it is an upgrade of TEGAL's traditional 1500 Series. The main difference is that in this machine, 2 series of magnets are placed: 1 on the upper electrode and one around the vertical walls of the reactor as shown in fig 1. In this way a very efficient magnetic confinement has been obtained : therefore this kind of equipment is called a Magnetically Confined Reactor (MCR). No magnets are placed near the lower electrode.
The upper electrode is always grounded: its diameter is large, approximately 50 cm.
There are several ways to apply power, as shown in fig. 1.c.
In Triode I mode, 13.56 MHz RF power is applied to the walls of the reactor.
In Triode II mode, 13.56 MHz RF power is applied to the bottom electrode, which has a diameter a little bit larger than the 125 mm wafer.
In both modes, 100 kHz power can be applied to the bottom electrode.
When no 100 kHz power is applied to the bottom electrode in Triode I mode, one can consider that this electrode is floating, as the matching networks form very high impedances.
In this way, we can compare the Triode I mode, without any AF, with the PF mode of the SWAFER and the Triode II mode with the RIE mode of the SWAFER, though one should not forget that for the SWAFER all power is applied at 25 kHz.
The bottom electrode can be cooled or heated. To promote heat transfer, He flows between the clamped wafer and the

electrode. The He backside pressure can be regulated : its maximum is 5 Torr. In all these tests, the electrode was cooled to 20°C.
There are 8 gases available: CF_4, SF_6, Cl_2, HBr, HCl, N_2, O_2, Ar. No NF_3 was available.

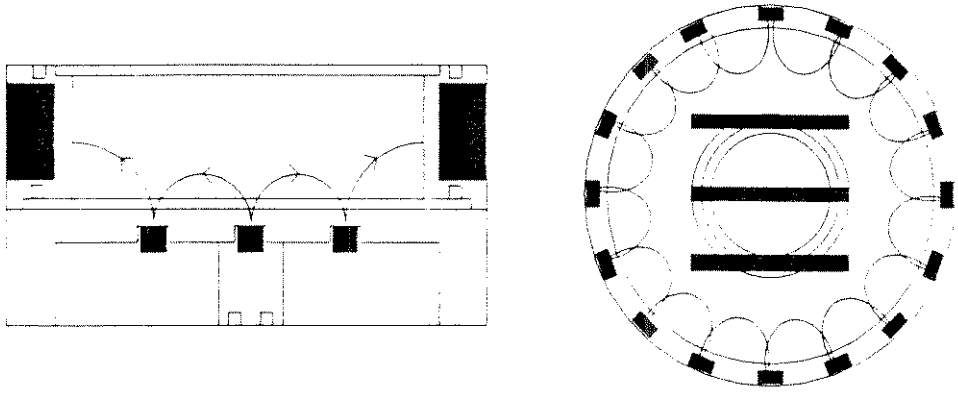

a) b)

Figure 1 : Top view (a) and side view (b) of the Triode reactor with magnetic confinement.

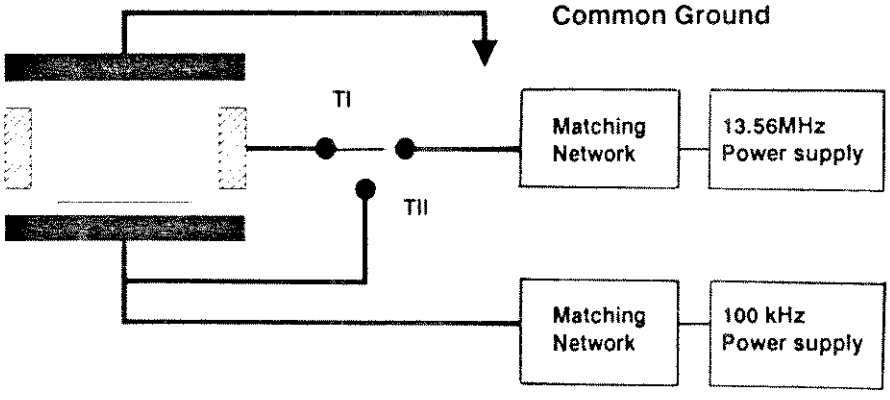

Figure 1.c : RF and AF configurations.

2 Preliminary tests.

Before the tests we shall describe below, some other tests were performed to characterize the equipment somewhat and to transfer a tungsten back etch process from another system to this one.
Tests were done primarily with a SF_6-O_2 chemistry. In these series of tests high selectivities towards photoresist were obtained both in Triode I as in Triode II mode. The resist etch rate increases more when 100 kHz AF power is applied to the lower electrode. Both W and resist etch rates increase when the He backside pressure is reduced to less than 5 Torr, with decrease of selectivity of W to resist. Therefore it was decided to leave the He backside pressure constant at 5 Torr.
These first results were very promising for vertical profile etching: in Triode II, with a SF_6-O_2 chemistry, vertical etching of the tungsten was obtained with selectivity towards the resist of over 4:1. Unfortunately, these tests proved non reproducible later. As we shall discuss later, passivation of the reactor is a probable cause of this non reproducibility.

3 Actinometry measurements.

As no large parameter range characterization of the machine had been done, a series of actinometry measurements were performed in a large parameter range :
- gas flows: SF_6 : 20 sccm to 80 sccm, O_2 : 0 to 16 sccm (0 to 80% of its maximum flow of 20 sccm of the used mass flow meter);
- pressure : 10 mTorr (minimum pressure for 96 sccm of flow is 9.5 mTorr) to 25 mTorr (which is approximately the highest pressure at which the magnetic confinement is still effective);
- power : at 13.56 MHz : 400 W to 700 W both Triode I (TrI) as Triode II (TrII), at 100 kHz : only 2 values : 0 W and 50 W.

Through the use of statistical design, the number of tests is reduced. The Response Surface Method (RSM) method was used for these test designs, because a large parameter area is investigated. This method is adequate for a screening test. A quadratic model was applied, which is a compromise between the accuracy/precision of the results and the number of tests. The accuracy can be evaluated through the correlation factor R^2 and analysis of variances, as explained in appendix I. In general, the results of these tests showed to be reliable.
A commercially available programme for statistical design of experiments, RS/Discover from BBN Software Products Corporation, was used to determine the test points and to analyse the results. These results can be shown in tables, graphs and formulas, using the RS/Explore and RS/1 programmes from the same company.

Most actinometry experiments use the 704 nm line to measure the intensity of the fluorine, I_F, and the 750 nm line to determine the intensity of the argon, I_{Ar}. In these experiments the signal to noise ratio of the 750 nm line signal was very low. Therefore the 697 nm Ar line was used. The main drawback to use the 697 nm line is that the light intensity which comes from the plasma at 697 nm is not zero when no Ar flows in the reactor. This light comes mainly from other strong emission peaks in the neighbourhood of the 697 nm line, e.g. from the 704 nm F line. As the increase of the 697 nm line intensity was linear with increasing Ar flow, it was possible to circumvent this problem by using the following method.
The intensity of the 697 nm line (and of the 704 nm line also) was measured for 4 plasmas with 4 different Ar flows : 0 sccm, 0.7 sccm, 1.7 sccm and 2.8 sccm : each plasma lasts for 30 seconds with intervals of 10 s to stabilize the gas flows of the following plasma. Figure 2 shows the intensities of the 704 nm line and the 697 nm line of the plasmas with constant SF_6 and O_2 flows and Ar flows of in chronological order 0 sccm, 0.7 sccm, 1.7 sccm and 2.8 sccm. The F intensity remains quite constant, while the Ar intensity increases.

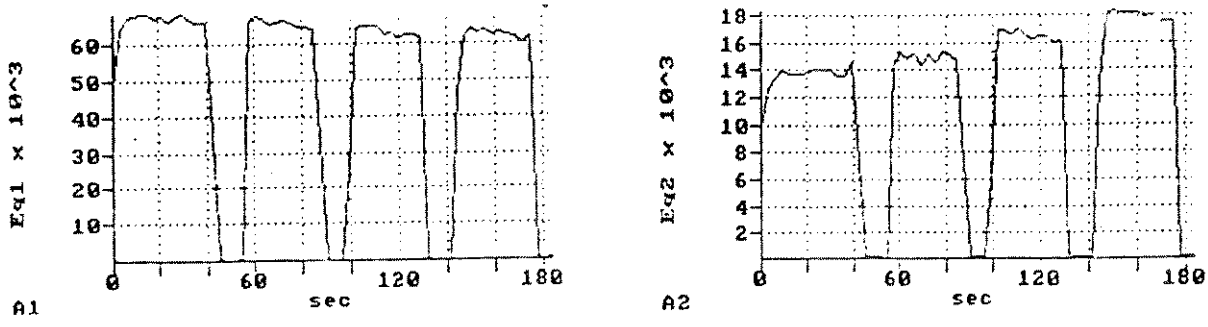

Figure 2 : Intensity of F (A1) and Ar (A2) peaks for Ar flows of 0, 0.7, 1.7 and 2.8 sccm.

An average of the argon intensities per argon flow was made and this was then plotted as a function of Ar flow, as shown in fig. 3 (The Ar mass flow controller (MFC) available was a 5 sccm N_2 MFC. As the thermal coefficient of Ar is 1.4 this means that 7 sccm of Ar can pass through it. As the minimum controllable flow through a MFC is typically 10% of its maximum value, 0.7 sccm of Ar was chosen as the first value. In the abcissa of fig. 3 is shown the percentage of maximum flow of Ar.)
On this plot a linear regression was performed. The value of I_{Ar} to be used in the expression I_F/I_{Ar} was determined in the following way (for historical reasons) : the product of

gradient of the regression with 0.5 times the total SF_6-O_2 flow (in sccm). For the example shown in fig. 3 the SF_6 flow was 50 sccm, the O_2 flow was 8 sccm.
The obtained I_{Ar} value therefore was:
0.057 x 0.5 x 58 = 1.65.

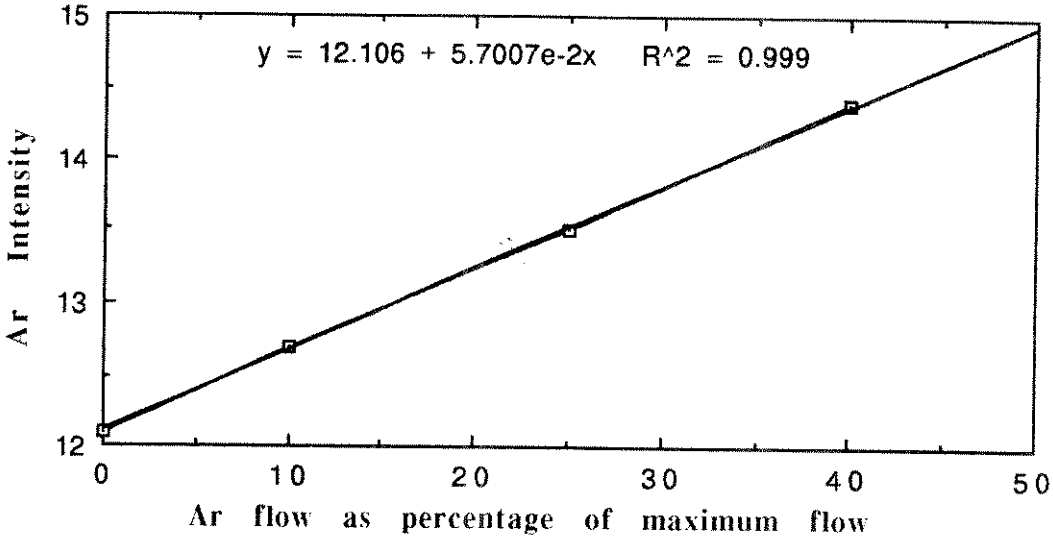

Figure 3 : Intensity of the Ar 697 nm line as a fuction of Ar flow, with linear regression.

An estimation of the error of the I_F/I_{Ar} quotient can be made in the following way. For the example in fig. 2 for which the flows were 80 sccm of SF_6 and 0 sccm of O_2, one can determine that:

$I_F = 65 \pm 1.5$ (A.U.)

$I_{Ar1} = 14 \pm 0.4$ (A.U.)

$I_{Ar4} = 17.5 \pm 0.4$ (A.U.)
(These values were obtained by averaging 10 measurement points.)

$I_{Ar4} - I_{Ar1} = 3.5 \pm 0.8$ (A.U.)

Then $I_F/I_{Ar} = 19 \pm 25\%$
Through a linear regression through z points (in this case to obtain the I_{Ar} value), we estimate that the error is a factor $(z)^{1/2}$ lower, if the correlation factor R^2 is at least 0.99. In this case that would mean that the error is a factor of 2 lower : $I_F/I_{Ar} = 19$ +- 13%, for this example. This example was a worst case example. In general the signal to noise of the Ar signal is better and/or the difference $I_{Arx} - I_{Ar1}$ is larger, in this way decreasing the relative error. In general the error of I_F/I_{Ar} is less than 10%.

When the correlation factor of the linear regression for determination of the I_{Ar} signal was lower than 0.99, the test was repeated. (The difference of the final results with the previous results was always less than 10%.)
To determine the final I_F/I_{Ar} value, the pressure has to be taken into account, as explained in appendix I. For our calculations a multiplication by 10% of the pressure (in mTorr) was performed. For the example in fig. 3 : the pressure was 18 mTorr. As I_F was 30, the final I_F/I_{Ar} value is:
30 x 1.8 / 1.65 = 33
The emission spectrometer used for these experiments was a EG&G Princeton Applied Research model 1470.
As substrate, always a bare 125 mm silicon wafer was used.

The results of the actinometry measurements are shown in table I, the fluorine concentrations are all in arbitrary units.

Table I : Overview of F concentration in function of process parameters.

Nr	Gas flows SF_6 [% of 100 sccm]	O_2 [% of 20 sccm]	Press [mTorr]	RF Power [W]	Fluorine Concentration in [A.U.] at 0W AF TrI	0W AF TrII	50W AF TrI	50W AF TrII
1	80	80	25	750	64	50	62	45
2	80	40	18	575	54	36	59	32
3	80	0	25	400	53	28	48	27
4	20	80	10	750	18	19	17	19
5	20	40	18	575	35	24	40	22
6	20	0	25	400	64	30	52	39
7	80	0	10	750	46	25	51	20
8	20	0	10	750	25	25	22	22
9	20	80	25	750	26	34	26	30
10	50	40	18	575	33	37	34	29
11	20	80	10	400	16	14	16	13
12	80	0	10	400	40	17	34	17
13	50	0	18	575	47	31	41	26
14	50	80	18	575	40	30	47	26
15	50	40	18	575	35	29	35	30
16	50	40	18	400	39	26	35	26
17	20	0	10	400	25	22	23	22
18	50	40	10	575	24	18	26	19
19	80	80	10	400	27	17	33	17
20	50	40	18	750	37	38	33	35
21	20	0	25	750	56	65	51	54
22	20	80	25	400	55	40	51	38
23	50	40	25	575	52	40	44	41
24	80	80	10	750	34	21	42	20
25	80	80	25	400	66	37	52	39
26	80	0	25	750	83	50	84	41

The general trends are the following:
1) Nearly no difference between 0 W AF and 50 W AF power is observed. Though the values of I_F and I_{Ar} are typically 30%

lower for plasmas with 50 W AF power, the difference in I_F/I_{Ar} between 0 W and 50 W AF is much less, typically 10%.
2) In this range of RF power, the F concentration does not change much with RF power.
3) In Triode I more F is generated than in Triode II mode.
4) Pressure increase leads to F concentration increase.
5) The influence of SF_6 and O_2 flows depends on the type of plasma and the values of the flows themselves.

The results of the 4 etch modes (Triode I and II, with and without 50 W AF power) will be discussed now in more detail.

a) Triode I, 0 W AF.

The correlation factor R^2 = 0.90, and the analysis of variances F(10,1) = 0.9947 show that the model fits well the experimental data.
The overall trends are shown in fig. 4.
Increase of SF_6 flow increases the F content, at SF_6 flows higher than 32 sccm; increase of O_2 flow decreases F content, increase of pressure increases the F content, increase of RF power does not change the F content, for powers higher than 497 W.

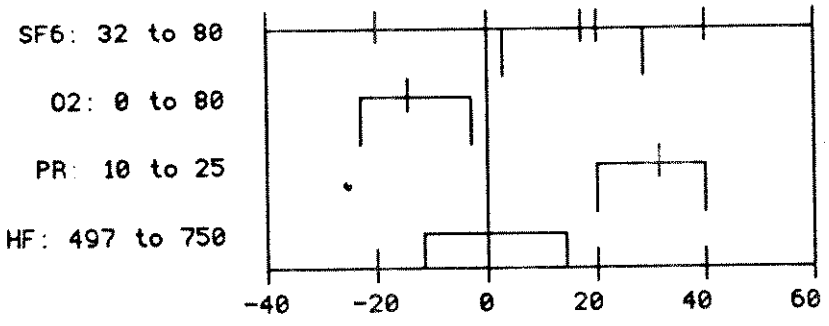

Figure 4 : Overall trends of the F concentration as function of SF_6 flow, O_2 flow, pressure and RF power in Triode I mode, for 0 W AF. The abcissa indicates the increase of the F content, a negative value indicates a decrease.

Figure 5 shows that at lower SF_6 flows the F content decreases with SF_6 flow, but increases at higher SF_6 flows. It shows that for high SF_6 flows, the traditional influence of O_2 on the F generation can be found. For low O_2 flows the F concentration increases due to a more efficient decomposition of the SF_6 molecule. At higher O_2 flows a dilution effect occurs, thereby decreasing the F concentration. This behaviour is not found at low SF_6 flows. For these flows, the magnetically confined plasma is so efficient in the decomposition of the SF_6 molecules that the addition of oxygen increases much less the formation of the free fluorine : mainly a dilution effect occurs. At higher

SF_6 flows, the decomposition of the SF_6 molecules is not as complete, therefore the oxygen influences the free fluorine generation as explained above.
Figure 6 shows that the F concentration is nearly independent of RF power and approximately linearly dependent on pressure.

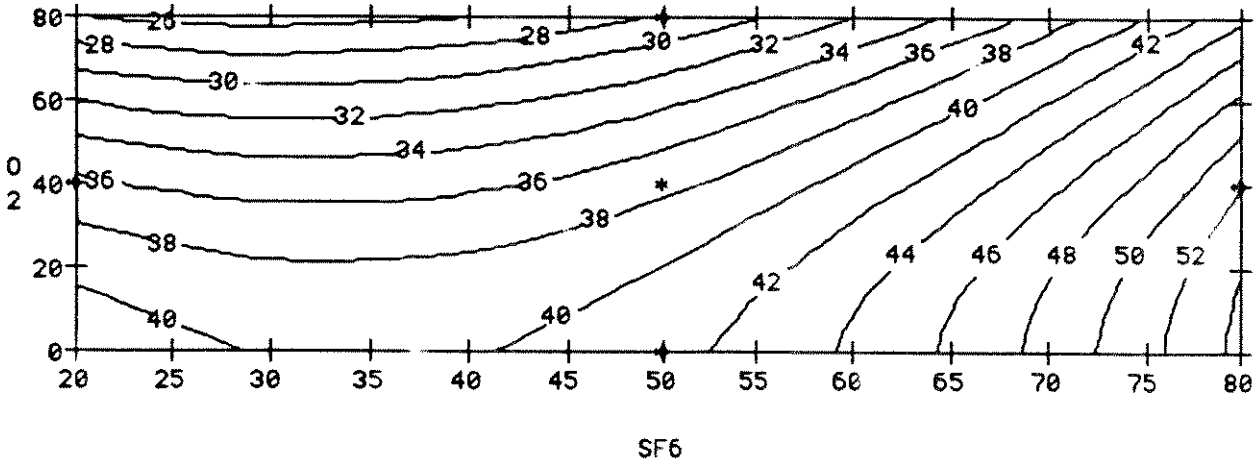

Figure 5 : Contourplot of F concentration in A.U. as a function of SF_6 flows and O_2 flows, at fixed pressure of 17.5 mTorr, Triode I mode, 400 W RF and 0W AF power.

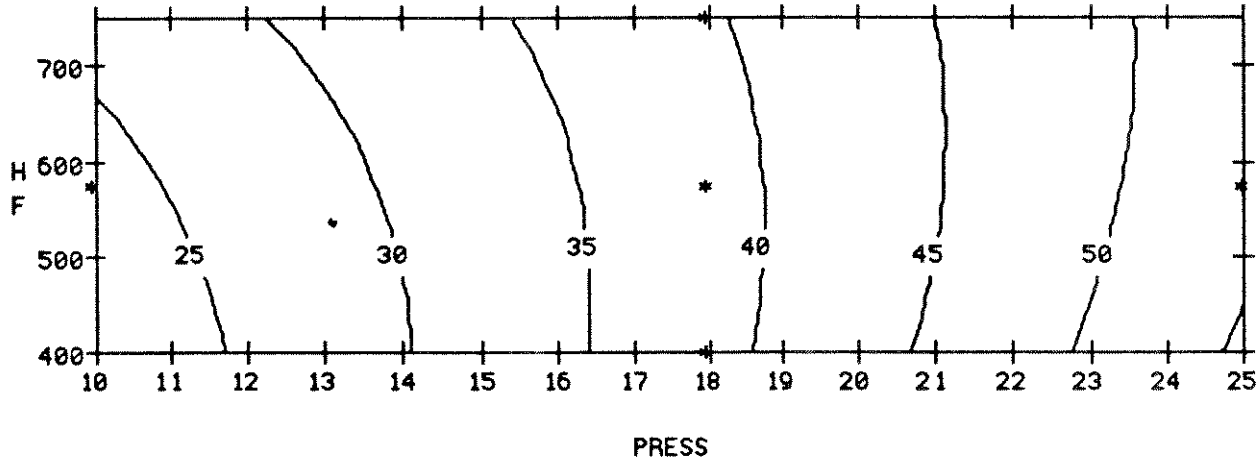

Figure 6 : Contourplot of F concentration in A.U. as a function of pressure and power for a SF_6 flow of 40 sccm and an O_2 flow of 8 sccm, Triode I mode, 0W AF power.

b) Triode I 50 W AF

The correlation factor R^2 = 0.85 and the analysis of variances F (10,1) = 206.9 show that the model does not fit well the experimental data. Therefore one has to be careful in the analysis of the results. In this case it is more secure to compare these plasmas with the corresponding plasmas at 0 W and evaluate if the same trends are valid. One can indeed assume that applying AF power to the lower electrode when RF power is applied to the walls of the

reactor will not influence very much the creation of free fluorine, but will enhance the ion bombardment, in this way increasing the etch rate of most thin films.
Table I shows indeed that the general trends are the same and that the absolute values are always of the same order of magnitude.
For sake of completeness, the results of the analysis are given below:
The overall trends are shown in fig. 7.
Increase of SF_6 flow increases the F content, at SF_6 flows higher than 44 sccm; increase of O_2 flow does not influence very much the F content, with a tendency to decrease it a little bit; increase of pressure increases the F content, increase of RF power does not change the F content much, for powers lower than 604 W.

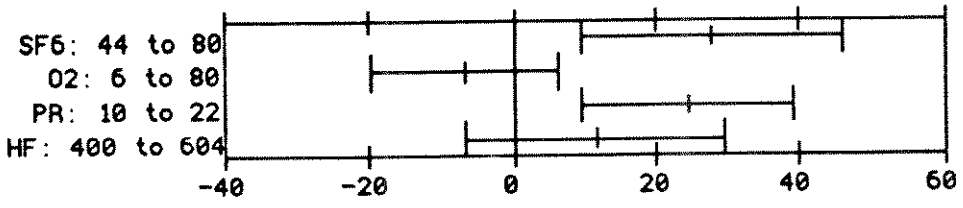

Figure 7 : Overall trends of the F concentration as function of SF_6 flow, O_2 flow, pressure and RF power in Triode I mode, for 50 W AF. The abcissa indicates the increase of the F content, a negative value indicates a decrease.

To do a more succesfull statistical analysis, a higher order model should be used. This means more tests. For our purpose here, we assume that the concordance between the plasmas with and without AF power should be quite good.

c) Triode II 0 W AF

The correlation factor $R^2 = 0.88$, and the analysis of variances $F(10,1) = 1.10$ indicate that the model fits well the experimental data. However one must take care with the analysis of variance as the reproducibility test for this mode was rather bad, as shown in table 1 by tests 10 and 15. This influences the analysis of variances so that it will indicate a good fit, even when the fit would be rather poor. The high correlation factor however indicates that the model is probably quite adequate.
The overall trends are shown in fig. 8.
Increase of SF_6 flow does not significantly influence the F content; the same is valid for the O_2 flow; increase of pressure increases the F content, increase of RF power increases the free F concentration, contrary to the results for Triode I mode.
It is clear from these results that the generation of free fluorine in Triode II mode is quite different from the

generation in Triode I mode. The main difference between the two modes which will mostly influence the generation of the F is the area of the powered electrodes, which is more than a factor of 5 larger in Triode I than in Triode II. Though the electric fields are less uniform in Triode I mode than in Triode II mode, the fact that magnets are places all along the wall of the reactor, helps very much to form a homogeneous and intense plasma in Triode I mode. These two factors together help to obtain a more intense plasma in the reactor in Triode I mode than in Triode II mode, what results in higher F concentrations.

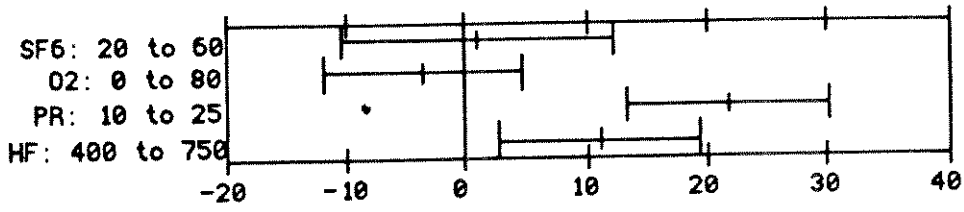

Figure 8 : Overall trends of the F concentration as function of SF_6 flow, O_2 flow, pressure and RF power in Triode II mode, for 0 W AF. The abcissa indicates the increase of the F content, a negative value indicates a decrease.

Some more detailed results are shown in fig. 9 and fig 10. The influence of the flows is clearly much less than the influence of pressure and even than the power. F concentration is approximately proportional to the pressure.

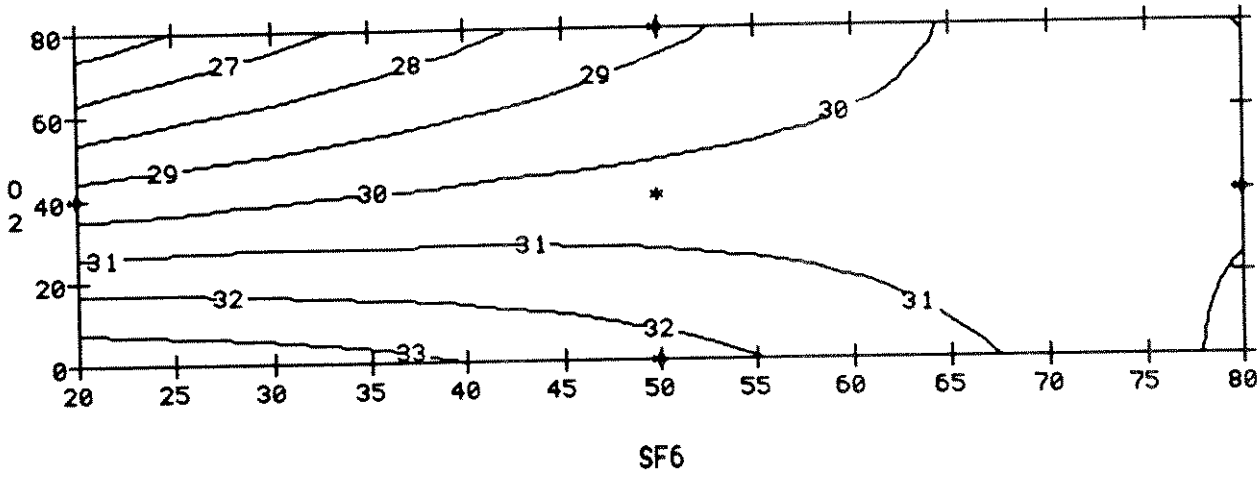

Figure 9 : Contourplot of F concentration in A.U. as a function of SF_6 flows and O_2 flows, at fixed pressure of 17,5 mTorr, Triode II mode, 400 W RF and 0W AF power.

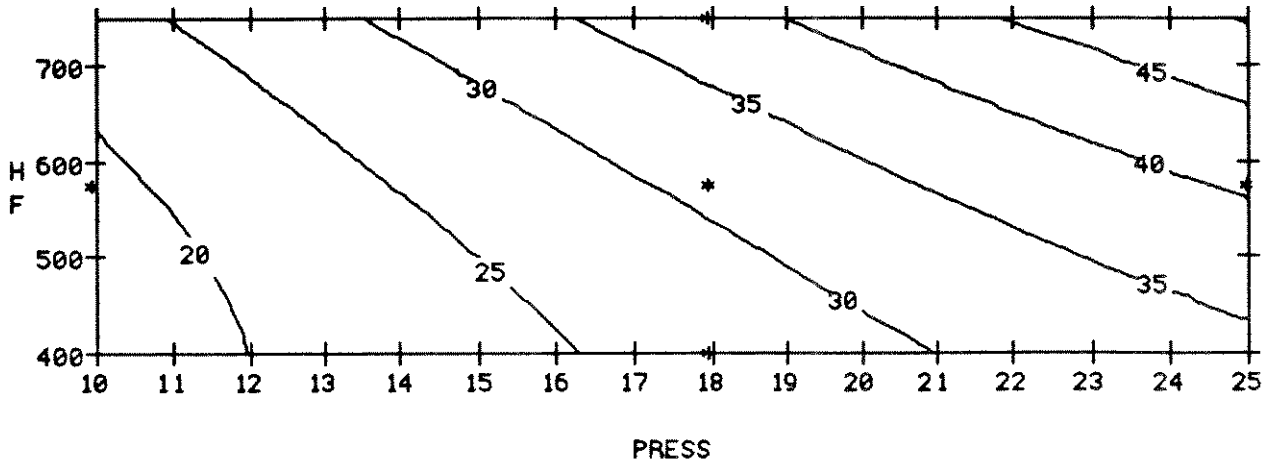

Figure 10 : Contourplot of F concentration in A.U. as a function of pressure and power for a SF_6 flow of 40 sccm and an O_2 flow of 8 sccm, Triode II mode, 0W AF power.

d) Triode II 50 W AF

The correlation factor R^2 = 0.90, and the analysis of variances F(10,1) = 13.2 show that the model fits well the experimental data.
The overall trends are shown in fig. 11.
Increase of SF_6 flow does not influence the F content for SF_6 flows lower than 50 sccm; the same yields for the O_2 flow ; increase of pressure increases the F content, increase of RF power increases the F content slightly for powers higher than 471 W. The general trends for Triode II, 50 W are remarkably similar to the ones for Triode II, 0 W AF, as the comparison of fig. 8 with fig. 11 shows.

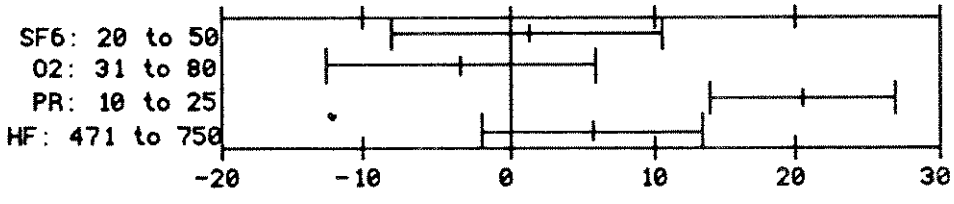

Figure 11 : Overall trends of the F concentration as function of SF_6 flow, O_2 flow, pressure and RF power in Triode II mode, for 50 W AF. The abcissa indicates the increase of the F content, a negative value indicates a decrease.

Figures 12 and 13 show a more detailed analysis.

Figure 12 shows very well the influence of the O_2 on the F generation. For low O_2 flows the F concentration increases due to a more effective decomposition of the SF_6 molecule. At higher O_2 flows a dilution effect occurs, thereby decreasing the F concentration. It is clear that the O_2 flow at which maximum free F concentration is found, increases with increasing SF_6 flow, as can be seen in both figures. Once again, the influence of the SF_6 flow is not very pronounced, whereas the influence of pressure is great, as shown in fig. 13.

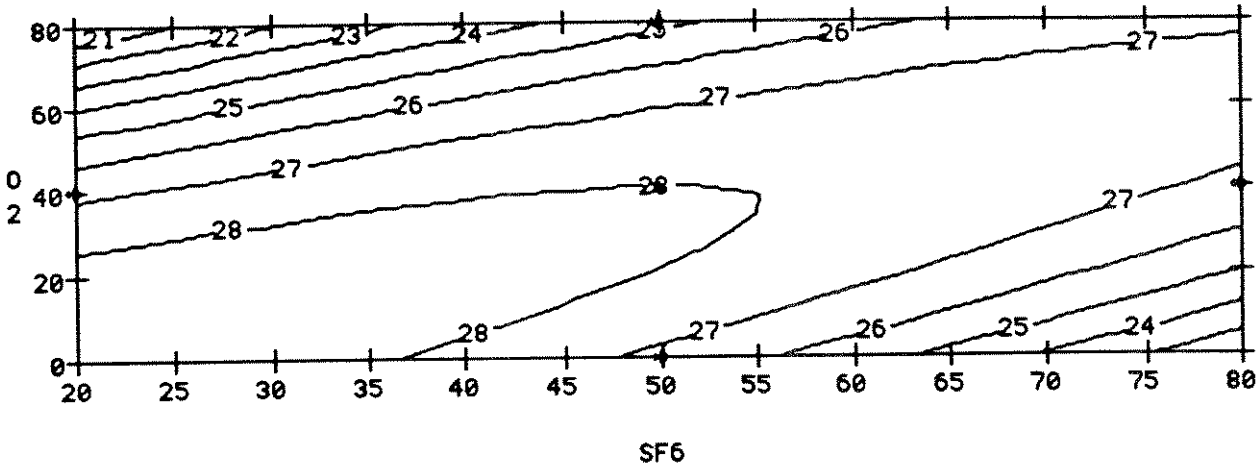

Figure 12 : Contourplot of F concentration in A.U. as a function of SF_6 flows and O_2 flows, at fixed pressure of 17.5 mTorr, Triode II mode, 400 W RF and 50W AF power.

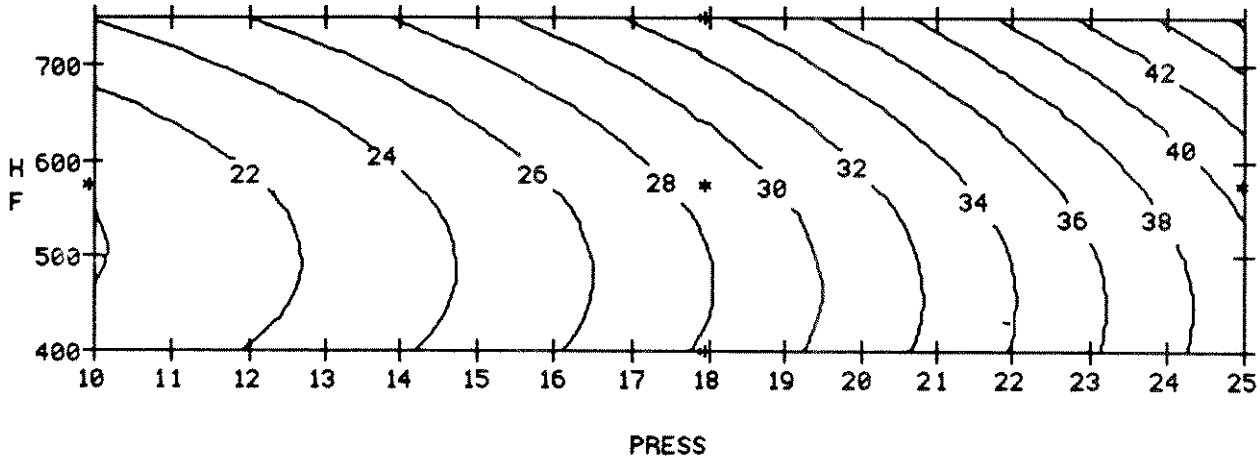

Figure 13 : Contourplot of F concentration in A.U. as a function of pressure and power for a SF_6 flow of 40 sccm and an O_2 flow of 8 sccm, Triode II mode, 50W AF power.

The results with and without 50 W AF are very similar, as can be expected: the extra 50 W AF, applied at the same electrode as the RF, will not influence very much the formation of the free F.

e) General conclusion on the addition of oxygen

The increase of free F concentration through addition of O_2 is much less than found in the SWAFER or in the literature for traditional, non MCR systems. Due to the magnetic confinement, the decomposition of the mother molecules is much more efficient in MCR systems than in traditional RIE or PE systems. Therefore, the addition of O_2 does influence much less, and in general works rather as a dilution element than as a F increasing element.

4) Polysilicon etching.

It is well reported that tungsten etching and silicon etching behave quite similar. As it is much simpler to obtain wafers with a polysilicon layer than with a tungsten layer and as measurement of the etch rates and uniformities is much simpler, it is useful to perform some polysilicon etchings before etching tungsten wafers, to obtain more information on processing in this machine. Besides, comparison of the results of polysilicon etching with the results of the tungsten etching will tell us more about etch mechanisms.
125 mm <100> wafers were used, on which 15 nm dry thermal oxide was grown and afterwards a 400 nm thick undoped polysilicon layer was deposited.
Measurement of the thickness of the polysilicon layers before and after etching were performed on an optical thickness measurement system : Prometrix 200 MS Spectramap.
The same software programme was used for the statistical design but the parameter range was reduced : the RF power was fixed at 400 W and the AF power at 0 W.
The results of the test are shown in table II.

Table II : overview of polysilicon etch rate in function of process parameters

Nr	SF_6 flow [% of 100 sccm]	O_2 flow [% of 20 sccm]	Press [mTorr]	Etch rates TrI [nm/min]	TrII [nm/min]
1	50	40	25	1169	802
2	20	0	25	592	476
3	50	40	10	1133	748
4	20	0	10	638	471
5	20	80	25	554	504
6	20	40	18	687	542
7	50	40	18	1201	802
8	20	80	10	574	445
9	50	80	18	1145	798
10	80	40	18	1402	927
11	50	0	18	1069	750
12	80	0	10	1362	811
13	80	80	10	1375	853
14	80	0	25	1250	803
15	50	40	18	1269	782
16	80	80	25	1540	904

The general trends are the following:
1) In Triode I mode the polysilicon etches faster than in Triode II mode.
2) The pressure is not important for the average etch rate, but is important for the uniformity of the etching. Uniformity increases from 0.70 to 0.90 in Triode II mode when decreasing pressure from 25 mTorr to 10 mTorr, analogue results can be found for Triode I mode.
3) The most important factor for the increase in etch rate is the flow of SF_6. The etch rate increases the most with SF_6 flow at low SF_6 flows.
4) At low O_2 flows the etchrate increases with O_2 flow, at higher flows the etch rate decreases with O_2 flow.
5) We did some tests at higher RF power and with AF power applied to the lower electrode, but the etch rate increase was minimal, certainly at low SF_6 flows.

The results of Triode I and Triode II modes will be discussed in more detail now.

a) Triode I etching.

The correlation factor R^2 = 0.909 and the analysis of variances F(5,1) = 1.525 show that the model fits well the experimental data.
The overall trends are shown in fig. 14.

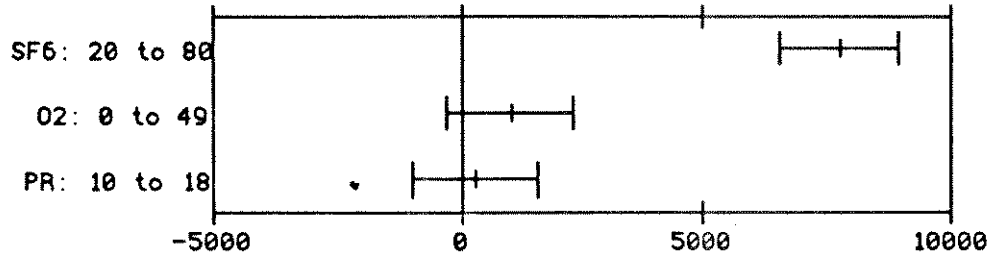

Figure 14 : Overall trends of the polysilicon etch rate as function of SF_6 flow, O_2 flow and pressure in Triode I mode. The abcissa indicates the increase of the etch rate in Å/min, a negative value indicates a decrease.

The dominant factor is the SF_6 flow: increase from 20 to 80 sccm more than doubles the etch rate. The oxygen flow does not influence the etch rate considerably; there also is little influence from the pressure.
Figures 15 and 16 show these trends in more detail.
It can be observed that the etch rate increases more with SF_6 at lower SF_6 flows. The influence of the O_2 in etch rate is very similar to what is discussed in the chapter on the actinometry tests above for the Triode II, 50W AF series.
The SF_6 flow is the main etch rate determining parameter. This becomes very clear by calculating how much fluor is consumed on the wafer for the different SF_6 flows. The

calculation procedure is explained in appendix I. For 20 sccm of SF_6 and no O_2, the etch rates are around 600 nm/min, while for 80 sccm of SF_6 and no O_2, the etch rates are around 1300 nm/min. It can be calculated that for the first case approximately 55 sccm of F is consumed, which means nearly 1 of every 2 F atoms that enter the reactor, for 1300 nm/min 120 sccm of F is consumed, or approximately 1 in 4. An efficiency of 1 in 2 - i.e. 50% of the available F atoms are used to remove the Si - is extremely high! This means this plasma is very efficient in decomposing the SF_6 gas. The magnetic confinement is very efficiently working in this reactor. But the consequence is also that enough F must be available which means that the incoming flows must be sufficiently high to furnish all this free fluorine. Therefore the SF_6 flow is the most important factor - input parameter for the etch rate.

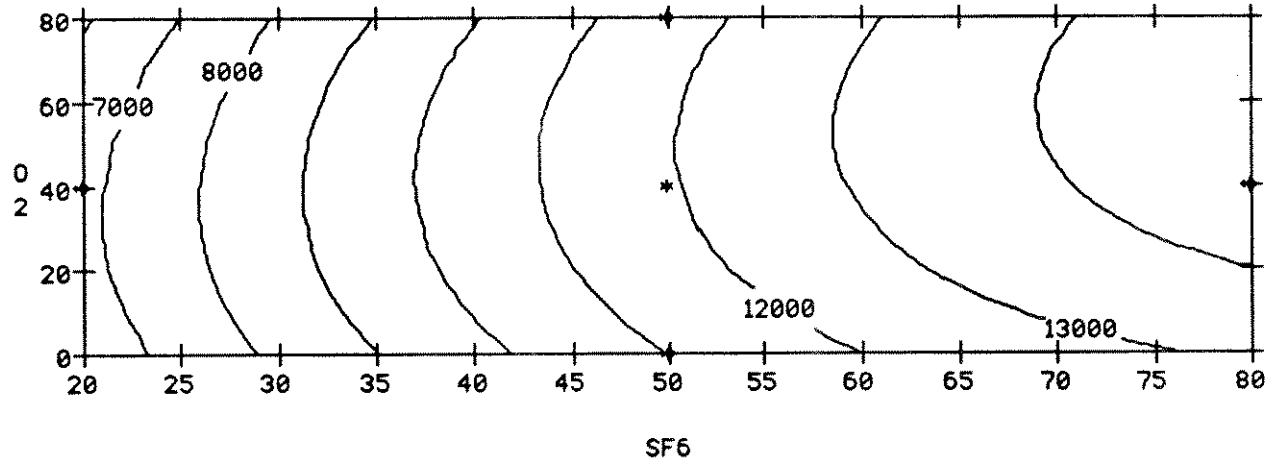

Figure 15 : Contourplot of polysilicon etch rate in Å/min as a function of SF_6 flows and O_2 flows, at fixed pressure of 17,5 mTorr, Triode I mode, 400 W RF and 0W AF power.

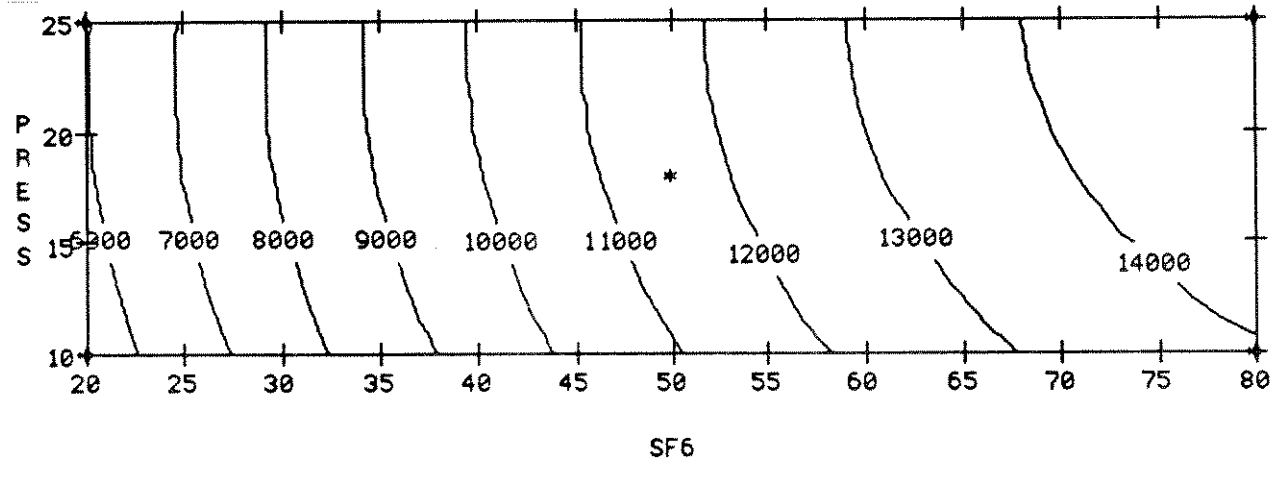

Figure 16 : Contourplot of polysilicon etch rate in Å/min as a function of SF_6 flows and pressure, at fixed oxygen flow of 16 sccm, Triode I mode, 400 W RF and 0W AF power.

The etch rate increases with O_2 at lower O_2 flows because of increase in the decomposition of the SF_6 molecule. At higher O_2 flows the etch rate decreases because of the dilution effect of the O_2 flow. The influence of the O_2 flow is more outspoken at higher SF_6 flows because at these higher flows the oxygen increases the free fluorine concentration much more than at low flows, as discussed in item 3 above.
Pressure influences the etch rate only very little; the relative changes are the same all over the SF_6 flow range.
The largest influence of the pressure is on the uniformity of the polysilicon etching. All polysilicon etchings with a 25 mTorr pressure have uniformities between 0.45 and 0.55, the 18 mTorr etchings have a 0.62 uniformity and the 10 mTorr etchings have uniformities between 0.72 and 0.75. The pressure is clearly the most determining factor. The uniformity increase with lower pressure can be explained by the fact that the diffusion coefficient is inversely proportional to the pressure: therefore at the lower pressure, diffusion of fluor is much higher. What limits the etch rate is the fact that the free fluorine must reach the wafer surface. When the diffusion coefficient is higher, this will happen easier and the fluorine concentration gradients will be lower. The nonuniformity will be caused by a F gradient, which will be lower at this higher diffusion coefficient at lower pressures.
Besides these etch tests some extra tests were performed to test some trends found in the actinometry tests.
The first test was done to determine if the etch time influences the etch rate. Three different times yielded a difference of less than 3% between highest and lowest etch rate, though the etch time was doubled. Therefore we may conclude that the etch time is not an etch rate determining parameter.
The other results are shown in table III. The uniformity is defined as the minimum etch rate at the wafer divided by the maximum etch rate.

Table III : overview of polysilicon etch rate in function of SF_6 - O_2 flows and different pressures in Triode I mode.

Nr	SF_6 flow [sccm]	O_2 flow [sccm]	Pressure [mTorr]	Etch rate [nm/min]	Uniformity [%]
1	90	6	10	1482	69
2	48	48	10	679	61
3	70	26	10	1355	73
4	80	16	10	1374	74
5	96	0	10	1440	71
6	48	0	10	1109	73
7	96	33	10	1349	72
8	50	8	25	1169	54
9	50	8	10	1133	76
10	50	8	18	1201	69
11	50	16	18	1145	70
12	50	0	18	1069	68

The main purpose of the first 7 tests was to investigate how etch rate and uniformity would change with still higher SF_6 flow and higher O_2 flow (before these tests the maximum O_2 flow was only 16 sccm).
These tests in fact confirm the fact that the SF_6 flow is by far the most determining factor. They show more clearly than the tests done before that the O_2 flow increases the etch rate only at low O_2 flows. Tests 1,3,4,5 and even 7 show a maximum etch rate for 6 sccm of O_2, at 16 sccm the etch rate decreases, decreasing even somewhat more at 26 sccm of O_2. Tests 10, 11 and 12 show an analogue result. One should however observe that the F consumption per incoming F atom is the highest still at testpoint 3! For those parameters, there is only 27 % possibly available F less as for testpoint 1, while the etch rate is still 91 % of the etch rate for point 1. Test 11 however indicates that for lower total flows, the increase of the O_2 flow over 24 % of the total flow, decreases the global effect of fluorine generation: other mechanisms start to become more important than the fact that O_2 helps in the decomposition of SF_6, as will be discussed in more detail in appendix V.
When the O_2 flow is as high as the SF_6 flow, as in test 2, the dilution effect is very pronounced and even influences the uniformity in a bad way.
The influence of the pressure is confirmed in tests 8 to 10 : the influence on etch rate is very little, while the influence on uniformity is much more important.
These checks confirm the trends indicated by the statistical design of experiments test series.
The following tests show that the influence of the RF and AF power is not strong: all processes: 20 sccm of SF_6, 0 sccm of O_2, 10 mTorr:
1) 400 W RF, 0 W AF : r = 638 nm/min, U = 0.73
2) 600 W RF, 0 W AF : r = 750 nm/min, U = 0.77
3) 400 W RF,50 W AF : r = 702 nm/min, U = 0.82
The influence of AF power on etch rate is very low, the uniformity improves, probably due to the higher ion bombardment, which influences slightly the etch rate. In fact : the highest etch rate on the wafer remains approximately the same, it is the lowest etch rate that increases.
A 50% RF power increase causes a 18% etch rate increase, which is much lower than for most plasmas in traditional RIE or PE systems.
The reason is once again that in these plasmas, the decomposition of the SF_6 molecules is much more complete than for traditional RIE or PE plasmas. Therefore, the extra power does not increase the F content very much, as also seen in the actinometry measurements. As an increase of AF power does not increase very much the etch rate, DC bias voltage will not influence the etch rate very much for these plasmas. Therefore an increase of voltage over the dark sheath caused by an increase in RF power, wil not increase the etch rate.

b) Triode II etching

The correlation factor R^2 = 0.997, and the analysis of variances F(5,1) = 0.86 show that the model fits well the experimental data.
The overall trends are shown in fig. 17.

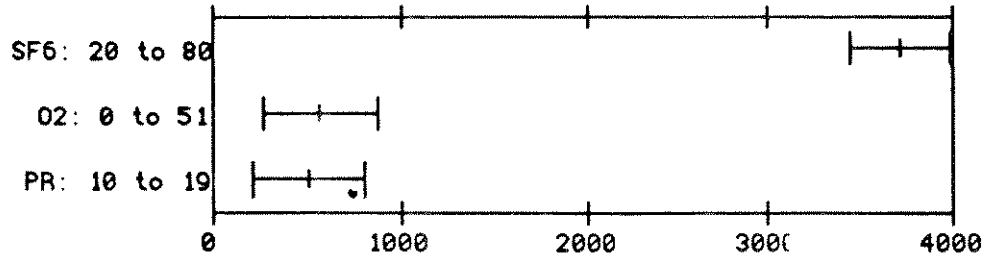

Figure 17 : Overall trends of the polysilicon etch rate in Å/min as function of SF_6 flow, O_2 flow and pressure in Triode II mode. The abcissa indicates the increase of the etch rate.

As for the Triode I etchings, the main responsible for etch rate increase is the SF_6 flow. The etch rate also increases with a factor of 2 when SF_6 flow increases from 20 sccm to 80 sccm. O_2 flow increase from 0 to 51 sccm also increases slightly the etch rate, whereas pressure increase from 10 to 19 mTorr also increases slightly the etch rate.
Figures 18 and 19 show these results in more detail.

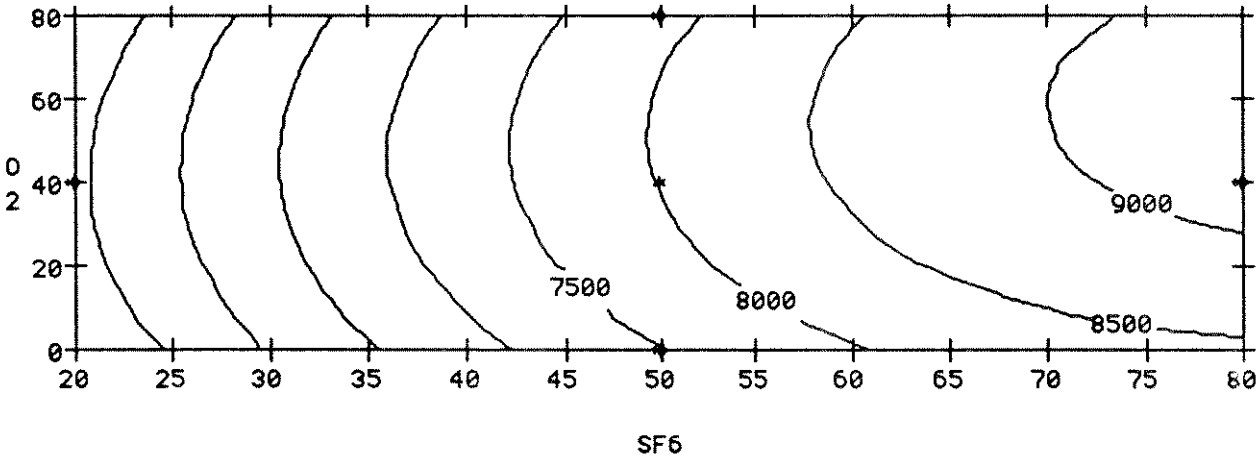

Figure 18 : Contourplot of polysilicon etch rate in Å/min as a function of SF_6 flows and O_2 flows, at fixed pressure of 17,5 mTorr, Triode II mode, 400 W RF and 0W AF power.

They show once again that the SF_6 flow is the determining factor for the etch rate. Though the etch rates are lower

than for the Triode I mode, the fluorine consumption is still very high, much higher than for traditional RIE or PE systems. For a flow of 20 sccm of SF_6 and no O_2, the etch rates are around 475 nm/min, while for a flow of 80 sccm of SF_6 and no O_2, the etch rates are around 810 nm/min. Using formula (1) of appendix I, one can calculate that for the first case approximately 44 sccm of F is consumed, which is more than one third of all available F. For the second case, approximately 74 sccm of F is consumed, a little bit less than 1 atom of 6 available, which is still a high value. The trend of the influence of the O_2 flow is the same as for Triode I and as decribed in the actinometry series of Triode II, 50 W AF.

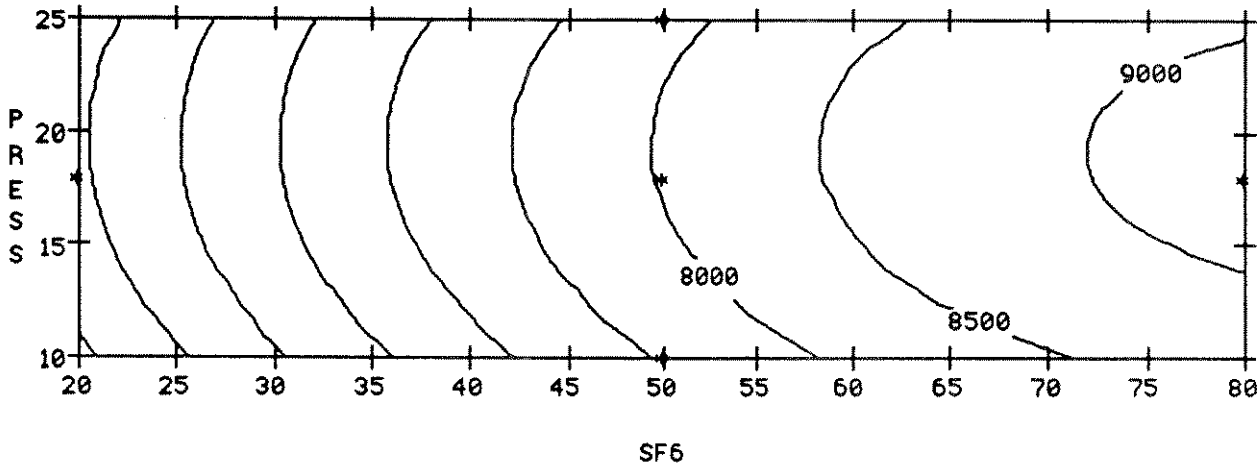

Figure 19 : Contourplot of polysilicon etch rate in Å/min as a function of SF_6 flows and pressure at fixed O_2 flow of 8 sccm, Triode II mode, 400 W RF and 0W AF power.

A pressure increase causes the etch rate to increase slightly with a maximum around 18 mTorr, but at higher pressure the etch rate tends to decrease.

Some extra tests were performed to investigate higher SF_6 and O_2 flows, as shown in table IV.

Table IV : overview of polysilicon etch rate for different SF_6/O_2 ratios in Triode II mode.

Nr	SF_6 flow [sccm]	O_2 flow [sccm]	Pressure [mTorr]	Etch rate [nm/min]
1	96	0	10	881
2	80	16	10	853
3	70	26	10	830
4	48	48	10	425
5	90	6	10	909

These tests show again that the increase in decomposition of the SF_6 molecule due to the presence of O_2 is set off by the

decrease of SF_6 flow in these tests (the total flow was held constant). One should however observe that the F consumption per incoming F atom is the highest still at testpoint 3! For those parameters, there are 27% less available F atoms as for testpoint 1, while the etch rate is still 94% of the etch rate for point 1.
The influence of the pressure is illustrated by the following table:

Table V : overview of polysilicon etch rate for different pressures, in Triode II mode.

Nr	SF_6 Flow [sccm]	O_2 Flow [sccm]	Pressure [mTorr]	Etch Rate [nm/min]	Uniformity [%]
1	50	8	25	802	71
2	50	8	10	748	81
3	50	8	18	802	74

As in Triode I mode, the pressure does not influence very much the etch rate, but rather the uniformity, with again the higher uniformity at the lower pressure. This can be explained once again by the higher diffusion coefficient at lower pressure. The uniformity is higher than in Triode I mode, because of the ion bombardment: this will certainly help the uniformity as also shown in the tests with higher RF and AF power in Triode I mode.

Though Triode I and Triode II are very different modes, the etch rate behaviour as a function of SF_6 and O_2 flow is very similar, while the difference for the pressure influence is also quite small. This indicates that the etch mechanisms or at least the etch limiting step(s) are very similar.

5) Comparison actinometry - polysilicon etch rate results.

Comparing the results of the actinometry tests with the results of the polysilicon etch tests, there are some agreements but also some disagreements. Most of the disagreements can be adequately explained.

Agreements.

1) The RF and the AF power influence very little. This is a strange result at first sight, as it is most uncommon for plasma etching that the etch rate is not very much influenced by AF and RF power. However, in these cases, the small influence can be explained by the huge decomposition of the SF_6 molecules already at the lowest investigated power levels and the fact that the etch rate limiting step is the arrival of free F at the wafer surface, therefore ion bombardment does also not influence very much the etch rate.
One of the main positive effects of the actinometry tests was exactly that for the etch tests we could remove the RF and AF power as parameters to be investigated, in this way

decreasing the number of tests for the polysilicon (and later for the tungsten) etching.
2) Certainly in Triode II, the influence of the O_2 flow shows the same trends for actinometry as for the polysilicon etch. As this was already a well known phenomenon, this feature served just to confirm the validity of our methods.

Contradictions or paradoxes.

1) The main paradox is the fact that the F content in the actinometry measurements is almost proportional to the pressure, while pressure does not influence the etch rate very much. This can be explained however by the pressure influence on the diffusion coefficient. The diffusion coefficient is inversely proportional to the pressure [2]. In this way the product diffusion coefficient times concentration of fluorine is approximately a constant for these plasmas. The SF_6 and therefore the F flow is more or less homogeneous over the reactor. As very much fluor is consumed, up to 50% in some cases, it is important that the fluorine from all over the reactor reaches the wafer. Therefore the diffusion constant is a very important parameter in these cases. One can imagine that when relatively less free fluorine is consumed, the diffusion coefficient is not so extremely important, as will be shown in appendix V.
2) The influence of the SF_6 flow is much less clear in the actinometry measurements than in the polysilicon etch measurements. SF_6 flow is the dominant factor for the polysilicon etch rate whereas it is not very significant in the F concentration.
The fluorine which remains in the plasma is the difference between the generated free fluorine and the fluorine consumed by the etching.
The overall free fluorine generating reaction is :

$$SF_X \rightarrow SF_{X-1} + F \qquad (1)$$

With $x = 6 \rightarrow 1$.
These reactions have equilibrium constants:

$$K_X = \frac{[\ SF_{X-1}\ ]\ [F]}{[\ SF_X\ ]} \qquad (2)$$

with [F] the concentration of the fluorine which remains in the plasma. A chemical system will try to keep its equilibrium, even when F is consumed by other chemical reactions. Therefore, if one compares two processes, which have the same pressure (therefore the same density of species) but different flows, in a first approximation, they both will have the same density of remaining free fluorine in the plasma (as the K constants for both processes will be

approximately the same). It is exactly this free fluorine density which is measured through actinometry.
Therefore it is possible that a process with higher SF_6 flows consumes much more free fluorine than a process with lower SF_6 flows, but that the concentration of the remaining free fluorine remains approximately the same.

6) Tungsten Etching.

These tests were done on 125 mm (100) wafers which received the following treatment: deposition of 500 nm of PECVD oxide, sputter deposition of 40 nm of Ti, sputter deposition of 80 nm of TiN, CVD deposition of 1000 nm of W at 425°C , patterning of 1.2 µm IX I-line resist from JSR. There were 2 masks used: 1 light field with 95 % clear area, 1 dark field with 5% clear area. Postbake was 1 minute hot plate at 95°C. These are the same wafers as of type W_{III} in appendix II.
Resist thickness was measured before and after etching with a Dektak II step height meter, as was the step in the tungsten after the dry strip in a pure oxygen plasma. Step heights were measured in the center, at 4 points at the border and at 1 point halfway the center and the border.
Because of the roughness of the tungsten film, we used a special way of determining the step height. This is shown in fig. 20. After levelling and zeroing of the bottom line, the average is calculated (automatically) from the points at the bottom line. Then the average of the heights of the top line is calculated and afterwards the difference between these averages is made. The structure used was a 150 µm by 150 µm square. This method is valid for these wafers as they were extremely flat. For bowed wafers another method should be used. We estimate that the final error on a step height is less than 10 nm, by measuring twice the structure the error becomes less than 7 nm.

6.1) Tests to investigate the influence of the oxygen flow in SF_6 - O_2 plasmas.

A first series of tests was performed to investigate the influence of the oxygen flow on the etch behaviour of the tungsten film. From these tests we can make comparisons with the etch tests on the SWAFER which are reported in appendix II.
Tests were done in Triode I mode. The RF power was fixed at 400 W and AF power at 0 W. Etch time was 30 seconds.
The results are shown in table VI.

a)

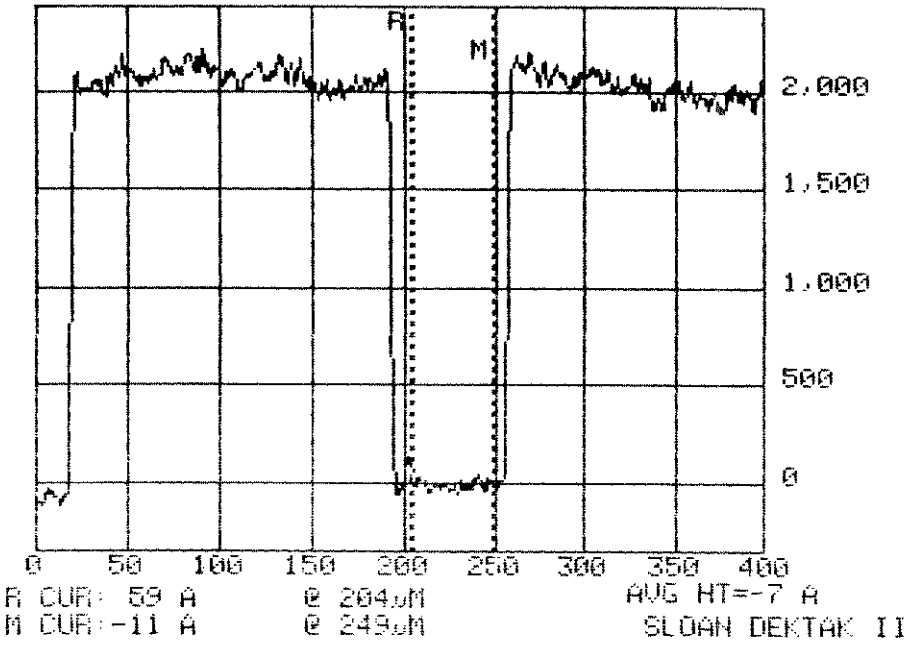

b)

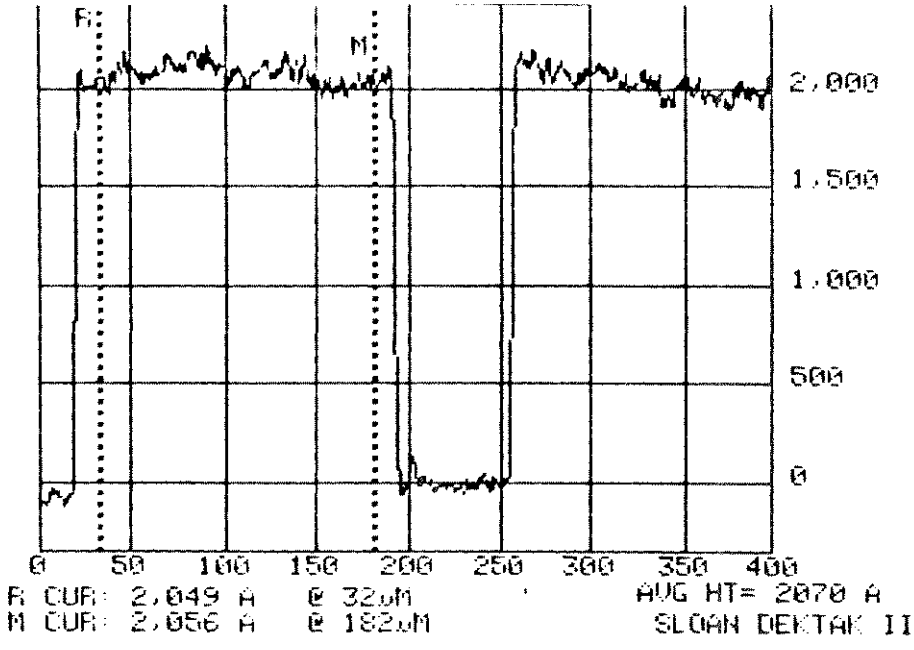

Figure 20 : Step height meter profiles, after levelling and zeroing; determination of the height of bottomline (a) and of top (b).

The following symbols are used :

r_W : tungsten etch rate in the center of the wafer, in [nm/min]
U : uniformity of the tungsten etching defined as minimum etch rate divided by maximum etch rate, in [%].
r_{PR} : resist etch rate at the center of the wafer, in [nm/min]
U_{PR} : uniformity of the resist etching in [%]
S : selectivity tungsten towards resist in the center of the wafer

Table VI : tungsten and resist etch characteristics for several SF_6-O_2 flows, for Triode I mode plasmas.

Nr	SF_6 flow sccm	O_2 flow sccm	Press mTorr	r_W nm/min	U %	r_{PR} nm/min	U_{PR} %	S
1	96	0	10	564	86	184	86	3.1
2	80	16	10	752	88	160	90	4.7
3	70	26	10	724	87	169	87	4.9
4	48	48	10	683	84	97	95	7.0

Figure 21 shows the etch rates of the tungsten and the polysilicon for these wafers.

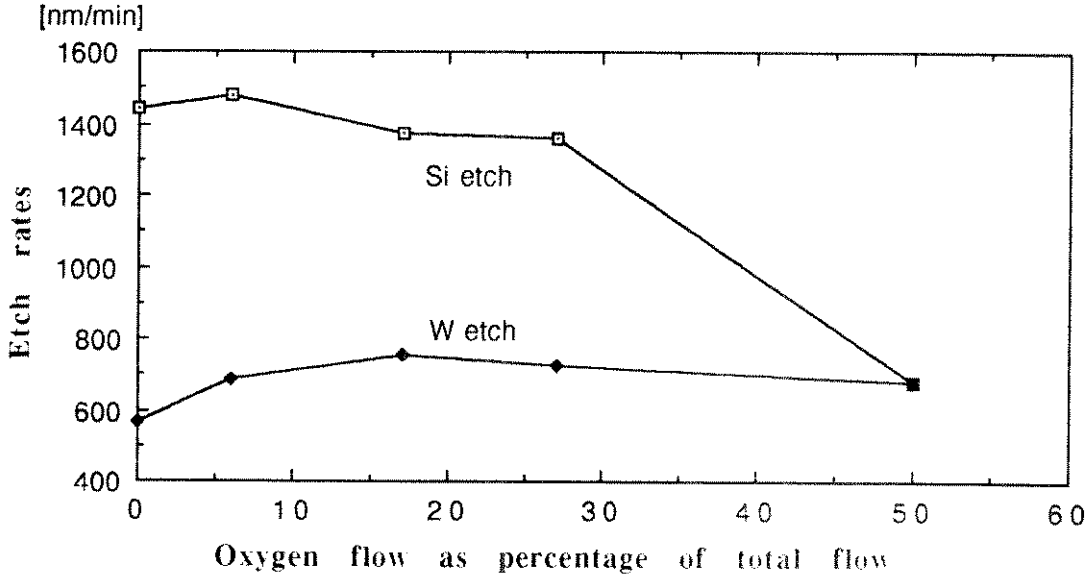

Figure 21 : Polysilicon and tungsten etch rate as a function of oxygen content in Triode I mode.

The lowest tungsten etch rate for this etch mode was always found halfway between the center and the border of the wafer. This seems to be a characteristic of this etching system in Triode I mode for tungsten. For polysilicon this phenomenom was not observed.

The tungsten etch rate as a function of the place on the wafer for processes 1 and 2 are shown in fig. 22. Place 2 is at 10 mm of the border of the wafer, place 7 is the center of the wafer.

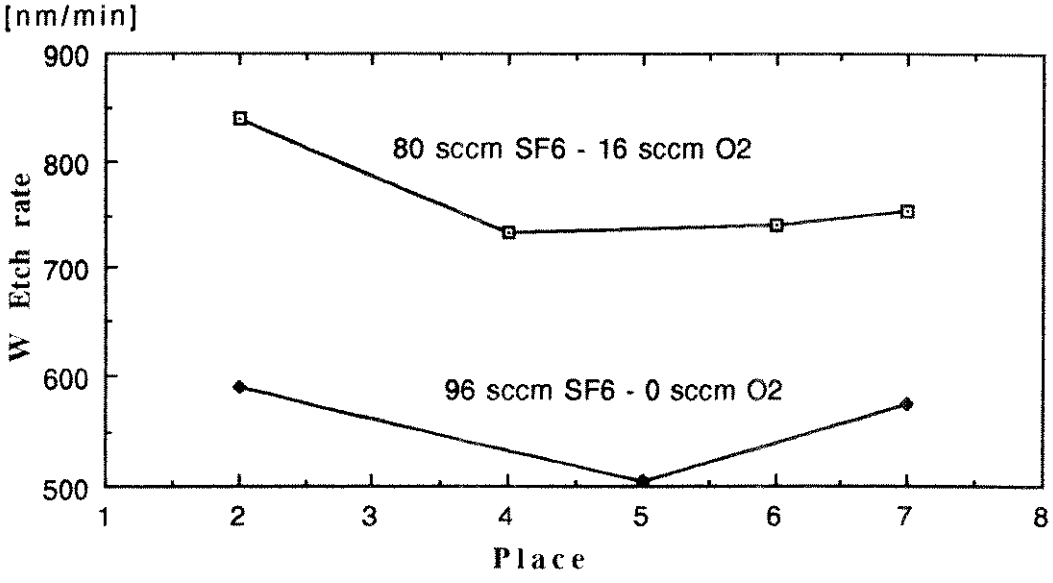

Figure 22 : Tungsten etch rate as a function of the place on the wafer, in Triode I mode.

These results are surprisingly similar to the results obtained by the SWAFER in PF mode, although there NF3 was used (see appendix II). The main points of agreement are:
- Etch rate is lowest with no oxygen added, even with a 50% O_2 flow, the etch rate remains very high.
- The selectivity towards the resist does not decrease with O_2 flow, on the contrary. The selectivity is lowest when no O_2 flow is present.

A difference is there in the fact that in the Tegal 15xx, the polysilicon etch rate starts decreasing with small O_2 flows, while for the tungsten etch rate, its maximum is at a higher O_2 flow, indicating the formation of a volatile WOF_4.
The selectivities of tungsten towards resist is lower in the Tegal 15xx : the etch rate of the resist is much higher. This indicates a certain ion bombardment in Triode I mode. One should observe that the pressure in the Tegal 15xx is much lower than in the Swafer and that in the Swafer at pressures lower than 70 mTorr the selectivities of tungsten towards resist are only 1:1.

Similar tests were performed in Triode II mode. The RF power was fixed at 400 W and AF power at 0 W. Etch time was 60 seconds.
The results are shown in table VII.

Table VII : tungsten and resist etch characteristics for several SF_6-O_2 flows, for Triode II mode plasmas, with fixed RF and AF power of respectively 400 W and 0 W.

Nr	SF_6 flow sccm	O_2 flow sccm	Press mTorr	r_W nm min	U %	r_{PR} nm min	U_{PR} %	S
1	96	0	10	488	96	508	98	0.96
2	90	6	10	484	93	520	97	0.93
3	80	16	10	470	88	500	90	0.94
4	70	26	10	467	92	600	97	0.78

The tungsten and polysilicon etch rates of these processes are shown in fig. 23. The following trends are clear:
- the tungsten etch rate is not much influenced by the oxygen content, at least not till 26% of O_2 flow, while the polysilicon etch rate increases initially, decreasing afterwards. This behaviour is very similar to the tungsten etching in RIE mode with NF_3 in the SWAFER (as shown in appendix II);
- the tungsten etch rate is lower than in Triode I mode;
- the uniformity is much higher than for Triode I mode. The maximum etch rate is always found at the border of the wafer, but the minimum etch rate can be found both in the center as halfway the wafer. These differences in etch rate are always of the order of 1%, thus well within the precision of the measurement.
- the resist etch rate is much higher than in Triode I mode and in general increases with higher O_2 flows, certainly at higher flows.

Figure 23 also shows the etch rates of polysilicon and tungsten in Triode I mode, to facilitate comparison.

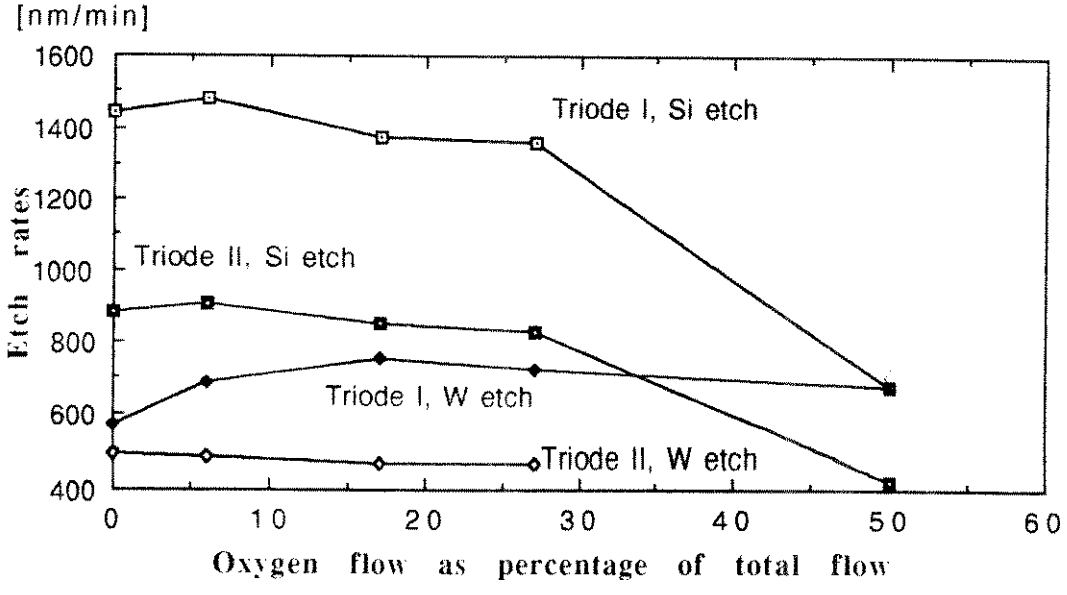

Figure 23 : Tungsten and polysilicon etch rates as a function of oxygen content and etch mode.

6.2) Tests through the statistical design of experiments method of SF_6 - O_2 plasmas.

The same software programme as for the polysilicon etch test series was used for the statistical design, but only a linear model with interactions was used. As the model fitted quite well for the etchings of the light field wafers, no extra tests with a quadratic model were performed. The parameter range was the same as for the polysilicon etchings.
Applied power was always 400 W RF, 0 W AF. As increase of RF and AF power had only a marginal influence on the tungsten etch rate, the lowest values of the investigated range were used, as for these values the selectivity of tungsten towards the underlying silicon dioxide will be highest.
The etch mode was always Triode II, as previous tests had indicated that the best loading effect was achieved in Triode II mode (as expected: chemical etching is much more loading sensitive than ion bombardment enhanced etching).
Uniformity is also better in Triode II mode than in Triode I mode.
Etch time was always 1 minute.
The main goal of these tests is to find the point where less loading effect occurs, i.e. where quotient of the light field patterned wafer etch rate divided by the the dark field patterned wafer etch rate is maximum. This is an important characteristic for tungsten back etching: the etching of the plugs should not be much faster than the etching of the blanket tungsten layer. The uniformity of the etching is also important, as is the selectivity towards the underlying films: at least the oxide should not be etched very much.
The results of this test series are shown in table VIII.
The following symbols are used:
r_{cLF} : tungsten etch rate at the center of a LF patterned wafer, in [nm/min]
r_{bLF} : tungsten etch rate at the border of a LF patterned wafer, in [nm/min]
U_{LF} : uniformity of the LF patterned wafer, in [%]
r_{cDF} : tungsten etch rate at the center of a DF patterned wafer, in [nm/min]
r_{bDF} : tungsten etch rate at the border of a DF patterned wafer, in [nm/min]
U_{DF} : uniformity of the DF patterned wafer, in [%]
LE_C : loading effect in the center, defined as quotient of the etch rate of the LF patterned wafer divided by the etch rate of the DF patterned wafer, in the center of the wafer, in [%].
LE_b : loading effect at the border, defined as quotient of the etch rate of the LF patterned wafer divided by the etch rate of the DF patterned wafer, at the border of the wafer, in [%].

Table VIII: overview of tungsten etch rates, uniformities and loading effects in function of process parameters for SF_6 - O_2 plasmas in Triode II mode.

Nr	Gas flows SF_6 sccm	O_2 % of 100 sccm	Press mTorr	r_{cLF} nm min	r_{bLF} nm min	U_{LF} %	r_{cDF} nm min	r_{bDF} nm min	U_{DF} %	LE_c %	LE_b %
1	80	80	25	542	623	87	736	808	91	74	77
2	20	80	10	386	381	99	557	575	97	69	66
3	80	80	10	525	559	94	652	651	99	81	86
4	20	0	10	304	327	93	462	506	91	66	65
5	80	0	25	467	537	87	668	737	91	70	73
6	80	0	10	495	544	91	632	646	98	78	84
7	50	40	18	469	521	90	740	767	96	63	68
8	50	40	18	487	524	93	733	775	94	67	68
9	20	80	25	442	451	98	738	772	96	60	58
10	80	0	25	278	305	91	475	534	89	59	57

The general trends for these tungsten etch processes are:
1) Dark field etch rate is always higher than light field etch rate.
2) Etch rate is (almost) always higher at the border than in the center of the wafer, a traditional bull's eye is found.
3) DF etching is in general more uniform than LF etching.
4) Etch rate is determined mostly by the SF_6 flow: the higher the flow, the higher the etch rate.
5) Uniformity increases with decreasing pressure, decreasing SF_6 flow and increasing O_2 flow, but remains always very high.
6) Loading effect ameliorates with increasing SF_6 flow and decreasing pressure, while the influence of the oxygen flow is neglectable.
A value of 0.81 in the center of the wafer and 0.86 at the border of the wafer was obtained, which is a very good result. Furthermore the uniformity of this process is quite good with values of 94% for the LF and 99% for the DF wafer.

We shall analyse in more detail the different responses of this test series.

a) Etch rate in the center of a light field patterned wafer.

The correlation factor $R^2 = 0.944$ and the analysis of variances $F(2,1) = 11.9$ show that the model fits well the experimental data.
The overall trends are shown in fig. 24.
The main etch rate determining factor is the SF_6 flow : increasing it increases the etch rate. The O_2 flow also does influence the etch rate in the same direction, though less pronounced. The influence of pressure is not important for the etch rate.

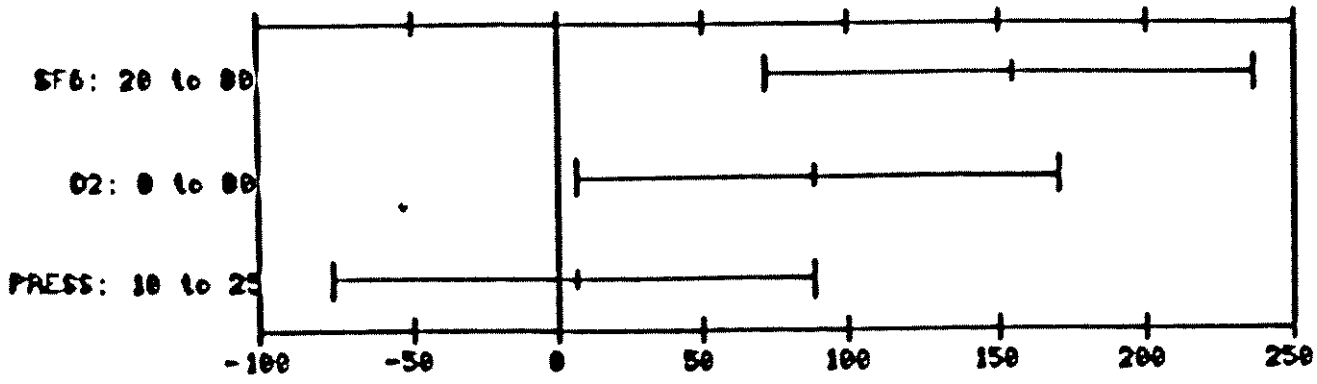

Figure 24 : Overall trends of the tungsten etch rate as function of SF_6 flow, O_2 flow and pressure at the center of a LF patterned wafer. The abcissa indicates the increase of the etch rate in nm/min, a negative value indicates a decrease.

Figures 25 and 26 shows this in more detail.

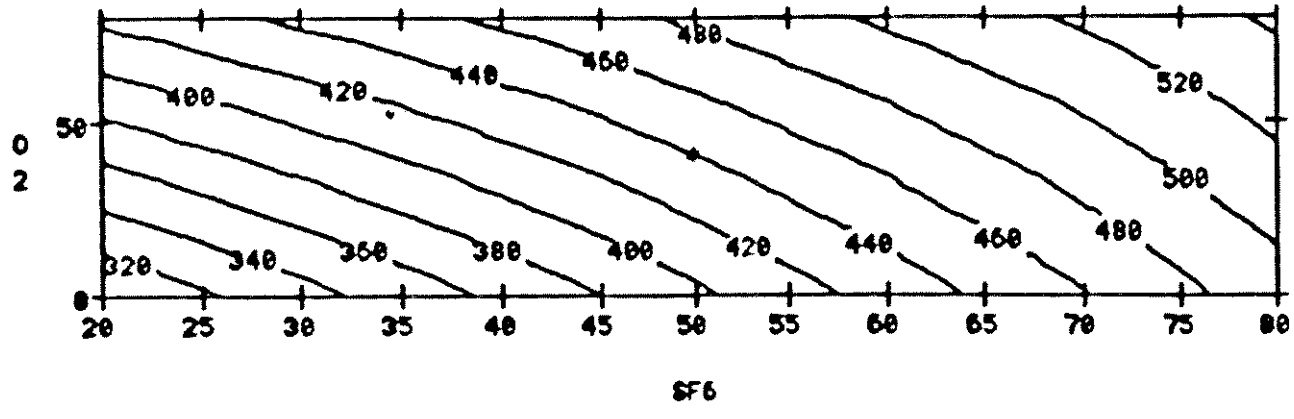

Figure 25 : Contourplot of tungsten etch rate in nm/min at the center of a LF patterned wafer, as a function of SF_6 flow and O_2 flow, at fixed pressure of 17,5 mTorr, Triode II mode, 400 W RF and 0 W AF power.

An increase of the SF_6 flow from 20 sccm to 80 sccm increases the etch rate typically by 60%.
The influence of the O_2 flow is higher at smaller SF_6 flows where it increases the etch rate by 30% when increasing from 0 to 16 sccm, at higher SF_6 flows, the increase of etch rate is less than 10% for the same O_2 flow increase.
The influence of the pressure is really minimal.

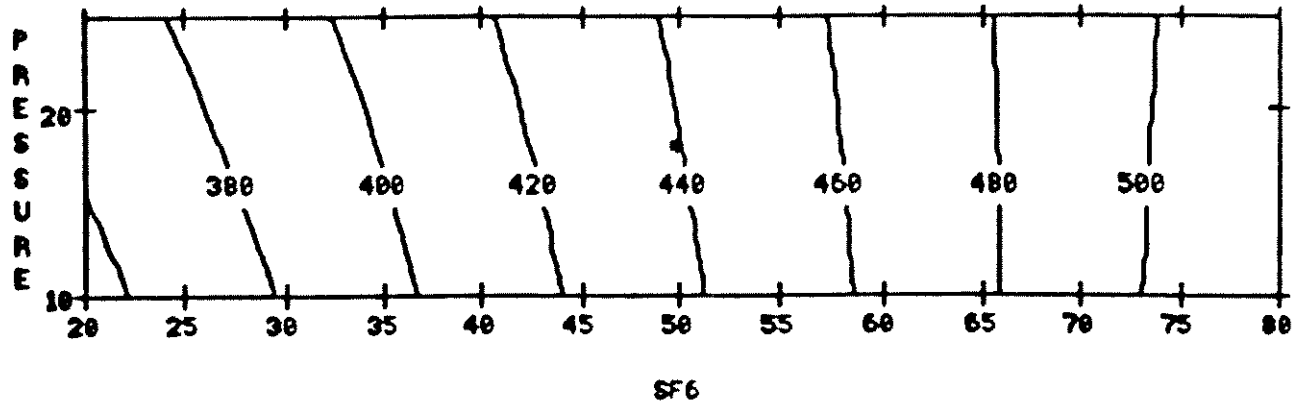

Figure 26 : Contourplot of tungsten etch rate in nm/min at the center of a LF patterned wafer, as a function of SF_6 flow and pressure at fixed O_2 flow of 8 sccm, Triode II mode, 400 W RF and 0 W AF power.

b) Etch rate at the border of a light field patterned wafer.

The correlation factor R^2 = 0.951 and the analysis of variances F(2,1) = 558 show that the model perhaps does not fit well the experimental data. It can be observed that the difference between the etch rates at the 2 centerpoints is only 0.6%, which is very little. Therefore the analysis of variances will automatically show a worse result than for the former case, where the difference was 3%. As the correlation factor is very good, we can consider the model as acceptable at least for general analysis.
The overall trends are shown in fig. 27.

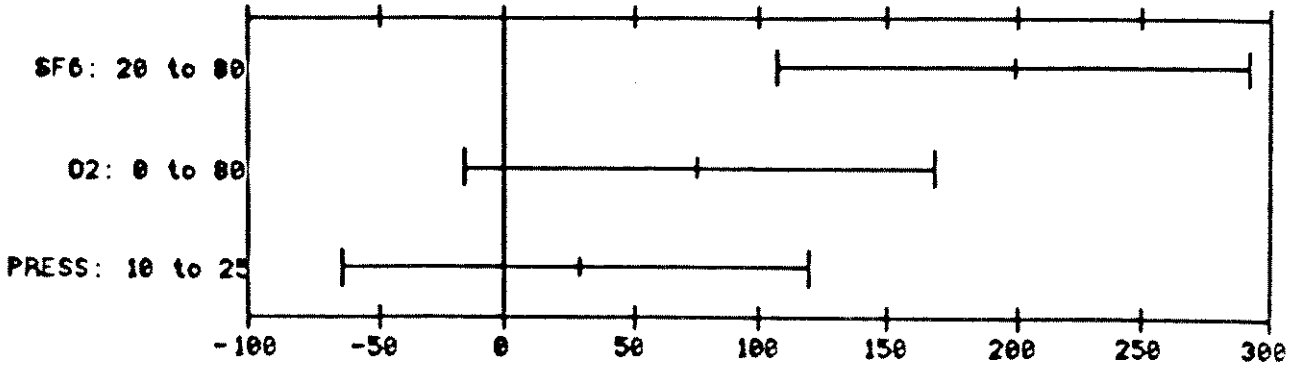

Figure 27 : Overall trends of the tungsten etch rate as function of SF_6 flow, O_2 flow and pressure at the border of a LF patterned wafer. The abcissa indicates the increase of the etch rate in nm/min, a negative value indicates a decrease.

An increase of the SF_6 flow increases the etch rate, the same is valid in a lesser way for the O_2 flow, while there is little influence of the pressure.
Figures 28 and 29 show this in more detail. At lower SF_6 flows the etch rate increases more rapidly with O_2 flow. A pressure increase causes a very slight increase in etch rate. The trends are extremely similar to the ones discussed in section a above, as can be expected.

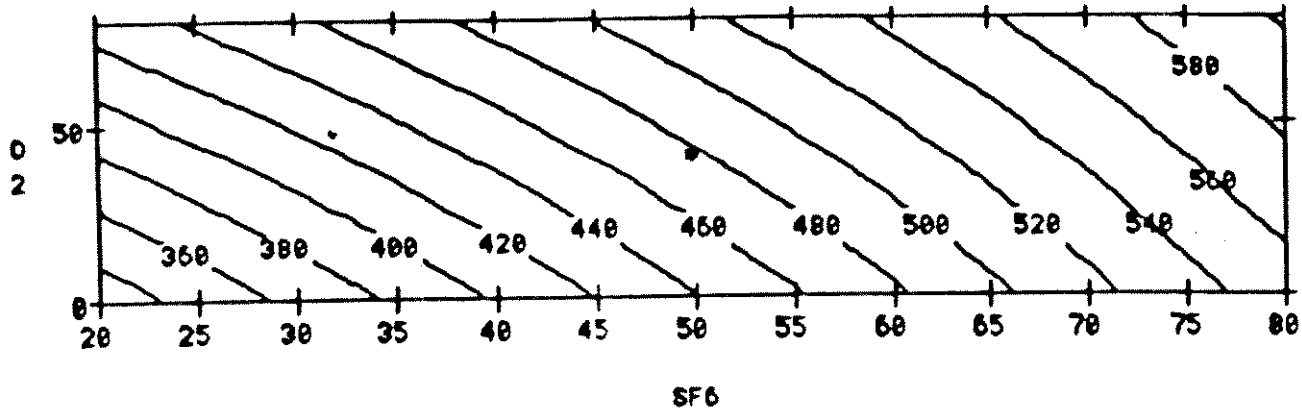

Figure 28 : Contourplot of tungsten etch rate in nm/min at the border of a LF patterned wafer, as a function of SF_6 flow and O_2 flow, at fixed pressure of 17,5 mTorr, Triode II mode, 400 W RF and 0 W AF power.

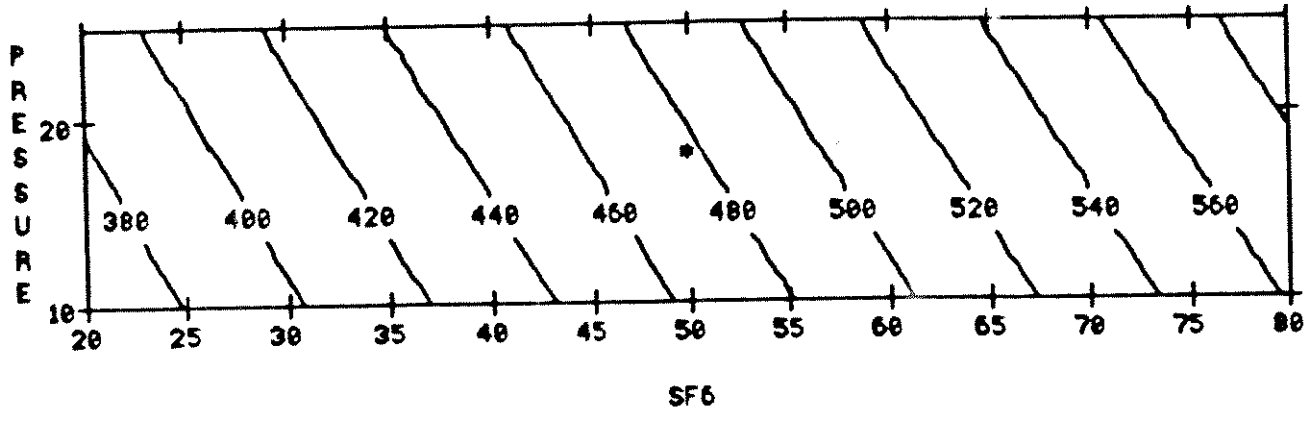

Figure 29 : Contourplot of tungsten etch rate in nm/min at the border of a LF patterned wafer, as a function of SF_6 flow and pressure at fixed O_2 flow of 8 sccm, Triode II mode, 400 W RF and 0 W AF power.

c) Uniformity of a light field patterned wafer.

The correlation factor $R^2 = 0.947$ and the analysis of variances $F(2,1) = 0.360$ show that the model fits well the experimental data.
The overall trends are shown in fig. 30.

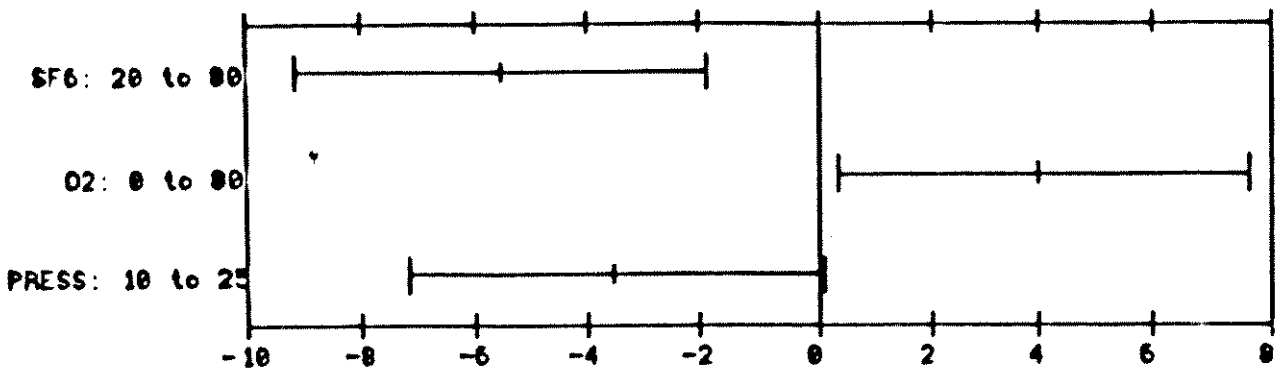

Figure 30 : Overall trends of the tungsten etch rate uniformity as function of SF_6 flow, O_2 flow and pressure of a LF patterned wafer. The abcissa indicates the increase of the uniformity in percentage points, a negative value indicates a decrease.

The uniformity increases with : decrease of SF_6 flow, increase of O_2 flow and decrease of pressure. But as the values are already high, the influences are very small. Figures 31 and 32 show this in more detail.
These figures show clearly that the most uniform processes are those at lowest pressure, lowest SF_6 flow and highest O_2 flow. It is clear that the higher diffusion coefficient at the lower pressure is again an important factor in the increase of the uniformity with decreasing pressure, as for the polysilicon etching.

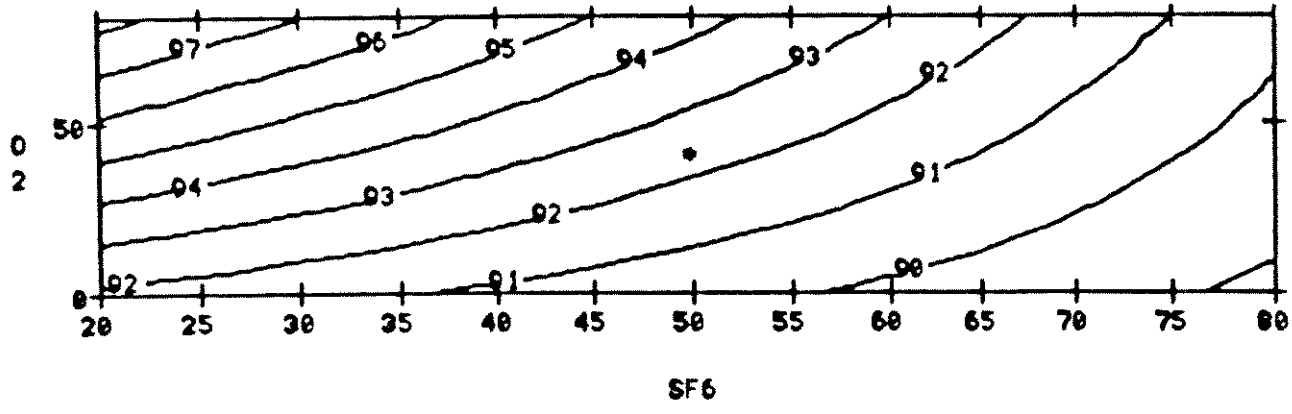

Figure 31 : Contourplot of tungsten etch rate uniformity in percentage points of a LF patterned wafer, as a function of SF_6 flow and O_2 flow, at fixed pressure of 17,5 mTorr, Triode II mode, 400 W RF and 0 W AF power.

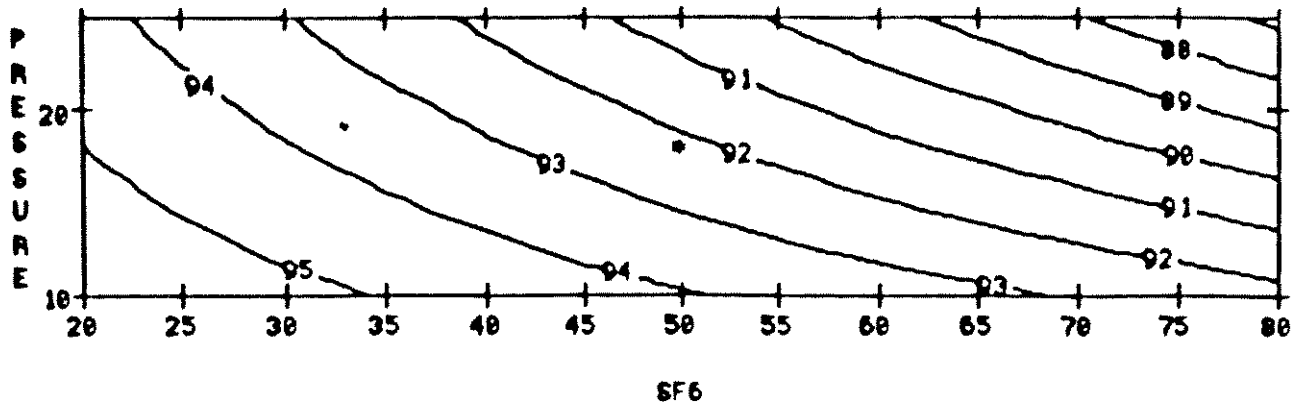

Figure 32 : Contourplot of tungsten etch rate uniformity in percentage points of a LF patterned wafer, as a function of SF_6 flow and pressure at fixed O_2 flow of 8 sccm, Triode II mode, 400 W RF and 0 W AF power.

d) Etch rate in the center of a dark field patterned wafer.

The correlation factor R^2 = 0.766 and the analysis of variances F(2,1) = 498 show that the model does not fit the experimental data. Therefore the following analysis must be treated very carefully.
The overall trends are shown in fig. 33.

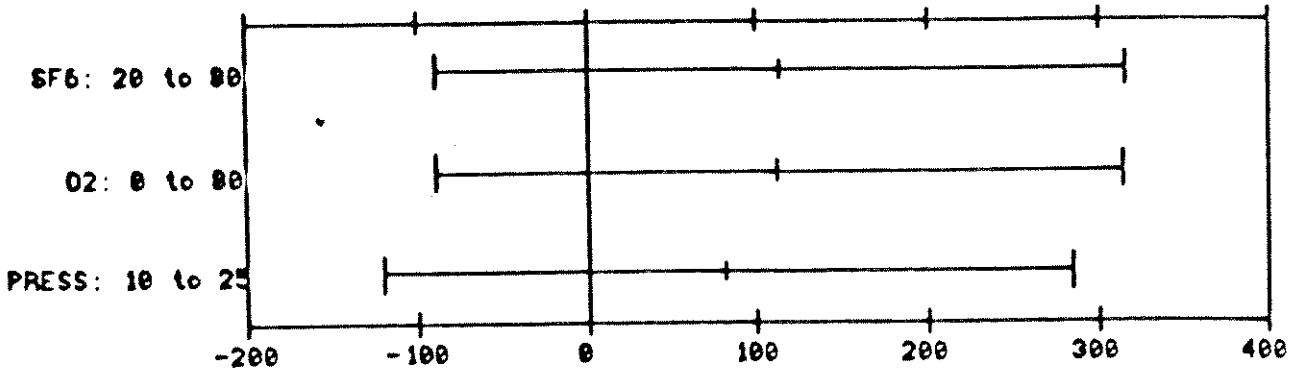

Figure 33 : Overall trends of the tungsten etch rate as function of SF_6 flow, O_2 flow and pressure at the center of a DF patterned wafer. The abcissa indicates the increase of the etch rate in nm/min, a negative value indicates a decrease.

They show a very small etch rate increase for the increase of the three parameters: SF_6 flow, O_2 flow and pressure.
When plotting the parameter set we normally use for the more detailed study, we see that the trends are somewhat similar to the LF patterned wafer: increase in etch rate with SF_6 flow, but only with 30% over the whole flow range (against

60% for the LF wafer), and with 25% with O_2 flow over the whole range, and somewhat in pressure, as shown in figures 34 and 35.

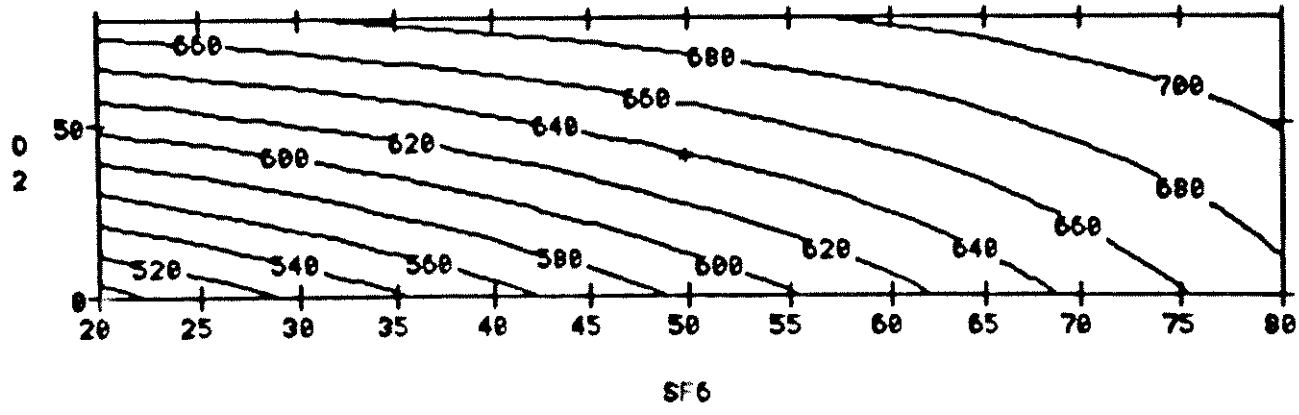

Figure 34 : Contourplot of tungsten etch rate in nm/min at the center of a DF patterned wafer, as a function of SF_6 flow and O_2 flow, at fixed pressure of 17,5 mTorr, Triode II mode, 400 W RF and 0 W AF power.

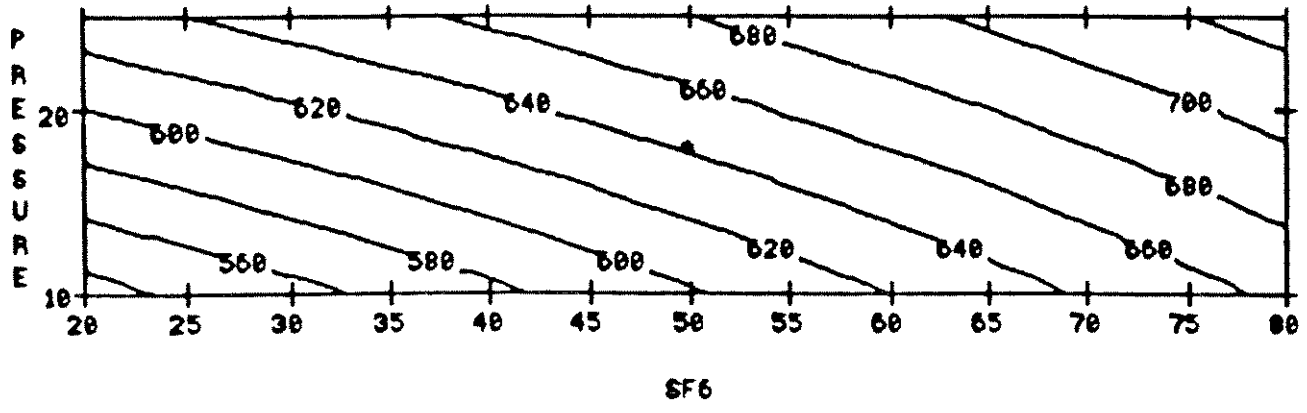

Figure 35 : Contourplot of tungsten etch rate in nm/min at the center of a DF patterned wafer, as a function of SF_6 flow and pressure at fixed O_2 flow of 8 sccm, Triode II mode, 400 W RF and 0 W AF power.

For a DF wafer, the F consumption is much less severe than for a LF wafer. This has in this case 2 immediate consequences : the overall etch rate of a DF wafer is higher and the influence of the SF_6 flow is much smaller than for the LF wafers.
Different from the LF wafer, a pressure increase slightly increases the etch rate. At higher pressure, the concentration of free F is higher, but the diffusion coefficient is lower. For the LF wafer, these 2 effects cancel each other. For the DF wafer, there is much less F consumption, therefore, the F has "to travel less" to reach

the wafer surface. In this case, it is logical that the F concentration is a more important factor than the diffusion coefficient.
Remark: there is also some F consumption in the removal of the resist: for a DF wafer this should not be completely neglected, as we did before for the tests in part A, for LF wafers.

e) Etch rate at the border of a dark field patterned wafer.

The correlation factor R^2 = 0.799 and the analysis of variances F(2,1) = 342 show that the model does not fit the experimental data. Therefore the following analysis must be treated very carefully.
The overall trends are shown in fig. 36.

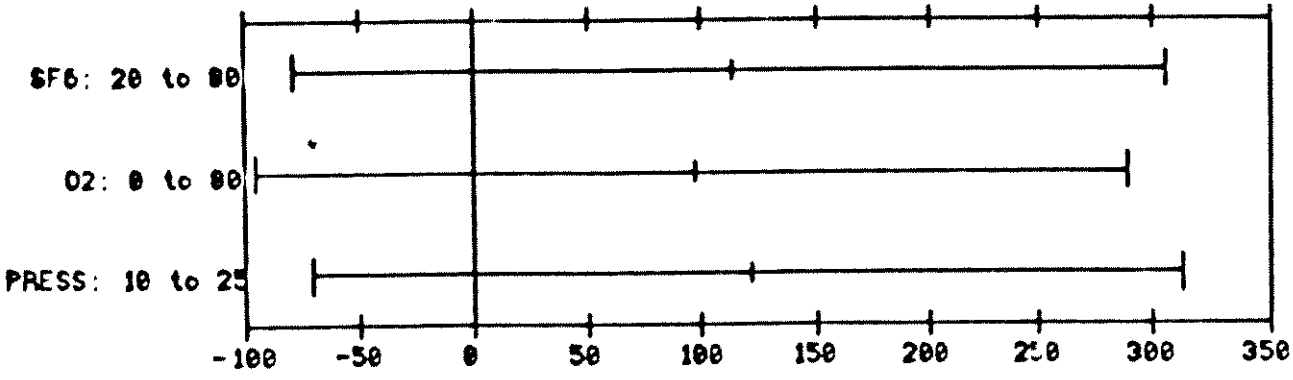

Figure 36 : Overall trends of the tungsten etch rate as function of SF_6 flow, O_2 flow and pressure at the border of a DF patterned wafer. The abcissa indicates the increase of the etch rate in nm/min, a negative value indicates a decrease.

These are very similar to the ones for the center of the wafer. The detailed plots show also the same results, what is expected if one looks at the good uniformity of the etching. Therefore, we shall not repeat the same conclusions here.

f) Uniformity of a dark field patterned wafer.

The correlation factor R^2 = 0.958 and the analysis of variances F(2,1) = 0.650 show that the model fits well the experimental data.
The overall trends are shown in fig. 37.
The uniformity increases with increase of O_2 flow but mainly by the decrease of pressure. But as the values are already high, the influences are only a few percent. The SF_6 flow is not important for this response.

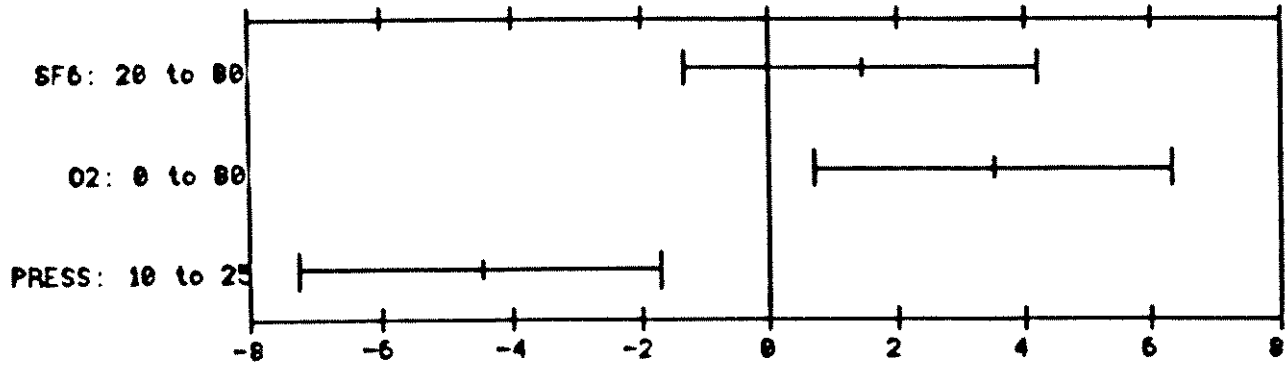

Figure 37 : Overall trends of the tungsten etch rate uniformity as function of SF_6 flow, O_2 flow and pressure of a DF patterned wafer. The abcissa indicates the increase of the uniformity in percentage points, a negative value indicates a decrease.

Figures 38 and 39 show this in more detail.
As the reproducibility tests (points 7 and 8 in table VIII) indicate a non reproducibility of 2% and most uniformity values are within this interval, the results of this analysis of variances do not yield much information in this case. But the overall main result is important: the uniformity of these processes is extremely high.

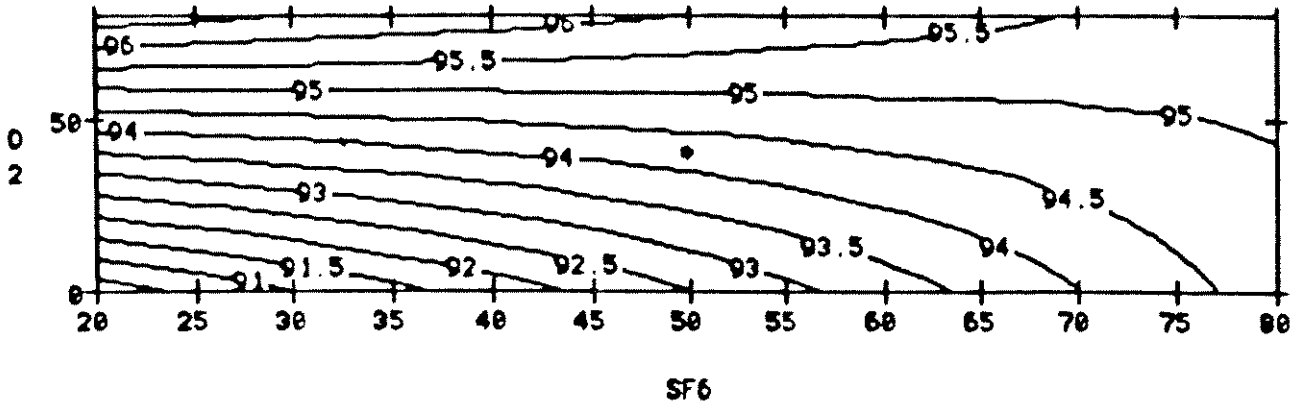

Figure 38 : Contourplot of tungsten etch rate uniformity in percentage points of a DF patterned wafer, as a function of SF_6 flow and O_2 flow, at fixed pressure of 17,5 mTorr, Triode II mode, 400 W RF and 0 W AF power.

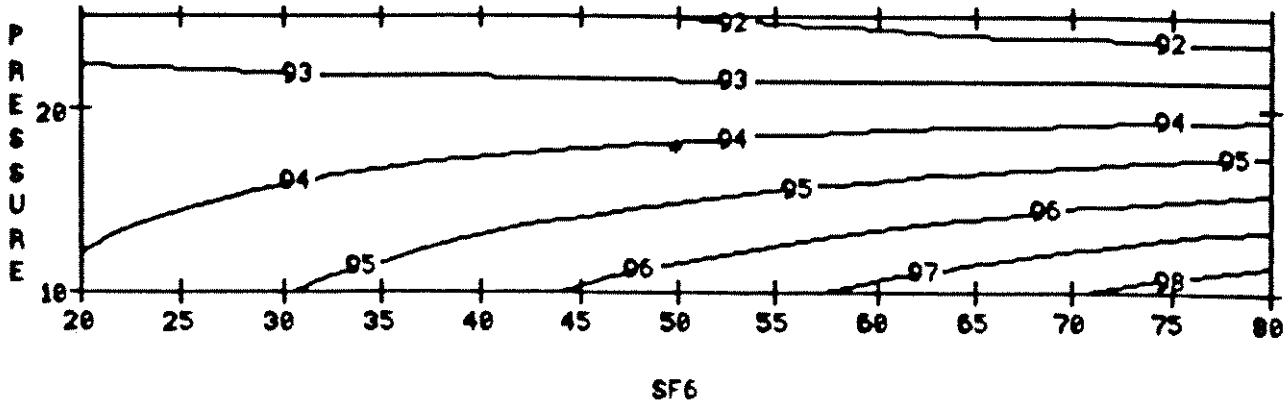

Figure 39 : Contourplot of tungsten etch rate uniformity in percentage points of a DF patterned wafer, as a function of SF_6 flow and pressure at fixed O_2 flow of 8 sccm, Triode II mode, 400 W RF and 0 W AF power.

g) Loading effect at the center of the wafer.

The most important response of these tests is the loading effect that occurs for these processes, as it is one of the most important effects (and often the killing one) in the W back etching to obtain plugs.
We quantified this loading effect LE in the following way: LE is the quotient of the etch rate of the LF patterned wafer divided by the etch rate of the DF patterned wafer, in this case in the center of the wafer. We expressed it in general in percent. The correlation factor $R^2 = 0.917$ and the analysis of variances $F(2,1) = 1.975$ show that the model fits well the experimental data.
The overall trends are shown in fig. 40.

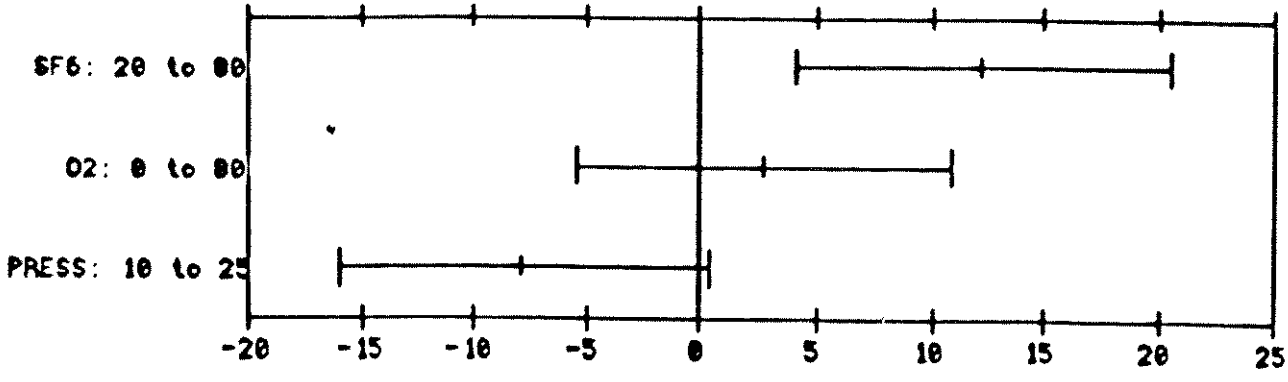

Fig. 40: Overall trends of LE as function of SF_6 and O_2 flow and pressure at the center of the wafer. The abcissa indicates the improvement of LE in percent, a negative value indicates a decrease in LE.

The most important factor is the SF_6 flow: increasing it from 20 to 80 sccm, yields an average LE improvement of 12%. Pressure is also quite important: decreasing from 25 mTorr to 10 mTorr yields an average LE improvement of 8%. The influence of the O_2 flow is not important.

These results are shown in more detail in figures 41 and 42.

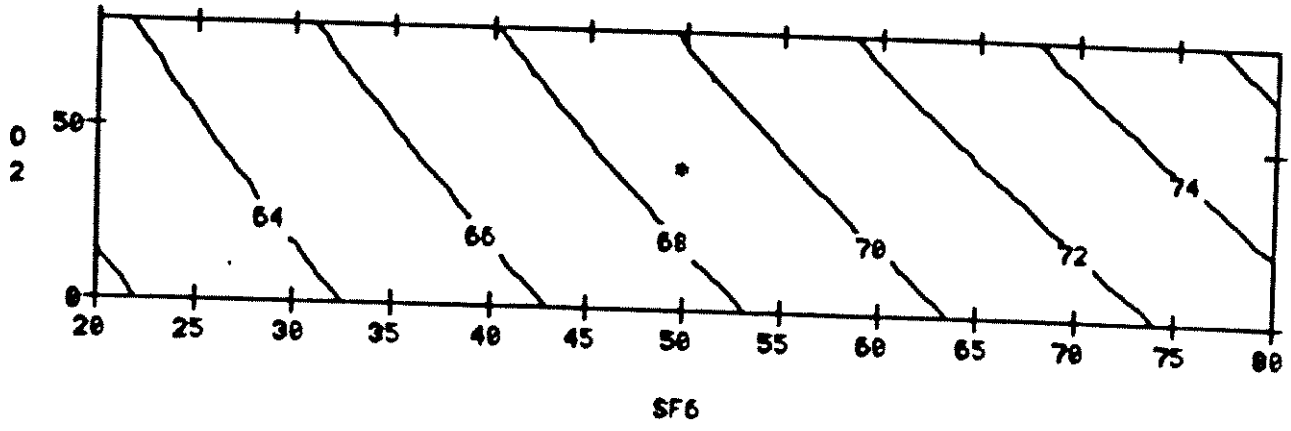

Figure 41 : Contourplot of LE in percentage points at the center of the wafer, as a function of SF_6 flow and O_2 flow, at fixed pressure of 17,5 mTorr, Triode II mode, 400 W RF and 0 W AF power.

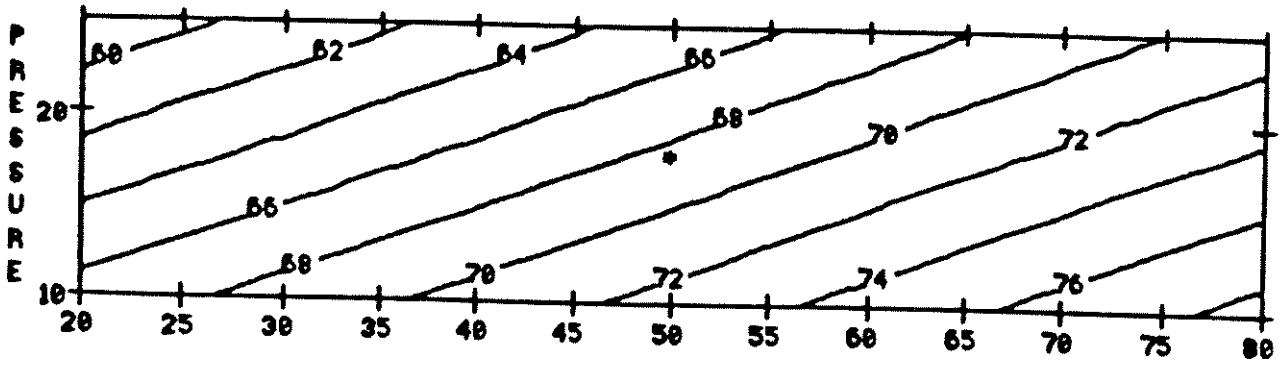

Figure 42 : Contourplot of LE in percentage points at the center of the wafer, as a function of SF_6 flow and pressure at fixed O_2 flow of 8 sccm, Triode II mode, 400 W RF and 0 W AF power.

The lines of equal LE effect are linear, indicating that there is not much of an interaction between the different factors. They show clearly that SF_6 flow must be as high as possible and pressure as low as possible, with still a marginal improvement of loading effect when increasing the O_2 flow.

We know that at higher SF_6 flow, the etch rate increases, that more free F reaches the wafer surface, certainly for a LF wafer. For a DF wafer, the consumption of free F is much less, therefore its etch rate will not increase as much with increase of free F. Then it is normal that the best LE is obtained when most free F reaches the wafer, thus with a high SF_6 flow.
For the LF wafer, the etch rate is not influenced by the pressure, for the DF wafer, etch rate increases with pressure, as explained in section d above. Therefore a pressure decrease will improve the loading effect.
O_2 flows have no major influence on etch rates of both types of wafers.

h) Loading effect at the border of the wafer.

The correlation factor $R^2 = 0.988$. As the results of the controle points were the same, it was not possible to perform an analysis of variances. But with this high correlation factor and knowing that the analysis of variances of the model in the center of the wafer was OK, we assume that the model is quite adequate. The results are approximately the same as in section g, as expected.
The overall trends are shown in fig. 43.

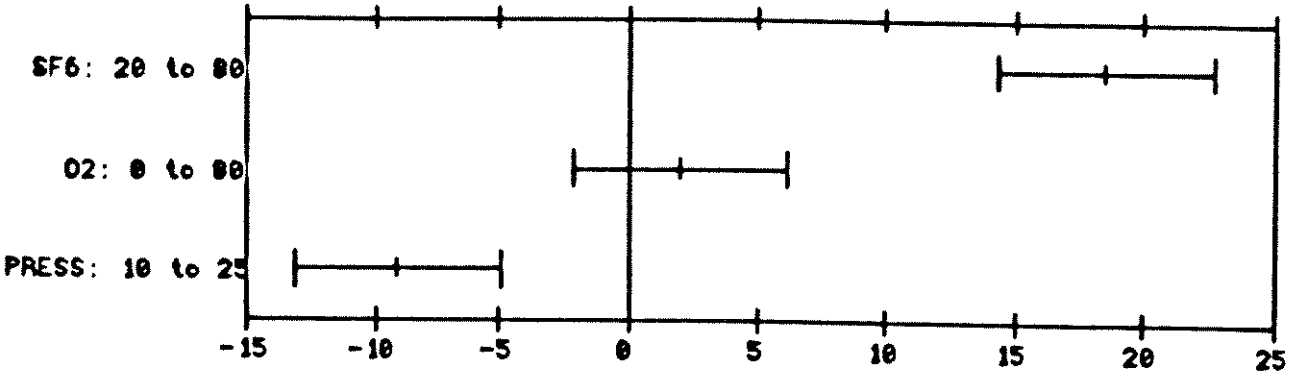

Figure 43 : Overall trends of LE as function of SF_6 flow, O_2 flow and pressure at the border of the wafer. The abcissa indicates the increase of LE in percentage points, a negative value indicates a decrease.

On the abcissa one can read the percentage points increase of LE (a negative value indicates a decrease in LE)
As expected, they are the same as for section g : SF_6 flow increase and pressure decrease improve the loading effect, O_2 flow is of little importance.
Figures which show the loading effect in more detail give similar results as above and are therefore not included.

i) Conclusion.

The best process for back etching of tungsten to form plugs is a process with flows of 80 sccm SF_6 and 16 sccm O_2, a pressure of 10 mTorr, 400 W RF power, 0 W AF power, Triode II mode.
This process results in an etch rate of 530 nm/min, uniformity of 94% and difference in etch rate between DF and LF patterned wafers of less than 20%.

j) Comparison tungsten etching - polysilicon etching.

Comparing figures 24 and 27 with figure 17, one can find the following agreements between tungsten and polysilicon etching:
- the dominant factor for the etch rates is the SF_6 flow;
- the oxygen flow is in both cases much less important.
However, when comparing e.g. fig. 25 with fig. 18, one can see that the increase in oxygen flow increases always the tungsten etch rate, while a parabole is formed for the polysilicon etch rate. This can be explained by the formation of WOF_4 product molecule in the case of the tungsten etching, as explained in more detail in appendices II and III.
A pressure increase does not influence the tungsten etch rate, while it increases very slightly the polysilicon etch rate. Though even in this case this result is only valid from 10 to 19 mTorr, which means that from 20 to 25 mTorr, there is no visible influence.
Therefore, we can conclude that in general the same factor influences both etch rates in the same way.
This can also be said of the uniformity, though we did not perform an as detailed study as for the etch rate.

6.3) Tests with SF_6 - Cl_2 plasmas.

Mixtures of SF_6 and Cl_2 gases are investigated to obtain a process for tungsten back etching. A quick screaning test was performed to have a first idea of the overall behaviour and performance of these processes. The pressure was kept constant at 10 mTorr and the power at 400 W RF power and 0 W AF power. The results are shown in table IX. The same symbols are used as for table VIII.
By adding Cl_2 to the SF_6, the etch rate of the tungsten decreases. When adding 80 sccm of Cl_2 to 20 sccm and 80 sccm of SF_6, the etch rates decrease with respectively 28% and 25% for a LF wafer. The uniformities for the LF wafers decrease slightly. The LE decreases for the wafer with high SF_6 flow, but increases for the wafer with low SF_6 flow.
These results are worse than for SF_6 - O_2 plasmas: the uniformity of the LF wafer etching is lower and the loading effect is worse than the 80 sccm SF_6, 20 sccm O_2 flow process. Therefore, no more tests were performed on these gas combination processes.

Table IX : overview of tungsten etch rates, uniformities and loading effects in function of process parameters, for SF_6 - Cl_2 plasmas.

Nr	Gas flows SF_6 [sccm]	Cl_2 [sccm]	r_{cLF} nm min	r_{bLF} nm min	U_{LF} %	r_{cDF} nm min	r_{bDF} nm min	U_{DF} %	LE_c %	LE_b %
1	80	0	495	544	91	632	646	98	78	84
2	80	80	372	432	88	532	575	92	70	74
3	20	0	304	327	93	462	506	91	66	65
4	20	80	218	245	89	298	304	98	73	81
5	50	40	379	432	88	574	626	92	66	69

Addition of Cl_2 to SF_6 does not increase the free F formation, as the addition of O_2 does. Generation of active Cl atoms occurs. It is known [3,4] that Cl containing gases etch W, forming the volatile WCl_6 compound. This compound is much less volatile than the WF_6 compound. For these gas mixtures there will be competition between F and Cl atoms to form a W-Halogen bond. When comparing test 3 with test 4, one can observe that with 80 sccm Cl_2 added, the etch rate decreases. As there are more halogen molecules available, one can suppose that there will be more generation of halogen atoms. With 80 sccm of SF_6 flow the etch rate is much higher than with 20 sccm of SF_6 flow, therefore the reason of the decrease of etch rate when adding 80 sccm of Cl_2 is not that the residence time of the particles in the reactor is too low. This indicates that the reason for etch rate decrease is the reduction of the volatility of the etch product : WCl_6 is much less volatile than WF_6. As the tungsten layer gets covered by more Cl than by F, the etch rate will decrease.
During these experiments, the resist etch rate was also measured. Addition of Cl_2 increases the etch rate of the resist for the LF wafers, therefore the selectivity from tungsten to resist halves when adding 80 sccm of Cl_2. Therefore, these processes are also not useful for etching tungsten anisotropically.

References:

[1] P. Laporte, L. Van den hove, Y. Melaku, "Dry Etching for sylilated resist development", Proceedings of the SPIE vol. 1392, eds. Bondur, Turner, 196 (1990)
[2] R.C. Reid, T.K. Sherwood, "The properties of gases and liquids", second edition, Mc.Graw - Hill, 1966
[3] D. Fischl, D. Hess, "Plasma Enhanced Etching of Tungsten and Tungsten Silicide in Chlorine Containing Plasmas", J. Electrochem. Soc. 134, 2265 (1987)
[4] Fischl e.a., "Etching of Tungsten and Tungsten Silicide Films by Chlorine Atoms", J. Electrochem Soc. 135, 2016 (1988)

Appendix V : Mechanisms for plasma etching of tungsten.

INDEX

Appendix V : Mechanisms for plasma etching of tungsten.

Introduction.

As mentioned in appendix I, general principles of plasma etching are well known and well described in the literature. Modelling of plasma etching is much more difficult, because it is very hard to quantify the different phenomena which occur within the plasma and at the wafer-plasma interface. In this appendix, we shall try to do some quantitative analysis of - mainly tungsten - plasma etching and propose some, simplified, models which will allow us to draw some conclusions on the etch limiting steps in plasma etching.

This appendix was divided in four parts:

1: Basic calculations for verification of plasma etch models.

2: Qualitative modelling : chemical etching versus bombardment enhanced etching and the influence of tungsten oxide.

3: General conclusions.

4: Suggestions for further research and development.

1) Basic calculations for verification of plasma etch models, applied to tungsten etching.

As explained in appendix I, the plasma etch process can be divided in several subprocesses. We shall distinguish the following steps:
- the plasma generates reactive particles, i.c. atomic F
- the reactive particle reaches the tungsten film
- the reagent adsorbs at the surface
- the reagent chemisorbs: a chemical W-F bound is formed
- other reagent particles react with the surface atom, so that the volatile product molecule is formed, typically WF_6
- the product molecule desorbs from the surface, and is pumped away.

To determine some mechanisms and to make some calculations, we shall make some assumptions which are in general valid, though sometimes simplified.
For tungsten we have the following material constants :
density ρ : 19.35 kg/dm^3 = 19.35 g/cm^3
atomic weight M: 184 g/mole
overall etch reaction: $W + 6\ F \rightarrow WF_6$
For silicon:
density ρ = 2.33 kg/dm^3 = 2.33 g/cm^3
atomic weight M: 28 g/mole
overall etch reaction: $Si + 4\ F \rightarrow SiF_4$

In appendix I, it was shown that it is possible to calculate the fluorine consumption J_F during etching of a (bare) wafer by the following formula:

$J_F = 2.24\ 10^{-3}\ .\ \pi\ .\ (d/2)^2\ .$ etch rate $.\ \rho\ .\ X\ /\ M$ (1)

with:
J_F : flow of atoms consumed in [sccm]
d : diameter of the wafer in [cm]
etch rate : of the film in [nm/min]
ρ : density of the film material in [kg/dm^3]
X : coefficient of the overal reaction :
Mat + X Hal -> $MatHal_X$
M : atomic weight of the film material in [g/mol]

As these flows are proportional to the etch rate, a F flow of 0.173 sccm is consumed and a WF_6 flow of 0.029 sccm comes free from the surface, per nm/min of W etch rate, for 125 mm wafers. For silicon for the same type of wafers, the fluorine consumption = 0.092 sccm, with formation of a SiF_4 flow of 0.023 sccm per nm/min etch rate.

1.1) Generation of the active species.

The generation of active species is very hard to determine, as explained in appendix I. When combining generation with diffusion, it will be possible to obtain quantitative data, as shown in 1.2, below.

1.2) Flow of reactive particles reaching the surface.

What needs to be known to determine the etch rate is the flow of free fluorine atoms that reach the surface. This flow is determined by two mechanisms:
1: the generation of free fluorine atoms.
2: the transport of these atoms to the surface.
By evaluating the transport mechanism, we shall be able to evaluate also the generation of the free fluorine.
We shall consider the following two cases: depletion and no depletion of the free fluorine source.

A) There is no depletion of free fluorine.
This means that the concentration of free fluorine remains constant all over the reactor. This assumption would be valid if the generation of free fluorine is extremely high and consumption of free fluorine low.
Then the movement of the free fluorine species is determined by the random thermal movement.
One can assume that the concentration of free fluorine is constant in the bulk of the plasma and that it is a fraction Y of the total number of particles in the plasma.

The average thermal speed, $\bar{c}$, is [1]

$$\bar{c} = (8kT/\pi.m)^{1/2} \quad (2)$$

with:
k : Boltzmann constant
T : absolute temperature in [K]
m : molecular mass in [g/mol]
It can be calculated that at 20°C $\bar{c}$ is equal to:
570 m/s for F
144 m/s for WF_6.
The impingement flux f_i in number of particles i per unit area, is [1] :

$$f_i = n_i \bar{c} / 4 \quad (3)$$

where n_i is the total density of particles i in the plasma. To calculate the impingement flux of fluor f_F, the concentration of fluor C_F in the plasma has to be known. From each mother molecule (e.g. NF_3 or SF_6), an average of G fluorine atoms are generated by the plasma. Therefore the concentration of fluor is a factor G/(G+1) of the concentration of all species n, assuming there is no recombination.

$$C_F = n \ (G/G+1 \ )$$

n is proportional to the pressure, therefore a proportionality factor p' is introduced. At 200 mTorr :

$$p' = 200 / 760000$$

At 200 mTorr, for a wafer of 125 mm, there is a flow of F because of thermal movement from plasma to wafer of:

$$f_F = \bar{c} \ . \ p' \ . \ G \ . \ A \ / \ [4 \ (G+1)] \quad (4)$$

with:
A : area of the wafer (which is 123 cm^2 for a 125 mm wafer)
A factor of 60 has to be introduced to convert seconds to minutes.

$$f_F = 57000 \times 60 \times 200 \times G \times 123 \ / \ [4 \times 760000 \times (G+1)] = 27675 \ G/(G+1) \ sccm$$

A typical value for G is 0.1 : 10% of the molecules yield 1 free fluorine atom [1,2], this is an assumption at the lower end of the range for G.
For these assumptions, an etch rate of :
0.1 x 27675/ [1.1 x 0.173] = 14543 nm/min would be supported, if this mechanism could be applied (assuming WF_6 as the sole volatile product).

B) The free fluorine source is depleted.

During etching, the fluorine will be consumed. In this way a gradient of free fluorine species will be created. Through diffusion, fluorine from further away in the reactor will reach the surface of the wafer.
The flow J of particles from the bulk of the plasma to the wafer is proportional to the concentration gradient dC/dx and the diffusion constant D and the area of the wafer A.

$$J = - A D \, dC/dx \qquad (5)$$

Ref [3] dedicates a chapter on diffusion coefficients. For a binary gas system at low pressure, the following formula is proposed:

$$D_{12} = 0.001858 \, T^{3/2} \, [(M_1 + M_2)/M_1 \, M_2]^{1/2} \, P \, \sigma_{12}^2 \, \Omega_D \qquad (6)$$

With :
D_{12} : the diffusion constant in [cm^2/s]
T : absolute temperature in [K]
M_1 M_2 : molecular weights in [mol/g]
p : pressure in [atmosphere]
σ_{12} : the Lennard-Jones force constant, which can be calculated from tables found in ref [3]
Ω_D : the Lennard-Jones potential function, which can be determined from tables in ref [3].
As the values of σ and Ω_D for NF_3 and atomic F were not published, we used values for BF_3 for calculations with NF_3 and HF to determine σ and F_2 to determine Ω_D for F.
We shall calculate D here for 2 examples: F in NF_3 at 200 mTorr and F in SF_6 at 10 mtorr, both at 20°C;
we obtain for example 1: $\sigma_{12}^2 = 3.67$, $\Omega_D = 1.07$, then
$D = 636$ cm^2/s
we obtain for example 2: $\sigma_{12}^2 = 4.14$, $\Omega_D = 1.105$, then
$D = 9129$ cm^2/s .
The diffusion constant of example 2 is much higher, because the pressure is a factor of 20 lower.
The concentration gradient is harder to determine. The arrival of active species is the limiting mechanism if at the wafer side the concentration is zero: it means that all F that arrives will immediately be adsorbed-chemisorbed. The concentration C_F in the plasma is unknown in general. Qualitative measurements are possible, determining absolute values is hard to impossible. It is clear that this value is dependent on the type of plasma and all the plasma parameters mentioned in appendix I.
For a first order approximation, one can assume that the free fluorine concentration increases linearly from the wafer on, till a certain distance x_s in the plasma i.e. the concentration gradient is constant in this plasma region - in

this plasma "slab" as we will call this region from now on. Therefore the total fluorine content in this slab is exactly half what it would be without any gradient, or if no F would be consumed, as can be seen in fig. 1.

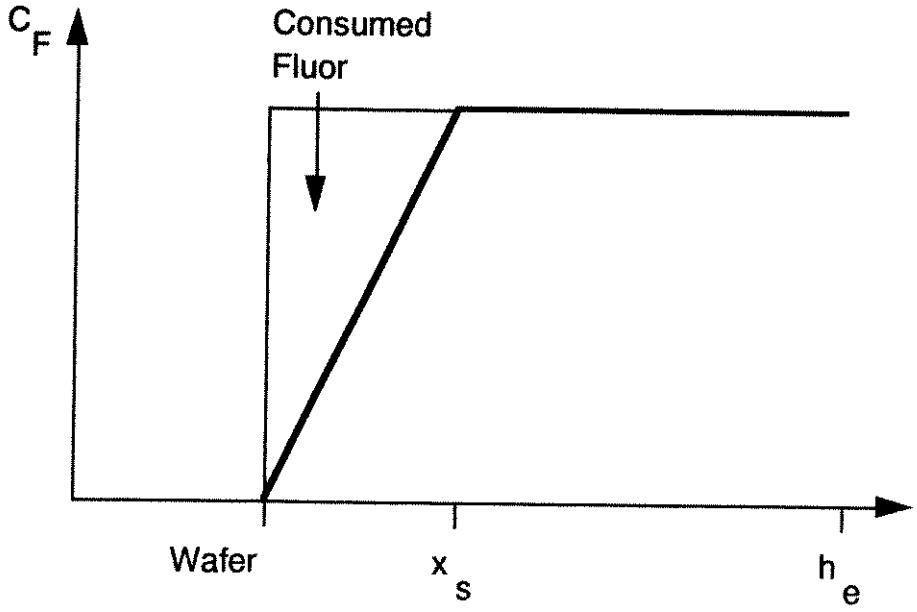

Figure 1 : Free fluorine concentration in the plasma.

Outside this plasma slab the concentration C_F is constant, i.e. the gradient is zero.
Therefore equation (5) becomes for fluorine diffusion:

$$J_F = D\ A\ C_F/x_S \qquad (7)$$

From each mother molecule (e.g. NF_3 or SF_6), an average of G fluorine atoms is generated by the plasma. Therefore the concentration of fluor is a factor G/(G+1) of the concentration of all species, n; assuming that there is no recombination.

$$C_F = n\ (\ G/G+1\ ) \qquad (8)$$

The density n is determined by the pressure of the plasma.

To calculate distance x_S in the plasma, the following assumptions can be made:
1) the flow of the used gases is homogeneous between the two electrodes;
2) free fluorine will only be consumed from the place where the wafer is placed till distance x_S in the plasma.
This assumption is a logical conclusion from the fact that outside the plasma slab the fluorine gradient is zero, therefore, no fluorine will diffuse from that region to the wafer.
It is necessary to have a certain concentration gradient in this slab, if not, no diffusion would take place in this

area. We shall consider the assumption of a constant gradient as sufficiently adequate, if the results of the following calculations prove to be consistent. In reality, the gradient will depend very much on the type of reactor and also on the way the atoms move through the reactor chamber. The total content of free fluorine per unit area in the slab is : 0.5 C_F x_S : half of the fluor is consumed, half remains, as can be seen in fig. 1: the upper triangle represents the consumed fluor.

3) From each mother molecule (e.g. NF_3 or SF_6), an average of G fluorine atoms are generated by the plasma. As in these plasma reactors the pressure remains constant by adjusting a throttle valve, the total gas flow is higher than the flow of entering mother molecules f: total flow of all the particles is then: (G+1)f, the flow of F atoms is G f.

As shown before, it is possible to calculate the flow of consumed fluor J_F, when the etch rate and wafer characteristics are known. This flow is exactly the flow that comes from the plasma slab described just above.

From assumptions 1 and 3 above, we conclude that without F consumption the F flow per unit of interelectrode distance between the electrodes would be a constant: G f / h_e with h_e the interelectrode distance.

The flow of consumed fluorine, J_F, is half the flow that would pass the plasma slab with thickness x_S if no F would be consumed (or half of the flow that passes through a region with thickness x_S outside the plasma slab).

$$J_F = 0.5\ G\ f\ x_S\ /\ h_e \qquad (9)$$

thus

$$x_S = 2\ J_F\ h_e\ /\ [G\ f] \qquad (10)$$

We have now 2 equations : (7) and (9), in which only x_S and G are unknown. Combining equations (7) and (8) yields:

$$J_F = A\ D\ n\ G\ /\ [(G+1)\ x_S]$$

Combining this with (10) yields:

$$x_S = [\ A\ D\ n\ 2h_e\ /\ [(G+1)\ f]]^{1/2} \qquad (11)$$

Substituting x_S in (9) and rearranging yields:

$$G^2\ A\ D\ n\ f\ -\ G\ 2\ J_F^2\ h_e\ -\ 2\ J_F^2\ h_e = 0$$

therefore:

$$G = (2J_F^2\ h_e + [J_F^4\ 4h_e^2 + 8A\ D\ n\ f\ J_F^2\ h_e]^{1/2})/[2(A\ D\ n\ f)] \qquad (12)$$

These formulas are valid for any plasma system, for which the assumptions stated above can be applied.
As a first example we take an experiment from appendix II: etching in the SWAFER system with the following process : 100 sccm of NF_3, 200 mTorr pressure with 50 W AF power in Plasma Float mode yields an etch rate of 200 nm/min. One can calculate then from formula (1) that the flow of consumed F is 34.7 sccm or $9.323\ 10^{20}$ atoms per minute : this is the flow J_F that has to arrive at the surface. One can calculate that there are $0.660\ 10^{16}$ species/cc at 200 mTorr and 20°C [1].
The height between the two electrodes in the SWAFER is 5 cm. The area of a 125 mm wafer is 123 cm^2. The diffusion constant has been calculated above. The flows have to be expressed in species per second.

$f = 4.48\ 10^{19}$ molecules/s
$J_F = 1.55\ 10^{19}$ atoms/s

Substituting all these values in equations (11) and (12) gives :

$G = 0.378$
$x_S = 9.15$ cm

The fact that the calculated x_S is greater than the interelectrode distance means that the reaction is limited by the generation of the free F atoms, not by the diffusion. The diffusion would only limit the etch rate if the reactor would be larger than this distance x_S.
Another example is taken from appendix IV : etching in a Tegal 15xx system with the following process : 80 sccm of SF_6, 10 mTorr pressure with 400 W RF power in Triode I mode yields an etch rate of 750 nm/min.
The distance between lower and upper electrode, h_e, is 10 cm. One can calculate that there are $0.033\ 10^{16}$ species/cc at 10 mTorr and 20°C [1]. The diffusion coefficient is calculated above. For this example, the flows are :

$f = 3.59\ 10^{19}$ molecules/s
$J_F = 5.81\ 10^{19}$ atoms/s

This results in :

$G = 5.93$
$x_S = 5.76$ cm

This means that the etch rate is limited by the combined mechanism generation - diffusion : if the generation rate would be higher, the etch rate would be faster : C_F increases and consequently J_F increases; if the diffusion was faster, the etch rate would also increase (F atoms from further off

in the reactor could also participate in the etching). One can observe that the generation rate is very high: nearly all the SF_6 molecules which enter the reactor, are completely decomposed.
This model is extremely simple, mainly in the modelling of the gas flow, which is always more complicated. A weak point is the importance of the diffusion constant: from formula (12) one can observe that if J_F is high, G is nearly linearly proportional to the inverse of this constant. Therefore, errors in D will greatly influence G, and also x_s.
It is very hard to quantitatively determine the concentration C_F and the distance x_s through experiments. Spatially resolved LIF measurements could give some indications, but a special reactor would be necessary, with access for the laser beam to several heights above the wafer. So a special design of windows in the reactor would be needed, which is normally not available in commercial systems.

1.3) Adsorption and chemisorption.

In this chapter, we shall not dedicate much attention to these mechanisms, as we found out that they are in general not the etch rate limiting steps, as shown below, in section 2.
The description in appendix I is adequate for our purposes here.

1.4) Formation of the volatile product.

As for the chemisorption, the treatment of this step as given in appendix I is sufficiently adequate, because this step is not the etch rate limiting mechanism, in general.

1.5) Desorption

The volatile product, for tungsten : WF_6, must leave the surface. This process can be described by equation (13) [4]:

$$\tau = \tau_o \exp (Q/RT_s) \qquad (13)$$

With τ_o: vibration time : typically 10^{-13} s
T_s : surface temperature in [K]
R : universal gas constant : 8.31 J/mol K
Q : activation energy in [J/mol]
τ : residence time of an adsorbed molecule in [s]

Q can be determined through tests of "Temperature Programmed Desorption" (TPD) [5].
For desorption of WF_6 at least 4 desorption peaks between 300 and 600 K were found, as shown in fig. 2. These peaks were designated to strongly adsorbed multilayer WF_6. Desorption activation energies of 87, 109, 127 and 145 kJ/mol could be estimated. A gamma peak was found at lower temperature: around 170 K, thought to be generated by weakly physisorbed

WF_6. Knowing that the desorption of the alfa 1 peak occurred at 360 K, we can calculate that the desorption activation energy of the gamma peak is approximately 41 kJ/mol.

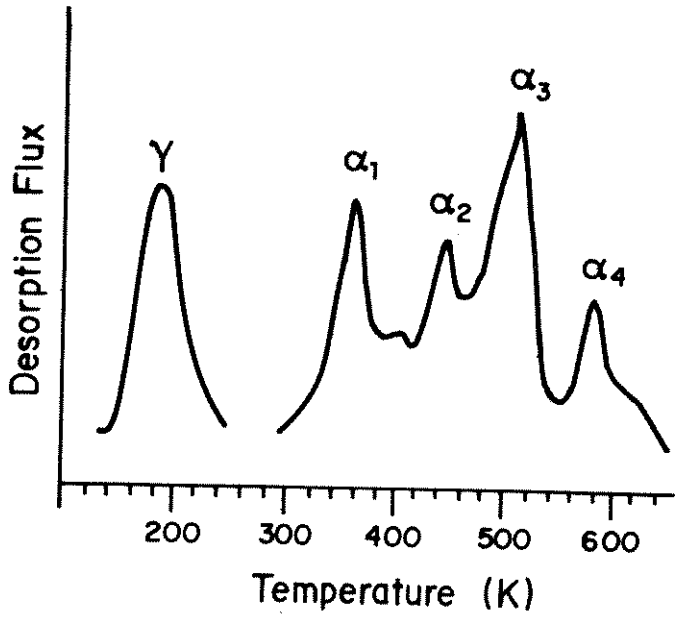

Figure 2 : WF_6 TPD spectra from clean W [5].

Using equation (13) at 300 K :
$\tau = 10^{-13}$ exp (41000/8.31 x 300) = 1.44 10^{-6} s
One monolayer of W (100) or W (111) consists of approximately 10^{15} atoms per square cm [6].
Then it is possible to calculate the number of desorbed molecules per second per cm^2 if desorption would be the rate limiting step:
$N_S = 10^{15} / 1.44\ 10^{-6} = 6.97\ 10^{20}$ molecules/s cm^2.
This is the equivalent of the following flow over a complete 125 mm wafer (if the WF_6 coverage would be 100% all the time):
$f = 123 \times 60 \times N_S = 5.13\ 10^{24}$ molecules/min = 191000 sccm .
So, desorption of physisorbed WF_6 will not be a rate limiting step.
Using equation (13) for the strongly adsorbed WF_6:
$\tau = 10^{-13}$ exp (87000/ 8.31 x 300) = 143 s
This corresponds with a flow of only $1.89\ 10^{-3}$ sccm.
WF_6 in this state will only be desorbed at an extremely low rate : this is not compatible with the etch rates observed.
Conclusion: WF_6 in a weakly bound physisorbed state is the main participant of the desorption, unless other energy, e.g. by ion bombardment, is added.

1.6) Summary

We introduced a simple model which allows us to make some calculations on generation of free fluorine and its diffusion towards the wafer. As shown in the next section of this appendix, the arrival of free fluorine at the wafer surface is often the etch rate limiting step. The examples in this section indicate that for low etch rates (as for the SWAFER etching) the generation of free F is the etch limiting step. On the other hand, for high etch rates the limiting steps are a combination of F generation and diffusion (as for the Tegal 15xx example).

2) Qualitative modelling: Chemical etching versus bombardment enhanced etching and the influence of tungsten oxide.

As discussed in appendix I, there are some contradictions in the literature on the following 2 topics:
- chemical etching of tungsten is possible or not, and how much is it accelerated by ion bombardment
- the formation of tungsten oxide inhibits etching of tungsten.
A lot of tests, as described in appendices II to IV, were performed to address these two items.

2.1) Chemical etching versus ion bombardment enhanced etching.

In an afterglow etcher one is sure that the etching is merely chemical, but in systems where the wafers rest on an electrode, it is always possible that there is some ion bombardment. In fact, if the wafer remains within the plasma, a dark sheath will be formed between the plasma and the wafer and there will always be some ion bombardment. The voltage across this sheath can be minimized by leaving the electrode, and therefore the wafer, on a floating potential. This can be done by physically isolating the electrode or place some very high impedance devices between the electrode and the ground. The second solution is often the most elegant, but also less reliable, as sometimes the devices can have a high impedance for DC currents but not for high frequency AC currents (as happened for some tests in the SWAFER equipment, see appendix II). Therefore one should always verify the different characteristics of an etching to check if they are all compatible with chemical etching before drawing conclusions.

2.1.1) SWAFER etchings.

As reported in appendix II, several dedicated tests were performed to investigate the mechanisms which govern the tungsten etching. For this purpose, tests were also performed with polysilicon wafers. Besides, data obtained before and described in ref. [7] are available. From these data conclusions of this section and sections 2.2, 2.3 and 2.4 could be drawn.

2.1.1.1) SF_6 based plasmas.

In RIE mode, the plasma etching characteristics are:
- "high" etch rates for all investigated films: tungsten, polysilicon, but also resist and oxide; resulting in low selectivities of tungsten (and polysilicon) towards resist and oxide.
- vertical walls for etching of tungsten, polysilicon and also silicon nitride.
All this indicates that there is a large amount of bombardment enhanced etching, as can be expected from an equipment with AF voltages in the RIE mode. The fact that no undercut is observed can be explained in two ways: there is (nearly) no chemical etching, or a sidewall protection is formed, by carbon containing particles, originated from the resist. With SF_6 we did not determine which of the 2 factors is the main reason for the vertical wall profile, but we assume it is the same as for NF_3 etchings, which are reported below.
In PF mode, the etch rates are extremely low for all the films. Ref. [7] mentions that etch rates of polysilicon at 50 W AF power are a factor of 3 lower than for RIE etching. Increasing power to 100 W increased the polysilicon etch rate by a factor of 3. It was observed that there is a large loading effect: a resist patterned wafer etches 50% faster than a blanket polysilicon wafer. Furthermore undercut was observed for both polysilicon and silicon nitride: processes are purely isotropic.
The etch rate for tungsten was so low that not many tests were done. For tungsten we had to increase the power to 150 W to obtain etch rates of the same order of magnitude as for RIE etchings at 50 W.
This means that in this equipment both polysilicon and tungsten etch chemically with SF_6, but at very low rates.

2.1.1.2) NF_3 based plasmas.

As reported in appendix II, more tests were performed with NF_3 than with SF_6. The main reason is that in PF mode several interesting phenomena occurred, as will be discussed later. As the etch rate in PF was higher than with SF_6 plasmas, we could study more easily the different characteristics of the etch processes. Besides, in PF mode we obtained an excellent process for part of a tungsten back etch process, as described in appendix II.
The overall results in RIE mode are similar to etching with SF_6, certainly what concerns the determination of the ion bombardment etching:
- the etch rates are in general higher than for SF_6, but the selectivities remain of the same order of magnitude, they are a little bit lower than for SF_6 in general;
- the wall profiles remain vertical, as well for tungsten layers patterned with resist as for them patterned with a

PECVD oxide. With a resist mask it was not possible to observe any undercut, while there was an undercut of typically 100 nm with the oxide mask. This indicates that there is some chemical etching, but very little. Furthermore, the resist erosion helps to prevent undercut, but even without resist erosion vertical walls can be obtained;
- Ref [7] reports similar trends for polysilicon and nitride etching.
This indicates very clearly that etching in RIE mode with NF_3 based plasmas is bombardment enhanced.
For the PF mode, the results are quite different from the SF_6 based plasmas, mainly in the etch rates: for tungsten the etch rate with NF_3 is a factor of 20 higher at 50W AF power than with SF_6, for polysilicon a factor of 5. Etch rates with NF_3 in PF mode are in general less than 50% lower than in RIE mode, but the difference depends very much on the process parameters..
One has to distinguish processes with pressures higher than 100 mTorr and lower than 70 mTorr (the intermediate region has not been investigated).
For processes with pressure higher than 100 mTorr the overall characteristics of the NF_3 based PF plasmas are :
- "high" etch rates for polysilicon, tungsten and silicon nitride. Much lower etch rates for resist and oxide, resulting in good to excellent selectivities. Selectivities of tungsten towards TiN are also excellent.
- always undercut for polysilicon, tungsten and silicon nitride etch processes: purely isotropic processes. Undercut of tungsten is independent of the mask type: resist or PECVD oxide. Undercut can be very severe and does not stop in time: several microns of tungsten can be removed from under the mask. This deep undercut is the best prove that it is not necessary to have any kind of bombardment to etch tungsten.
This indicates very strongly that the etching is merely chemical.
Therefore, we can conclude that it is possible to perform merely chemical etching of tungsten, provided there is enough free fluorine available, as will be discussed further below.
The loading effect for these plasmas has a rather strange behaviour: for resist patterned wafers the etch rate decreases with resist coverage, while for PECVD oxide patterned wafers the etch rate increases with oxide coverage. This will be discussed in more detail below.
For processes with pressures lower than 70 mTorr, the characteristics are rather different:
- the resist etch rate increases very much, so that the selectivity tungsten to resist is reduced to approximately 1:1;
- no undercut is observed for tungsten layers covered with resist.
Furthermore 2 other characteristics, typical for the RIE plasmas are observed: high uniformity and no resist popping when the wafer leaves the reactor. All this indicates that

at these pressures, the plasma behaves rather as an RIE plasma, with bombardment enhancement.
In general we can observe that in PF the higher the pressure, the more chemically the plasma behaves, e.g. what considers undercut.

2.1.2) Tegal 15xx etchings

Only SF_6 based plasmas were investigated, as no NF_3 was available on this equipment.
In Triode I mode RF power is applied to the walls of the reactor, while the wafer rests on the bottom electrode, which remains on a floating potential. This etch mode is very similar to the PF etch mode of the SWAFER. The main characteristics of etch processes in this mode are :
- etch rates of tungsten and polysilicon are very high, while the etch rate of resist is quite low, resulting in good selectivities;
- if no AF power is applied, undercut is observed for polysilicon and for tungsten etch processes.
This indicates that the etching is predominantly chemical.
When even only 10 W of AF power is applied to the bottom electrode, the characteristics change completely : vertical tungsten wall profiles can be obtained, but the etch rate of the resist increases considerably.
In Triode II mode, a typical RIE configuration is used : bottom electrode RF powered and all other conducting parts of the reactor are grounded. The main characteristics are then:
- still high etch rates, but lower than with Triode I mode for tungsten and polysilicon, but higher etch rates for the resist, with much lower selectivities as a consequence;
- vertical tungsten wall profiles.
This indicates that the etching became ion bombardment enhanced.

2.1.3) General conclusions

For tungsten etching it is possible to have both ion bombardment enhanced etching and chemical etching, as long as there is enough free F available . It is possible to obtain higher etch rates in the same reactor with chemical etching than with bombardment enhanced etching, both for tungsten and polysilicon.

2.2) Determination of the etch rate limiting steps.

The last observation of the former section is a strong indication that the etch rate will be mainly limited by the arrival of active particles at the wafer surface. Also the fact that very high etch rates are possible in Triode I mode (in the Tegal 15xx), therefore with chemical etching, indicates the same. Another indication is the loading effect that occurs for all etchings, when an appropriate mask is used.

Dedicated tests were performed to compare the phenomena which occur for polysilicon and tungsten etchings. By comparing the etch rates and the fluorine consumption of the polysilicon and the tungsten etching, we can draw more conclusions. At the same time the role of the oxygen in these plasmas will be explained.

2.2.1) The role of oxygen in the SWAFER etch processes.

2.2.1.1) SF_6 based plasmas.

We only investigated plasmas in RIE mode in more detail. The influence of oxygen content on the etch rates of polysilicon and tungsten is shown in fig. 3. Initially the etch rates increase with oxygen content, until a maximum is reached, after which the etch rate decreases. It can be observed that the maximum etch rate is reached at a lower oxygen content for polysilicon etching than for tungsten etching. This behaviour is the same as described in the literature and explained in appendix I: for low oxygen content the F content increases with oxygen flow, thereby increasing the etch rate.

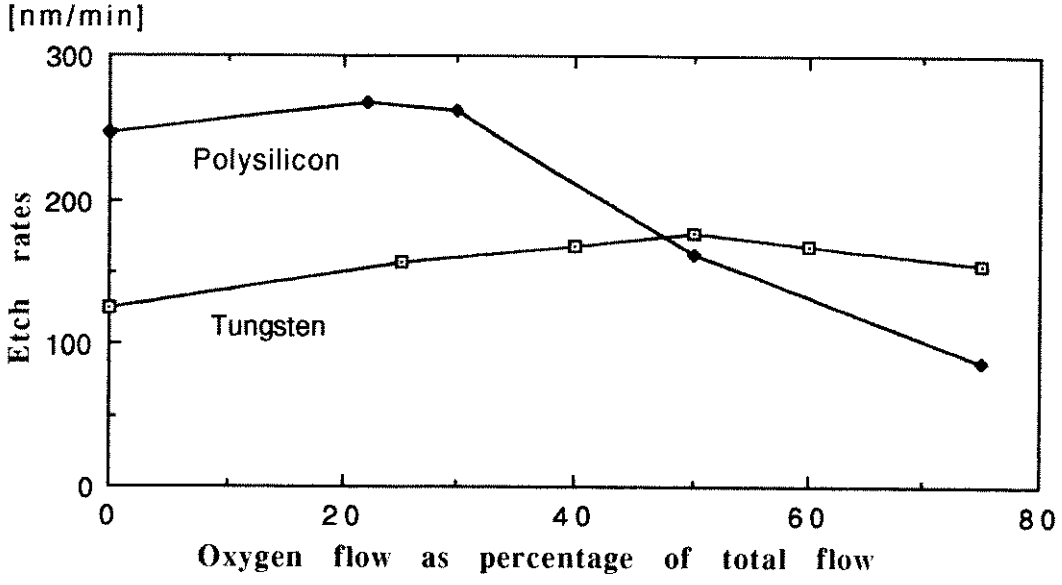

Figure 3 : Polysilicon and tungsten etch rates as a function of oxygen content for SF_6 based plasmas in RIE mode.

At higher oxygen flows, there are two effects that decrease the etch rate: firstly competition between F and O atoms to make a bond with the Si or W atoms of the layer to be etched and secondly a simple dilution effect. For the polysilicon etching the competition is certainly a strong factor, as SiO is formed which can turn into non volatile products : SiO_2 or $SiOF_2$. For W, WOF_4 was detected as a possible volatile compound, together with WF_6 [8-10]. In this way the etch rate will remain high or even increase at higher oxygen contents than for Si etching. Tungsten etch rate probably

decreases because of dilution effect. (For these tests the total flow was held constant : therefore an increase of oxygen flow means a decrease in halogen flow.)

2.2.1.2) NF_3 based plasmas.

For the RIE mode, the influence of oxygen on the polysilicon and tungsten etching is shown in fig. 4.

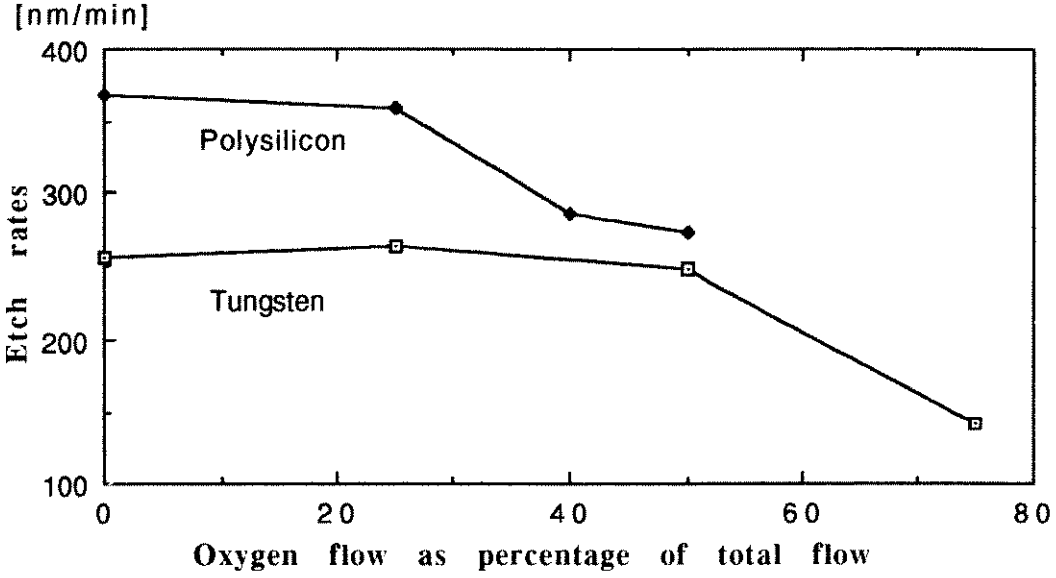

Figure 4 : Polysilicon and tungsten etch rates as a function of oxygen content for NF_3 based plasmas in RIE mode.

Etch rates do not increase (significantly) with increasing oxygen content, nor for polysilicon, nor for tungsten. At higher flows, the etch rates start to decrease. The fact that the etch rates remain practically constant for quite a large oxygen content range, could indicate that the etch rate limiting step is the chemisorption step. However, chemisorption should not be slower for these processes than for the processes in Triode I mode in the Tegal 15xx. In the Tegal 15xx, the wafer temperature will (probably) be lower than in the SWAFER.
The ion bombardment factor is hard to evaluate. In RIE mode in the SWAFER, the powered electrode receives ions at much higher energies than in the case of the Triode I mode of the Tegal 15xx. As the Tegal 15xx plasmas in Triode I mode are much intenser, one can suppose that the densities of the impinging ions are much higher than for the SWAFER plasmas. Comparing the ion bombardment factor for RIE plasmas in the SWAFER with Triode I mode plasmas in the Tegal 15xx, one can suppose that it still will be more effective for the SWAFER because of the much higher ion energies. However, if one would compare PF mode in the SWAFER with Triode I mode in the Tegal 15xx, the ion bombardment factor will be larger for the Tegal 15xx, because of the much higher ion densities, while ion energies are of the same order of magnitude for both these types of plasmas.

The fact that etch rates in the Tegal 15xx in Triode I mode are a factor of 3 higher than for RIE plasmas in the SWAFER, while chemisorption and formation of the volatile product should be higher for the SWAFER RIE mode plasmas, indicates that neither chemisorption nor the formation of the volatile product is the etch rate limiting step for these RIE processes.
The etch rates are always much higher than for SF_6 based plasmas (the other process parameters were the same for the tests reported here). This is caused by the much easier decomposition of the NF_3 molecule, because of the lower binding energies between N and F atoms, as shown in appendix I. As this molecule decomposes easily, oxygen addition does not increase the formation of free fluorine. The polysilicon etch rate decreases because of the competition between O and F molecules and forming SiO_2 or $SiOF_2$, while for W WOF_4 is formed, which is volatile in these types of plasma. At higher oxygen flows occurs probably a dilution effect.
For the PF mode, completely different mechanisms occur, as shown in fig. 5.

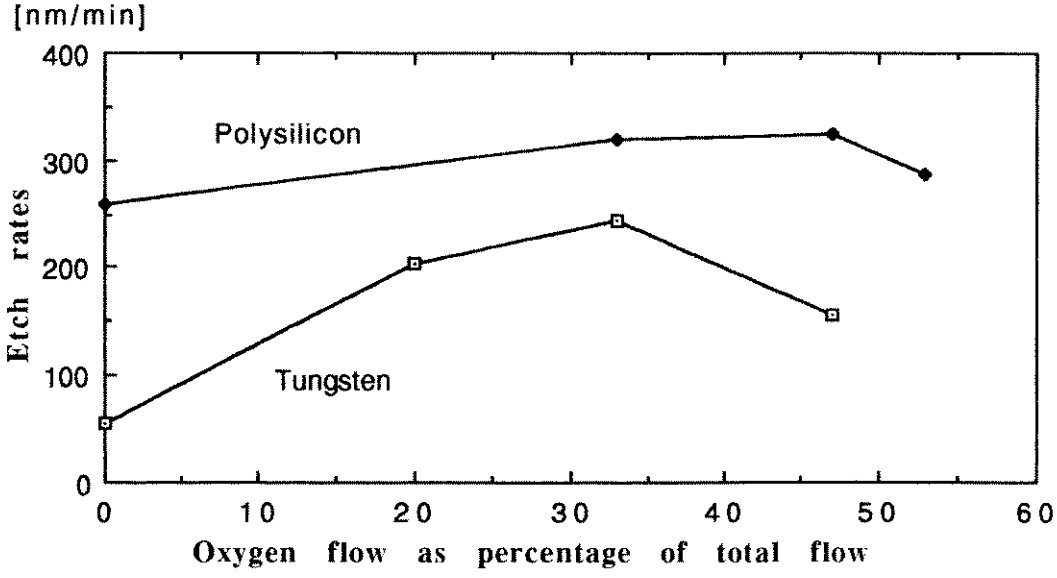

Figure 5 : Polysilicon and tungsten etch rates as a function of oxygen content for NF_3 based plasmas in PF mode.

Both polysilicon and tungsten etch rates increase with increasing oxygen content, till they reach a maximum after which they decrease. The difference is that the maximum for the tungsten etching is at a much lower oxygen content : approximately 30%, even lower than the maximum for the polysilicon etching. The mechanism for the polysilicon etching is probably the same: etch rate decrease because of competition. For the tungsten, another explanation must be given. A possible explanation lies in the high boiling point of the WOF_4 molecule: 188°C. This indicates that extra energy may be required to remove this molecule from the surface. In RIE mode, there is a lot of ion bombardment

which can remove this molecule from the surface, but in PF mode, this is not the case. Therefore it is possible that this molecule remains at the surface, inhibiting further etching, or at least retarding further etching, instead of promoting it. For a WOF_4 molecule, the O to F rate is only 25%, whereas for $SiOF_2$, it is 50%. Therefore the retarding effect of WOF_4 will be found at lower oxygen contents than $SiOF_2$. Ref [11] reports that no WOF_4 was found, but those tests were done in a RIE mode.

2.2.2) Fluorine consumption for SWAFER etch processes.

Through formula (1), it is possible to calculate the fluorine which is consumed during the etching. When using this formula for the etch processes described above and using an 80% free area for the W wafers (using a LF mask), the obtained results are shown in figures 6-8, when no fluorine consumption by the resist is assumed.

2.2.2.1) For SF_6 based plasmas in RIE mode, fig 6.

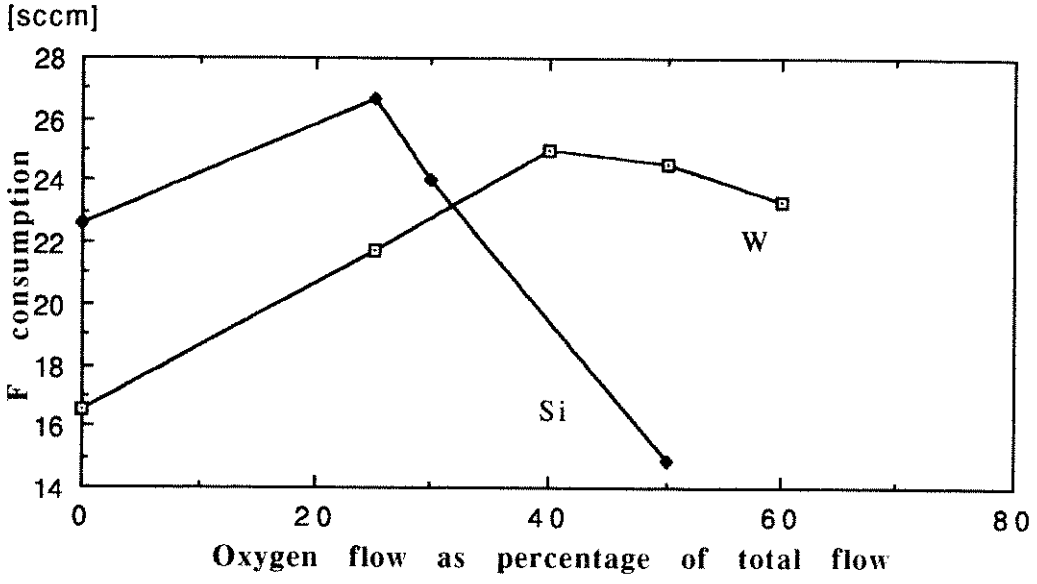

Figure 6 : Fluorine consumption for polysilicon and tungsten etch processes as a function of oxygen content for SF_6 based plasmas in RIE mode.

Only in the 25% to 40% oxygen content range is the consumption of F for silicon and tungsten the same. The maxima of consumption are approximately the same for W and Si. This indicates that in this range the arrival of the fluorine at the surface is the etch rate limiting factor. If chemisorption would be the etch rate limiting step, it would be an enormous coincidence that the F consumption of polysilicon and tungsten etching would be the same, as the energies to form the Si-F bound and the W-F bound are different. However, if for both materials, the arrival of

free fluorine is the etch rate limiting step, it would be normal that the consumption of the free F would be the same, as the generation of the free fluorine is not (very much) dependent on the material which is etched.
The fact that the polysilicon etch rate increases with oxygen flow at low oxygen flows is an extra argument that the arrival of free F is the etch rate limiting step, as at these flows the oxygen increases the formation of free fluorine as discussed before and also in appendices I and II.
At higher oxygen contents it is clear that another mechanism limits the etch rate of the silicon, in this case the competition between O and F molecules. For the case of no oxygen, it seems that another mechanism limits the tungsten etch rate : the F consumption for polysilicon is 37% higher than for tungsten: this difference is too big to be explained only by experimental errors. This anomaly at 0% oxygen will be observed also for other plasmas. We assume that for all these plasmas an interaction tungsten-carbon-plasma is reponsible for the etch rate decrease, as explained in section 2.4.2.
Maximum fluorine consumption is around 25 sccm of oxygen flow, for total gas flows of 100 sccm for these tests. This means that in general only 1 F atom per 3 SF_6 molecules is consumed. Therefore it is very probable that the etch rate limiting step is the generation of the F, not diffusion.
The generation factor, G, and the width of the plasma slab, x_s, can be calculated using formulas (10) and (12), after using formula (6) for determining the diffusion constant.
As shown in appendix II, the etch rate for processes with SF_6 gas flow of 100 sccm, no oxygen, pressure of 100 mTorr and AF power of 50 W in RIE mode is in average 140 nm/min, while having a 20% resist coverage of the wafer. For this case one obtains :
$G = 0.24$
$x_s = 8.2$ cm.
For processes with gasflows of 50 sccm of SF_6 and 50 sccm of O_2, with same pressure and power, the etch rate increases to 180 nm/min. For this case one obtains :
$G = 0.47$
$x_s = 10.6$ cm
Both results indicate that diffusion of the free fluorine is not the etch rate limiting step. In example 2, the generation of the free fluorine is the etch rate limiting step.

2.2.2.2) For NF_3 based plasmas.

Fig. 7 shows that for RIE plasmas the fluorine consumption is the same for the tungsten etching and the polysilicon etching at low oxygen contents. Afterwards, it decreases for the polysilicon etching.

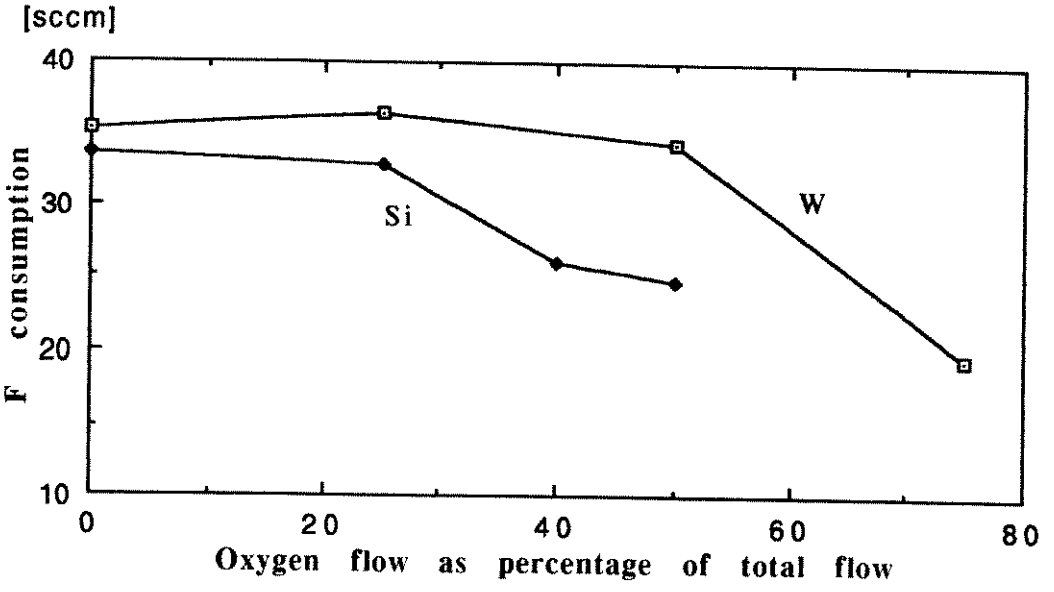

Figure 7 : Fluorine consumption for polysilicon and tungsten etch processes as a function of oxygen content for NF_3 based plasmas in RIE mode.

Once again, this is a strong indication that at low oxygen contents, the arrival of F at the wafer surface is the etch limiting mechanism. When the consumption for the polysilicon etching starts to decrease, the competition between O and F atoms to form bonds with the Si atoms begins, as the fluorine consumption remains high for the tungsten etching.
Fig. 8 shows the evolution of the F consumption for PF plasmas.
In the range from 20% to 33% of oxygen content, the F consumption is approximately the same for polysilicon and tungsten etching. This indicates that in this range, the arrival of F atoms at the wafer surface is the etch rate limiting mechanism. For other oxygen contents, the silicon F consumption is always higher, indicating that other mechanisms determine the etch rate of the tungsten. At higher oxygen contents, a possible explanation is the formation of WOF_4, which is not sufficiently volatile in PF mode, as explained above. But this figure also indicates that another etch rate limiting mechanism occurs at 0% oxygen content, just as for the SF_6 RIE plasmas, as will be discussed in 2.4.2.
Just as for the SF_6 case, the consumption of fluorine is quite low, the maxima are found around 35 sccm of oxygen flow. Total flows are 100 sccm for the RIE mode, 75 sccm for

the PF mode. Therefore approximately 1 F atom per 2 NF_3 molecules is consumed. This indicates that the etch rate limiting step will probably not be the diffusion, but the generation of the free fluorine.

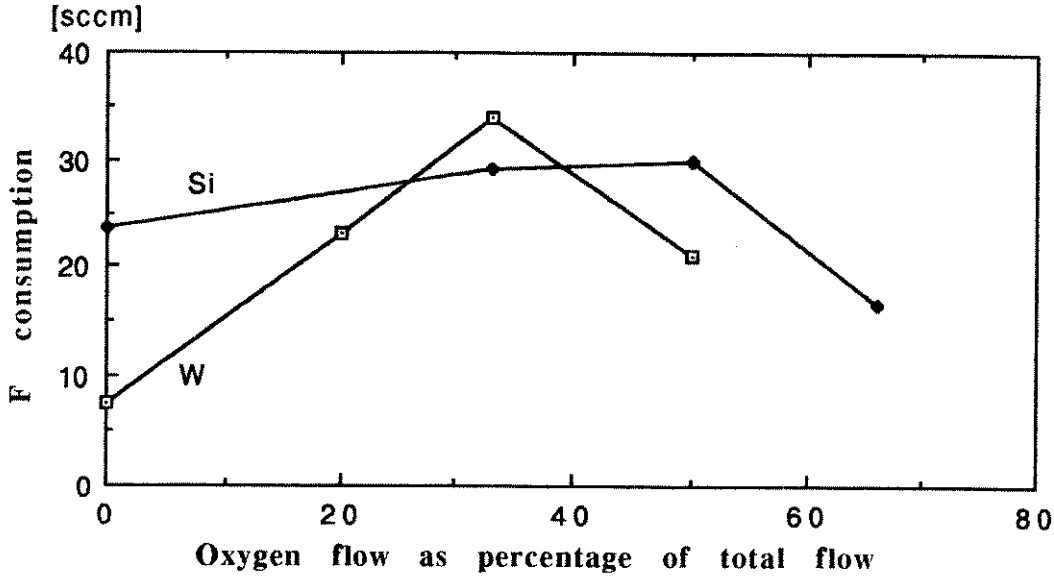

Figure 8 : Fluorine consumption for polysilicon and tungsten etch processes as a function of oxygen content for NF_3 based plasmas in PF mode.

Just as for the SF_6 - O_2 mixtures, one can calculate G and x_s for NF_3 - O_2 mixtures. The example in section 1.2 was for a PF plasma with gas flows of NF_3 of 100 sccm, O_2 of 20 sccm, pressure of 200 mTorr and power of 50W; the etch rate was then 200 nm/min. The result is :
G = 0.38
x_s = 9.2 cm
For a typical RIE plasma with NF_3 flow of 100 sccm, pressure of 150 mTorr, 50 W AF power, with etch rate of 254 nm/min, the calculations yield :
G = 0.38
x_s = 9.1 cm
Both these results indicate that generation of free fluorine is the etch rate limiting step.

2.2.3) The role of oxygen in the Tegal 15xx etch processes.

For Triode I mode, the influence of oxygen content (when mixed with SF_6) on polysilicon and on tungsten etch rate is shown in fig. 9.
The polysilicon etching remains nearly constant, until it starts decreasing at higher oxygen flows. This decrease is probably due to the competition of F and O atoms for the Si atoms.
For the tungsten etching, a significant etch rate increase occurs from 0% to approximately 15% of oxygen content.

Afterwards, the etch rate remains constant, at least for the oxygen range investigated.

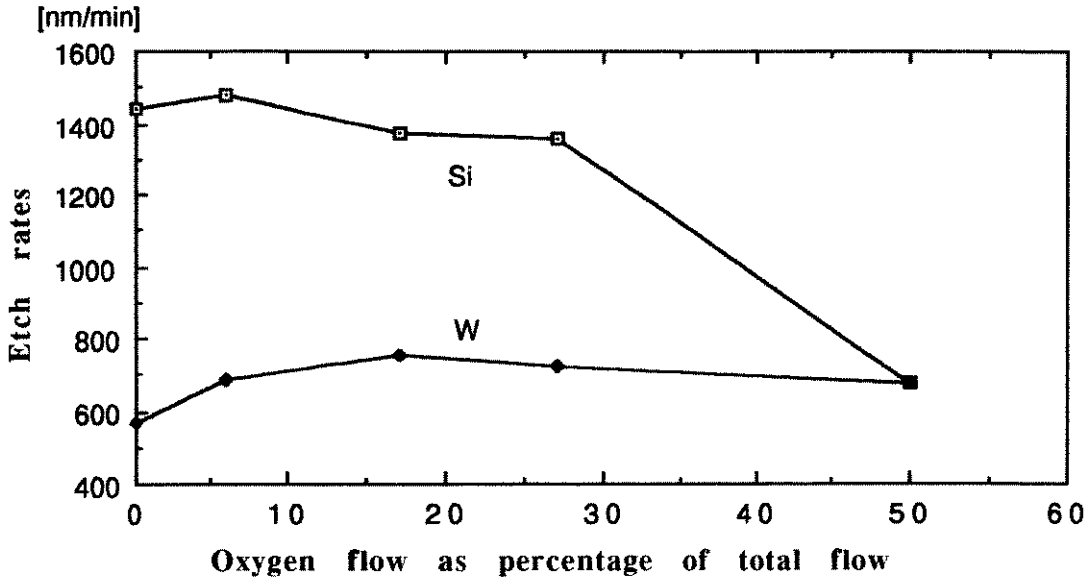

Figure 9 : Polysilicon and tungsten etch rates as a function of oxygen content in Triode I mode.

The results of these etch processes are surprisingly similar to the results obtained in the SWAFER in PF mode, although there NF_3 was used (see above and appendix II). The main points of agreement are:
- the tungsten etch rate is lowest with no oxygen added; even with a 50% O_2 flow, the etch rate remains very high;
- the selectivity towards the resist does not decrease with O_2 flow, on the contrary. The selectivity is lowest when no O_2 flow is present.

There is a difference between the SWAFER and Tegal 15xx etch results in the fact that in the Tegal 15xx the polysilicon etch rate starts decreasing at small O_2 flows, while for the tungsten etch rate, its maximum is at a higher O_2 flow than for the polysilicon etch rate.
The reason for the fact that the polysilicon etch rate does not significantly increase with oxygen content, even at low oxygen contents, is that the efficiency of the magnetically confined plasmas is extremely high, therefore, oxygen addition does nearly not help the formation of free fluorine. This was observed in the actinometry measurements, as reported in appendix IV, and used in the explanation of the polysilicon etch rate behaviour. In section 2.2.4, we shall quantify this phenomenom.
The fact that the tungsten etch rate drops at a much lower oxygen content in the SWAFER than in the Tegal 15xx can be attributed to the difference in ion bombardment. As explained before in section 2.2.1., the ion bombardment is more intense in Triode I mode of the Tegal 15xx than in PF mode in the SWAFER. Therefore it is possible that the ion bombardment in the Triode I mode is sufficient to remove the

WOF_4, where it did not succeed in the PF mode in the SWAFER. Then the etch rate in the Tegal 15xx remains high at higher oxygen flows, while it decreases in PF mode in the SWAFER, as explained above.
The possible mechanisms behind the low tungsten etch rate at 0% O_2 flow will be discussed in section 2.4.2.
For Triode II mode, the influence of the oxygen content on the polysilicon and tungsten etch rates is shown in fig. 10.

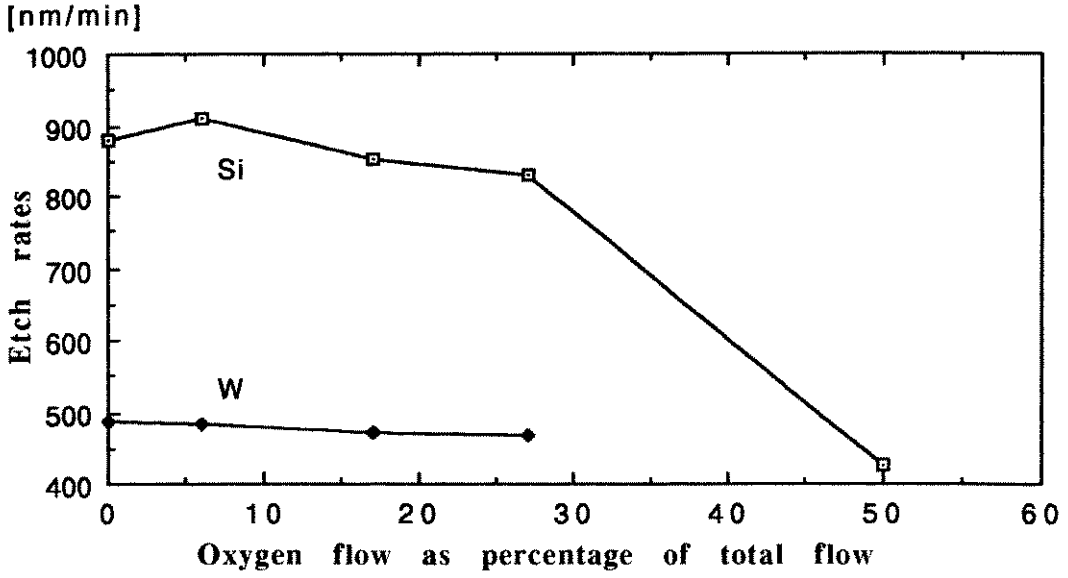

Figure 10 : Polysilicon and tungsten etch rates as a function of oxygen content in Triode II mode.

In this case no (significant) increase of etch rate is observed nor for polysilicon, nor for tungsten. The etch rate of the polysilicon decreases at the higher oxygen content. This decrease is probably due to the competition of F and O atoms to form a bond with the Si atoms.
These results are surprisingly similar to the RIE etching with NF_3-O_2 mixtures in the SWAFER : compare fig. 4 with fig. 10.
Further characteristics of this etching, as already commented in appendix IV:
- the tungsten etch rate is lower than in Triode I mode;
- the uniformity is much higher than for Triode I mode;
- the resist etch rate is much higher than in Triode I mode .

At low oxygen flows the resist etch rate is almost independent of oxygen flow. At high oxygen flows, the resist etch rate increases with higher O_2 flow.

2.2.4) Fluorine consumption for Tegal 15xx etch processes.

It is possible to calculate the F consumption of an etch process as shown in appendix I, using formula (1). For the W wafers, we assumed a free W area of 90 % (a different mask with less resist at the border of the wafer was used than for

the SWAFER etchings). No F consumption by the resist is assumed. This results in fig. 11.

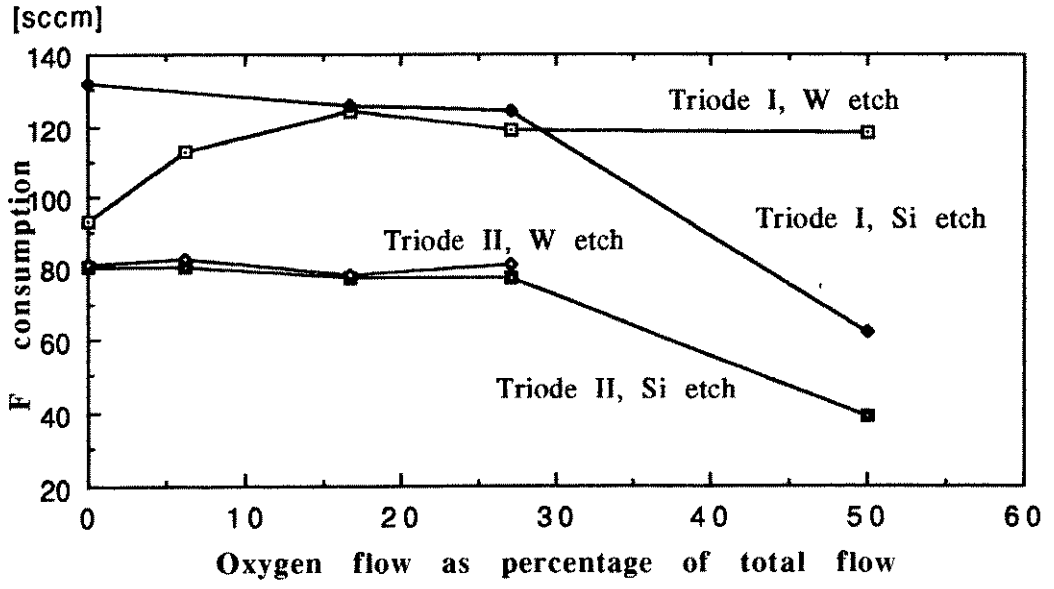

Figure 11 : Fluorine consumption for polysilicon and tungsten etch processes as a function of oxygen content in Triode I and Triode II modes.

This figure shows that there is an extremely good agreement in fluorine consumption for the Triode II mode between the tungsten and the polysilicon etching. This is a very strong indication that the etch rate limiting mechanism is the same for both etchings at low oxygen contents: the limited number of fluorine particles that reaches the wafer surface. As there is no W etch test done at 50 % oxygen content, it is not possible to determine what causes the fluorine consumption of the silicon etching to decrease at the 50% oxygen content. Analogy with the SWAFER results suggests the competition of O with F atoms to react with the silicon atoms at the wafer surface. The fact that oxygen addition does not increase fluorine consumption is explained in section 2.2.3 above. The fluorine consumption is much higher for these plasmas than for the SWAFER plasmas. For a total flow of 96 sccm, 80 sccm of F is consumed. This means that 1 atom of F is consumed per molecule of SF_6.
As shown in appendix IV, section 4, for the polysilicon etching, at low flows this ratio is still higher: the discharge decomposes very efficiently the SF_6 molecules.
This is also the reason why there is little influence of the oxygen addition on the etch rate.
For the Triode I mode, there is good agreement in the range from approximately 10% to 30% oxygen content. For higher oxygen content, the tungsten etch process consumes much more fluorine than the polysilicon etch process. We propose the traditional explanation: the etch rate and the fluorine consumption of the polysilicon etching decreases because of the competition between F and O atoms at the silicon surface:

the oxygen atoms form a Si-O bound, that afterwards SiO can form the non-volatile SiO_2 or $SiOF_2$ molecules, in this way decreasing the etch rate. The same competition between O and F occurs also at the W surface, but there one can also form a WOF_4 molecule, which is volatile in these plasmas, thereby not limiting the etch rate. As the F consumption of the W etching is still high, and much higher than the F consumption of the polysilicon etching, one can conclude that the reason of the etch rate decrease of the polysilicon etching is not the lack of free fluorine atoms, but rather another mechanism, i.c. the formation of non-volatile products on the wafer surface.
The difference in F consumption at 0% oxygen is harder to explain. The polysilicon F consumption shows that there is sufficient free F to obtain etch rates similar to the processes with more O_2. This means that there is another etch rate limiting mechanism for the tungsten etching when there is little or no O_2 flow in Triode I mode. In Triode II this phenomenom does not occur, but one has to observe that in Triode I even for the 0 sccm O_2 flow etching, the etch rate and thus also the F consumption is higher than for whatever Triode II etching. Once again, the similarity with the PF etching with NF_3 and no O_2 gas in the SWAFER is striking. This indicates that the oxygen plays an active role in the (chemical) etching of the tungsten, not only in the formation of the free fluorine atoms. In section 2.4.2 we shall discuss this fenomenom within a larger context and try to explain it.
For both Triode I mode and Triode II mode, one can calculate the generation factor G and the width of the plasma slab, x_s, using formulas (10) and (12) after determining the diffusion constant from formula (6).
In section 1.2 an example of Triode I mode was already been calculated :
$G = 5.93$
$x_s = 5.76$ cm.
For the same process parameters in Triode II mode, i.e. : 80 sccm of SF_6 flow, 10 mTorr pressure, 400 W RF power, with a wafer with 5% resist coverage, the etch rate was 492 nm/min. One calculates then :
$G = 2.93$
$x_s = 7.3$ cm.
For both cases, the etch rate is limited by both the generation of the free fluorine and the diffusion of these atoms to the wafer.

2.3) Formation of tungsten oxide through oxidation of a fluorinated layer.

As described in appendix II, sections 3.3.3.1 and 2, and in appendix III, tungsten oxide layers are formed when tungsten leaves the reactor after being partially etched by a fluorine rich, chemically etching plasma. The fact that this oxidation occurs in two completely different systems, the

SWAFER and the Matrix 303, indicates that it is a general phenomenom, not related to a certain equipment.
The main results of the Auger measurements and the observations made in appendix II, which will help us to explain this oxidation, are:
- the wafer oxidizes when it arrives into air, it does not oxidize in a nitrogen atmosphere, nor in the plasma itself;
- the depth profiles of the F and the O concentrations are very similar;
- no F is found in a wafer which remained in air for a few hours.
We propose the following mechanism for the formation of these oxides: in the NF_3-O_2 plasmas a lot of free fluorine is formed. A lot of free fluorine arrives at the wafer surface. A part of the fluorine is used to remove the tungsten, forming mainly the volatile molecule WF_6, through a mechanism called associative desorption, as described in ref [6], a part is able to diffuse into the tungsten. When a wafer comes into air, which always contains water vapour, we assume that the following reaction occurs:
W-F + H-H-O -> W-O + H-F + H .
The HF evaporates into air and the W-O bounds are formed, resulting in the tungsten oxide layer observed. This explains why the depth of the oxygen in the tungsten sample which came in contact with air is the same as the depth of the fluorine in the tungsten of a sample which came not in contact with air.
The reason that there is no F or O found in the samples that have been etched in RIE mode is in the first place that the formation of free fluorine is much less in this mode. At 25 kHz it is very hard to perform accurate actinometry to verify this [11].
Furthermore, as shown above and in appendix IV, the etch rate is higher in RIE than in PF mode: this can easily be explained through the ion bombardment which increases the etch rate [12]. Therefore, the adsorbed fluorine at the surface of the tungsten film will be much less than in PF mode. In PF mode, one can assume a completely saturated tungsten surface, full of WF_3 and WF_4 compounds. In the RIE mode, there will be much less - if any - of these, because of the ion bombardment. Therefore, there will be no F in excess to diffuse into the bulk.
The oxide layers created by the Matrix 303 are thicker than the oxide layers of the SWAFER. Oxide layers in the SWAFER differ in thickness: near large resist areas, where the etching is slower, the oxide is thicker than far away from the resist, see also below. The Matrix 303 is an afterglow etcher: the wafer is not inbedded in the plasma. Therefore, no bombardment occurs: the etching is really completely chemical. Therefore, even for higher fluorine concentrations in the Matrix 303, the etch rate can be lower than in the SWAFER, where always some ion bombardment occurs [13]. Thus the fluorinated layer in the Matrix 303 will be thicker than in the SWAFER, explaining the thicker oxides.

The fact that no F is discovered in the wafers with SF_6 etchings in the SWAFER can be attributed to the fact that much less free fluorine is formed in these etch processes, as can be seen in the much lower etch rates if the same power is applied in PF mode.
Perhaps the formation of the oxide is linked to the presence of NF_3, as no oxidation was observed in Triode I mode in the Tegal 15xx, when SF_6 based plasmas were used. On the other hand, there is more ion bombardment in Triode I mode in the Tegal 15xx than in PF mode in the SWAFER. Therefore it is possible that this ion bombardment removes the fluorinated layer. This is compatible with the fact that there is also enough ion bombardment to remove the WOF_4 product molecules in the Tegal 15xx, while they were not removed in the SWAFER in PF mode. The only way to verify the possible difference between SF_6 and NF_3 plasmas is to perform experiments in the Tegal 15xx with NF_3 or in the Matrix 303 with SF_6.
Unfortunatley, this was not possible, as these equipment were used for standard processing and therefore the gas configurations could not be changed.

2.4) Tungsten oxide formation in general and its influences.

2.4.1) Influence of pre-treatments.

In the literature contradictions were found on the formation of tungsten oxide [9,14] and its influence on the etch rate. We did several tests with the SWAFER, see appendix II, sections 3.2 and 3.3, and drew the following conclusions:
- leaving the wafer a long time (weeks) in the air or submitting it to an oxygen plasma at temperatures under 200°C (before etching), does not form a tungsten oxide which decreases the etch rate;
- when submitting the wafer to an oxygen plasma at temperatures higher than 250°C, a tungsten oxide layer is formed which decreases the etch rate;
- a tungsten oxide formed through oxidation of a fluorinated tungsten layer, as described in section 2.3 above, decreases the etch rate.
The Auger spectra, discussed in section 2.3 and appendix II, section 3.3.3.2, indicate that if a WO_3 like compound is found at the wafer surface, the oxide is formed by chemical bonds and resists the plasma, as is the case for the oxides formed in the PF mode in the SWAFER. Wafers that were left in an air ambient for weeks had WO_x compounds at the surface, with $x<2$: in this case the oxygen was only adsorbed and the oxide forms no impedance for the plasma etching.

2.4.2) Influence of the resist.

The influence of the resist coverage is normal for most processes. What occurs typically is a loading effect: the etch rates of the underlying films will be higher when these films are covered more by a mask, typically a resist. In

this way, one can characterize the loading effect that occurs during back etching of tungsten plugs, as described in appendices I, II, and IV. The reason for the higher etch rates is the fact that when less film surface is available for etching, this smaller area will be etched faster with the same concentration of active particles, in our cases fluorine atoms, because on the whole, less free fluorine will be consumed.
This behaviour is observed for Triode II processes in the Tegal 15xx and in the SWAFER for processes in the RIE mode. (No tests were done in Triode I mode in the Tegal 15xx.)
In the SWAFER, the inverse was observed for PF processes: the less resist coverage, the higher the etch rate. Increase of AF power did not increase the tungsten etch rate of a DF patterned wafer. Ref [7] however mentions a traditional loading effect for polysilicon etching in PF mode with SF_6.
Tests with blanket tungsten wafers and with PECVD oxide masked wafers show that the etch rates are highest for a PECVD oxide DF patterned wafer. The etch rate decreases in the following order : PECVD oxide LF patterned wafer, followed immediately by : blanket wafer, then resist BF patterned wafer, and the lowest etch rate occurs for a resist DF patterned wafer.
Furthermore, we observed that in PF mode near large resist areas, the etch rate decreases : this is best illustrated by the type of non-uniformity for the PF etch processes: for a blanket wafer, the etch rates are highest at the border; for a resist patterned wafer, with resist in the outer 8 mm of the wafer: the etch rate is lowest at the border. A similar phenomenom happened near a region where the resist was not patterned, already inside the wafer : as reported in appendix II, section 3.3.3.4, near this area, the etch rate is lower: the influence of the resist is observed several mm from the area. On the other side, lines up to 20 µm wide do not influence the etch rate: the rates are the same in spaces between 2 µm wide lines as between 20 µm wide lines.
The presence of the resist does also alter the tungsten oxide colours for some PF processes. As described in appendix II, section 3.3.3.2: nearby a large resist area, oxygen was found till 2.5 times the depth it was found at places 6 mm from this area. Therefore, we assume that the F has diffused a factor 2.5 more near the resist than far away from the resist. This indicates that the etch rate decrease by the resist is not due to lack of fluorine atoms. This is also consistent with the fact that the resist etches very slowly in PF mode, therefore, it will not consume nor F nor O atoms.
The fact that the F arrives at the tungsten surface, but the etch rate is lower indicates that some mechanism either inhibits the formation of the volatile molecule or that it inhibits the desorption of this molecule.
This mechanism probably is governed by the presence of carbon. It was not possible to establish exactly which mechanism is responsible for the etch rate decrease, but it is probably the same one which is responsible for the

following aspects of tungsten etching and resist stripping in other equipment :
- it is found that the particulate count in afterglow strippers increases very much after stripping of tungsten wafers;
- particulate count in etchers also increases very much when resist patterned tungsten wafers are etched in a system, and cleaning is very difficult.

These phenomena indicate a strong interaction resist-tungsten-plasma, though this interaction has not been identified, and not even been acknowledged in the literature.
Another phenomenom which indicates that tungsten etching still guards some secrets, is the fact that after etching tungsten wafers in a reactor, even with "innocent" gases such as SF_6, the etch rates of other materials decrease, even after strict plasma cleaning procedures. The first results of the SF_6 etchings in the SWAFER also indicate a certain passivation process which decreases the etch rate. As no specific research was done to identify the problem, no stringent conclusion can be drawn. But the same resist-tungsten-plasma interaction occurred and could, as least for a part, be responsible for this phenemenom.
It is known that the presence of carbon in the deposition of W from WF_6, causes the formation of beta W : which has a much lower conductivity, but also lower etch rate [14]. An X-Ray Diffraction (XRD) analysis was performed on a wafer, oxidized after a PF process, but no beta W was detected. Therefore, the formation of beta W is probably not the reason for all these phenomena.
Another explanation can be the formation of W-C bonds, which inhibit the etching. There is always some ion bombardment of whatever surface which is placed in a plasma [1]. Therefore, even in PF mode, some low energetic ions bombard the wafer surface. This bombardment will not be enough to break the W bonds, but possibly it can remove some carbon from the resist, which is redeposited onto the W surface, where it can form W-C bonds. At these sites, it will be more difficult to form W-F bonds and therefore the etch rate decreases. This is a reasonable explanation for the decrease in fluorine consumption for the etching in PF mode in the SWAFER and for Triode I mode in the Tegal 15xx for a 0% oxygen content. Indeed, in RIE mode, the W-C bonds can be destroyed by the ion bombardment and when oxygen is available in the plasma, it will bind itself easily with the C, forming CO and CO_2. These molecules are also much more stable than the W-C complex. Special tests should be performed to sustain this theory, e.g. by etching blanket wafers, also in the Tegal 15xx. (The fact that blanket tungsten layers etch faster than tungsten patterned with resist in PF mode in the SWAFER, is compatible with this theory.)
Another explanation can be the influence of the oxygen molecules on the voltage over the plasma sheath. SF_6 and NF_3 are both very electronegative molecules; they tend to capture free electrons. Very often other gases are added to make their plasmas more stable. The capture of free electrons

leads to lower DC bias voltages and lower plasma sheath voltages. Therefore, the addition of oxygen will increase the DC bias voltage and the voltage over the plasma sheath. As ref [13] states that very low ion energies cause considerable tungsten etch rate differences, and as the experiences with the MATRIX 303, as also commented in appendix III above, indicate, this small plasma sheath voltage can have a serious impact. Therefore, it is possible that the addition of small quantities of oxygen changes the etch rate and even the etch rate limiting mechanism.
The fact that several µm of undercut can be found in some etch processes, indicates that this last mechanism alone is not a sufficient explanation. Combination of the last 2 mechanisms is not contradicted by the experiments.

3) General conclusions.

The overall mechanisms as described in the literature and discussed in appendix I were confirmed in this work. On the part of the contradictions, we were able to draw the following conclusions :
1: It is possible to etch tungsten in a merely chemical way, as long as enough free fluorine is available.
2: It is possible to etch tungsten in an anisotropic way if enough ion bombardment occurs.
3: Leaving wafers in air or submitting them to an oxygen plasma, at low temperatures, does not form a tungsten oxide which inhibits etching of the tungsten layer.
4: When tungsten comes in contact with oxygen at high temperatures (>250°C) or when a wafer comes in contact with air after being etched with a gas mixture containing NF_3 in a chemical way, a tungsten oxide is formed which inhibits (or delays) etching of the underlying tungsten.
5: The presence of resist decreases the etch rate of tungsten for a chemical etch process with a NF_3 - O_2 mixture. The complex resist-tungsten-plasma causes several strange phenomena which are not all understood.
6: The etch rate limiting mechanisms for tungsten etching discovered in this study, are :
- in general the limited arrival of free fluorine atoms;
- at zero (or low) oxygen flow, the interaction tungsten - plasma - carbon decreases the etch rate;
- at high oxygen flow, the main responsible of the etch rate decrease can be the competition between F and O atoms to form the product molecule or the dilution effect, decreasing again the arrival of the free fluorine.

4) Suggestions for further research, with the existing equipment.

1: Investigate more thoroughly the influence of process parameters and pre-treatments on the tungsten oxide formation in chemical etch processes with NF_3.
2: Investigate the influence of the resist on the chemical etch process, mainly in the Tegal 15xx and the Matrix 303.

3: Investigate the use of other gas mixtures for tungsten etching, e.g. using HBr as an additive gas to SF_6, NF_3 or even Cl_2.
4: Combine the knowledge of polysilicon etching and tungsten etching to develop tungsten silicide etching.

References

[1] B. Chapman, "Glow Discharge Plasmas", John Wiley and sons (1980).
[2] J. Coburn, "Plasma Etching and Reactive Ion Etching", IV Oficina Brasileira de Microeletronica, pp. 41-80, edt Mammana (1983)
[3] R.C. Reid, T.K. Sherwood, "The properties of gases and liquids", second edition, Mc.Graw - Hill, 1966
[4] Vacuumtechniek - L. Wolterbeek Muller, Kluwer Technische boeken, 1989
[5] Hindmann and Raupp, "Coadsorption of WF_6 and H_2 on polycrystalline tungsten: implications for the hydrogen reduction reaction", Advanced Metallization for ULSI Applications, October 1991, extended abstracts.
[6] A. Durandet, Y. Arnal, J. Pelletier, G. Pomot, "Anisotropy and Kinetics of the Etching of Tungsten in SF6 Multipolar Microwave Plasma", J. Appl. Phys. 67, 2298 (1990)
[7] J. Vandersmissen, "Characterization of polysilicon and nitride processes in the SWAFER", internal Cobrain report, 1991.
[8] Mutsukura, Turban, "Reactive Ion Etching of Tungsten in SF6-N2 plasmas", J. Electrochem. Soc, 137, 225 (1990)
[9] T. Bestwick, G. Oehrlein, "Tungsten Etching Mechanisms in CF4/O2 Reactive Ion Etching Plasmas", J. Appl. Phys. 66, 5034 (1989)
[10] Collumeau e.a., "RIE of a T-shape refractory ohmic contact for a self-aligned heterojunction bipolar transistor", J. Electrochem. Soc. 137, 671 (1990)
[11] A. Richards, B. Thompson, K. Allen, H. Sawin, "Atomic Chlorine Concentration Measurements in a Plasma Etching Reactor", J. Appl. Phys. 62, 792 (1987)
[12] W. Greene, D. Hess, W. Oldham, "Ion-bombardment-enhanced Plasma Etching of Tungsten with NF3/O2", J. Vac. Science Technol. B 6, 1570 (1988)
[13] F. Fracassi, J. Coburn, "Plasma-assisted Etching of Tungsten Films: a quartz-crystal Microbalance Study", J. Appl. Phys. 63, 1758 (1988)
[14] Adachi, Susa, "Reactive Ion Etching of Tungsten Films Sputter Deposited on GaAs", J. Electrochem. Soc. 132, 2980 (1985)

List of Symbols

A : area of the wafer
c : average thermal speed of species
C : concentration
C_F : concentration of atomic fluorine
d: diameter of the wafer
D : diffusion constant
E : electron energy
E_a : activation energy (used for etch rate)
E_S : excitation efficiency
f : incoming flow of species
f(E): electron energy distribution function
G : generation factor (of atomic fluorine)
h : Planck's constant
h_e : height between the electrodes of a parallel plate reactor
h_i : step height of measurement i
I_X : light intensity emitted by species X
J_F : Flow of consumed F during etching
J_{WF6} : Flow of desorbed WF6 during etching
k : Boltzmann constant
LE : loading effect
LE_b : loading effect at the border
LE_c : loading effect in the center
m : molecular mass
M_i : atomic weight of species i
n_i : density of species i in the plasma
ODF : wafer covered with a PECVD oxide dark field mask
OLF : wafer covered with a PECVD oxide light field mask
p : : pressure
Q : activation energy (used for desorption)
r : etch rate
r_{PR} : resist etch rate
r_{SiO2} : oxide etch rate
r_W : tungsten etch rate
r_{bDF} : tungsten etch rate at the border of a DF patterned wafer
r_{bLF} : tungsten etch rate at the border of a LF patterned wafer
r_{cDF} : tungsten etch rate in the center of a DF patterned wafer
r_{cLF} : tungsten etch rate in the center of a LF patterned wafer
R : universal gas constant
R^2: correlation factor
RDF : wafer covered with a resist dark field mask
RLF : wafer covered with a resist light field mask
R_{sp} : resistivity of the material
R_{sq} : sheath resistance of a layer
S : selectivity
t : time

t_l : thickness of the layer
t_{PR} : thickness of resist layer
t_W : thickness of the tungsten layer
T : temperature
T_S : wafer surface temperature
U : uniformity of tungsten etch rates
U_{PR} : uniformity of resist etch rates
U_{LF} : uniformity of tungsten etch rates of a light field patterned wafer
U_{DF} : uniformity of tungsten etch rates of a dark field patterned wafer
v(E) : electron velocity, as a function of the electron energy
w : weight of the wafer
x_S : width of the plasma slab
y : average value of the measured results
y_i : experimental result, as measured
y_{ci} : result as predicted by the model

ν : frequency of the foton
ρ : density of the material
σ : standard deviation
$\sigma_S(E)$: collision cross section for excitation
σ_{12} : Lennard-Jones force constant
τ : residence time of an adsorbed molecule
τ_o: vibration time
Ω_D: Lennard-Jones potential function